Computational Modeling of Ferromagnetics and Magnetorheological Elastomers

Gautam Ethiraj

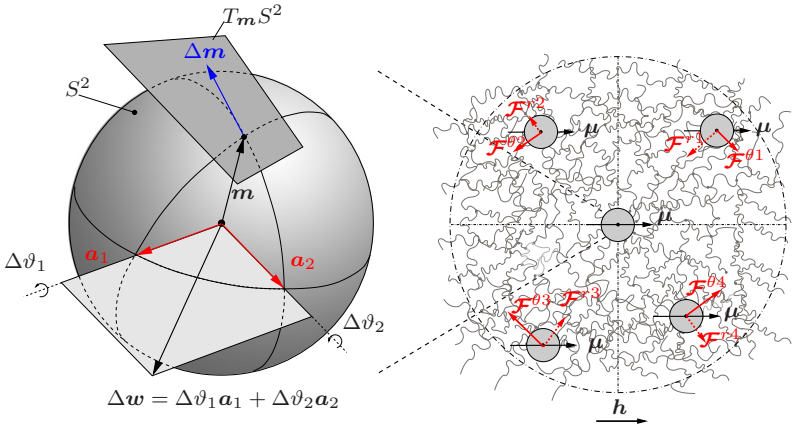

$$E' = \int_{\mathcal{S}} \rho[\psi_{mat}(\nabla\boldsymbol{\varphi}, \boldsymbol{\mu}, \nabla\boldsymbol{\mu}) + \mu_0\boldsymbol{\mu}\cdot\nabla\widetilde{\phi}]\, dv - \frac{\mu_0}{2}\int_{\Omega} |\nabla\widetilde{\phi}|^2\, dv$$

Bericht Nr.: I-33 (2014)
Institut für Mechanik (Bauwesen), Lehrstuhl I
Professor Dr.-Ing. C. Miehe
Stuttgart 2014

Computational Modeling of Ferromagnetics and Magnetorheological Elastomers

Von der Fakultät Bau- und Umweltingenieurwissenschaften der Universität Stuttgart
zur Erlangung der Würde eines Doktor-Ingenieurs (Dr.-Ing.)
genehmigte Abhandlung

von

Gautam Ethiraj

aus Chennai, Indien

Hauptberichter : Prof. Dr.-Ing. Christian Miehe
1. Mitberichter : Prof. Dr.-Ing. Andreas Menzel
2. Mitberichter : Jun.-Prof. Björn Kiefer, Ph.D.

Tag der mündlichen Prüfung: 5. Dezember 2014

Institut für Mechanik (Bauwesen) der Universität Stuttgart
2014

Herausgeber:

Prof. Dr.-Ing. habil. C. Miehe

Organisation und Verwaltung:

Institut für Mechanik (Bauwesen)
Lehrstuhl I
Universität Stuttgart
Pfaffenwaldring 7
70550 Stuttgart
Tel.: +49(0)711/685-66378
Fax: +49(0)711/685-66347

© Gautam Ethiraj
Institut für Mechanik (Bauwesen)
Lehrstuhl I
Universität Stuttgart
Pfaffenwaldring 7
70550 Stuttgart
Tel.: +49(0)711/685-66377
Fax: +49(0)711/685-66347

ISBN 3-937859-21-7 (D 93 Stuttgart)

Abstract

The aim of this work is to present new variational-based computational modeling approaches for selected materials that have coupled magnetic and mechanical properties. In order to solve the magnetomechanically coupled boundary value problems, we employ the finite element method and also discuss certain aspects that are peculiar to magnetomechanical problems such as the unity constraint on the magnetization, the incorporation of the surrounding free space, the micromechanics of the coupled response etc. Thus, we present continuum models motivated by underlying physical phenomena at the micro- and nano-scale that are embedded in appropriate variational-based finite element frameworks allowing the simulation and visualisation of finite-sized bodies. Specifically, we present the computational modeling of two types of *magnetostrictive materials,*

- Ferromagnetic materials with magnetic domain microstructures that evolve dissipatively. This is based on Brown's theory of micromagnetics and now extended and implemented within the computationally powerful finite element method in which the focus is on the geometric consistency.
- Magnetorheological Elastomers (MREs) where we will introduce a modular approach for the construction of micromechanically motivated models for the constitutive response of such materials. Motivated by Toupins work on the elastic dielectric, we will discuss the variational principle and the implementation in the finite element framework.

In modeling the above materials, we span the range of scales involved in continuum magnetomechanics, and also highlight the variety of challenges that exist in the field. From the theoretical and computational standpoint, this work aims to contribute to the ultimate goal of construction of a compatible hierarchy of models for magnetomechanically coupled materials.

Ferromagnetic Materials: We present a *new geometrically exact, three-field rate-type variational principle for dynamic dissipative micro-magneto-mechanics.* This is done by first constructing functionals of micro-magneto-elasticity based on three fields which govern the coupled problem. Of utmost importance are the energy-enthalpy and dissipation functionals. They are formulated in terms of a general framework of an objective, first-order gradient-type material. Inside of the solid domain, the energy density splits up into a free space or vacuum contribution plus a term due to the solid matter. The latter contains the stored elastic energy, including the magnetostrictive coupling, the non-convex magnetic anisotropy density that determines the easy axes of magnetization (due to spin-orbit interactions) and the so-called exchange energy (due to spin-spin interactions) that contains the gradient of the magnetization director. We assume a Rayleigh-type function for the dissipation. and introduce mechanical and magnetic loading functionals by focussing on magnetic-field-driven as well as stress-driven scenarios. The mechanical loading functional contains a *prescribed average macro-stress within the solid domain.* The magnetic loading functional is defined in terms of a *prescribed average macro-field within the full space*, including solid domain and free space. With these functionals at hand, we develop variational principles for the coupled evolution problem. To this end, we first outline in a continuous setting the variational principle for stationary problems, in line with

the classical work of Brown [21], formulated however, in terms of the loading quantities stated above.

A central and new aspect of the work is the formulation of an *incremental variational principle for dynamic (quasi-static) evolution problems.* This incremental principle, which governs the rates of the primary variables based on a potential, that is formulated in terms the energy-enthalpy and the dissipation functionals. We show that the Euler equations of this variational principle are the static stress equilibrium condition, the magnetostatic equilibrium condition, often denoted as the third Maxwell equation or the Gauss-Faraday law, and the Landau-Lifshitz equation for the evolution of the magnetization director.

Based on this framework, we developed *a new geometrical consistent finite element model of micro-magneto-elasticity*, that accounts for the geometric structure of the magnetization director $\boldsymbol{m} \in \mathcal{S}^{d-1}$. Starting from the algorithmic version of the variational principle for dynamic evolution problems associated with finite time increments, we propose a finite element method which preserves exactly this geometric property of the director field at the nodes of the mesh. This time-space-discrete formulation is variational in nature, yielding a symmetric monolithic system of the coupled multifield problem. The key ingredient is the *exact rotational treatment of the magnetization director*, resulting in nonlinear incremental updates of the nodal variables. The method preserves the geometric structure in each iteration step of a typical Newton-Raphson update. As a consequence of the nonlinear update of the magnetization director, the finite element tangent matrix splits into characteristic material and geometric contributions. We outline the formulation in the full three-dimensional context. Its reduction to two-dimensional problems yields a substantial simplification due to the scalar nature of the incremental rotation. Numerical simulations to demonstrate the modeling capacity of the proposed formulation for domain wall motions in magnetic field- and stress-driven loading processes, including their coupling with the surrounding free space have been carried out.

We have gone further to develop a *projection method based on an operator split* as an alternative computational approach to the above monolithic solution strategy. This method is based on the same variational principles mentioned above, but avoids the nonlinear update and geometric matrices of the geometrically exact method thus leading to straightforward and efficient implementation. The unity constraint of the magnetization director is preserved by a post-processing projection step and a staggered solution scheme is employed for solving for the primary variables. Also, due to the successful implementation of both methods, *a comparison* of computational performance between the geometrically exact method and projection method has also been made possible for the first time.

Magnetorheological Elastomers (MREs): A *new incremental variational principle for dissipative magneto-mechanics of MREs in the finite deformation regime* has been formulated in this dissertation. We have first considered the non-dissipative elastic scenario. This is based on the classical work on elastic dielectrics by Toupin [156] and the work on MREs by Kankanala & Triantafyllidis [88, 89]. A *three-field formulation in terms of the deformation map, magnetization (per unit mass) and magnetic scalar potential of the self-field* is presented. In a similar manner to Miehe & Ethiraj [115], we begin with constructing the required functionals. Of foremost importance is the energy enthalpy functional of finite deformation magnetoelasticity. The loading contributions are taken in terms of the applied magnetic field and mechanical body forces and tractions. With these functionals at hand, we construct the variational principle for finite deforma-

tion magnetoelasticity. The Euler equations of the variational principle are the balance of linear momentum, the Gauss' law for magnetism, the (time-discrete) Biot equation for the evolution of the internal variables and a local equation relating the magnetic field with the magnetization.

From the material modeling perspective, we have presented *a modular framework for the construction of constitutive models for isotropic MREs that allow the incorporation of statistically based kernels*. The presented framework has two salient features that are to be highlighted. Firstly, we employ a *multiplicative split of the deformation gradient into stress-free (magnetostrictive) and stress-producing parts*. This gives rise to the second salient feature namely *the exploitation of micromechanically-motivated, statistically-based (network) kernels* in the model without any change. While we use an Ising model for the pure magnetic response, the elastic response is governed by the non-affine microsphere model of Miehe, Göktepe & Lulei [118].

We further extend the above methods to cover irreversible effects. Here, we focus on the viscoelastic response that arises due to the rubber matrix. With the functionals for the reversible (magnetoelastic) case defined, we present a *new four-field incremental variational principle for magneto-viscoelasticity* with the fourth field representing viscous strain-like variables. This is based on the construction of a rate-type variational potential that yields in addition to the balance equations of the elastic case, the Biot equation for the local evolution of the viscous strain-like variables as the Euler equations. The incremental variational potential follows by an algorithmic time integration. Following this, the modular framework for free-energy functions for magnetoelasticity of MREs is now extended to cover magneto-viscoelasticity. This involves an addition to the energetic part of the model and a dissipation function as well. Once again the modular framework allows the inclusion of the *statistically-based network kernels,* this time, *for viscoelasticity*. For our specific implementation, we use the viscoelastic model of Miehe & Göktepe [116].

We have implemented the frameworks for finite deformation magnetoelasticity and magnetoviscoelasticity within a finite element code and thus are able to perform fully-coupled magnetomechanical simulations for application-oriented problems.

Zusammenfassung

Das Ziel dieser Arbeit ist es für ausgewählte Materialien mit sowohl magnetischen als auch mechanischen Eigenschaften neue numerische Modellierungsansätze darzustellen. Das magnetomechanische Randwertproblem wird mit der Finite Elemente Methode gelöst und wir diskutieren einige einzigartigen Gesichtspunkte solcher Probleme. Dazu gehören unter anderem die Einheitslänge der Magnetisierung, die Betrachtung des umgebenden luftleeren Raums sowie die Mikromechanik der gekoppelten Systemantwort. Wir präsentieren kontinuumsmechanische Modelle welche durch die zugrundeliegenden physikalischen Phänomene auf der Mikro- oder sogar Nanonskale motiviert sind. Diese Modelle sind im Rahmen der Finiten Elemente Methode implementiert, basieren auf Variationsprinzipien und erlauben die Simulation sowie Visualisierung von Festkörpern endlicher Größe. Im Einzelnen betrachten wir die computergestützte Modellbildung zweier magnetostriktiver Materialien:

- Ferromagnetische Materialien bestehen aus Mikrostrukturen mit magnetischen Domänen, welche sich dissipativ entwickeln. Diese Modelle basieren auf der *mikromagnetischen Theorie von Brown* und werden so erweitert, dass sie in leistungsstarke Finite Elemente Codes implementiert werden kö nnen.
- Magnetorheologische Elastomere (MREs) werden durch die Einführung eines modularen Ansatzes zur Konstruktion mikromechanisch motivierter Modelle beschrieben. Die Modelle basieren auf *Toupins Theorie für ideale Dielektrika* und wir diskutieren deren Implementation in die Finite Elemente Methode.

Die oben genannten Materialien spannen die komplette Bandbreite der beteiligten Skalen für mikromagnetische Modelle auf und heben die vielseitigen Herausforderungen in diesem Forschungsfeld hervor. Genauer gesagt zielt diese Arbeit darauf ab, seinen Teil zum ultimativen Ziel einer ganzheitlichen Beschreibung von magnetomechanisch gekoppelten Materialien beizutragen, und dies sowohl von theoretischen als auch rechentechnischen Gesichtspunkten. Dementsprechend konstruieren und implementieren wir neue inkrementelle Variationsprinzipien für die Modellierung dissipativer Reaktionen für magnetomechanisch gekoppelte Mehrfeldprobleme auf der Mikro- und Makroskale.

Ferromagnetische Materialien: Wir präsentieren ein neues, geometrisch exaktes, ratenabhängiges Variationsprinzip für dissipative Mikromagnetomechanik. In einem ersten Schritt werden Funktionale der Mikromagnetoelastizität konstruiert. Diese basieren auf drei Primärvariablen welche das gekoppelte Randwertproblem beschreiben. Von größter Wichtigkeit sind hierbei die Energie-Enthalpie sowie Dissipationsfunktionale. Diese sind in einem allgemeinen Rahmen in Abhängigkeit eines objektiven Gradientenmaterials ersten Grades beschrieben. Innerhalb des betrachteten Gebiets teilt sich die Energiedichte in einen Anteil resultierend aus der Präsenz des luftleeren Raums (Vakuum) und des Festkörpers auf. Der letztgenannte Anteil des Festkörpers enthält die gespeicherte elastische Energie. Diese ist zusammengesetzt aus der magnetostriktiven Kopplung, der nicht konvexen, richtungsabhängigen magnetischen Dichte (aufgrund der Spin-Bahn Wechselwirkung), welche die Vorzugsrichtung der Magnetisierung bestimmt, und der sogenannten Austauschenergie (aufgrund der Spin-Spin Wechselwirkung), welche den Gradienten der Magnetisierungsrichtung enthält. Die dissipativen Prozesse werden durch eine Rayleigh Funktion beschrieben. Zusätzlich führen wir mechanische sowie magnetische Belastungsfunktionale ein, welche Prozesse charakterisieren die entweder durch magnetische Felder

oder durch Spannungen getrieben werden. Das mechanische Belastungsfunktional ist formuliert in Abhängigkeit der makroskopischen Durchschnittsspannungen des Festkörpers. Das magnetische Belastungsfunktional ist durch den vorgegeben Mittelwert des magnetischen Feldes im gesamten Kontrollraum definiert, welcher sowohl den Festkörper als auch das Vakuum umfasst. Stehen diese Funktionale zur Verfügung, entwickeln wir Variationsprinzipien für das gekoppelte Evolutionsproblem. Zu diesem Zweck erläutern wir in einem ersten Schritt das kontinuierliche *Variationsprinzip für stationäre Probleme*. Dieses ist im Einklang mit der klassischen Arbeit von Brown Jr. [20], berücksichtigt jedoch die oben genannten Belastungsfunktionale.

Ein zentraler sowie neuer Aspekt dieser Arbeit ist die Formulierung eines *inkrementellen Variationsprinzips für dynamische (quasistatische) Evolutionsprobleme*. Dieses inkrementelle Prinzip, welches die Raten der Primärvariablen basierend auf einem Potential bestimmt, ist in Abhängigkeit der Energie-Enthalpie sowie Dissipationsfunktionale formuliert. Hierbei wird aufgezeigt, dass die Euler Gleichungen dieses Variationsprinzips die statischen Gleichgewichtsbedingung, das Gaußsche Gesetz für Magnetfelder (dritte Maxwellgleichung), sowie die Landau-Lifshitz Gleichung für die Evolution der Magnetisierungsrichtung sind.

Basierend auf diesem Rahmenkonzept wird ein neues, geometrisch konsistentes finites Elementmodel der Mikromagnetoelastizität entwickelt, welches die geometrische Struktur (Einheitslänge) der Magnetisierungsrichtung berücksichtigt. Wir starten hierbei von der, für endliche Zeitschrittweiten formulierten, algorithmischen Darstellung des dynamischen Variationsprinzips. Daraufhin beabsichtigen wir eine Methode zu entwickeln, welche diese geometrische Eigenschaft der Richtung der Magnetisierung an den Knoten des Finite Elemente Netzes exakt erfüllt. Diese variationelle zeit- und raumdiskrete Formulierung liefert ein symmetrisches, monolithisches Gleichungssystem des gekoppelten Mehrfeldproblems. Der zentrale Aspekt ist die exakte Behandlung der Drehung der Magnetisierungsrichtung, welche in einem nichtlinearen Update der inkrementellen Knotenvariablen resultiert. Die entwickelte Finite Elemente Methode behandelt inkrementelle Größen als Primärvariablen. Im Besonderen sind hierbei die inkrementellen Rotationsfreiheitsgrade zu nennen, welche die Variation und Linearisierung der Magnetisierungsrichtung bestimmen. Die Methode bewahrt die geometrische Struktur in jedem Iterationsschritt eines typischen Newton-Raphson Updates. Als Konsequenz des nichtlinearen Updates der Magnetisierungsrichtung spaltet sich die Tangentenmatrix in einen charakteristischen Material- sowie geometrischen Anteil auf. Wir erläutern die Formulierung im vollen dreidimensionalen Kontext. Die Reduktion auf zweidimensionale Probleme liefert eine erhebliche Vereinfachung aufgrund der skalaren Natur der inkrementellen Rotation. Numerische Simulationen zeigen die Leistungsfähigkeit des Modells für durch magnetische Felder sowie Spannungen getriebene Bewegungen der Domänenwände auf. Zusätzlich wird die Kopplung mit dem umgebenden Vakuum berücksichtigt.

Des weiteren wurde eine Projektionsmethode basierend auf einem Operator Split als alternativer rechnergestützter Ansatz zur oben erwähnten monolithischen Lösungsstrategie entwickelt. Diese Methode basiert auf den genannten Variationsprinzipien, jedoch vermeidet sie nichtlineare Updates und geometrische Tangentenmatrizen der geometrisch exakten Formulierung welches wiederum zu einer einfachen und effizienten Implementierung führt. Die Einheitslänge der Magnetisierungsrichtung wird durch eine Nachbearbeitung mit einem Projektionschritt sichergestellt. Zusätzlich wird eine gestaffelte Lösungsstrategie zur

Bestimmung der Primärvariablen angewendet. Durch die erfolgreiche Implementierung beider Methoden ist es zum ersten Mal möglich, die Leistungsfähigkeit der geometrisch exakten und Projektionsmethode miteinander zu vergleichen.

Magnetorheologische Elastomere (MREs): Diese Dissertation formuliert ein neues inkrementelles Variationsprinzip für dissipative Magnetomechanik für MREs im Bereich großer Verformungen. Zu aller erst behandeln wir das nicht dissipative, elastische Szenario. Dieses basiert auf der klassischen Arbeit von Toupin [156] über das ideale Dielektrikum sowie der Arbeit von Kankanala & Triantafyllidis [88, 89] über magnetorheologische Elastomere. Es wird eine dreifeld Formulierung bezüglich der Deformationsabbildung, Magnetisierung (pro Masseneinheit) und magnetischem Skalarpotential des Eigenfeldes präsentiert. Auf die gleiche Weise wie Miehe & Ethiraj [115] beginnen wir mit der Konstruktion aller benötigten Funktionale. Von großer Bedeutung ist hierbei das Energie-Enthalpie Funktional der Magnetoelastizität. Die Beiträge durch externe Belastungen wie das angelegte magnetische Feld, mechanische Gewichtskraft und Randspannungen werden als Totlasten angenommen. Sind diese Funktionale bestimmt, konzentrieren wir uns auf den Aufbau des Variationsprinzips der finiten Magnetoelastizität. Die Euler Gleichungen dieses Variationsprinzips sind die mechanische Impulsbilanz, das Gaußsche Gesetz für Magnetfelder, die (zeitdiskrete) Biot Gleichung für die Evolution der internen Variablen und eine lokale Gleichung, welche das magnetische Feld mit der Magnetisierung in Zusammenhang bringt.

Es wird ersichtlich, dass es kein eindeutiges Rahmenkonzept für die Struktur der freien Energiefunktion für magnetorheologische Elastomere gibt. Dies ist eine Kluft die wir beabsichtigen zu füllen. Wir fokussierten uns mit Erfolg auf isotrope MREs, jedoch ist zu erwarten, dass Anisotropie in das selbe Konzept eingepflegt werden kann. Das vorgelegte Rahmenkonzept hat zwei Besonderheiten, welche wir im folgenden kurz hervorheben. Zum einen verwenden wir eine multiplikative Aufteilung des Deformationsgradienten in einen spannungsfreien (magnetostriktive) und spannungsproduzierenden Anteil. Dies führt zur zweiten hervorstechenden Eigenschaft, die daraus besteht, *mikromechanisch motivierte*, auf *statistischer Mechanik basierte (Netzwerk-) Kerne* ohne jegliche änderung im Modell zu nutzen. Während wir für die rein magnetische Systemantwort ein Ising Modell verwenden, wird die elastische Reaktion durch das nicht-affine Mikrosphärenmodell von Miehe et al. [118] beschrieben.

Des weiteren werden die obigen Methoden erweitert um irreversible Effekte zu beschreiben. Hierbei konzentrieren wir uns auf viskoelastische Reaktionen aufgrund der Gummimatrix. Die anhand des reversiblen (magnetoelastischen) Falls bereits definierten Funktionale werden auf ein inkrementelles vierfeld Variationsprinzip für Magnetoviskoelastizität erweitert. Das vierte Primärfeld stellt hierbei eine interne, verzerrungsähnliche Variable dar, welche viskose Effekte beschreibt. Diese Erweiterung basiert auf der Definition eines ratenanhängigen Variationspotentials, welches als Euler Gleichungen zusätzlich zu den Bilanzgleichungen des elastischen Falls die Biot Gleichung für die lokale Evolution der viskosen internen Variable liefert. Das inkrementelle Variationspotential folgt durch eine algorithmische Zeitintegration. Dementsprechend wurde das modulare Konzept zur Beschreibung magnetorheologischer Elastomere so erweitert, dass viskose Effekte mit einbezogen werden können. Dies beinhaltet sowohl eine Ergänzung des energetischen Anteils als auch der Dissipationsfunktion. Abermals erlaubt die modulare Struktur die Einbeziehung der auf statistischer Mechanik basierten Netzwerkkerne, nur diesmal für *Viskoelastizität*.

Konkret benutzten wir das viskoelastische Modell von Miehe & Göktepe [116] für die numerische Implementierung.

Wir haben jegliche Konzepte der finiten Magnetoelastizität sowie Viskoelastizität in einem Finiten Elemente Code implementiert. Dadurch ist es möglich, voll gekoppelte magnetomechanische Simulationen für anwendungsorientierte Probleme durchzuführen und die verwendeten Materialmodelle mit experimentellen Ergebnissen zu vergleichen. Diese Modelle zeigen dabei eine sehr gute Übereinstimmung.

Acknowledgements

First and foremost, I would like to thank Prof. Dr.-Ing. Christian Miehe for his guidance and for the opportunity to work on an extremely interesting and challenging area of research. I am especially thankful for the unique learning environment that he created at the institute and for readily entrusting me with responsibilities from the very start.

I would also like to thank Prof. Dr.-Ing. Andreas Menzel for agreeing to be a reviewer for the dissertation and for his open and friendly attitude throughout our interaction. My sincere thanks goes to Bjoern Kiefer, Ph.D. for his support through the MSc thesis and right up to the point as a reviewer for this dissertation.

I would like to thank all my former colleagues at the institute for the jovial atmosphere at the institute, their friendship and laughter-filled company at conferences. Additionally, the efforts of Daniele, Felix and Ilona in ensuring that one was never too far away from a coffee-break are gratefully acknowledged. I sincerely thank Fadi for his support in COMMAS administration, for introducing me to Arslan Kebab, and for accompanying me in my quest for "an exercise that is easy and gives a lot of muscles". My heartfelt thanks goes to Vasantha, Ashish and the COMMAS HiWis for their invaluable contributions and support in research and administrative matters which made this dissertation possible while being the COMMAS Course Director at the same time. I am greatly indebted to Heike for being a source of encouragement and support in the final steps of the dissertation.

Finally, I am most grateful to my family in India including Sheila Atha, Mohan Mama and Shabari Atha because of whom it was possible for me to pursue this particular studies-cum-career route, and specifically to Papa who has always set a good example, been a pillar of support, and been the best dad ever.

Contents

1. Introduction **1**
1.1. Motivation 1
1.2. State of the Art 5
1.2.1. Micro-Magneto-Mechanics of Ferromagnetic Materials 5
1.2.2. Finite Deformation Magneto-Mechanics of MREs 7
1.3. Objectives and Outline 9
1.3.1. Geometrical Aspects in Computational Micro-Magneto-Mechanics . 9
1.3.2. Micromechanically Based Modular Approach for Modeling of MREs 10
1.3.3. Outline of the Work 11

2. Fundamentals of Magnetostatics **13**
2.1. Governing Principles of Magnetostatics 13
2.1.1. First Principle of Magnetostatics: Conservation of Electric Charge . 13
2.1.2. Second Principle of Magnetostatics: Conservation of Magnetic Flux 14
2.1.3. Third Principle of Magnetostatics: Maxwell-Lorentz Aether Relation 14
2.2. Equations of Field-Matter Interactions in Magnetostatics 14
2.2.1. Field due to Prescribed Current Distribution 14
2.2.2. A Magnetizable Body in the Vicinity of a Current Distribution . . . 15
2.2.3. Global Forms and Jump Conditions 16
2.2.4. Units of Magnetic Field Variables 16

3. Fundamentals of Continuum Magneto-Mechanics **17**
3.1. Geometrical Aspects of Finite Deformation Kinematics 17
3.1.1. Placement Map and Deformation Map 17
3.1.2. Strain Measures and Mapping Properties 18
3.1.3. Stress Measures and Mapping Properties 20
3.1.4. Geometric Transformation of Magnetic Variables 21
3.2. Balance Laws of Thermo-Magneto-Mechanics 23

4. Geometrically Exact Micro-Magneto-Elasticity **27**
4.1. Small Deformations for Mechanically Hard Ferromagnets 27
4.2. Basic Functionals in Micro-Magneto-Elasticity 28
4.2.1. Primary Fields: Displacement, Magnetization, Potential 28
4.2.2. Boundary Conditions and Loading Functionals 29
4.2.3. Objective State Variables: Theory of Grade One 31
4.2.4. Energy-Enthalpy and Dissipation Potential Functionals 31
4.2.5. Energy-Enthalpy Function of Micro-Magneto-Elasticity 34
4.2.6. Dissipation Potential for Micro-Magnetic Evolution 34
4.3. Variational Formulation of Micro-Magneto-Elasticity 34
4.3.1. Variational Formulation for Stationary Problems 34
4.3.2. Variational Formulation for Dynamic Problems 36

4.4. Discrete Incremental Variational Formulations 38
4.4.1. Time-Discrete Field Variables in Incremental Setting 38
4.4.2. Time-Discrete Incremental Variational Principle 40
4.4.3. Space-Time-Discrete Incremental Variational Principle 42
4.5. FE Discretization of 2D-Problems 45
4.5.1. Specification of Nodal Variable Vectors 45
4.5.2. Constitutive State, Generalized Stresses and Moduli 45
4.5.3. Specification of the Finite Element Matrices 46
4.5.4. Nonlinear Update of Nodal Variables 46
4.6. Selected Initial Boundary Value Problems 46
4.6.1. Example to Demonstrate the Rotation of the Magnetization 47
4.6.2. Formation of Magnetic Domains in Thin Film of Permalloy 48
4.6.3. Growth of Magnetic Domains in Thin Permalloy Sample 51
4.6.4. Magnetic Domain Evolution in Stress-Driven Loading 51

5. A Projection Method for Micro-Magneto-Elasticity 55
5.1. Variational Principles for Micro-Magneto-Elasticity 55
5.1.1. Variational Formulation for Dynamic Problems 55
5.1.2. Decoupling via Operator Split 57
5.2. Time-Discrete Incremental Variational Formulations 58
5.2.1. Time-Discrete Field Variables in Incremental Setting 58
5.2.2. Magnetic Predictor-Corrector Algorithm $ALGO_{\boldsymbol{m}}$ 59
5.2.3. Magneto-Mechanical Corrector Algorithm $ALGO_{\boldsymbol{u}\tilde{\phi}}$ 60
5.3. Space-Time-Discrete Staggered Finite Element Solution 61
5.3.1. Space-Time Discrete Magnetic Predictor-Corrector 62
5.3.2. Space-Time Discrete Magnetomechanical Corrector 64
5.4. Numerical Results 65
5.4.1. Formation of Magnetic Domains in Thin Ferromagnetic Film 65
5.4.2. Evolution of Magnetic Domains in an Applied Magnetic Field 67
5.4.3. Evolution of Magnetic Domains under Applied Mechanical Stress . . 68
5.4.4. A Comparison of the Two Methods 69

6. Magnetoelasticity of MREs 71
6.1. Motivation and Physical Background of MREs 71
6.2. Basic Functionals of Magnetoelasticity 72
6.2.1. Primary Fields: Displacement, Magnetization, Potential 72
6.2.2. Energy-Enthalpy Functional of Magneto-Elasticity 73
6.2.3. Loading Functional of Magneto-Elasticity 74
6.3. Variational Principle for Stationary Problems 75
6.3.1. The Variational Statement 75
6.3.2. Euler-Lagrange Equations in Reference Configuration 76
6.4. Finite Element Implementation of the Coupled Problem 77

6.5. Properties of the Free Energy Function 79
6.5.1. Objectivity 79
6.5.2. Material Symmetry 80
6.5.3. Magnetic Symmetry 80
6.5.4. Invariants 80
6.6. Constitutive Framework Modeling MREs 80
6.6.1. Ingredient 1: Additive Split of Energy-Enthalpy Density 81
6.6.2. Ingredient 2: Energy of the Magnetic State 81
6.6.3. Ingredient 3: Volumetric-Isochoric Split of Local Deformation 84
6.6.4. Ingredient 4: Magnetostrictive Deformation 84
6.6.5. Ingredient 5: Local Isochoric Mechanical Network Kernel 85
6.7. The Stress and Magnetic Induction 88
6.8. Coupled Tangent Moduli for FEM Implementation 89
6.9. Numerical Examples 90
6.9.1. Saturation Effect in Magnetostriction 90
6.9.2. Spherical Magnetorheological Elastomer Sample in Free Space 91
6.9.3. MRE for a Finger Actuator 94
6.9.4. Inhomogeneous Large Magnetically-Induced Strains in MRE 95
6.9.5. Magnetorheological Elastomer as Actuator in Valve 97

7. Magneto-Viscoelasticity of MREs 101
7.1. Primary Variables for Magneto-Viscoelasticity 101
7.2. Variational Principle for Rate-Dependent Problems 101
7.3. Time-Discrete Incremental Variational Principle 103
7.4. Finite Element Implementation of the Coupled Problem 104
7.5. Constitutive Ingredients for Constructing the Model 106
7.5.1. Ingredient 1: Additive Split of Energy-Enthalpy Density 107
7.5.2. Ingredient 2: Energy of the Magnetic State 107
7.5.3. Ingredient 3: Volumetric-Isochoric Split of Local Deformation 107
7.5.4. Ingredient 4: Magnetostrictive Deformation 107
7.5.5. Ingredient 5: Local Isochoric Mechanical Network Kernel 108
7.6. The Stress and Magnetic Induction 110
7.7. Numerical Results 111
7.7.1. Qualitative Demonstration of Magnetic Relaxation 111
7.7.2. Dynamic Compression Test 113

8. Conclusion 117
8.1. Computational Micro-Magneto-Mechanics 117
8.2. Finite Strain Computational Modeling of MREs 118

1. Introduction

The aim of this work is to present new variational-based computational modeling approaches for selected materials that have coupled magnetic and mechanical properties. In order to solve the magnetomechanically coupled boundary value problems, we employ the finite element method and also discuss certain aspects that are peculiar to magnetomechanical problems such as the unity constraint on the magnetization, the inclusion of the surrounding free-space, the micromechanics of the coupled response etc. Thus, we present continuum models that are motivated by the underlying physical phenomena at the micro- and nano-scale that are also embedded in appropriate variational-based finite element frameworks allowing the simulation and visualisation of finite-sized bodies. Specifically, we will present the computational modeling of two types of *magnetostrictive materials* namely,

- *Ferromagnetic materials* with magnetic domain microstructures that evolve with dissipation. This is based on Brown's theory of micromagnetics and now extended and implemented within the computationally powerful finite element method.
- *Magnetorheological Elastomers (MREs)* where we will introduce a modular approach for the construction of micromechanically motivated models for such materials. We will also discuss their implementation in the finite element method.

In modeling the above materials we cover the range of scales involved in continuum magnetomechanics, and also highlight the variety of challenges that that exist in the field. More specifically, from the theoretical and computational standpoint, this work aims to contribute a building block to the ultimate goal of construction of a compatible hierearchy of models for magnetomechanically coupled materials.

1.1. Motivation

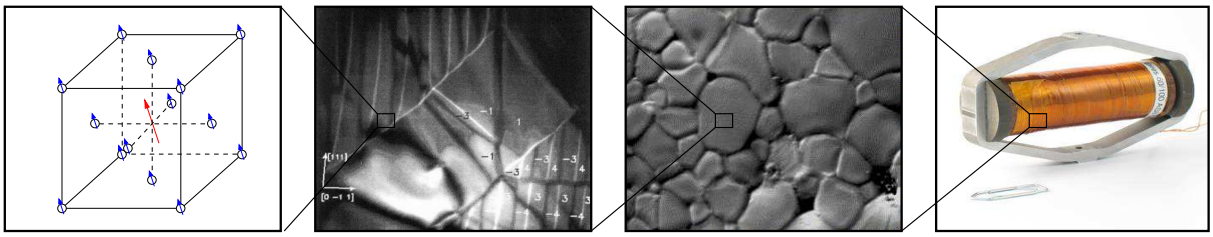

Figure 1.1: Typical length scales involved in continuum magnetomechanics

Miniaturization and high-performance are usually the driving force to create new materials. As a result, a number of smart materials (also called multifunctional materials), have been developed and are still continuing to be developed and optimized by researchers in order to be used in new components or replace existing ones with an (even more) optimized performance which consequently brings the need for modeling and simulation of such materials[1]. Some examples follow.

[1]Modeling concepts may also provide motivation for discovery of new phenomena in materials. In 1956, Tavger & Zaitsev [150] and in 1957, Dzialoshinskii [47] proved, by symmetry considerations

Figure 1.2: Applications of magnetostrictive smart materials. Terfenol-D and Galfenol were originally developed by the US Navy for sonar equipment. These materials are being considered by automotive firms for high pressure fuel injectors, see PIRATLA [127]. Feonic PLC. [71] uses the high magnetostriction for transducers.

Terfenol-D ($Tb_{1-x}Dy_xFe_2$, $x \approx 0.3$) was developed by the US military to have a large magnetostriction to enable its use in higher-powered sonar equipment having greater bandwidth and reliability while reducing transducer size and weight by a factor of three [70]. Ever since it was commercially available[2], several other applications have been identified for this material and its derivatives for military, civilian or industrial purposes, see Figure 1.2. For example, Robert Bosch GmbH is developing Terfenol-D based fuel injectors capable of a higher performance than piezoelectric injectors thus signalling a possible comeback for solenoid-based injectors even in the high performance segment (traditional solenoid injectors continue to be the mainstay of low-cost injection technology). Feonic PLC develops Terfenol-D-based transducers that act as "invisible speakers" by using walls, floors and other resonant surfaces as amplifiers, see [71]. Clearly, there is a need to model such materials in order to optimize their performance. With the advent of high performance computing, large scale atomic level simulations are possible. However computations for macro-sized bodies via such approaches remains impracticable. Accurate continuum models as well as their numerical implementation in a robust manner are the need of the hour. This scenario forms the motivation for micromechanically motivated computational models of magnetomechanically coupled materials.

As was said earlier, miniaturization of components is a motivation for developing new materials. The case of magnetic materials is no different. As a result, modeling approaches need to evolve according to the scales involved. The schematic in Figure 1.3 highlights this for the case of magnetic recording devices that have steadily made use of knowledge of smaller and smaller scales. Clearly, newer storage devices require a precise knowledge of magnetic domain behavior and its response to externally applied magnetic fields and mechanical loads. As shown in Figure 1.3, magnetic domains are used to store data in bits. An improved knowledge of magnetic domain behavior enables more compact storage of data and higher capacities as is seen in Figure 1.3. The schematic Figure 1.3 shows how this is achieved in two examples. With an improved knowledge of magnetic domain behavior, an earlier method of longitudinal magnetic recording (LMR) could be replaced with a denser perpendicular magnetic recording (PMR). While the longitudinal method required in-plane domains to store bits of 0 and 1, the perpendicular method used spins pointed up and down to denote 0 and 1 bits. This was shown in 1976 by

alone, that piezomagnetism could occur in MnF_2 and CoF_2. Later in 1960, BOROVIK-ROMANOV [10] examined these materials and experimentally observed and measured the effect for the first time, see BOROVIK-ROMANOV [11]. The researchers had collaborated in the above mentioned works.

[2]Currently, there are only two commercial producers of Terfenol-D in the world i.e. ETREMA Products, Inc. in the USA and Gansu Tianxing Rare Earth Functional Materials Co. Ltd. in China.

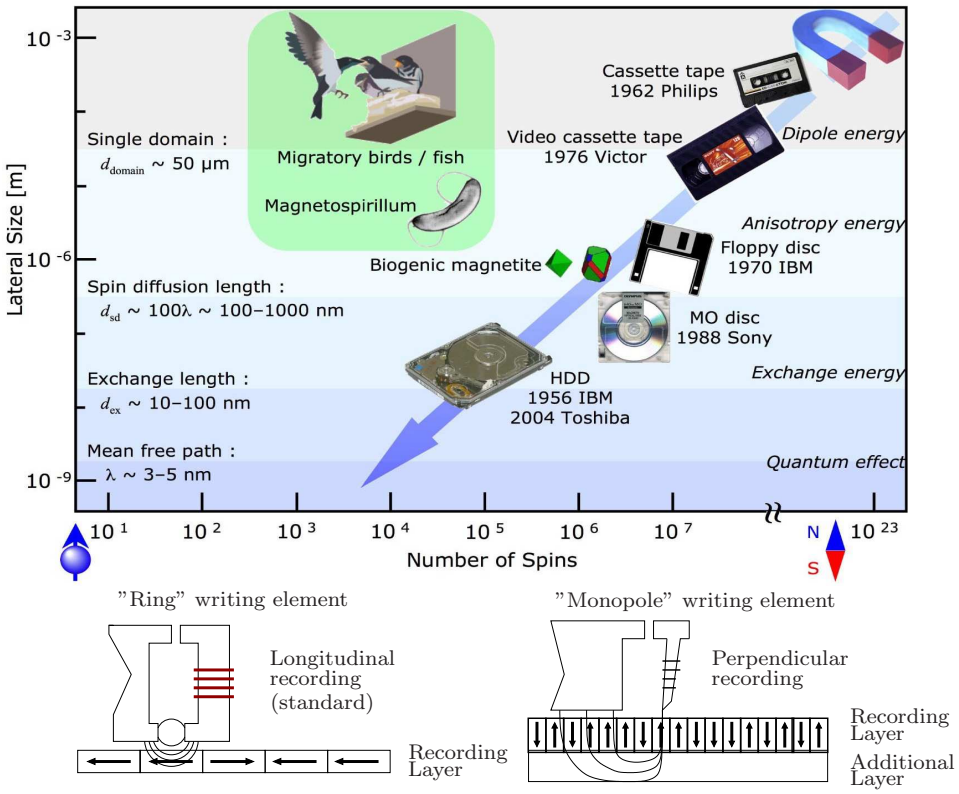

Figure 1.3: Typical length scales involved in the development of magnetic recording devices, taken from Hirohata & Takanashi [68]. Longitudinal recording and (improved) perpendicular recording, two types of writing heads on a hard disk, taken from *Wikipedia*.

Shun-ichi Iwasaki, then professor in Tohuku University in Japan, see also Iwasaki & Takemura [77, 78]. IBM Almaden Research Center in collaboration with researchers of Data Storage Systems Center- a National Science Foundation Engineering Research Center at Carnegie Mellon University, made the first industry-standard demonstration in 1998. The first commercially successful implementation was in 2005. Clearly macroscopic models (for applications lying in the upper-right part of the graph in Figure 1.3) are not adequate since finer resolution is required for applications operating at smaller scales. Thus continuum modeling approaches need to be adapted for different length scales.

Of late, there is a lot of interest in materials that display a (thermo-) electro-magneto-mechanical coupled character. There are a variety of such materials in focus with the prime emphasis today being on *multiferroics*. Often, these materials are constructed by combining materials that are individually uncoupled (or weakly coupled). The composite however has the desired coupled character. This motivates many researchers to explore homogenization methods by simulating the microstructure under different loading conditions. The homogenization process is used for bridging the scales but there is plenty of work to be done in providing models at the individual scales. Thus, homogenization leaves two aspects to be take care of. Firstly, the requirement for accurate microscale models (of the single phases), and secondly the macroscopic phenomenological models at a higher scale (which use the results of homogenization in order to simulate life-size components). We do not deal with homogenization here but address the other two aspects via the chosen materials to be modeled. While the modeling of ferromagnetic domain structures

Figure 1.4: Magnetorheological elastomers find use in hte automotive industry as actuators and variable stiffness devices. It is used as an active component in a magnetic valve (Fraunhofer ISC) and as a variable suspension device in cars (Ford Motor Company). According to Martin [108] these materials are also a candidate for artificial muscles.

addresses the first requirement, the modeling of magnetorheological elastomers shows the construction of micromechanically sound models for large bodies, thus addressing the second concern. To summarize, magnetic materials and hence magnetomechanically coupled computational models are developed for the following purposes (adapted from Venkataraman [162]):

- *Magnetostrictive sensors and actuators:* Magnetostrictive materials change show changes in dimension upon changing the magnetization state. Conversely, if a force is applied on them, the magnetization changes. This property is harnessed in application of actuators and sensors. The magnetostrictive effect observed in pure metals like Cobalt, Iron etc. is of the order of a few microstrains and room temperature. By alloying the metals, a giant magnetostrictive response is obtained. For example, Terfenol-D , Galfenol (Ga_xFe_{1-x} with $0.1 < x < 0.4$), Cobalt-Iron-Oxide ($CoFe_2O_4$) and Nickel-Iron-Oxide ($NiFe_2O_4$) which show mechanical deformations of the order of a couple of hundreds to thousands of microstrains induced by the application of magnetic fields, see Piratla [127].

- *Variable stiffness devices:* Magnetorheological elastomers were developed by laboratories in the automotive industry like the Ford Co., Toyota and Lord Co. as variable stiffness devices. These materials are now available in a variety of different compositions and microstructures but are actively optimized and developed in academia and industry. MREs are easily manufactured and their uses are in Figure 1.4. The variation in stiffness due to magnetization is sometimes referred to as the ΔE effect.

- *Magnetic recording in hard disk drives:* In magnetic recording media, each bit (0 or 1) stored, is a region with a single domain state. These may be altered by a magnetic field applied by the recording head. Thus the stability of these domain states is essential for the longevity of any recording medium. Various factors like constitution of layers in the recording medium, thickness of the layers, grain size and magnitude of external field have an influence here For an account on magnetic recording, one may refer to the book by Spaldin [147] and Bertram [8].

- *Paleomagnetism:* Naturally occurring magnetite grains act as carriers of paleomagnetic information. The natural remnant magnetization is an indicator of earth's magnetic field in the past. This field calls for an understanding of not only rock-composition, but also of magnetization structures.

1.2. State of the Art

Research on magnetomechanically coupled materials has its beginnings in the discovery of the effect in Joule [84, 85], after which a number of derived magnetomechanical effects were identified, see Lee [101] for a compact review. For the physical theory the work by Bozorth [14, 15] is of immense value as well as those of Kittel [91] and Cullity [28]. With regard to to theoretical formulations for continuum (electro-)magneto-mechanics, some of the major contributors are Toupin [156], Brown [17, 18, 21] and Tiersten [152, 153]. In what follows, we briefly look at the developments in micro-magneto-elasticity and magnetorheological elastomers separately. Although several areas of overlap are expected, this treatment allows us to highlight the individual character of each of the topics.

1.2.1. Micro-Magneto-Mechanics of Ferromagnetic Materials

The phenomenon of ferromagnetism in solids is characterized on the macroscopic level by a local magnetization that remains even after a complete withdrawal of the applied magnetic field and the stresses. At the microscale level, ferromagnetic materials are composed of several homogeneously magnetized regions, called *magnetic domains*, whose evolution in time is driven by external magnetic fields and stresses applied to a sample of the material. This causes the characteristic 'butterfly' field-induced strain and ferromagnetic hysteresis curves on the macroscale. It is this property of *dissipative magnetostriction*, that ferromagnetic materials exhibit a magneto-mechanical coupled response and hence find use as the active components in sensors and actuators. Some examples of this class of materials are Terfenol-D ($Tb_{1-x}Dy_xFe_2$), Cobalt-Iron-Oxide ($CoFe_2O_4$) and Nickel-Iron-Oxide ($NiFe_2O_4$) which show mechanical deformations induced by the application of magnetic fields. Elementary effects and the modeling ideas for ferromagnetic materials are described in Kittel [92], Cullity [28] and Spaldin [147]. Recent interest focuses on the construction of new, so-called *multiferroic composites* with strong magnetic-electric (ME) coupling, see for example Fiebig [58], Eerenstein, Mathur & Scott [49] or Nan et al. [124]. The macroscopic properties of ferromagnetic materials are determined through the evolution of the domain walls and the rotation of the magnetic moment between the *easy axes* under the application of external magnetic field and stresses. These time dependent changes are dissipative in nature and therefore result in magnetic hysteresis that is typically observed at the macroscale. The description of these effects through numerical models of continuum physics is a subject of present research and may broadly be classified into two categories namely, phenomenological macro-modeling approaches that do not resolve the magnetic domains and micromagnetics that involves the explicit characterization of the domain walls. For *macroscopic models* that describe the dissipative effects in ferromagnetic materials based on the concept of internal variables, the reader is directed to magnetostrictive models that are described in the works Smith, Dapino & Seelecke [145], Linnemann, Klinkel & Wagner [104] and Miehe, Kiefer & Rosato [119]. The work Miehe, Rosato & Kiefer [120] considers a dissipative model for multiferroic composites.

In order to improve the predictive quality of such macroscale models and to have a better understanding of the underlying micromechanical driving forces, a greater emphasis on the construction of micro-mechanically motivated experiments as well as microscale models is called for. The development of such models started with the seminal work of Landau & Lifschitz [100], where the fundamentals of the so-called *domain theory* of magnetization in rigid bodies as a consequence of energy minimization have been laid. In

the 1960s, Brown [20, 21] laid the basis of the theory of *micromagnetics*, which is based on variational principles. The essential difference between domain theory and micromagnetics is that the former assumes a certain structure of the domains a priori and proceeds by optimizing this assumed structure with respect to the energy, while the latter delivers an optimum microstructure directly by solving the micromagnetic equations. Here, traditional approaches are restricted to the description of ferromagnetic effects in rigid bodies and neglect magneto-mechanical coupling. The magnetization vector

$$\boldsymbol{M} = m_s \boldsymbol{m} \quad \text{with} \quad \boldsymbol{m} \in \mathcal{S}^{d-1} \tag{1.1}$$

is introduced as a continuum field variable, which describes the continuous evolution of the magnetization on a microscale. The saturation magnetization m_s is taken as a constant, or more precisely, only temperature dependent. The underlying geometric structure of the magnetization director $\boldsymbol{m}$ in (1.1), where $\mathcal{S}^{d-1}$ denotes the hypersphere in the $\mathcal{R}^d$, constitutes the essential difference with respect to the microelectric problems (e.g. phase-field models for ferroelectric domains in Zhang & Bhattacharya [168], Schrade, Müller, Xu & Gross [138] and Miehe, Zäh & Rosato[121]) that employ a polarization vector as the order parameter which has no constraint on its magnitude. This so-called Heisenberg-Weiss relation create a special demand on the theoretical formulations and in particular, their numerical implementation. The foundations of the ferromagnetic domains in literature is well developed. We refer to the classic overview provided by Kittel [92] and a more recent outlook in Hubert & Schäfer [72]. When ignoring for a moment the magneto-mechanical coupling effects, the domain theory for *rigid bodies* is based on the Landau-Lifschitz energy functional

$$E(\boldsymbol{m}) = \int_{\mathcal{B}} \left[\frac{\alpha}{2} |\nabla \boldsymbol{m}|^2 + \varphi(\boldsymbol{m}) - m_s \boldsymbol{m} \cdot \boldsymbol{h} \right] dV + \frac{\kappa}{2} \int_{\mathcal{R}^3} |\nabla \phi|^2 \, dV \ , \tag{1.2}$$

the minimization of which, for a given external magnetic field $\boldsymbol{h}$, gives the shape of the magnetic domain. Here, the functional is valid along with the additional constraint $\mathrm{div}[m_s \boldsymbol{m} - \nabla \phi] = 0$, i.e. the third Maxwell equation, where for a given magnetization $\boldsymbol{m}$, ϕ is the corresponding magnetic potential. The contributions to the free energy comprise the gradient term, the non-convex term $\varphi(\boldsymbol{m})$, whose energy landscape characterizes the easy axes of magnetization, and finally, the magnetostatic part. The central problem in the solution of such *equilibrium theories* is the presence of the non-convex energy term φ. This applies equally to micro-magneto-elastic theories, where we additionally have elastic and magnetostrictive terms in the free energy, see Kittel [92] and Hubert & Schäfer [72]. This is the motivation behind considering *relaxation methods* for the solution of non-convex variational problems which are dealt with, in the works of James & Kinderlehrer [80], DeSimone [32] and DeSimone & James [33]. Here, laminate-type structures are adopted to characterize the magnetic microstructure. Further, in a 'large body limit,' the gradient term in (1.2) and thus the boundary of the microstructure is neglected ($\alpha = 0$). Relaxation methods for rigid ferromagnetic materials are described in DeSimone et al. [34]. Formulations that include elastic couplings are outlined in the work DeSimone & James [33]. Numerical algorithms for implementation in non-convex variational problems are found in Prohl [129] as well as Kruzik & Prohl [95]. In contrast, classical approaches to *dynamic theories* of domain evolution consider the celebrated Landau-Lifschitz-Gilbert Equation (LLG, see Gilbert [63]), which describes

a) 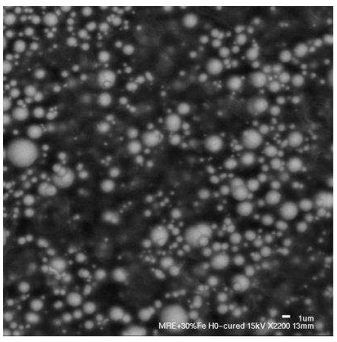 b) 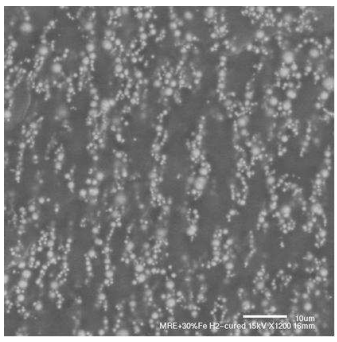

Figure 1.5: Scanning electron microscope (SEM) pictures of microstructure of MRE-iron particles in silicone M4601 matrix, Kallio [87]. a) Isotropic or random distribution of iron particles in polymer matrix and b) iron particles aligned in a preferred direction (transversally anisotropic).

the temporal evolution of the magnetization. This equation characterizes a phase-field that is consistent with the geometric constraint $(1.1)_2$. Micro-magneto-elastic theories with domain evolution based on the LLG are found in Zhang & Chen [166, 167], as well as the recent descriptions on the magneto-electric effects in multiferroic materials are in Li et al. [103]. Brown [20] presents a principle of virtual work for micromagnetics. It also covers briefly the treatment of dissipation with a Rayleigh-type functional that yields the LLG equation, as well as the topic of magnetostriction.

Literature does however appear to be lacking geometrically consistent Finite Element frameworks arising from variational principles of an incremental dissipative nature, where the LLG equation arises as an Euler equation. This motivates the extension of the incremental variational principles for macro-magneto-mechanical problems with *locally* evolving internal variables proposed in Miehe, Kiefer & Rosato [119], towards *gradient-extended* dissipative structures with *balance-type* evolution equations for order parameters which describe the magnetization. Furthermore, the algorithmic implementation of the LLG equation involving the space- and time-discretization that is consistent with the geometric structure of the magnetization director field is particularly challenging. This has led to the implementation of projection techniques or different norm preserving numerical methods, in order to have the discretized problem capture the aforementioned geometric structure. Weinan & Wang [163], Prohl [129] and Kruzik & Prohl [95] present some solutions. In Lewis & Nigam [102] aspects of the geometrical integration on spherical manifolds is considered with a particular emphasis on micromagnetic problems. A consistent and descriptive numerical treatment within the framework of finite elements is however, not given. The problem of satisfying the constraint $(1.1)_2$ bears a striking resemblance to the geometrically exact descriptions of finite deformation of shell structures with inextensible directors as described in Simó, Fox & Rifai [142].

1.2.2. Finite Deformation Magneto-Mechanics of MREs

MREs (magnetorheological elastomers) are a class of solids that consist of rubber matrix embedded with micro- or nano-sized magnetizable particles such as iron. MREs may be classified into two categories on the basis of the arrangement of the magnetizable particles in the polymeric matrix namely, *i*) isotropic and *ii*) anisotropic. Isotropic MREs have the magnetizable particles uniformly distributed throughout the matrix while anisotropic MREs have these particles aligned along a particular direction, see Figure 1.5. Such an

arrangement is brought about by applying a magnetic field during the curing process such that the particles form chain like structures in that direction. As a result of this specific *composite* nature, the shape and mechanical properties of these materials can be varied by the application of magnetic fields. This fact gives a wide scope for the exploitation of such materials in industry as actuators and tunable stiffness components. It is therefore of great interest to be able to reliably model or predict the properties of such materials by constitutive equations and present the solution and analysis of representative boundary value problems. Also, since deformations of elastomers are typically large, there is an added need to develop the constitutive theory in a *finite strain context*.

Although exchange effects are neglected, the main challenge still appears to be the *construction of accurate material models* that capture the coupled response of the MRE, see concluding remarks in Salas & Bustamante [133]. This appears to be a serious challenge in part due to the paucity of experimental data in literature, and partly due to the lack of a consensus on the the choice of magnetic variables employed for the continuum modeling framework. While there appears to be a steady increase in experimental data available over the last decade, the difference on continuum formulations seems to be a more recent occurrence (relevant works are cited below). Some appear to prefer to choose the magnetization while others prefer to avoid it. This lack of consensus sometimes makes the interpretation of experimental results ambiguous. Experimental work and simple one dimensional models for isotropic and anisotropic MREs have been presented in Jolly et al. [83], Davis [31], Bellan & Bossis [6], and Varga, Filipcsei & Zrínyi [160, 161]. These contributions focus on estimating the change in shear modulus of the material motivated by ab initio calculations for magnetic dipole-dipole interaction and experiment. Bednarek [5] captures magnetostriction of MREs and presents detailed micromechanical explanations for elastic and inelastic regimes. The dissertation by Kallio [87] covers preparation and characterization of MREs with valuable data on static and dynamic properties. The work by Diguet [36] addresses additionally, micromechanically-based modeling aspects and considers the shape effect in detail, among other aspects. Both works provide valuable data and hints for continuum approaches of the type presented here.

The works on continuum formulations in electro-mechanics are also of relevance here. Toupin's work on the elastic dielectric [156] presents an unconstrained variational formulation for electromechanics and is probably the most relevant in this field. Brown's contributions [17, 18, 21] are also fundamental. Other important contributions are by Tiersten [152, 154, 155] and Maugin & Eringen [110], Maugin [109]. These works form the fundamentals for more recent work on magnetomechanically coupled finite deformation. The work Kankanala & Triantafyllidis [88, 89] presents a *three-field* unconstrained minimization variational approach with a view to examine stability issues. They also present material models for isotropic MREs. The framework is used by Danas, Kankanala & Triantafyllidis [30] which focusses on anisotropic response of MREs. Micromechanics of anisotropic MREs are suggested and the presented material model is fitted carefully with experimental results. Danas & Triantafyllidis [29] then focus on identifying bifurcation points of anisotropic MREs under loading which, are important for applications in haptic technology. We also mention the contributions by Ericksen [51, 50, 52] which comment on the existing continuum electro-magneto-mechanical formulations without focusing on MREs. Dorfmann et al. [16, 42, 43, 44, 45, 46, 23] also model MREs but differ from the previously mentioned approaches in that they do not

use the magnetization as a primary variable and consequently do not consider "applied" and "self" fields separately. Thus they work with a *two-field-formulation*. The works Steigmann [148] and Bustamante et al. [24] compare some of these different existing approaches. In line with remarks of Bustamante et al. [24] and from our experience in [54, 57] formulations following this approach appear to be simpler but might obscure the micromechanics behind the proposed material models in the process. In any case, Saxena, Hossain & Steinmann [135, 136] use these approaches and consider anisotropy and viscoelasticity. We also mention closely related works on some aspects common to those covered in the presented approach. Ask, Menzel & Ristinmma [3, 4] deal with phenomenological approaches to modeling electrostriction and electro-viscoelasticity in the finite strain regime. Sansour et al. [134] have proposed the multiplicative split for the deformation gradient for materials with electromechanical coupling. Thylander, Menzel & Ristinmaa [151] use the microsphere model for electro-active-polymers. Within the microsphere approach one method of dealing with anisotropy is given in Menzel & Waffenschmidt [111].

Some other approaches to modeling MREs are also mentioned here. Borcea & Bruno [9] consider pair-wise interaction of magnetic dipoles to obtain constitutive relations that are exact to second-order in the volume-fraction of the particles. They assume however that the particles are single-domains and hence saturated. This could be true for the particle-sizes that they mention, but does not always have to be the case. Ivaneyko et al. [74, 75, 76] consider ab initio calculations taking dipole-dipole interaction energy for different particle arrangements thus giving an insight into micromechanics of MREs. Ponte Castañeda & Galipeau [128] and Galipeau & Ponte Castañeda [60] use a homogenization approach to model the constitutive response for magnetorheological elastomers at finite strain. Similarly Steinmann et al. [82, 27] also present approaches to the problem via homogenization.

Miehe et al. [119, 120] propose variational frameworks for small strain magneto-electro-elasticity with dissipative response that is suitable for computational implementation but literature on variational-based finite element simulations of finite-sized MREs in the large strain regime appears to be scant. Moreover, there is no clear framework for the construction of free-energy functions for such formulations. This work aims to fill this gap with a focus on computational implementation. Although we focus on the isotropic category of MREs anisotropy is expected to fit easily in the presented framework with minor modifications. It is also shown how viscous effects may be accounted for within this framework.

1.3. Objectives and Outline

With the above mentioned literature as background, we state our objectives in the two categories of interest and then outline the structure of this work.

1.3.1. Geometrical Aspects in Computational Micro-Magneto-Mechanics

Here, the *construction of geometrically exact, variational-based numerical models for the dynamic (or quasi-static) temporal evolution of magnetic domains in ferromagnetic and magnetostrictive materials* is the key focus of this work. The challenge on the theoretical side is the formulation of a *variational principle* in terms of the rates of the primary variables of the multi-field problem of micro-magneto-elasticity which, among other things,

returns a Landau-Lifschitz-Gilbert-type evolution equation for the magnetization as an Euler equation. On the computational side, the key challenge is the construction of a new space- and time-discrete *algorithmic procedure* for micromagnetic problems that preserves the geometric properties of the magnetization director.

We propose a geometrically exact finite element method for micro-magneto-elasticity that accounts for the rotational nature of the magnetization director. Our work is inspired by Lewis & Nigam [102] on geometric integration on spheres with application to micromagnetics, and also by the sequence of works by Simó and coworkers [141, 142] on geometrically exact shell models that account for an exact rotational treatment of the shell directors. These ideas on the parametrization of rotations and their consistent implementation into time-space-discrete finite element methods serve as guideline for the construction of geometrically exact numerical methods in micromagnetics. In our proposed formulation, we consider the magnetization director as a geometric object, that is treated appropriately. With that guideline at hand, we outline a computational scenario for the evolution of magnetic domains that is characterized by the following three ingredients:

- *Variational nature:* Variational principles for the coupled evolution problem of dissipative micro-magneto-elasticity, in the continuous as well as the time-discrete setting.
- *Non-standard BVPs:* Embedding of solids with evolving magnetic domains, loaded by consistently homogenized magnetic fields and stresses, into the free space.
- *Geometrically exact nodal updates:* Symmetric FE solver with exact rotational updates of the magnetization directors at the nodes of the finite element mesh.

While those are the main objectives, we also consider an alternative computational method based on an operator split which may be considered as an approximation to the previous method but easier to implement. In presenting this method we also make a comparison of the two approaches.

1.3.2. Micromechanically Based Modular Approach for Modeling of MREs

With the mentioned literature as background, we aim to fill in what is missing, namely *a three-field variational-based finite element implementation with the of coupled finite deformation magnetoelasticity with the magnetization and magnetic scalar potential* that is suited for modeling MREs and *a framework for the modular construction of magnetorheological elastomers that is motivated from micromechanics*. For the first case, we have addressed the elastic and viscoelastic cases. The approach is similar to the classical work Toupin [156] on the elastic dielectric and also contrasted with the work on MREs by Kankanala & Triantafyllidis [88, 89] that uses a vector potential formulation. As opposed to the work here, both cited works do not present any finite element simulations. Here, a three-field formulation in terms of the deformation map $\boldsymbol{\varphi}$, magnetization (per unit mass) $\boldsymbol{\mu}$ and magnetic scalar potential $\widetilde{\phi}$ of the self-field is presented. In a similar manner to Miehe & Ethiraj [115], we begin with constructing the required functionals. Of foremost importance is the energy enthalpy functional, of finite deformation magnetoelasticity. The loading contributions are taken in terms of the applied magnetic field and the mechanical body forces and tractions are taken as "dead" loads. With these

functionals at hand, we construct the variational principle for finite deformation magnetoelasticity. The Euler equations of the variational principle are the balance of linear momentum, Gauss' Law for magnetism, the (time-discrete) Biot equation for the evolution of the internal variables and a local equation relating the magnetic field with the magnetization.

The material modeling approach is directly motivated by considering the existing magnetomechanical interactions on the microscale of such composite materials. that allows to include all of possible network models in a modular format. Conceptually, this is achieved by assuming a split of the energy function into an *elastic contribution* and an *magnetostatic part*

$$\Psi(\boldsymbol{F}, \boldsymbol{\mu}) = \Psi_{mec}(\boldsymbol{F}, \boldsymbol{\mu}) + \Psi_{mag}(\boldsymbol{\mu}) \ , \tag{1.3}$$

where $\boldsymbol{F} = \nabla\boldsymbol{\varphi}$ is the deformation gradient and $\boldsymbol{\mu}$ is the Eulerian magnetization per unit mass. The two contributions account for the two micromechanical ingredients mentioned above. The first part will be designed to include the *mechanical network model*, while the second part covers the *pure magnetic energy* which is the energy possessed by virtue of the magnetization of the body alone. A key aspect of this work is a modeling of the elastic contribution based on a kinematic assumption for the *macroscopic* network deformation

$$\Psi_{mec}(\boldsymbol{F}, \boldsymbol{\mu}) = \Psi_{net}(\boldsymbol{F}_{net}) \quad \text{with} \quad \boldsymbol{F}_{net} = \boldsymbol{\mathcal{E}}\boldsymbol{F} \tag{1.4}$$

which includes a left (Clifton-type) *multiplicative decomposition* of the deformation gradient into *stress free* and *stress producing parts*. Here, $\boldsymbol{\mathcal{E}}^{-1}$ is an magnetically induced stretch tensor that depends on the *Eulerian magnetization per unit mass*. The above ansatz allows for the incorporation of energy functions Ψ_{net} associated with complex mechanical network models *without any change*. The objective in this part of the the work is thus to present a robust computational (FEM) framework with the following features

- *Variational nature:* Variational principles for the coupled problem of finite deformation magneto-(visco-)elasticity, in the continuous as well as the time-discrete setting.
- *Non-standard BVPs:* Simulations of large deformations and rotations of macro-sized bodies under applied magnetic and mechanical loads as well as accounting for the surrounding free space.
- *Modular framework for constructing free energy functions:* A multiplicative split of the deformation gradient allows us to capture the coupled response and use a variety of existing models including statistically-based kernels.

1.3.3. Outline of the Work

The work is organized as follows. Chapter 2 introduces the fundamental variables and equations of continuum magnetostatics. Our approach here is in line with modern approaches of electromagnetic theory which rely on the acceptance of the *Maxwell-Bateman laws* namely, the *conservation of charge* and *conservation of magnetic flux* as a starting point. We then postulate the *aether relations* and obtain the necessary equations and boundary conditions of magnetostatics.

Chapter 3 outlines the fundamentals of continuum magnetomechanics. The purpose of the chapter is to introduce the mechanical variables involved in the used in rest of the thesis and the mapping properties of the magnetic and mechanical variables.

Chapter 4 presents a new *geometrical consistent finite element model for dissipative micromagnetics* which is shown to result from a geometrically exact rate-type variational principle. Details of the implementation are discussed and then numerical simulations of ferromagnetic bodies with evolving magnetic microstructure including a surrounding frees-space are presented.

Chapter 5 describes an alternative computational method for micro-magneto-elasticity that is based on an operator split. This uses a *robust staggered scheme* for solving for the primary variables and enables a straightforward extension into three dimensions. Numerical examples showing the capability of the approach are presented with a comparison to the geometrically exact method.

Chapter 6 deals with the *finite deformation magnetomechanics of magnetorheological elastomers*. The variational principle is discussed following which, we outline *a modular approach for the construction of free energy functions* for such materials. Some aspects of the computational finite element implementation are discussed and numerical results of finite deformation coupled problems are presented.

Chapter 7 deals with an extension of the framework of the previous chapter to *accommodate inelastic effects, such as viscoelasticity*.

Chapter 8 summarizes the work and gives some ideas for future work in the context of the approaches presented in the dissertation. Note that part of the work presented in this dissertation also appears in recently submitted publications Ethiraj et al. [56, 55].

2. Fundamentals of Magnetostatics

We now introduce the variables of magnetostatics. This is done by stating the balance laws and then by applying them consistently, we motivate the choice of variables. The presentation here is adapted from those of TRUESDELL & TOUPIN [159] and KOVETZ [94]. Here however, we deal with magnetostatics where we assume steady currents only and no electric field.

2.1. Governing Principles of Magnetostatics

2.1.1. First Principle of Magnetostatics: Conservation of Electric Charge

The law of conservation of charge means that charge cannot be created or destroyed. In order to derive a formal statement of the law, we assume an Euclidean space with a time and space dependent *charge density* ρ^e, see Figure 2.1. Consider a region of this space $\mathcal{P}$ which is bounded by $\partial\mathcal{P}$. Applying the law to $\mathcal{P}$, would mean that the rate of change of charge in $\mathcal{P}$ is equal to the net flux of charge into $\mathcal{P}$ through $\partial\mathcal{P}$. In order to write this formally, we introduce the vector $\mathbf{j}$ as the *current density* (charge per unit area per unit time) at the surface $\partial\mathcal{P}$ of the volume $\mathcal{P}$. Thus,

$$\frac{d}{dt}\int_{\mathcal{P}} \rho^e \, dv + \int_{\partial\mathcal{P}} \mathbf{j}\cdot\mathfrak{n} = 0 \; . \tag{2.1}$$

Using the divergence theorem we get the local form of (2.1) which is a *continuity equation*

$$\dot{\rho}^e + \operatorname{div}\mathbf{j} = 0 \quad \text{everywhere.} \tag{2.2}$$

Being in the magnetostatic regime, we consider steady currents only, i.e. there is no change in the net charge density anywhere in space or $\dot{\rho}^e = 0$ everywhere. This reduces the continuity equation to the local form of the first principle of magnetostatics

$$\boxed{\operatorname{div}\mathbf{j} = 0 \quad \text{everywhere}} \tag{2.3}$$

that is current density has no sources or sinks. As a corollary to (2.3), we can therefore assume that a *current potential* $\mathfrak{h}$ exists such that

$$\mathbf{j} = \operatorname{curl}\mathfrak{h} \; . \tag{2.4}$$

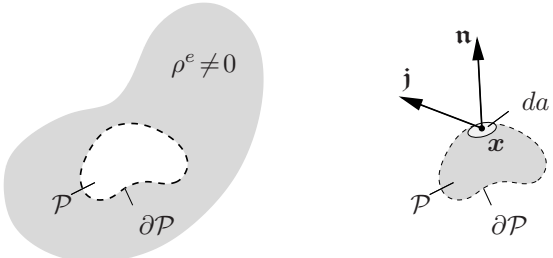

Figure 2.1: Conservation of electric charge applied to an *arbitrary control volume* $\mathcal{P}$. A time and space dependent *charge distribution* $\rho^e(\boldsymbol{x}, t)$ defines a *current density* $\mathbf{j}(\boldsymbol{x}, t)$. For magnetostatics, the time dependence is dropped.

2.1.2. Second Principle of Magnetostatics: Conservation of Magnetic Flux

The second principle introduces the vector field $\mathfrak{b}$ which we call the *magnetic induction* and it states that its flux through an arbitrary closed surface is zero. Sometimes, this principle is also stated as a consequence of the *absence of magnetic monopoles*. Under this concept, the field lines of $\boldsymbol{b}$ are said to originate from north poles and terminate on south poles. However, since monopoles do not actually exist, all lines of $\mathfrak{b}$ close upon each other or originate and terminate at infinity. Formally, for an arbitrary control volume $\mathcal{P}$,

$$\oint_{\partial\mathcal{P}} \mathfrak{b} \cdot \mathfrak{n}\, da = 0 \tag{2.5}$$

which, in the above form is also referred to the *Gauss' law of magnetism*. Using the divergence theorem and localization argument, we get the differential equation

$$\boxed{\operatorname{div} \mathfrak{b} = 0 \quad \text{everywhere}} \tag{2.6}$$

that is the magnetic flux has no sources or sinks. As a corollary to (2.6), we can therefore assume that a *magnetic vector potential* $\mathfrak{a}$ exists such that

$$\mathfrak{b} = \operatorname{curl} \mathfrak{a}\ . \tag{2.7}$$

2.1.3. Third Principle of Magnetostatics: Maxwell-Lorentz Aether Relation

The third principle of magnetostatics aims to connect the first two principles which until now, were independent of each other. It states that an Euclidean inertial frame exists in which the following relation holds at all times,

$$\boxed{\mathfrak{b} = \mu_0 \mathfrak{h}} \tag{2.8}$$

where μ_0 is a universal constant called the magnetic constant or the magnetic permeability of vacuum. In other words it postulates the existence of at least one frame, in which the magnetic induction $\mathfrak{b}$ is proportional to the current potential $\mathfrak{h}$. This principle is similar to the second law of mechanics that postulates the existence of at least one inertial frame in which force is proportional to acceleration. The value of μ_0 in SI units is $4\pi \times 10^{-7}$T-m/A.

2.2. Equations of Field-Matter Interactions in Magnetostatics

2.2.1. Field due to Prescribed Current Distribution

The problem reduces to the following equations by application of the three principles

$$\overline{\boldsymbol{j}} = \operatorname{curl} \overline{\boldsymbol{h}}\ , \qquad \overline{\boldsymbol{b}} = \operatorname{curl} \overline{\boldsymbol{a}}\ , \quad \text{and} \quad \overline{\boldsymbol{b}} = \mu_0 \overline{\boldsymbol{h}}\ . \tag{2.9}$$

Thus if we are given or if we solve for the vector potential $\overline{\boldsymbol{a}}$ satisfying

$$\mu_0 \overline{\boldsymbol{j}} = \operatorname{curl}(\operatorname{curl} \overline{\boldsymbol{a}}) \quad \text{in everywhere.} \tag{2.10}$$

we have the solution fields for the current distribution. For situations with a certain amount of symmetry, like those sketched in Figure 2.2, the above equations may be easily solved analytically, see also *Biot-Savart Law* in Stratton [149]. In the general, a numerical solution should be obtained, using a vector potential formulation. In any case, once the vector potential $\overline{\boldsymbol{a}}$ is known, the other associated fields can be derived from it. In this work we assume that $\overline{\boldsymbol{a}}$ (or equivalently $\overline{\boldsymbol{h}}$ or $\overline{\boldsymbol{b}}$) are known.

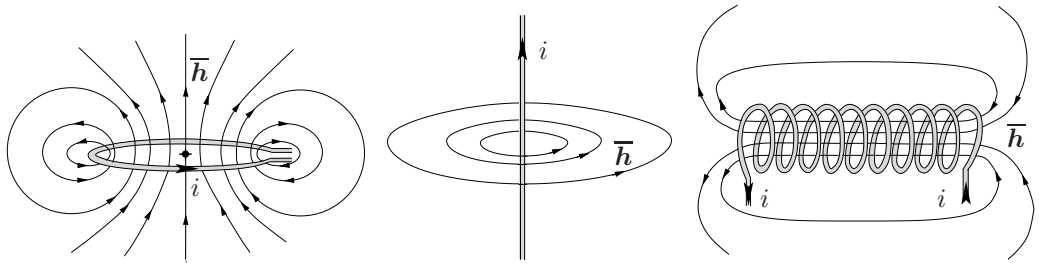

Figure 2.2: Some examples of prescribed current distributions and their associated field $\overline{\boldsymbol{h}}$, see STRATTON [149]: a) On the axis of a current carrying loop with radius R, at a distance z from the center, $\overline{\boldsymbol{h}}$ has the magnitude $\overline{h}_z^{axis}$. b) At some distance r away from a straight current carrying conductor, $\overline{\boldsymbol{h}}$ is circular with magnitude $\overline{h}_\theta^{out}$. c) At the center of an infinitely long solenoid, $\overline{\boldsymbol{h}}$ is uniform and has a magnitude $\overline{h}_z^{in}$.

2.2.2. A Magnetizable Body in the Vicinity of a Current Distribution

It is known that materials, in general, *respond* to magnetic fields by setting up currents and magnetic fields of their own. If $\widetilde{\boldsymbol{j}}$ denotes the *induced currents* on the body $\mathcal{S}$ due to the existing fields caused by the prescribed current distribution, then the application of the conservation of charge gives

$$\overline{\boldsymbol{j}} + \widetilde{\boldsymbol{j}} = \operatorname{curl} \boldsymbol{h}' \ . \tag{2.11}$$

According to the principle of superposition, the total magnetic flux is $\boldsymbol{b} = \widetilde{\boldsymbol{b}} + \overline{\boldsymbol{b}}$. Application of the conservation of magnetic flux, using $\operatorname{div} \overline{\boldsymbol{b}} = 0$ gives

$$\operatorname{div} \boldsymbol{b} = 0 \quad \Rightarrow \quad \operatorname{div} \widetilde{\boldsymbol{b}} = 0 \ . \tag{2.12}$$

The Maxwell-Lorentz aether relation implies

$$\boldsymbol{b} = \mu_0 \boldsymbol{h}' \ . \tag{2.13}$$

Since the total current $\overline{\boldsymbol{j}} + \widetilde{\boldsymbol{j}}$ must satisfy the continuity equation of magnetostatics, it is easily seen that $\operatorname{div} \widetilde{\boldsymbol{j}} \stackrel{!}{=} 0$. Thus, we introduce the *magnetization* $\boldsymbol{m}$ such that

$$\widetilde{\boldsymbol{j}} = \operatorname{curl} \boldsymbol{m} \ . \tag{2.14}$$

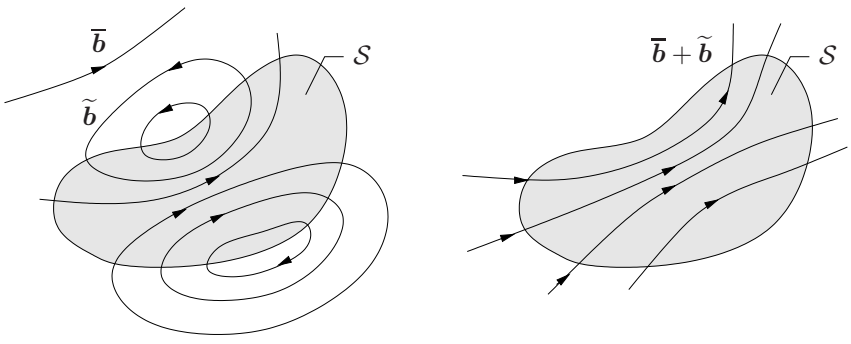

Figure 2.3: A magnetizable body placed in a field $\overline{\boldsymbol{b}}$ is gets magnetized and hence creates its own magnetic field $\widetilde{\boldsymbol{b}}$. The resultant field is shown in the figure on the right.

The magnetization $\boldsymbol{m}$ is dependent on the state of the material only and is obtained through a constitutive assumption. It is taken to be zero outside the body. Note that $\boldsymbol{m}$ is determined by the magnetization current $\widetilde{\boldsymbol{j}}$ *as well as* the prescribed fields. Its curl however is determined by the induced currents alone. By eliminating the current potential $\boldsymbol{h}'$, we can write the relation

$$\overline{\boldsymbol{j}} = \operatorname{curl}\left(\frac{\boldsymbol{b}}{\mu_0} - \boldsymbol{m}\right) . \tag{2.15}$$

This motivates the definition of the *magnetic field* vector $\boldsymbol{h}$ whose *curl depends on the prescribed currents only.* Therefore we introduce,

$$\boldsymbol{h} := \frac{\boldsymbol{b}}{\mu_0} - \boldsymbol{m} . \tag{2.16}$$

For our purposes we make one further simplification in order to eliminate all prescribed quantities from the expression. Using $\boldsymbol{b} = \widetilde{\boldsymbol{b}} + \overline{\boldsymbol{b}}$ and $\overline{\boldsymbol{b}} = \mu_0 \overline{\boldsymbol{h}}$ in (2.15), and using $(2.9)_1$,

$$\operatorname{curl}\left(\frac{\widetilde{\boldsymbol{b}}}{\mu_0} - \boldsymbol{m}\right) = \boldsymbol{0} \tag{2.17}$$

where we have identified the (magnetic) *self-field* of the body $\mathcal{S}$ as

$$\widetilde{\boldsymbol{h}} := \frac{\widetilde{\boldsymbol{b}}}{\mu_0} - \boldsymbol{m} . \tag{2.18}$$

Due to (2.17) and (2.18) we introduce a *magnetic scalar potential of the self-field* so that

$$\widetilde{\boldsymbol{h}} := -\nabla\widetilde{\phi} . \tag{2.19}$$

2.2.3. Global Forms and Jump Conditions

The differential equations of magnetostatics for a magnetically active body in the presence of a prescribed electric current distribution or field are

$$\operatorname{div}\widetilde{\boldsymbol{b}} = 0 \quad \text{and} \quad \operatorname{curl}\widetilde{\boldsymbol{h}} = \boldsymbol{0} . \tag{2.20}$$

These may be written in an integral form as

$$\oint_{\partial\mathcal{P}} \widetilde{\boldsymbol{b}} \cdot \boldsymbol{n}\, da = 0 \quad \text{and} \quad \oint_{\mathcal{C}} \widetilde{\boldsymbol{h}} \cdot d\boldsymbol{x} = 0 , \tag{2.21}$$

where $\mathcal{C}$ is a closed curve in space. Applying the above equations across the surface $\partial\mathcal{S}$ we obtain the "jump conditions" as

$$[\![\widetilde{\boldsymbol{b}}]\!] \cdot \boldsymbol{n} = 0 \quad \text{on } \partial\mathcal{S} \quad \text{and} \quad [\![\widetilde{\boldsymbol{h}}]\!] \times \boldsymbol{n} = \boldsymbol{0} \quad \text{on } \partial\mathcal{S} . \tag{2.22}$$

2.2.4. Units of Magnetic Field Variables

It follows from formula (2.14) that the vector $\boldsymbol{m}$ has the dimensions of the current per unit length. Hence, from (2.18) $\boldsymbol{m}$ and $\widetilde{\boldsymbol{h}}$ are measured in amperes per metre (A/m). Then, if the units of $\widetilde{\boldsymbol{b}}$ is taken to be Tesla, the unit of μ_0, is (T-m/A). The reader is referred to [2] and [22] for discussions on the topic of units of magnetic variables.

3. Fundamentals of Continuum Magneto-Mechanics

This chapter introduces the variables of coupled magnetomechanics from a continuum standpoint to consolidate the notation for the subsequent chapters. This content has been taken from the master thesis Ethiraj [54]. After a detailed look at the mechanical variables, we take a quick look at the mapping properties of the magnetostatic variables that were introduced in the previous chapter. Finally, for completeness, we state the balance laws of thermo-magneto-mechanics.

3.1. Geometrical Aspects of Finite Deformation Kinematics

3.1.1. Placement Map and Deformation Map

A *material body* B is mathematically defined as the open set of material points P, which can be identified with geometrical points in the three-dimensional Euclidean space $\mathbb{R}^3$ via the one-to-one *configuration placement map* $\boldsymbol{\chi}$. The *motion* of a body is the time-parameterized family of configurations

$$\boldsymbol{\chi}_t := \begin{cases} B \to \mathcal{S} \in \mathbb{R}^3 \ , \\ P \in B \mapsto \boldsymbol{x}_t = \boldsymbol{\chi}_t(P) \in \mathcal{S} \ . \end{cases} \tag{3.1}$$

This relation therefore describes the configuration of the body B in $\mathbb{R}^3$ at time t. In the *referential description of motion* one defines the *reference* or *Lagrangian configuration* as the placement of the body at time t_0, i.e. $\mathcal{B} := \boldsymbol{\chi}_{t_0}(B)$, with the *reference coordinates* $\boldsymbol{X} := \boldsymbol{\chi}_{t_0}(P) \in \mathcal{B}$. The *current* or *Eulerian configuration* at time t is defined as $\mathcal{S} := \boldsymbol{\chi}_t(B)$, with the *spatial coordinates* $\boldsymbol{x} := \boldsymbol{\chi}_t(P) \in \mathcal{S}$. The motion of the body with respect to the

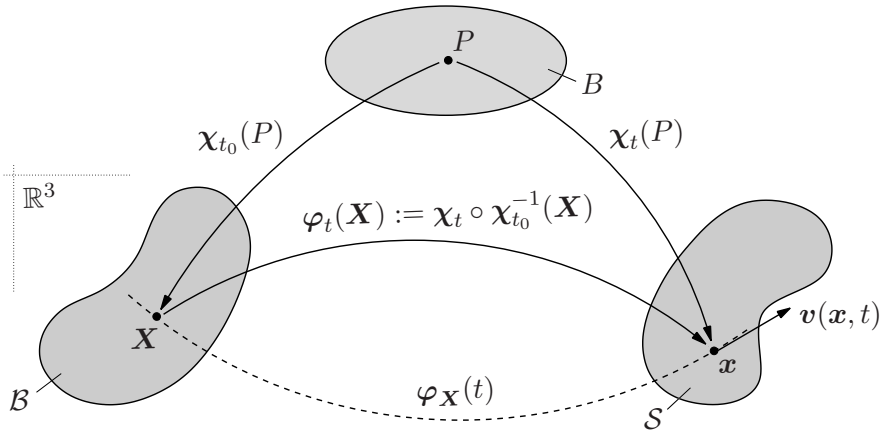

Figure 3.1: Identification of the position $\boldsymbol{X} \in \mathcal{B}$ of a particle $\boldsymbol{P} \in B$ in three-dimensional Euclidian space $\mathbb{R}^3$ through the configuration map $\boldsymbol{\chi}_t$ and description of the motion of a material point w.r.t the reference configuration via the deformation map $\boldsymbol{\varphi}_t$.

reference configuration is then defined by the nonlinear *deformation map*

$$\boldsymbol{\varphi} := \begin{cases} \mathcal{B} \times \mathbb{R}_+ \to \mathcal{S} \in \mathbb{R}^3 \ , \\ (\boldsymbol{X}, t) \mapsto \boldsymbol{x} = \boldsymbol{\varphi}(\boldsymbol{X}, t) = \boldsymbol{\varphi}_t(\boldsymbol{X}) \ , \end{cases} \tag{3.2}$$

which maps the material points $\boldsymbol{X} \in \mathcal{B}$ onto their deformed spatial positions $\boldsymbol{x} \in \mathcal{S}$ as shown in Figure 3.1.

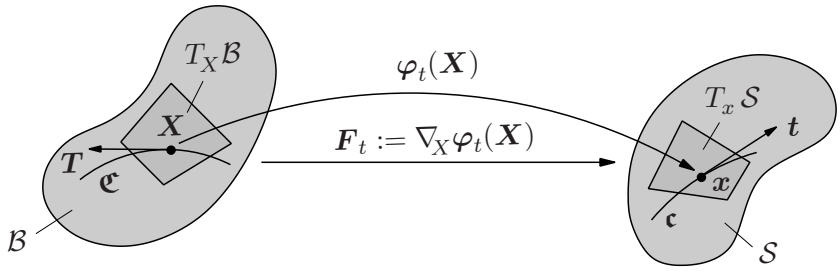

Figure 3.2: The deformation gradient acting as the linear tangent map, which transforms the material vector $\boldsymbol{T} \in T_X\mathcal{B}$, tangent to a material curve $\mathfrak{C}$ at $\boldsymbol{X}$, onto the associated spatial vector $\boldsymbol{t} \in T_x\,\mathcal{S}$, tangent to the material curve $\mathfrak{c}$ at $\boldsymbol{x}$.

3.1.2. Strain Measures and Mapping Properties

Mathematically, the *deformation gradient* $\boldsymbol{F}$ is defined as the Fréchet derivative of the deformation map, i.e. $\boldsymbol{F}_t(\boldsymbol{X}) := \operatorname{Grad} \boldsymbol{\varphi}_t$. Geometrically, the deformation gradient can be interpreted as the *linear tangent map* which maps tangents $\boldsymbol{T}$ to material curves, i.e. elements of the tangent spaces $T_X\mathcal{B}$ of the manifold $\mathcal{B}$, onto tangents $\boldsymbol{t}$ of the deformed material curves, i.e. elements of the tangent space $T_x\,\mathcal{S}$ of the manifold $\mathcal{S}$, according to

$$\boldsymbol{F}_t := \begin{cases} T_X\mathcal{B} \to T_x\,\mathcal{S} \ , \\ \boldsymbol{T} \mapsto \boldsymbol{t} = \boldsymbol{F}_t\boldsymbol{T} \ , \end{cases} \tag{3.3}$$

as visualized in Figure 3.2. Note that, since $\boldsymbol{\varphi}_t$ is a one-to-one mapping and must prohibit material interpenetration, the deformation gradient is subject to the following constraints $J := \det \boldsymbol{F} > 0$. The determinant of the deformation gradient can further directly be interpreted as another fundamental mapping, the *volume map*, which relates infinitesimal reference volume elements dv to their deformed spatial counterparts dV via the relation

$$J = \det \boldsymbol{F} := \begin{cases} \mathbb{R}_+ \to \mathbb{R}_+ \ , \\ dV \mapsto dv = \det \boldsymbol{F}\, dV \ . \end{cases} \tag{3.4}$$

The *co-factor* of the deformation gradient $\operatorname{cof} \boldsymbol{F}$ is defined as the derivative of the volume map with respect to $\boldsymbol{F}$. It can geometrically be interpreted as the *area map*, which maps infinitesimal reference area elements onto the associated spatial ones via the relation $\boldsymbol{n}\, da = J\boldsymbol{F}^{-T}\boldsymbol{N}\, dA = (\operatorname{cof} \boldsymbol{F})\boldsymbol{N}\, dA$, also known as *Nanson's formula*. Moreover, $\boldsymbol{F}^{-T}$ can thus be identified as the *normal map*, that maps normals of material surfaces, or, again from the differential geometry view point, elements of the co-tangent space $T_X^*\mathcal{B}$, onto normals of the deformed spatial surfaces, i.e. elements of the co-tangent space $T_x^*\mathcal{S}$. Therefore, if we have $\tilde{\boldsymbol{n}} = J\boldsymbol{n}$, we may write

$$\boldsymbol{F}^{-T} := \begin{cases} T_X^*\mathcal{B} \to T_x^*\mathcal{S} \ , \\ \boldsymbol{N} \mapsto \tilde{\boldsymbol{n}} = \boldsymbol{F}^{-T}\boldsymbol{N} \ . \end{cases} \tag{3.5}$$

For the specification of coordinate representations one introduces the Cartesian frames $\{\boldsymbol{E}_i\}$ for $T_X\mathcal{B}$, $\{\boldsymbol{E}^i\}$ for $T_X^*\mathcal{B}$, $\{\boldsymbol{e}_i\}$ for $T_x\,\mathcal{S}$ and $\{\boldsymbol{e}^i\}$ for $T_x^*\mathcal{S}$. Capital letter indices $i = \{A, B, C\}$ are used for Lagrangian and lower case indices $i = \{a, b, c\}$ for Eulerian

settings.[3] The reference and spatial coordinates are thus expressed as $\boldsymbol{X} = X^A \boldsymbol{E}_A$ and $\boldsymbol{x} = x^a \boldsymbol{e}_a$. The deformation gradient then admits the representation $\boldsymbol{F} = F^a{}_A \boldsymbol{e}_a \otimes \boldsymbol{E}^A$, with $F^a{}_A = \partial \varphi^a / \partial X^A$. Likewise, the component forms of the mappings (3.3) and (3.5) read $t^a = F^a{}_A T^A$ and $n_a = (F^{-1})^A{}_a N_A$.

In order to be able to measure geometric quantities such as the length of vectors, however, one must additionally introduce *metric tensors*. In global Cartesian frames the *covariant* and *contravariant Lagrangian metric tensors* admit the reduced representation $\boldsymbol{G} = \delta_{AB} \boldsymbol{E}^A \otimes \boldsymbol{E}^B$ and $\boldsymbol{G}^{-1} = \delta^{AB} \boldsymbol{E}_A \otimes \boldsymbol{E}_B$, where δ_{AB} and δ^{AB} are Kronecker deltas. Similarly, the *covariant* and *contravariant Eulerian metric tensors* reduce to $\boldsymbol{g} = \delta_{ab} \boldsymbol{e}^a \otimes \boldsymbol{e}^b$ and $\boldsymbol{g}^{-1} = \delta^{ab} \boldsymbol{e}_a \otimes \boldsymbol{e}_b$, respectively. The metric tensors represent mappings of vectors, i.e. elements of the tangent spaces, onto normals (co-vectors), i.e. elements of the co-tangent spaces. For the Lagrangian and the Eulerian manifolds these mappings are defined by

$$\boldsymbol{G} := \begin{cases} T_X \mathcal{B} \to T_X^* \mathcal{B} \ , \\ \boldsymbol{T} \mapsto \boldsymbol{N} = \boldsymbol{G}\boldsymbol{T} \ , \end{cases} \qquad \boldsymbol{g} := \begin{cases} T_x \mathcal{S} \to T_x^* \mathcal{S} \ , \\ \boldsymbol{t} \mapsto \boldsymbol{n} = \boldsymbol{g}\boldsymbol{t} \ . \end{cases} \tag{3.6}$$

These mappings can also be interpreted as *index lowering* or *raising procedures* since the coordinate representations of (3.6) read $N_A = G_{AB} T^B = \delta_{AB} T^B$ and $n_a = g_{ab} t^b = \delta_{ab} t^b$, respectively. It is

Commutative diagrams, such as the ones displayed in Figure 3.3, significantly facilitate the geometric meaning of the introduced mappings. Based on the definitions of the mappings

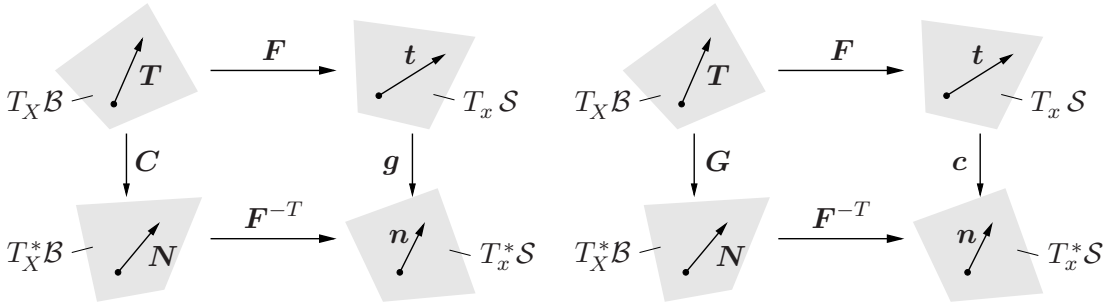

Figure 3.3: Commutative diagram illustrating the *'push-forward'* and *'pull-back'* of the covariant reference metric $\boldsymbol{G}$ and spatial metric $\boldsymbol{g}$.

(3.3), (3.5), (3.6) and their respective inverse mappings, one can introduce additional deformation measures. The *right Cauchy-Green tensor* $\boldsymbol{C}$ can in this context be defined as the *'pull-back'* of the spatial metric

$$\boldsymbol{C} := \boldsymbol{\varphi}^*(\boldsymbol{g}) = \boldsymbol{F}^T \boldsymbol{g} \boldsymbol{F} \ , \qquad \text{or} \qquad C_{AB} = F^a{}_A g_{ab} F^b{}_B \ , \tag{3.7}$$

in coordinate representation, and can thus be interpreted as the 'representation of the current metric in the Lagrangian setting' or 'convected spatial metric'. Similarly, the *inverse right Cauchy-Green tensor* $\boldsymbol{C}^{-1}$ is defined as

$$\boldsymbol{C}^{-1} := \boldsymbol{\varphi}^*(\boldsymbol{g}^{-1}) = \boldsymbol{F}^{-1} \boldsymbol{g}^{-1} \boldsymbol{F}^{-T} \ , \qquad \text{or} \qquad \big(C^{-1}\big)^{AB} = \big(F^{-1}\big)^A{}_a g^{ab} \big(F^{-1}\big)^B{}_b \ . \tag{3.8}$$

[3] Note that these frames will typically coincide, but they have formally been considered here for the sake of clarity.

Accordingly, via appropriate *'push-forward'* operations, one defines the *left Cauchy-Green tensor* $\boldsymbol{b}^f$, often called the *Finger tensor*, and the *inverse left Cauchy-Green tensor* $\boldsymbol{c}$, respectively, as

$$\boldsymbol{b}^f := \boldsymbol{\varphi}_* \left(\boldsymbol{G}^{-1}\right) = \boldsymbol{F}\boldsymbol{G}^{-1}\boldsymbol{F}^T \ , \qquad \text{or} \qquad b^{ab} = F^a{}_A G^{AB} F^b{}_B \ , \tag{3.9}$$

$$\boldsymbol{c} = \left(\boldsymbol{b}^f\right)^{-1} := \boldsymbol{\varphi}_* \left(\boldsymbol{G}\right) = \boldsymbol{F}^{-T}\boldsymbol{G}\boldsymbol{F}^{-1} \ , \qquad \text{or} \qquad c_{ab} = \left(F^{-1}\right)^A{}_a G_{AB} \left(F^{-1}\right)^B{}_b \ . \tag{3.10}$$

The reader is again referred to Figure 3.3 for a graphical representation of the geometrical mapping properties of the introduced metric tensors.

3.1.3. Stress Measures and Mapping Properties

Consider an arbitrary *part* $\mathcal{P} \subset \mathcal{B}$ cut out of the undeformed body in the reference configuration and its deformed counterpart $\mathcal{P}_t \subset \mathcal{S}$ with the respective closed surfaces $\partial\mathcal{P}$ and $\partial\mathcal{P}_t$, as shown in Figure 3.4. In the current configuration one replaces the mechanical action of the rest of the body on the cut-out part by the spatial traction field $\boldsymbol{t}$. According

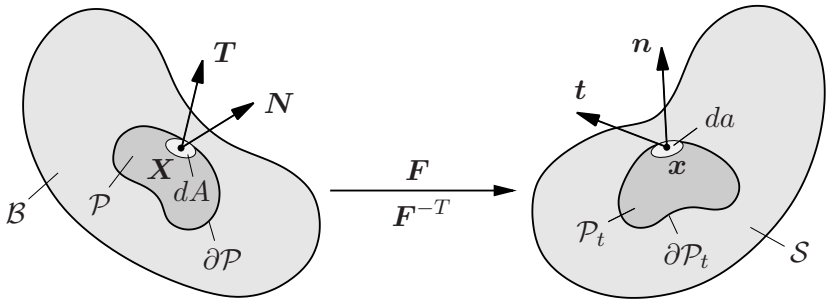

Figure 3.4: The material and spatial traction vectors $\boldsymbol{T}(\boldsymbol{X}, t; \boldsymbol{N}) \in T_X\mathcal{B}$ and $\boldsymbol{t}(\boldsymbol{x}, t; \boldsymbol{n}) \in T_x\,\mathcal{S}$ representing the forces per unit area exerted by the cut-off remainder of the body on the surfaces $\partial\mathcal{P}$ and $\partial\mathcal{P}_t$ of the cut-out parts in the material and spatial settings, respectively.

to *Cauchy's theorem*, $\boldsymbol{t}$ is assumed to be a linear function of the orientation of the cut, represented by the spatial unit normal $\boldsymbol{n} \in T_x^*\mathcal{S}$ to the surface $\partial\mathcal{P}_t$, or specifically

$$\boldsymbol{t}(\boldsymbol{x}, t; \boldsymbol{n}) := \boldsymbol{\sigma}(\boldsymbol{x}, t)\boldsymbol{n} \ , \qquad \text{or} \qquad t^a = \sigma^{ab} n_b \ . \tag{3.11}$$

Therein $\boldsymbol{\sigma}$ is the *Cauchy stress tensor*, which in our considered geometrical framework can be understood as a contravariant mapping of the form

$$\boldsymbol{\sigma} := \begin{cases} T_x^*\mathcal{S} \to T_x\,\mathcal{S} \ , \\ \boldsymbol{n} \mapsto \boldsymbol{t} = \boldsymbol{\sigma}\boldsymbol{n} \ . \end{cases} \tag{3.12}$$

Another common spatial stress measure is the *Kirchhoff stress tensor*, or *weighted Cauchy stress tensor*, $\boldsymbol{\tau} := J\boldsymbol{\sigma}$, which, due to the scalar nature of J, preserves the geometric mapping properties of $\boldsymbol{\sigma}$.

One can further introduce a scaled spatial traction vector $\tilde{\boldsymbol{t}} \in T_x\,\mathcal{S}$ that produces a resultant force on an element of the reference surface which is equal to the force exerted by $\boldsymbol{t}$ on an element of the deformed surface, such that $\boldsymbol{t}\,da = \tilde{\boldsymbol{t}}\,dA$. The *nominal* or *first Piola-Kirchhoff stress tensor* $\boldsymbol{P}$ is then defined via the Cauchy-theorem-type relation $\tilde{\boldsymbol{t}} := \boldsymbol{P}\boldsymbol{N}$,

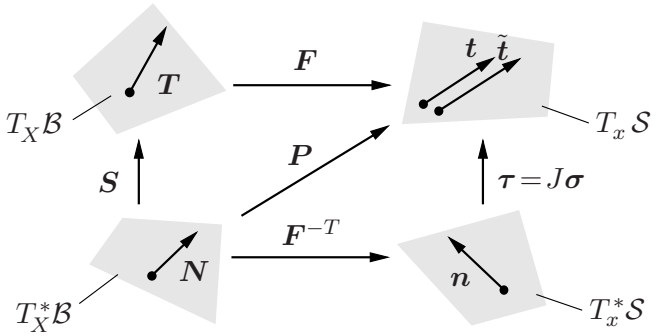

Figure 3.5: Commutative diagram illustrating the geometric mapping properties of the introduced stress tensors.

or $\tilde{t}^a = P^{aA} N_A$. Additionally, using Nanson's formula, one obtains the following relation between the introduced stress tensors $\boldsymbol{P} = J\boldsymbol{\sigma}\boldsymbol{F}^{-T} = \boldsymbol{\tau}\boldsymbol{F}^{-T}$. Note that $\boldsymbol{P}$ is a two-point (mixed-variant) tensor possessing the geometrical mapping properties

$$\boldsymbol{P} := \begin{cases} T^*_X\mathcal{B} \to T_x\mathcal{S} \ , \\ \boldsymbol{N} \mapsto \tilde{\boldsymbol{t}} = \boldsymbol{P}\boldsymbol{N} \ . \end{cases} \tag{3.13}$$

The Lagrangian traction vector $\boldsymbol{T} \in T_X\mathcal{B}$ may be defined as the *'pull-back'* of the spatial traction field $\tilde{\boldsymbol{t}} \in T_x\mathcal{S}$, i.e. $\boldsymbol{T} = \boldsymbol{\varphi}^* \left(\tilde{\boldsymbol{t}}\right) = \boldsymbol{F}^{-1}\boldsymbol{T}$ as displayed in Figure 3.4. The *second Piola-Kirchhoff stress tensor* $\boldsymbol{S}$ is then defined via the relation $\boldsymbol{T} := \boldsymbol{S}\boldsymbol{N}$, or $T^A = S^{AB} N_B$, and has the mapping properties

$$\boldsymbol{S} := \begin{cases} T^*_X\mathcal{B} \to T_X\mathcal{B} \ , \\ \boldsymbol{N} \mapsto \boldsymbol{T} = \boldsymbol{S}\boldsymbol{N} \ . \end{cases} \tag{3.14}$$

The commutative diagram of Figure 3.5 depicts the geometrical relations between the introduced stress tensors. It is immediately apparent that the following *'pull-back'* operations on the mixed-variant and spatial stress tensors hold.

$$\boldsymbol{S} := \boldsymbol{\varphi}^* (\boldsymbol{P}) = \boldsymbol{F}^{-1}\boldsymbol{P} \ , \qquad \text{or} \qquad S^{AB} = \left(F^{-1}\right)^A{}_a P^{aB} \ , \tag{3.15}$$

$$\boldsymbol{S} := \boldsymbol{\varphi}^* (\boldsymbol{\tau}) = \boldsymbol{F}^{-1}\boldsymbol{\tau}\boldsymbol{F}^{-T} \ , \qquad \text{or} \qquad S^{AB} = \left(F^{-1}\right)^A{}_a \tau^{ab} \left(F^{-1}\right)^B{}_b \ . \tag{3.16}$$

Accordingly, the converse *'push-forward'* relations of the mixed-variant and reference stress tensors are given by

$$\boldsymbol{\tau} = J\boldsymbol{\sigma} := \boldsymbol{\varphi}_* (\boldsymbol{P}) = \boldsymbol{P}\boldsymbol{F}^T \ , \qquad \text{or} \qquad \tau^{ab} = P^{aA} F^b{}_A \ , \tag{3.17}$$

$$\boldsymbol{\tau} := \boldsymbol{\varphi}_* (\boldsymbol{S}) = \boldsymbol{F}\boldsymbol{S}\boldsymbol{F}^T \ , \qquad \text{or} \qquad \tau^{ab} = F^a{}_A S^{AB} F^b{}_B \ . \tag{3.18}$$

3.1.4. Geometric Transformation of Magnetic Variables

The *governing equations of magnetostatics* were derived earlier and are given by the following global and local expressions Using the geometrical framework of finite kinematics introduced above, one can derive the material description of Maxwell's equations. From the area map by Nanson's formula it follows

$$0 = \oint_{\partial\mathcal{P}_\mathcal{S}} \widetilde{\boldsymbol{b}} \cdot \boldsymbol{n}\, da = \oint_{\partial\mathcal{P}_\mathcal{B}} \widetilde{\boldsymbol{b}} \cdot J\boldsymbol{F}^{-T}\boldsymbol{N}\, dA = \oint_{\partial\mathcal{P}_\mathcal{B}} \widetilde{\boldsymbol{B}} \cdot \boldsymbol{N}\, dA \tag{3.19}$$

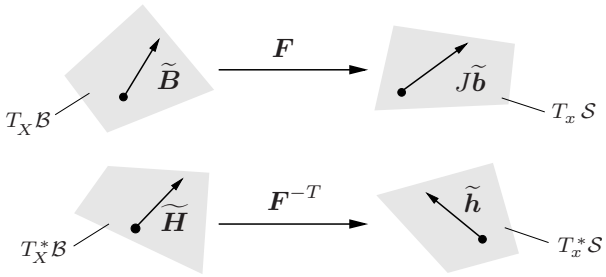

Figure 3.6: Geometric mapping properties of material and spatial magnetic induction and magnetic field.

where we have defined the *material magnetic induction* via the relation

$$\widetilde{\boldsymbol{B}} = J\boldsymbol{F}^{-1}\widetilde{\boldsymbol{b}} \,. \tag{3.20}$$

Consequently, the mapping property of the vector $\widetilde{\boldsymbol{h}}$ yields

$$0 = \oint_{\partial\mathcal{A}_\mathcal{S}} \widetilde{\boldsymbol{h}} \cdot d\boldsymbol{x} = \oint_{\partial\mathcal{A}_\mathcal{B}} \widetilde{\boldsymbol{h}} \cdot \boldsymbol{F}\, d\boldsymbol{X} = \oint_{\partial\mathcal{A}_\mathcal{B}} \widetilde{\boldsymbol{H}} \cdot d\boldsymbol{X} \,, \tag{3.21}$$

with the definition of the *reference magnetic field strength*

$$\widetilde{\boldsymbol{H}} = \boldsymbol{F}^T\widetilde{\boldsymbol{h}} \,. \tag{3.22}$$

The derived geometric relations are visualized in Figure 3.6. Thus we obtain the *balance equations of magnetostatics in the Lagrangian setting* in global and local form as

$$\begin{aligned} \int_\mathcal{B} \widetilde{\boldsymbol{B}} \cdot \boldsymbol{N}\, dA = 0 \quad &\Leftrightarrow \quad \operatorname{Div} \widetilde{\boldsymbol{B}} = 0 \\ \oint_\mathcal{C} \widetilde{\boldsymbol{H}} \cdot d\boldsymbol{X} = 0 \quad &\Leftrightarrow \quad \operatorname{Curl} \widetilde{\boldsymbol{H}} = \boldsymbol{0} \end{aligned} \tag{3.23}$$

In a similar manner one may motivate the mappings of the magnetization and induced current densities. Starting with (2.14): $\widetilde{\boldsymbol{j}} = \operatorname{curl} \boldsymbol{m}$ and integrate it over an arbitrary surface $\mathcal{A}_\mathcal{S}$ bounded by contour $\partial\mathcal{A}_\mathcal{S}$

$$\int_{\mathcal{A}_\mathcal{S}} \widetilde{\boldsymbol{j}} \cdot \boldsymbol{n}\, da = \int_{\partial\mathcal{A}_\mathcal{S}} \boldsymbol{m} \cdot d\boldsymbol{x} \tag{3.24}$$

which, by use of Nanson's formula and the mapping of a tangent vector (as we have already done earlier), results in the referential form

$$\int_{\mathcal{A}_\mathcal{B}} \widetilde{\boldsymbol{J}} \cdot \boldsymbol{N}\, dA = \int_{\partial\mathcal{A}_\mathcal{B}} \boldsymbol{M} \cdot d\boldsymbol{X} \,, \tag{3.25}$$

where we identify

$$\widetilde{\boldsymbol{J}} = J\boldsymbol{F}^{-1}\widetilde{\boldsymbol{j}} \quad \text{and} \quad \boldsymbol{M} = \boldsymbol{F}^T\boldsymbol{m} \tag{3.26}$$

With the geometric transformations defined, we have the essentials required for finite deformation magnetostatic constitutive modelling and boundary value problems.

3.2. Balance Laws of Thermo-Magneto-Mechanics

For any *admissible thermo-magneto-mechanical process* the following global balance laws must hold for every part $\mathcal{P}_t \subset \mathcal{S}$ of the material body, along with the equations for the magnetic variables introduced in the previous section. These balance equations contain, in addition to the classical contributions, the *ponderomotive body force field* $\rho\boldsymbol{\gamma}^m(\boldsymbol{x},t)$, the *ponderomotive body couple field* $\rho\boldsymbol{l}^m(\boldsymbol{x},t)$ and the *magnetic energy source field* $\rho r^m(\boldsymbol{x},t)$, which are due to the *field-matter-interactions* of the deforming magnetizable body and the magnetic field.[4]

In the following equations $\mathfrak{M}$ denotes the *mass*, $\mathfrak{L}$ the *linear momentum*, $\mathfrak{F}$ the *resultant magnetomechanical force*, $\mathcal{A}_0$ the *angular momentum* and $\mathfrak{M}_0$ the *resultant magnetomechanical moment* about the origin, $\mathfrak{K}$ the *kinetic energy*, $\mathfrak{E}$ the *internal energy*, $\mathfrak{P}$ the *power due to external magnetomechanical forces*, $\mathfrak{Q}^h$ the *thermal power*, $\mathfrak{Q}^m$ the *additional magnetic power*[5], Γ the *total rate of entropy production*, $\mathfrak{H}$ the *entropy* and finally $\mathfrak{S}$ the *entropy power* of the considered part $\mathcal{P}_t$. We further introduce the *spatial mass density field* $\rho(\boldsymbol{x},t)$, the *spatial velocity field* $\boldsymbol{v}(\boldsymbol{x},t) := \partial_t\boldsymbol{\varphi}(\boldsymbol{X},t)\circ\boldsymbol{\varphi}_t^{-1}(\boldsymbol{x})$, the mass specific *mechanical body forces* $\rho\boldsymbol{\gamma}(\boldsymbol{x},t)$, the *internal energy density* per unit mass $e(\boldsymbol{x},t)$, the mass specific *heat source* $r^h(\boldsymbol{x},t)$, the *surface heat flux vector* $\boldsymbol{q}(\boldsymbol{x},t)$, the *entropy production* per unit mass $\gamma(\boldsymbol{x},t)$, the mass specific *entropy* $\eta(\boldsymbol{x},t)$ and the *absolute temperature field* $\theta(\boldsymbol{x},t)$.

With these definitions at hand, one can express the *global balance laws of continuum thermodynamics for magnetizable media in the spatial setting* in the following form

Balance of mass

$$\frac{d}{dt}\mathfrak{M} = 0 \ , \quad \frac{d}{dt}\int\limits_{\mathcal{P}_t} \rho \, dv = 0 \ . \tag{3.27a}$$

Balance of linear momentum

$$\frac{d}{dt}\mathfrak{L} = \mathfrak{F} \ , \quad \frac{d}{dt}\int\limits_{\mathcal{P}_t} \rho\boldsymbol{v} \, dv = \int\limits_{\mathcal{P}_t} \left[\rho\boldsymbol{\gamma} + \rho\boldsymbol{\gamma}^m\right] \, dv + \int\limits_{\partial\mathcal{P}_t} \boldsymbol{t} \, da \ . \tag{3.27b}$$

Balance of angular momentum

$$\frac{d}{dt}\mathcal{A}_0 = \mathfrak{M}_0 \ , \quad \frac{d}{dt}\int\limits_{\mathcal{P}_t} \boldsymbol{x}\times\rho\boldsymbol{v} \, dv = \int\limits_{\mathcal{P}_t} \left[\boldsymbol{x}\times(\rho\boldsymbol{\gamma} + \rho\boldsymbol{\gamma}^m) + \rho\boldsymbol{l}^m\right] \, dv + \int\limits_{\partial\mathcal{P}_t} \boldsymbol{x}\times\boldsymbol{t} \, da \ . \tag{3.27c}$$

Balance of energy (first law of thermodynamics)

$$\frac{d}{dt}\left(\mathfrak{K} + \mathfrak{E}\right) = \mathfrak{P} + \mathfrak{Q}^h + \mathfrak{Q}^m \ , \tag{3.27d}$$

$$\frac{d}{dt}\int\limits_{\mathcal{P}_t} \left[\tfrac{1}{2}\,\rho\boldsymbol{v}\cdot\boldsymbol{g}\boldsymbol{v} + \rho e\right] \, dv = \int\limits_{\mathcal{P}_t} \left[(\rho\boldsymbol{\gamma} + \rho\boldsymbol{\gamma}^m)\cdot\boldsymbol{g}\boldsymbol{v}\right] \, dv + \int\limits_{\partial\mathcal{P}_t} \boldsymbol{t}\cdot\boldsymbol{g}\boldsymbol{v} \, da + \int\limits_{\mathcal{P}_t} \rho r^h \, dv - \int\limits_{\partial\mathcal{P}_t} \boldsymbol{q}\cdot\boldsymbol{n} \, da + \int\limits_{\mathcal{P}_t} \rho r^m \, dv \ .$$

[4] The specific form of electromagnetic source terms depends on the underlying model for field matter interactions, such as the *dipole-dipole*, or the *dipole-current loop* models discussed for example in [73], [125].

[5] We follow here the approach of Pao & Hutter [125] and include the work done by the magnetic body couple $\rho\boldsymbol{l}^m$ in the source term ρr^m.

Entropy inequality (second law of thermodynamics)

$$\Gamma := \frac{d}{dt}\mathfrak{H} - \mathfrak{S} \geq 0 \,, \quad \int_{\mathcal{P}_t} \rho\gamma \, dv := \frac{d}{dt}\int_{\mathcal{P}_t} \rho\eta \, dv - \left(\int_{\mathcal{P}_t} \frac{\rho r^h}{\theta} \, dv - \int_{\partial\mathcal{P}_t} \frac{\boldsymbol{q}\cdot\boldsymbol{n}}{\theta} \, da \right) \geq 0 \,. \quad (3.27e)$$

Note that body forces and couple of non-magnetic origin are not included here. The traction $\boldsymbol{t}$ includes the action of electromagnetic fields through the surface $\partial\mathcal{P}_t$. By using standard divergence, transport and localization theorems as well as the geometric mappings introduced above, the *local balance laws of continuum thermodynamics for magnetizable media in the spatial and material settings* are derived as

Balance of mass

$$\dot\rho + \rho \operatorname{div} \boldsymbol{v} = 0 \,, \qquad J\rho(\boldsymbol{\varphi}_t(\boldsymbol{X}), t) = \rho_0(\boldsymbol{X}) \,. \quad (3.28a)$$

Balance of linear momentum

$$\rho\dot{\boldsymbol{v}} = \operatorname{div}\boldsymbol{\sigma} + \rho\boldsymbol{\gamma} + \rho\boldsymbol{\gamma}^m \,, \qquad \rho_0\dot{\boldsymbol{V}} = \operatorname{Div}\boldsymbol{P} + \rho_0\boldsymbol{\Gamma} + \rho_0\boldsymbol{\Gamma}^m \,. \quad (3.28b)$$

Balance of angular momentum

$$\operatorname{skew}\boldsymbol{\sigma} = \rho\boldsymbol{L}^m \,, \qquad \operatorname{skew}\left(\boldsymbol{P}\boldsymbol{F}^T\right) = \rho_0\boldsymbol{L}^m \,. \quad (3.28c)$$

Balance of energy (first law of thermodynamics)

$$\rho\dot e = \boldsymbol{\sigma} : \boldsymbol{g}\boldsymbol{l} + \rho r^h - \operatorname{div}\boldsymbol{q} + \rho r^m \,, \qquad \rho_0\dot e = \boldsymbol{g}\boldsymbol{P} : \dot{\boldsymbol{F}} + \rho_0 R^h - \operatorname{Div}\boldsymbol{Q} + \rho_0 R^m \,. \quad (3.28d)$$

Entropy inequality (second law of thermodynamics)

$$\rho\gamma = \rho\dot\eta - \rho\frac{r^h}{\theta} + \frac{1}{\theta}\operatorname{div}\boldsymbol{q} - \frac{1}{\theta^2}\boldsymbol{q}\cdot\operatorname{grad}\theta \geq 0 \,, \quad (3.28e)$$

$$\rho_0\gamma = \rho_0\dot\eta - \rho_0\frac{R^h}{\theta} + \frac{1}{\theta}\operatorname{Div}\boldsymbol{Q} - \frac{1}{\theta^2}\boldsymbol{Q}\cdot\operatorname{Grad}\theta \geq 0 \,. \quad (3.28f)$$

In the material setting we have defined the *reference mass density field* $\rho_0(\boldsymbol{X})$, the *material velocity field* $\boldsymbol{V}(\boldsymbol{X},t) := \partial_t\boldsymbol{\varphi}(\boldsymbol{X},t)$, the *material body force term* $\boldsymbol{\Gamma}^{(m)} := \boldsymbol{\gamma}^{(m)}(\boldsymbol{x},t)\circ\boldsymbol{\varphi}_t(\boldsymbol{X})$, the *material heat source* $R^{(m)} := r^{(m)}(\boldsymbol{x},t)\circ\boldsymbol{\varphi}_t(\boldsymbol{X})$ and, using the area map, the *material heat flux vector* $\boldsymbol{Q} := J\boldsymbol{q}\boldsymbol{F}^{-T}$. The tensor $\rho\boldsymbol{L}^m$ in the angular momentum balance is the *dual* of the body couple $\rho\boldsymbol{l}^m$ and defined through the relation $\boldsymbol{L}^m\boldsymbol{a} = -\frac{1}{2}\boldsymbol{l}^m\times\boldsymbol{a}$, $\forall\boldsymbol{a}$.

The balance laws for magnetizable continua listed above are general. As mentioned, however, they require the specification of the ponderomotive force and couple terms as well as the magnetic energy source term. These terms must be justified based on a particular field-matter-interactions theory. For a broader discussion of this deep subject the reader is referred to Hutter & van de Ven[73]. In this work, we briefly mention the following two approaches. The approach originally due to Lorentz [106], which was further developed by Dixon & Eringen [38, 39] and Eringen & Maugin [53], relies on the evaluation of the interactions of elementary electrically-charged particles in a volume element with electromagnetic fields, followed by a homogenization procedure, based on volume or phase-space averaging, to derive the desired continuum model. The other model, which has been used in Ethiraj [54] is the *two-dipole model* in the so-called *Chu Formulation*, as discussed in detail by Penfield & Haus [126] and Hutter & van de Ven [125]. The two dipole model is built on the following three assumptions (cf. Hutter & van de Ven [73]):

(i) each material particle is equipped with a number of mutually noninteracting electric and magnetic dipoles,

(ii) each monopole experiences an electromagnetic body force as described by the *Lorentz force* $\rho \boldsymbol{F}^L := q^e \boldsymbol{e} + \mu_0 q^e \boldsymbol{v} \times \boldsymbol{h} + q^m \boldsymbol{h} - \varepsilon_0 q^m \boldsymbol{v} \times \boldsymbol{e}$, where q^e and q^m are the electric and (fictitious) magnetic charges of the monopoles later respectively related to the polarization and magnetization of an elementary volume, and

(iii) the monopoles of a particular dipole are only a small distance apart so that Taylor series expansions are justified.

See Ethiraj [54] for a the Coleman-Noll exploitation using the source terms derived by the latter approach.

4. Geometrically Exact Micro-Magneto-Elasticity

Here we present a rate-type *geometrically exaact incremental variational principle* for a dissipative micro-magneto-elastic model. It describes the quasi-static evolution of both *magnetic as well as mechanically driven* magnetic domains, which also *incorporates the surrounding free space*. The model incorporates characteristic size-effects that are observed and reported in the literature. The associated Euler equations arising from the variational principle for the coupled problem are shown to be consistent with the Landau-Lifschitz equation, containing the damping term of the Landau-Lifschitz-Gilbert equation that describes the time evolution of the magnetization. A particular challenge is the algorithmic preservation of the geometric constraint on the magnetization director field, that remains constant in magnitude (in contrast with the approach for ferroelectrics in Miehe, Zäh & Rosato[121]). We propose a novel finite element formulation for the monolithic treatment of the variational-based *symmetric three-field problem*, considering the mechanical displacement, the magnetization director, and the magnetic potential induced by the magnetization as the primary fields. Here, the geometric property of the magnetization director is exactly preserved pointwise by nonlinear *rotational updates at the nodes*. Numerical simulations treat domain wall motions for magnetic field- and stress-driven loading processes, including the extension of the magnetic potential into the free space.

4.1. Small Deformations for Mechanically Hard Ferromagnets

In our approach we assume small deformations of the body under consideration. This is quite valid since most ferromagnetic materials like iron, cobalt, Permalloy, and even Terfenol-D that have a large Youngs modulus and show a rather small magnetostrictive effect. In any case, the focus here is on the preservation of the geometric constraint on the magnetization in an algorithmic setting. The challenge remains nearly unchanged in the finite deformation context. We proceed as outlined in Rosato [132]. Under the small strain assumption, we have small stretches as well as vanishing rotations. Thus, using a polar decomposition of the deformation gradient into a rotation $\boldsymbol{R}$ and stretch $\boldsymbol{U}$, we have

$$\boldsymbol{F} = \boldsymbol{R}\boldsymbol{U}, \qquad \boldsymbol{R} \approx \boldsymbol{1}, \qquad \boldsymbol{U} \approx \boldsymbol{1} \tag{4.1}$$

Note that the exclusion of finite rotations renders the small strain assumption inadequate in bending scenarios where substantial rotations would accompany small stretches. With the assumptions above, we do not require to (geometrically) differentiate between material and spatial configurations. Then a linearization of the deformation gradient yields

$$\text{lin } \boldsymbol{F} = \text{grad}\, \boldsymbol{u} = \boldsymbol{\varepsilon} + \boldsymbol{\omega} \ , \tag{4.2}$$

where $\boldsymbol{\varepsilon}$ is the symmetric part (stretch-related) and $\boldsymbol{\omega}$ is the antisymmetric part (rotation-related). Thus the *small strain tensor* is nothing but the symmetric part

$$\boldsymbol{\varepsilon} = \frac{1}{2}[\text{grad}\, \boldsymbol{u} + (\text{grad}\, \boldsymbol{u})^T] \ . \tag{4.3}$$

Note that for a small-strain assumption to be valid, the scalar components of the *infinitesimal rotation tensor*

$$\boldsymbol{\omega} = \frac{1}{2}[\text{grad}\, \boldsymbol{u} - (\text{grad}\, \boldsymbol{u})^T] \ . \tag{4.4}$$

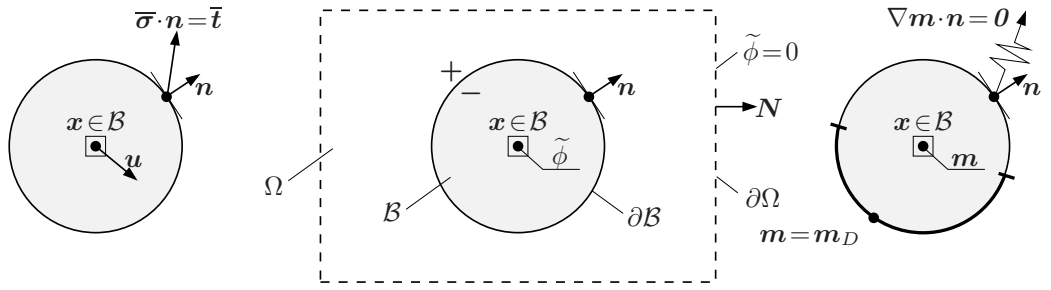

(a) displacement (b) magnetic potential (c) magnetization

Figure 4.1: Primary variable fields in micro-magneto-elasticity, for a solid $\mathcal{B} \subset \Omega$ embedded into a *free space box* $\Omega \subset \mathcal{R}^d$. (a) Associated with the *displacement field* $\boldsymbol{u}$ defined on $\mathcal{B}$ are Neumann-type boundary conditions for the macro tractions $\overline{\boldsymbol{\sigma}} \cdot \boldsymbol{n} = \overline{\boldsymbol{t}}$ on $\partial\mathcal{B}$. (b) The *magnetic potential field* $\widetilde{\phi}$ in Ω induced by the magnetization of the solid is continuous across the interface $\partial\mathcal{B}$, i.e. $[\![\widetilde{\phi}]\!] := \widetilde{\phi}^+ - \widetilde{\phi}^- = 0$ on $\partial\mathcal{B}$, and zero on the boundary $\partial\Omega$ of the free space box. (c) The *magnetization director field* $\boldsymbol{m}$ on $\mathcal{B}$ is constrained by the boundary conditions $\boldsymbol{m} = \boldsymbol{m}_D$ on $\partial\mathcal{B}_{\boldsymbol{m}}$ and its normal flux $\nabla\boldsymbol{m}\cdot\boldsymbol{n}=\boldsymbol{0}$ on $\partial\mathcal{B}_{\boldsymbol{d}}$, with $\partial\mathcal{B} = \partial\mathcal{B}_{\boldsymbol{m}} \cup \partial\mathcal{B}_{\boldsymbol{d}}$.

should be such that $|\omega_{ij}| << 1$. Additionally, in the small deformation scenario, we do not differentiate between Eulerian and Lagrangian magnetic variables or the objectivity of their time rates.

4.2. Basic Functionals in Micro-Magneto-Elasticity

Let $\Omega \subset \mathcal{R}^d$ denote a vacuum free space box with dimension $d \in [2, 3]$ and $\mathcal{B} \subset \Omega$ be the domain occupied by the material solid, as depicted in Figure 4.1. Ω is considered to be large enough such that the magnetic field induced by the magnetization of the body $\mathcal{B}$ is decayed at its surface $\partial\Omega \subset \mathcal{R}^{d-1}$. We study the deformation and the magnetization of the body under quasi-static, magneto-mechanical loading in the range $\mathcal{T} \subset \mathcal{R}$ of time. In what follows, $\nabla(\cdot) := \partial_{\boldsymbol{x}}(\cdot)$ and $\dot{(\cdot)} := \partial_t(\cdot)$ denote the spatial gradient and the time derivative of the field $(\cdot)$, respectively.

4.2.1. Primary Fields: Displacement, Magnetization, Potential

The boundary-value-problem of magneto-mechanics is a coupled multi-field problem. On the mechanical side, the primary variable field is the *displacement field* $\boldsymbol{u}$ of the material point $\boldsymbol{x} \in \mathcal{B}$ at time $t \in \mathcal{T}$. On the magnetic side, the *magnetization unit director* $\boldsymbol{m}$ describes the magnetization of the solid material at $\boldsymbol{x} \in \mathcal{B}$ and $t \in \mathcal{T}$. Hence, we focus on the two primary variable fields

$$\boldsymbol{u} : \begin{cases} \mathcal{B} \times \mathcal{T} \to \mathcal{R}^d \\ (\boldsymbol{x}, t) \mapsto \boldsymbol{u}(\boldsymbol{x}, t) \end{cases} \text{and} \quad \boldsymbol{m} : \begin{cases} \mathcal{B} \times \mathcal{T} \to \mathcal{S}^{d-1} \\ (\boldsymbol{x}, t) \mapsto \boldsymbol{m}(\boldsymbol{x}, t) \end{cases} \tag{4.5}$$

defined on the solid domain $\mathcal{B} \subset \Omega$. The magnetization director $\boldsymbol{m}$ defines the magnetization

$$\boldsymbol{M} = m_s \boldsymbol{m} \ , \tag{4.6}$$

where the material constant m_s is the spontaneous magnetization of the solid under consideration. The magnetization director is constrained by the condition

$$|\boldsymbol{m}| = 1 \ , \tag{4.7}$$

which restricts the manifold of the order parameters $\boldsymbol{m}$ to the unit sphere $\mathcal{S}^{d-1}$ in the $\mathcal{R}^d$. This geometric structure of the order parameter $\boldsymbol{m}$ is a key property in the description of

micro-magnetism and has to be considered consistently in the subsequent theoretical and computational setting. In contrast to the unconstrained evolution $\dot{\boldsymbol{u}}$ of the displacement, the evolution $\dot{\boldsymbol{m}}$ of the magnetization is constrained to be of the form

$$\dot{\boldsymbol{m}} = \boldsymbol{\omega} \times \boldsymbol{m} \ , \tag{4.8}$$

where the vector $\boldsymbol{\omega} \in \mathcal{R}^d$ is the *spin of magnetization*. Clearly, (4.8) satisfies the condition (4.6) for all times $t \in \mathcal{T}$. The magnetic field in the full free space box Ω induced by the magnetization $\boldsymbol{M}$ is described by a third field, the *magnetic potential*

$$\widetilde{\phi} : \begin{cases} \Omega \times \mathcal{T} \to \mathcal{R} \\ (\boldsymbol{x}, t) \mapsto \widetilde{\phi}(\boldsymbol{x}, t) \ . \end{cases} \tag{4.9}$$

This potential field is assumed to be continuous across the interface $\partial\mathcal{B}$ between the solid domain $\mathcal{B}$ and the surrounding free space $\Omega \setminus \mathcal{B}$, i.e.

$$[\![\widetilde{\phi}]\!] = 0 \ \text{ on } \partial\mathcal{B} \ , \tag{4.10}$$

where $[\![(\cdot)]\!] := (\cdot)_+ - (\cdot)_-$ denotes jump between the sides $\partial\mathcal{B}_+$ and $\partial\mathcal{B}_-$ of the interface as depicted in Figure 4.1. The gradients of the displacement field $\boldsymbol{u}$ and the potential $\widetilde{\phi}$ define the displacement gradient tensor and the magnetic field vector induced by the magnetization $\boldsymbol{m}$

$$\boldsymbol{f} := \nabla \boldsymbol{u} \ \text{ in } \mathcal{B} \quad \text{and} \quad \widetilde{\boldsymbol{h}} := -\nabla \widetilde{\phi} \ \text{ in } \Omega \ , \tag{4.11}$$

respectively. These definitions satisfy automatically the *deformation compatibility* $\operatorname{curl}[\boldsymbol{f}] = \boldsymbol{0}$ in $\mathcal{B}$ and *Amperes's law*, the fourth Maxwell equation, $\operatorname{curl}[\boldsymbol{h}] = \boldsymbol{0}$ in Ω for the quasi-static problem under consideration. The strains are assumed to be small, i.e. $|\nabla \boldsymbol{u}| < \epsilon$ is bounded by a small number ϵ. In contrast, the norm of the gradients of the magnetization director $|\nabla \boldsymbol{m}|$ and the magnetic potential $|\nabla \widetilde{\phi}|$ are not bounded.

4.2.2. Boundary Conditions and Loading Functionals

4.2.2.1. Mechanical Loading by Average Macro-Stress. We consider the magnetized body $\mathcal{B}$ to be mechanically loaded by a *constant external stress function* $\overline{\boldsymbol{\sigma}}(t)$, i.e. we assume the given traction

$$\overline{\boldsymbol{t}} = \overline{\boldsymbol{\sigma}} \cdot \boldsymbol{n} \ \text{ on } \partial\mathcal{B} \tag{4.12}$$

on the full surface of the body, where $\boldsymbol{n}$ is the outward normal on $\partial\mathcal{B}$. As a consequence, the stress inside the solid domain decomposes according to

$$\boldsymbol{\sigma}(\boldsymbol{x}, t) = \overline{\boldsymbol{\sigma}}(t) + \widetilde{\boldsymbol{\sigma}}(\boldsymbol{x}, t) \ \text{ in } \mathcal{B} \tag{4.13}$$

into the external part $\bar{\boldsymbol{\sigma}}$ and the stress fluctuation $\widetilde{\boldsymbol{\sigma}}$. The stress fluctuation is governed by the mechanical equilibrium equation

$$\operatorname{div} \widetilde{\boldsymbol{\sigma}} = \boldsymbol{0} \ \text{ in } \mathcal{B} \tag{4.14}$$

As a consequence of (4.12)–(4.14), we obtain

$$\int_{\mathcal{B}} \widetilde{\boldsymbol{\sigma}} \, dV = \int_{\partial\mathcal{B}} (\widetilde{\boldsymbol{\sigma}} \cdot \boldsymbol{n}) \otimes \boldsymbol{x} \, dA - \int_{\mathcal{B}} \operatorname{div}[\widetilde{\boldsymbol{\sigma}}] \otimes \boldsymbol{x} \, dV = \boldsymbol{0} \ . \tag{4.15}$$

With this result at hand, it is clear that the above introduced external stress

$$\overline{\boldsymbol{\sigma}} = \frac{1}{|\mathcal{B}|} \int_{\mathcal{B}} \boldsymbol{\sigma} \, dV \tag{4.16}$$

is the *averaged or homogenized stress* in the solid domain $\mathcal{B}$. We consider the magnetized body to be mechanically loaded by this average stress. It induces the *mechanical load functional*

$$\boxed{L_{\overline{\boldsymbol{\sigma}}}(\boldsymbol{u}; t) = \int_{\partial\mathcal{B}} \boldsymbol{u} \cdot (\overline{\boldsymbol{\sigma}}(t) \cdot \boldsymbol{n}) \, dA \; = \; \int_{\mathcal{B}} \nabla_s \boldsymbol{u} : \overline{\boldsymbol{\sigma}}(t) \, dV \; .} \tag{4.17}$$

Note that the pure Neumann-type loading (4.12) determines the displacement field $\boldsymbol{u}$ up to rigid body motions. They can be suppressed by suitable Dirichlet conditions, which do not give constraints on the deformation of the solid. Examples are single nodal supports in a typical finite element discretization.

4.2.2.2. Magnetic Loading by Average Macro-Field. The magnetized solid with magnetization $m_s\boldsymbol{m}$ *generates* the magnetic field $\widetilde{\boldsymbol{h}}$. Let the total magnetic field be decomposed according to

$$\boldsymbol{h}(\boldsymbol{x}, t) = \overline{\boldsymbol{h}}(t) + \widetilde{\boldsymbol{h}}(\boldsymbol{x}, t) \;\; \text{in } \Omega \; , \tag{4.18}$$

where $\overline{\boldsymbol{h}}$ is the *constant external contribution*. Considering the magnetization $m_s\boldsymbol{m}$ in the domain as given, $\widetilde{\boldsymbol{h}}$ follows from the Maxwell equations

$$\operatorname{curl}[\widetilde{\boldsymbol{h}}] = \boldsymbol{0} \quad \text{and} \quad \operatorname{div}[\widetilde{\boldsymbol{h}} + \hat{m}_s\boldsymbol{m}] = 0 \;\; \text{in } \Omega \; , \tag{4.19}$$

where the formal extension of the magnetization to the free space box Ω is obtained by defining

$$\hat{m}_s(\boldsymbol{x}) = \begin{cases} m_s & \text{for } \boldsymbol{x} \in \mathcal{B} \\ 0 & \text{otherwise,} \end{cases} \tag{4.20}$$

see James & Kinderlehrer [80] and DeSimone [32] for an account of this point. Condition $(4.19)_1$ is satisfied by equation $(6.6)_2$ in terms of the magnetic potential $\widetilde{\phi}$, which is formally assumed to satisfy the Dirchlet condition

$$\widetilde{\phi} = 0 \;\; \text{on } \partial\Omega \tag{4.21}$$

on the boundary $\partial\Omega$ of the free space box Ω. As a consequence, we have

$$\int_{\Omega} \widetilde{\boldsymbol{h}} \, dV = -\int_{\partial\Omega} \widetilde{\phi}\boldsymbol{N} \, dA = \boldsymbol{0} \; , \tag{4.22}$$

where $\boldsymbol{N}$ is the outward normal on the surface $\partial\Omega$ of the free space box, see Figure 4.1. Hence, we may view the external field $\overline{\boldsymbol{h}}$ as the *average* of the total magnetic field in the free space box Ω, i.e.

$$\overline{\boldsymbol{h}} = \frac{1}{|\Omega|} \int_{\Omega} \boldsymbol{h} \, dV \; . \tag{4.23}$$

We consider the magnetized body to be loaded by this external *magnetic loading functional*

$$\boxed{L_{\overline{\boldsymbol{h}}}(\boldsymbol{m};t) = \kappa_0 \int\limits_{\mathcal{B}} m_s \boldsymbol{m} \cdot \overline{\boldsymbol{h}}(t)\, dV \ ,} \tag{4.24}$$

where κ_0 is the magnetic permeability of the vacuum.

4.2.3. Objective State Variables: Theory of Grade One

The three fields $\boldsymbol{u}$, $\boldsymbol{m}$ and $\widetilde{\phi}$ defined in (6.4) and (4.9) are the primary variable fields for the coupled magneto-mechanical problem of a solid embedded into the free space. We consider a constitutive theory for simple materials of the grade one, by assuming constitutive functions to be dependent on these primary variables and their first gradient. For a generic scalar constitutive variable f, we constitute the functional dependence

$$f = \hat{f}(\mathfrak{c}_0) \quad \text{with} \quad \mathfrak{c}_0 := \{\boldsymbol{u}, \nabla\boldsymbol{u}, \boldsymbol{m}, \nabla\boldsymbol{m}, \widetilde{\phi}, \nabla\widetilde{\phi}\} \ . \tag{4.25}$$

However, for the quasi-static problem under consideration, these functions are constrained to satisfy the invariance condition

$$\hat{f}(\mathfrak{c}_0^+) = \hat{f}(\mathfrak{c}_0) \tag{4.26}$$

for superimposed rigid body motions $\boldsymbol{u}^+ = \boldsymbol{u} + \boldsymbol{w}\boldsymbol{x} + \boldsymbol{c}$ and a shift of the magnetic potential $\widetilde{\phi}^+ = \widetilde{\phi} + c$. Thus, we have $\mathfrak{c}_0^+ := \{\boldsymbol{u} + \boldsymbol{w}\boldsymbol{x} + \boldsymbol{c}, \nabla\boldsymbol{u} + \boldsymbol{w}, \mathfrak{m}, \nabla\mathfrak{m}, \widetilde{\phi} + c, \nabla\widetilde{\phi}\}$ for arbitrary skew tensors $\boldsymbol{w}$, vectors $\boldsymbol{c}$ and scalars c, respectively. The immediate consequence of (4.26) is that the constitutive function $\hat{f}$ cannot depend on the displacement $\boldsymbol{u}$, the skew part of the displacement gradient skew$[\nabla\boldsymbol{u}]$ and the magnetic potential $\widetilde{\phi}$. A reduced constitutive equation of the grade one follows

$$f = \hat{f}_{red}(\mathfrak{c}) \quad \text{with} \quad \mathfrak{c} := \{\nabla_s\boldsymbol{u}, \boldsymbol{m}, \nabla\boldsymbol{m}, -\nabla\widetilde{\phi}\} =: \{\boldsymbol{\varepsilon}, \boldsymbol{m}, \nabla\boldsymbol{m}, \widetilde{\boldsymbol{h}}\} \ , \tag{4.27}$$

depending on the *set of objective state variables* $\mathfrak{c}$, that satisfies a priori the constraint (4.26). Recall that the symmetric part of the displacement gradient is the classical small-strain tensor

$$\boldsymbol{\varepsilon} := \nabla_s\boldsymbol{u} = \tfrac{1}{2}[\boldsymbol{f} + \boldsymbol{f}^T] \in Sym(d) \ . \tag{4.28}$$

4.2.4. Energy-Enthalpy and Dissipation Potential Functionals

In order to describe the energy storage in micromagnetics in terms of the objective constitutive state defined in (4.27), we first introduce a constitutive free energy function and transform it later by a Legendre transformation to a mixed energy-enthalpy function, suitable for the above choice of the primary variables.

4.2.4.1. Contributions to the Energy Density. We need to describe two contributions to the energy density: a contribution Ψ_{vac} due to the presence of a magnetic field in the full free space box Ω and the additional contribution Ψ_{mat} in the domain $\mathcal{B} \subset \Omega$ due to the elastic deformation and the magnetization of the solid. Hence, in the solid domain $\mathcal{B}$, the total free energy density of the solid material embedded into the free space decomposes according to

$$\Psi(\boldsymbol{\varepsilon}, \boldsymbol{m}, \nabla\boldsymbol{m}, \widetilde{\boldsymbol{b}}) = \Psi_{mat}(\boldsymbol{\varepsilon}, \boldsymbol{m}, \nabla\boldsymbol{m}) + \Psi_{vac}(\boldsymbol{m}, \widetilde{\boldsymbol{b}}) \tag{4.29}$$

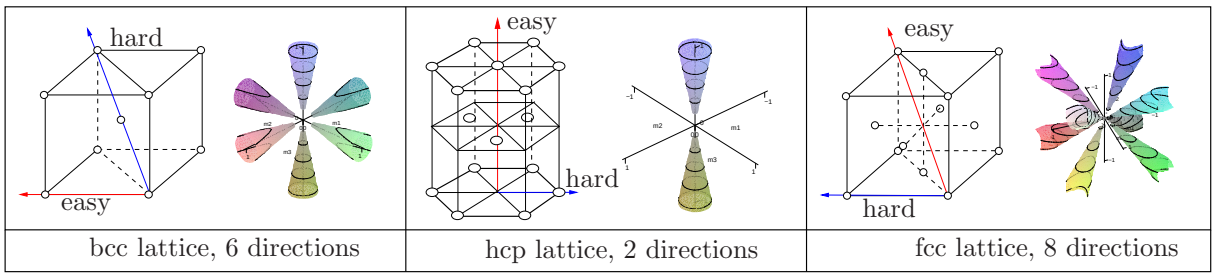

bcc lattice, 6 directions | hcp lattice, 2 directions | fcc lattice, 8 directions

Figure 4.2: Easy directions of different crystal lattice types.

into contributions from the material and the free space. Here, $\widetilde{\boldsymbol{b}}$ is the magnetic induction induced by the magnetization, see definition (4.37) below. The material part of the free energy is a function of the strain $\boldsymbol{\varepsilon}$, the magnetization director $\boldsymbol{m}$ and its gradient $\nabla\boldsymbol{m}$. It is assumed to consist of the three contributions

$$\Psi_{mat}(\boldsymbol{\varepsilon}, \boldsymbol{m}, \nabla\boldsymbol{m}) = \Psi_e(\boldsymbol{\varepsilon}, \boldsymbol{m}) + \Psi_a(\boldsymbol{m}) + \Psi_{ex}(\nabla\boldsymbol{m}) \ , \tag{4.30}$$

where Ψ_e is the elastic energy, Ψ_a the anisotropy energy and Ψ_{ex} the exchange energy.

4.2.4.2. Elastic Energy Density. The elastic energy $\Psi_e : Sym(d) \times \mathcal{S}^{d-1} \mapsto \mathcal{R}_+$ describes the energy storage due to elastic lattice distortions. Associated with the magnetization director $\boldsymbol{m}$, there exists a preferred local distortion of the crystalline solid. In line with DeSimone & James [33] and Zhang & Chen [166], we introduce an even function $\boldsymbol{m} \mapsto \boldsymbol{\varepsilon}_0(\boldsymbol{m}) \in Sym^3_+$, where $\boldsymbol{\varepsilon}_0(\boldsymbol{m})$ is the *stress-free strain* corresponding to the magnetization director $\boldsymbol{m}$. For our simple model, we assume this strain to be isochoric and fully isotropic in the lateral direction, yielding the deviatoric ansatz

$$\boldsymbol{\varepsilon}_0(\boldsymbol{m}) = \tfrac{3}{2}E\left[\boldsymbol{m}\otimes\boldsymbol{m} - \tfrac{1}{3}\boldsymbol{1}\right] \ , \tag{4.31}$$

where the material parameter $E > 0$ is the magnetostrictive constant. Clearly, E is the strain induced by the magnetization in the direction $\boldsymbol{m}$. With this ansatz at hand, we consider the elastic energy density to be a function of the elastic, stress-producing strains $\boldsymbol{\varepsilon}_e := \boldsymbol{\varepsilon} - \boldsymbol{\varepsilon}_0$. A quadratic form reads

$$\Psi_e(\boldsymbol{\varepsilon}, \boldsymbol{m}) = \tfrac{1}{2}[\boldsymbol{\varepsilon} - \boldsymbol{\varepsilon}_0(\boldsymbol{m})] : \mathbb{C} : [\boldsymbol{\varepsilon} - \boldsymbol{\varepsilon}_0(\boldsymbol{m})] \ , \tag{4.32}$$

where $\mathbb{C} := \lambda\boldsymbol{1}\otimes\boldsymbol{1} + 2\mu\mathbb{I}$ is the positive definite fourth-order elasticity tensor of the crystal. For simplicity, we modeled the elastic response to be isotropic based on the two Lamé constants $\lambda > 0$ and $\mu > 0$. Taking into account the constant length of $\boldsymbol{m}$ in (4.8), we obtain the invariant-based representation

$$\Psi_e(\boldsymbol{\varepsilon}, \boldsymbol{m}) = \frac{\lambda}{2}\mathrm{tr}^2[\boldsymbol{\varepsilon}] + \mu\,\mathrm{tr}[\boldsymbol{\varepsilon}^2] - 3\mu E\big\{\mathrm{tr}[\boldsymbol{\varepsilon}(\boldsymbol{m}\otimes\boldsymbol{m})] - \frac{1}{3}\mathrm{tr}[\boldsymbol{\varepsilon}]\big\} \ . \tag{4.33}$$

4.2.4.3. Anisotropy Energy Density. In a crystalline solid, there exist preferred directions of magnetization, often denoted as the *easy directions*. They are modeled by the even, non-negative anisotropy energy density $\Psi_a : \mathcal{S}^{d-1} \mapsto [0, +\infty]$. The zeros of Ψ_a define the easy directions, i.e. the directions along which the material is magnetized most easily. Specific representations of this non-convex energy contribution Ψ_a for different crystals are reported in Cullity [28], Kittel [90, 91] and Kittel & Galt [93]. The

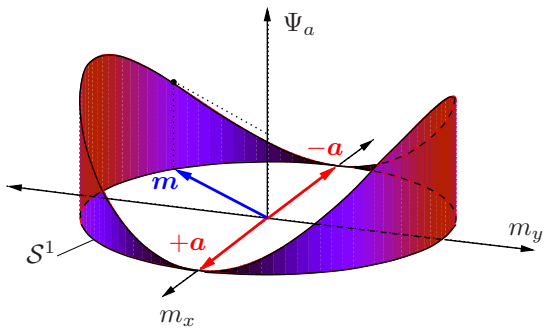

Figure 4.3: Simplified two-dimensional anisotropy energy density (two-well potential) characterized by a unit vector $\boldsymbol{a}$ for the uniaxial case. The magnetization director $\boldsymbol{m}$ evolves on the unit circle $\mathcal{S}^1$.

simplest form is obtained for the *uniaxial case*, where the set of zeros of Ψ_a are at the preferred directions $\mathcal{K} := \{+\boldsymbol{a}, -\boldsymbol{a}\}$, characterized by the structural unit vector $\boldsymbol{a}$. Then, the condition

$$0 = \Psi_a(\pm\boldsymbol{a}) < \Psi_a(\boldsymbol{m}) \quad \forall\, \boldsymbol{m} \neq \pm\boldsymbol{a} \tag{4.34}$$

is satisfied by the simple function

$$\Psi_a(\boldsymbol{m}) = \frac{K}{2}\big\{1 - \mathrm{tr}^2[\boldsymbol{m} \otimes \boldsymbol{a}]\big\} \ , \tag{4.35}$$

where the material parameter $K > 0$ is the anisotropy constant. Ψ_a governs the anisotropic energy landscape with two wells at the easy directions of magnetization. Functions which account for more than two easy directions are specified in Cullity [28], Kittel [90, 91] and Kittel & Galt [93].

4.2.4.4. Exchange Energy Density. The exchange energy $\Psi_{ex} : Lin(d) \mapsto [0, +\infty]$ models the tendency of neighboring magnetic atoms to align due to Heisenberg's exchange interaction. Focussing on an isotropic response, we consider the standard expression

$$\Psi_{ex}(\nabla\boldsymbol{m}) = \frac{A}{2}\,\mathrm{tr}\left[\nabla\boldsymbol{m} \cdot \nabla^T\boldsymbol{m}\right] \ , \tag{4.36}$$

where the material parameter $A > 0$ is the exchange energy coefficient. It is a material length scale related to the width of the magnetic domain walls.

4.2.4.5. Energy Density of the Free Space. The magnetization $m_s\boldsymbol{m}$ defines, together with the total magnetic field $\widetilde{\boldsymbol{h}}$, the magnetic induction induced by the magnetization

$$\widetilde{\boldsymbol{b}} \ = \ \kappa_0(\,\widetilde{\boldsymbol{h}} + \hat{m}_s\boldsymbol{m}\,) \ \text{ in } \Omega \tag{4.37}$$

with $\hat{m}_s$ defined in (4.20). The energy $\Psi_{vac} : \mathcal{R}^d \times \mathcal{R}^d \mapsto [0, +\infty]$ describes the energy due to the presence of a magnetic field in the free space, including the embedded solid material. Resolving (4.37) for the magnetic field $\widetilde{\boldsymbol{h}} = \hat{\boldsymbol{h}}(\boldsymbol{m}, \widetilde{\boldsymbol{b}})$, we define the quadratic form

$$\Psi_{vac}(\boldsymbol{m}, \widetilde{\boldsymbol{b}}) = \frac{\kappa_0}{2}\mathrm{tr}\big[\hat{\boldsymbol{h}} \otimes \hat{\boldsymbol{h}}\big] = \frac{1}{2\kappa_0}\mathrm{tr}\big[(\widetilde{\boldsymbol{b}} - \kappa_0\hat{m}_s\boldsymbol{m}) \otimes (\widetilde{\boldsymbol{b}} - \kappa_0\hat{m}_s\boldsymbol{m})\big] \tag{4.38}$$

governed by the magnetic permeability $\kappa_0 > 0$ of the vacuum.

4.2.5. Energy-Enthalpy Function of Micro-Magneto-Elasticity

With the above definition of the free energy function at hand, we obtain the mixed energy-enthalpy function by the partial Legendre transformation

$$\Psi'(\boldsymbol{\varepsilon}, \boldsymbol{m}, \nabla \boldsymbol{m}, \widetilde{\boldsymbol{h}}) = \inf_{\widetilde{\boldsymbol{b}}} \left[\Psi(\boldsymbol{\varepsilon}, \boldsymbol{m}, \nabla \boldsymbol{m}, \boldsymbol{b}) - \widetilde{\boldsymbol{h}} \cdot \widetilde{\boldsymbol{b}} \right] \tag{4.39}$$

with respect to the magnetic slot. This transformation affects only the free space part Ψ_{vac} of the free energy. The necessary condition of (4.39) gives (4.37). Using this as an elimination equation for $\widetilde{\boldsymbol{b}}$, we get from (4.39) the energy-enthalpy function

$$\Psi'(\boldsymbol{\varepsilon}, \boldsymbol{m}, \nabla \boldsymbol{m}, \widetilde{\boldsymbol{h}}) = \Psi_{mat}(\boldsymbol{\varepsilon}, \boldsymbol{m}, \nabla \boldsymbol{m}) - \frac{\kappa_0}{2} \widetilde{\boldsymbol{h}} \cdot \widetilde{\boldsymbol{h}} - \kappa_0 m_s \boldsymbol{m} \cdot \widetilde{\boldsymbol{h}} \ , \tag{4.40}$$

which includes the free energy density Ψ_{mat} of the solid material defined in (4.30). Note that the the energy-enthalpy function Ψ' is formulated in terms of the objective constitutive state variables $\mathfrak{c}$ defined in (4.27). With this function at hand, we finally obtain the *energy-enthalpy functional* of the magnetized solid $\mathcal{B}$ embedded into the free space Ω

$$\boxed{E'(\boldsymbol{u}, \boldsymbol{m}, \widetilde{\phi}) = \int_{\mathcal{B}} \left\{ \Psi_{mat}(\nabla_s \boldsymbol{u}, \boldsymbol{m}, \nabla \boldsymbol{m}) + \kappa_0 m_s \boldsymbol{m} \cdot \nabla \widetilde{\phi} \right\} dV - \frac{\kappa_0}{2} \int_{\Omega} |\nabla \widetilde{\phi}|^2 \, dV \ .} \tag{4.41}$$

4.2.6. Dissipation Potential for Micro-Magnetic Evolution

For a time-dependent, dynamic modeling of the evolution of the magnetization director $\boldsymbol{m}$, we need to define a kinetic law. This is achieved by the definition of a constitutive dissipation potential. We assume the simple quadratic structure

$$\Phi(\dot{\boldsymbol{m}}) = \frac{\eta}{2} |\dot{\boldsymbol{m}}^2| \ , \tag{4.42}$$

where the scalar parameter η is an inverse mobility coefficient, which governs the kinetics of the magnetic domain wall evolution. In order to account for the geometric structure $\boldsymbol{m} \in \mathcal{S}^{d-1}$ of the magnetization, the above dissipation potential is due to (4.8) effectively formulated in terms of the spin $\boldsymbol{\omega}$ and the magnetization director $\boldsymbol{m}$. With the above function at hand, we introduce the *dissipation potential functional*

$$\boxed{D(\dot{\boldsymbol{m}}) = \int_{\mathcal{B}} \Phi(\dot{\boldsymbol{m}}) \, dV \ .} \tag{4.43}$$

The four functionals $L_{\overline{\boldsymbol{\sigma}}}$, $L_{\overline{\boldsymbol{e}}}$, E' and D defined in (4.17), (4.24), (4.41) and (4.43) govern the variational principles of micro-magneto-mechanics outlined in the subsequent part of the work.

4.3. Variational Formulation of Micro-Magneto-Elasticity

4.3.1. Variational Formulation for Stationary Problems

Based on the energy-enthalpy functional (4.41), the mechanical loading functional (4.17) and the magnetic loading functional (4.24), we define the *stationary magneto-elastic potential*

$$\Pi'_{stat}(\boldsymbol{u}, \boldsymbol{m}, \widetilde{\phi}; t) := E'(\boldsymbol{u}, \boldsymbol{m}, \widetilde{\phi}) - L_{\overline{\boldsymbol{\sigma}}}(\boldsymbol{u}; t) - L_{\overline{\boldsymbol{h}}}(\boldsymbol{m}; t) \ , \tag{4.44}$$

yielding the form

$$\begin{aligned}\Pi'_{stat} = &\int_{\mathcal{B}} \big\{ \frac{A}{2}|\nabla \boldsymbol{m}|^2 + \Psi_e(\nabla \boldsymbol{u}_s, \boldsymbol{m}) + \Psi_a(\boldsymbol{m}) - \nabla_s \boldsymbol{u} : \overline{\boldsymbol{\sigma}}(t) \big\}\, dV \\ &- \int_{\Omega} \big\{ \kappa_0(\hat{m}_s \boldsymbol{m}) \cdot [\overline{\boldsymbol{h}}(t) - \nabla \widetilde{\phi}] + \frac{\kappa_0}{2}|\nabla \widetilde{\phi}|^2 \big\}\, dV \ ,\end{aligned} \tag{4.45}$$

where $\hat{m}_s$ defined in (4.20) is used for the extension of the magnetization to the full space Ω. We assume that the displacement $\boldsymbol{u}$, the magnetization director $\boldsymbol{m}$, and the magnetic potential $\widetilde{\phi}$ are governed by the variational principle

$$\boxed{\{\boldsymbol{u}, \boldsymbol{m}, \widetilde{\phi}\} = \arg \Big\{ \inf_{\boldsymbol{u} \in \mathcal{R}^d} \inf_{\boldsymbol{m} \in \mathcal{S}^{d-1}} \sup_{\widetilde{\phi} \in \mathcal{R}} \Pi'_{stat}(\boldsymbol{u}, \boldsymbol{m}, \widetilde{\phi}; t) \Big\} \ .} \tag{4.46}$$

The necessary condition of this principle is provided by the stationarity of the functional (4.45). Taking into account the geometric structure $\boldsymbol{m} \in \mathcal{S}^{d-1}$, we have

$$\delta \boldsymbol{m} \ = \ \delta \boldsymbol{w} \times \boldsymbol{m} \tag{4.47}$$

for the variation of the magnetization director in analogy to (4.8). The variation reads

$$\begin{aligned}\delta \Pi'_{stat} = &\int_{\mathcal{B}} - \operatorname{div}[\partial_{\nabla_s \boldsymbol{u}} \Psi_{mat}] \cdot \delta \boldsymbol{u}\, dV + \int_{\mathcal{B}} \big(\boldsymbol{m} \times [\delta_{\boldsymbol{m}} \Psi_{mat} - \kappa_0 m_s (\overline{\boldsymbol{h}} - \nabla \widetilde{\phi})] \big) \cdot \delta \boldsymbol{w}\, dV \\ &+ \int_{\partial \mathcal{B}} \big([\partial_{\nabla_s \boldsymbol{u}} \Psi_{mat} - \overline{\boldsymbol{\sigma}}] \cdot \boldsymbol{n} \big) \cdot \delta \boldsymbol{u}\, dA + \int_{\partial \mathcal{B}_{\mathfrak{h}}} \big(\boldsymbol{m} \times [\partial_{\nabla \boldsymbol{m}} \Psi_{mat} \cdot \boldsymbol{n}] \big) \cdot \delta \boldsymbol{w}\, dA \\ &- \int_{\Omega} \kappa_0 \operatorname{div}[-\nabla \widetilde{\phi} + \hat{m}_s \boldsymbol{m}] \delta \widetilde{\phi}\, dV + \int_{\partial \mathcal{B}} \kappa_0 \big([\![-\nabla \widetilde{\phi} + \hat{m}_s \boldsymbol{m}]\!] \cdot \boldsymbol{n} \big) \delta \widetilde{\phi}\, dA\end{aligned} \tag{4.48}$$

for the virtual fields $\{\delta \boldsymbol{u}, \delta \boldsymbol{w}, \delta \widetilde{\phi}\}$ with $\delta \boldsymbol{w} = \boldsymbol{0}$ on $\partial \mathcal{B}_{\boldsymbol{m}}$ and $\delta \widetilde{\phi} = 0$ on $\partial \Omega$. Thus, we end up with the Euler equations

$$\left.\begin{aligned} \operatorname{div}[\partial_{\nabla_s \boldsymbol{u}} \Psi_{mat}] &= \boldsymbol{0} \\ \boldsymbol{m} \times \big[\delta_{\boldsymbol{m}} \Psi_{mat} - \kappa_0 m_s (\overline{\boldsymbol{h}} - \nabla \widetilde{\phi}) \big] &= \boldsymbol{0} \\ \operatorname{div}[-\nabla \widetilde{\phi} + m_s \boldsymbol{m}] &= 0 \end{aligned}\right\} \text{ in } \mathcal{B} \tag{4.49}$$

in the solid domain $\mathcal{B}$, along with the boundary conditions

$$\partial_{\nabla_s \boldsymbol{u}} \Psi_{mat} \cdot \boldsymbol{n} = \overline{\boldsymbol{\sigma}} \cdot \boldsymbol{n} \ \text{ on } \partial \mathcal{B} \quad \text{and} \quad \boldsymbol{m} \times (\partial_{\nabla \boldsymbol{m}} \Psi_{mat} \cdot \boldsymbol{n}) = \boldsymbol{0} \ \text{ on } \partial \mathcal{B}_{\mathfrak{h}} \tag{4.50}$$

the jump condition

$$[\![-\nabla \widetilde{\phi} + \hat{m}_s \boldsymbol{m}]\!] \cdot \boldsymbol{n} = 0 \ \text{ on } \partial \mathcal{B} \tag{4.51}$$

at the interface between the solid domain and the surrounding free space, and the field equation

$$\Delta \widetilde{\phi} = 0 \ \text{ in } \Omega \setminus \mathcal{B} \tag{4.52}$$

in the surrounding free space $\Omega \setminus \mathcal{B}$, where $\Delta(\cdot) = \text{div}[\text{grad}[(\cdot)]]$ is the Laplace operator. Here, we introduced the variational or functional derivative of the free energy functions with respect to the magnetization director

$$\delta_{\boldsymbol{m}} \Psi_{mat} := \partial_{\boldsymbol{m}} \Psi_{mat} - \text{div}\left[\partial_{\nabla \boldsymbol{m}} \Psi_{mat}\right] . \tag{4.53}$$

The set (4.49) and (4.50) of equations is consistent with those outlined in Brown [21] p.27 for rigid micro-magnetics and p.75 for micro-magneto-elasticity. Note that $(4.49)_1$ and $(4.49)_3$ reflect the stress equilibrium equation and the third Maxwell equation. The third equation in $(4.49)_2$ governs the spin of the magnetization, but is *not well posed* due to the non-convexity of the free energy function Ψ_{mat}. This has motivated researchers to approach micromagnetics based on relaxation and convexification methods.

Optimizing the functional (4.45) with respect to the magnetic potential $\widetilde{\phi}$, we obtain the Maxwell equation $(4.19)_2$. This equation expresses the fact that the potential $\widetilde{\phi}$ in Ω is determined by the magnetization $\boldsymbol{m}$ in $\mathcal{B} \subset \Omega$. The Maxwell equation $(4.19)_2$ implies the condition

$$\int_{\Omega} |\nabla \widetilde{\phi}|^2 \, dV = \int_{\Omega} \hat{m}_s \boldsymbol{m} \cdot \nabla \widetilde{\phi} \, dV \ , \tag{4.54}$$

as pointed out by James & Kinderlehrer [80] p.220. Substituting this result into (4.45) and setting $A = 0$ in the exchange term yields the energy functional

$$E'_{stat} = \int_{\mathcal{B}} \left\{ \Psi_e(\nabla \boldsymbol{u}_s, \boldsymbol{m}) + \Psi_a(\boldsymbol{m}) - \nabla_s \boldsymbol{u} : \overline{\boldsymbol{\sigma}} - \kappa_0 m_s \boldsymbol{m} \cdot \overline{\boldsymbol{h}} \right\} dV + \frac{\kappa_0}{2} \int_{\Omega} |\nabla \widetilde{\phi}|^2 \, dV \ , \tag{4.55}$$

which appears in the constrained theory of magnetization for the large bodies proposed by DeSimone and James [33], p.288. If we make the opposite substitution, we obtain the following expression

$$E^{\star}_{stat} = \int_{\mathcal{B}} [\Psi_{mat}(\nabla \boldsymbol{u}_s, \boldsymbol{m}, \nabla \boldsymbol{m}) - \nabla_s \boldsymbol{u} : \overline{\boldsymbol{\sigma}} - \kappa_0 m_s \boldsymbol{m} \cdot \overline{\boldsymbol{h}} + \frac{\mu_0}{2} m_s \boldsymbol{m} \cdot \nabla \widetilde{\phi}] \, dV \ . \tag{4.56}$$

This expression appears as the quantity to be minimized in Brown [21] p.73–74 (here of course, we are in the small strain setting), in which we can identify the second term in the first integral as the *magnetostatic energy of the self-field* or the *demagnetization energy*. The third term is the *Zeeman energy*.

Both these functionals are understood to be constrained by the Maxwell equation $(4.19)_2$, which determines the magnetic potential $\widetilde{\phi}$ for a given magnetization director $\boldsymbol{m}$ or vice versa, for appropriate boundary conditions. In DeSimone and James [33], the functional (4.55) served as a starting point for the computation of laminate-type magnetic domains based on relaxation concepts in the calculus of direct variation of non-convex problems. We also refer to the work of DeSimone [32] on energy minimizers and relaxation methods for large ferromagnetic bodies, which are mechanically rigid. An overview about recent analytical developments in rigid micromagnetics is given in DeSimone et al. [35].

4.3.2. Variational Formulation for Dynamic Problems

For dynamic problems, which govern the evolution in time of the magnetization in the solid, we define a *rate-type variational principle*, which governs the rates $\{\dot{\boldsymbol{u}}, \dot{\boldsymbol{m}}, \dot{\widetilde{\phi}}\}$ at a

given state $\{\boldsymbol{u}, \boldsymbol{m}, \widetilde{\phi}\}$. This treatment also includes the *kinetics* of the magnetization, which is assumed to be dissipative in nature. It is described by the dissipation potential functional D introduced in (4.43). Based on the energy-enthalpy functional (4.41), the dissipation potential (4.42), the mechanical loading functional (4.17) and the magnetic loading functional (4.24), we define the rate-type *dynamic magneto-elastic potential*

$$\Pi'_{dyn}(\dot{\boldsymbol{u}}, \dot{\boldsymbol{m}}, \dot{\widetilde{\phi}}; t) := \frac{d}{dt} E'(\boldsymbol{u}, \boldsymbol{m}, \widetilde{\phi}) + D(\dot{\boldsymbol{m}}) - L_{\overline{\boldsymbol{\sigma}}}(\dot{\boldsymbol{u}}; t) - L_{\overline{\boldsymbol{h}}}(\dot{\boldsymbol{m}}; t) \tag{4.57}$$

at a given state $\{\boldsymbol{u}, \boldsymbol{m}, \widetilde{\phi}\}$. Note the appearance of the dissipation functional D in the potential. Using integration by parts, the rate functional takes the explicit form

$$\begin{aligned}
\Pi'_{dyn} = &\int_{\mathcal{B}} -\operatorname{div}[\partial_{\nabla_s \boldsymbol{u}} \Psi_{mat}] \cdot \dot{\boldsymbol{u}}\, dV + \int_{\mathcal{B}} \big([\delta_{\boldsymbol{m}} \Psi_{mat} - \kappa_0 m_s(\overline{\boldsymbol{h}} - \nabla\widetilde{\phi})] \cdot \dot{\boldsymbol{m}} + \frac{\eta}{2} \dot{\boldsymbol{m}} \cdot \dot{\boldsymbol{m}}\big)\, dV \\
&+ \int_{\partial\mathcal{B}} \big([\partial_{\nabla_s \boldsymbol{u}} \Psi_{mat} - \overline{\boldsymbol{\sigma}}] \cdot \boldsymbol{n}\big) \cdot \dot{\boldsymbol{u}}\, dA + \int_{\partial\mathcal{B}_{\mathfrak{h}}} (\partial_{\nabla \boldsymbol{m}} \Psi_{mat} \cdot \boldsymbol{n}) \cdot \dot{\boldsymbol{m}}\, dA \\
&- \int_{\Omega} \kappa_0 \operatorname{div}[-\nabla\widetilde{\phi} + \hat{m}_s \boldsymbol{m}] \dot{\widetilde{\phi}}\, dV + \int_{\partial\mathcal{B}} \kappa_0 \big([\![-\nabla\widetilde{\phi} + \hat{m}_s \boldsymbol{m}]\!] \cdot \boldsymbol{n}\big) \dot{\widetilde{\phi}}\, dA\,.
\end{aligned} \tag{4.58}$$

Note that this functional is linear in the rates $\{\dot{\boldsymbol{u}}, \dot{\boldsymbol{m}}, \dot{\widetilde{\phi}}\}$ up to the quadratic term $\eta\dot{\boldsymbol{m}}\cdot\dot{\boldsymbol{m}}/2$, which comes form the dissipation function. We assume that the *rates* of the displacement, the magnetization director, and the magnetic potential at a given state are governed by the variational principle

$$\boxed{\{\dot{\boldsymbol{u}}, \dot{\boldsymbol{m}}, \dot{\widetilde{\phi}}\} = \arg\Big\{ \inf_{\dot{\boldsymbol{u}} \in \mathcal{R}^d} \inf_{\dot{\boldsymbol{m}} \in T_{\boldsymbol{m}}\mathcal{S}^{d-1}} \sup_{\dot{\widetilde{\phi}} \in \mathcal{R}} \Pi'_{dyn}(\dot{\boldsymbol{u}}, \dot{\boldsymbol{m}}, \dot{\widetilde{\phi}}; t) \Big\}\,.} \tag{4.59}$$

Note carefully, that this variational principle accounts for the geometric structure of the magnetization. As a consequence of $\boldsymbol{m} \in \mathcal{S}^{d-1}$, we have $\dot{\boldsymbol{m}} \in T_{\boldsymbol{m}}\mathcal{S}^{d-1}$ where $T_{\boldsymbol{m}}\mathcal{S}^{d-1}$ is the *tangent space* of $\mathcal{S}^{d-1}$ at $\boldsymbol{m}$ as depicted in Figure 4.4. As a consequence, we have

$$\delta\dot{\boldsymbol{m}} \;=\; \delta\boldsymbol{\omega} \times \boldsymbol{m} \tag{4.60}$$

for the variation of the rate of the magnetization director at fixed $\boldsymbol{m}$ in analogy to (4.47). Then, the necessary condition of the above principle is provided by the variation

$$\begin{aligned}
\delta\Pi'_{dyn} = &\int_{\mathcal{B}} -\operatorname{div}[\partial_{\nabla_s \boldsymbol{u}} \Psi_{mat}] \cdot \delta\dot{\boldsymbol{u}}\, dV + \int_{\mathcal{B}} \big(\boldsymbol{m} \times [\delta_{\boldsymbol{m}} \Psi_{mat} - \kappa_0 m_s(\overline{\boldsymbol{h}} - \nabla\widetilde{\phi}) + \eta\dot{\boldsymbol{m}}]\big) \cdot \delta\boldsymbol{\omega}\, dV \\
&+ \int_{\partial\mathcal{B}} \big([\partial_{\nabla_s \boldsymbol{u}} \Psi_{mat} - \bar{\boldsymbol{\sigma}}] \cdot \boldsymbol{n}\big) \cdot \delta\dot{\boldsymbol{u}}\, dA + \int_{\partial\mathcal{B}_{\mathfrak{h}}} \big[\boldsymbol{m} \times (\partial_{\nabla \boldsymbol{m}} \Psi_{mat} \cdot \boldsymbol{n})\big] \cdot \delta\boldsymbol{\omega}\, dA \\
&- \int_{\Omega} \kappa_0 \operatorname{div}[-\nabla\widetilde{\phi} + \hat{m}_s \boldsymbol{m}] \cdot \delta\dot{\widetilde{\phi}}\, dV + \int_{\partial\mathcal{B}} \kappa_0 \big([\![-\nabla\widetilde{\phi} + \hat{m}_s \boldsymbol{m}]\!] \cdot \boldsymbol{n}\big) \delta\dot{\widetilde{\phi}}\, dA
\end{aligned} \tag{4.61}$$

for the virtual fields $\{\delta\dot{\boldsymbol{u}}, \delta\boldsymbol{\omega}, \delta\dot{\widetilde{\phi}}\}$ with $\delta\boldsymbol{\omega} = \boldsymbol{0}$ on $\partial\mathcal{B}_{\boldsymbol{m}}$ and $\delta\dot{\widetilde{\phi}} = 0$ on $\partial\Omega$. Note that (4.61) is identical to (4.48) up to the term that comes form the dissipation. Hence, the

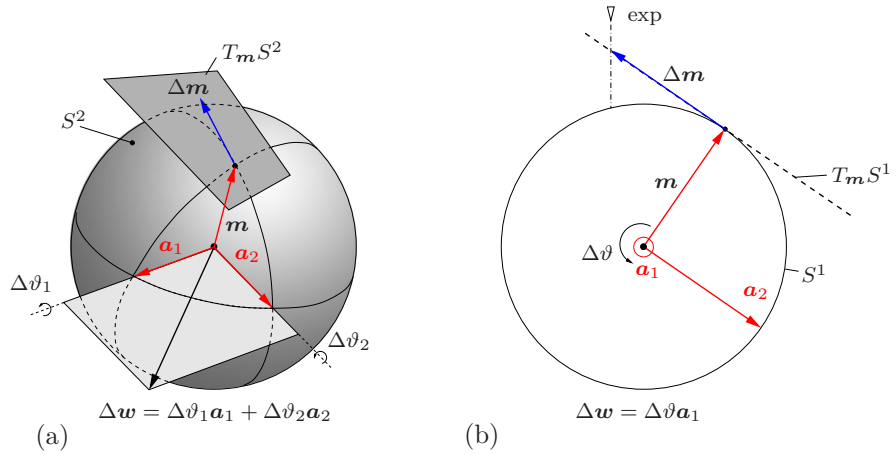

Figure 4.4: Illustration of the geometrically consistent exponential update for the magnetization director that ensures that $\boldsymbol{m} \in \mathcal{S}^{d-1}$. (a) $\Delta\boldsymbol{m}$ lies in the tangent space defined by $\boldsymbol{a}_1$ and $\boldsymbol{a}_2$. (b) Simplification to the two dimensional case with only a scalar required to update the rotation.

Euler equations are identical with (4.49)–(4.52) of the stationary variational principle up to $(4.49)_2$, which now appears in the form

$$\eta\boldsymbol{m}\times\dot{\boldsymbol{m}} + \boldsymbol{m}\times\left[\delta_{\boldsymbol{m}}\Psi_{mat} - \kappa_0 m_s(\overline{\boldsymbol{h}} - \nabla\widetilde{\phi})\right] = \boldsymbol{0} \quad \text{in } \mathcal{B}\,. \tag{4.62}$$

It extends the stationary equation $(4.49)_2$ by the kinetic term $\eta\boldsymbol{m}\times\dot{\boldsymbol{m}}$. Taking the cross product of this equation with the vector $\boldsymbol{m}$, we end up with the evolution equation for the magnetization director

$$\dot{\boldsymbol{m}} = \frac{1}{\eta}\boldsymbol{m}\times\left(\boldsymbol{m}\times[\delta_{\boldsymbol{m}}\Psi_{mat} - \kappa_0 m_s(\overline{\boldsymbol{h}} - \nabla\widetilde{\phi})]\right) \quad \text{in } \mathcal{B}\,. \tag{4.63}$$

This is consistent with the celebrated Landau-Lifschitz equation, see Landau & Lifschitz [100]. It contains the damping term of the Landau-Lifschitz-Gilbert equation of the non-stationary micromagnetics, see Gilbert [62]. Note that this evolution equations satisfies the constraint $\dot{\boldsymbol{m}}\cdot\boldsymbol{m} = 0$. The boundary value problem of dynamic, quasi-static micromagnetics is governed by equations (4.49)–(4.50), where $(4.49)_2$ is replaced by the Landau-Lifschitz equation (4.63).

4.4. Discrete Incremental Variational Formulations

4.4.1. Time-Discrete Field Variables in Incremental Setting

4.4.1.1. Finite Increments. We now outline variational principles for time-discrete problems. To this end, we consider time-discrete solutions of the field variables at the discrete times $0, t_1, t_2, \ldots, t_n, t_{n+1}, \ldots, T$ of the process interval $[0, T]$. In order to advance the solution within a typical time step, we focus on the finite time increment $[t_n, t_{n+1}]$, where

$$\tau_{n+1} := t_{n+1} - t_n > 0 \tag{4.64}$$

denotes the step length. In the subsequent treatment, all field variables at time t_n are assumed to be *known*. The goal then is to determine the fields at time t_{n+1} based on variational principles valid for the time increment under consideration. In particular, we

assemble the time-discrete spatial fields (displacement, magnetization, potential) at the discrete times t_n and t_{n+1} in the discrete solution vectors

$$\mathfrak{v}_{n+1} := \{\boldsymbol{u}_{n+1}, \boldsymbol{m}_{n+1}, \widetilde{\phi}_{n+1}\} \quad \text{and} \quad \mathfrak{v}_n := \{\boldsymbol{u}_n, \boldsymbol{m}_n, \widetilde{\phi}_n\} \ . \tag{4.65}$$

In order to obtain a compact notation, we drop in what follows the subscript $n+1$ and consider all variables without subscript to be evaluated at time t_{n+1}. The link between the variables at the two time-discrete states is obtained in *iterative steps*, which must preserve the geometric nature of the variables involved. Here, the particular challenge is to preserve the property $\boldsymbol{m} \in \mathcal{S}^{d-1}$ of the magnetization director within each step, yielding in contrast to the standard *linear* updates of the displacements $\boldsymbol{u} \in \mathcal{R}^d$ and the potential $\widetilde{\phi} \in \mathcal{R}$ a *nonlinear formulation*. To this end, we first outline the variation, the linearization and the update equation of the magnetization director within an incremental setting.

4.4.1.2. Variation and Linearization of Magnetization Director. The variation and linearization of the magnetization director appear in the form

$$\delta\boldsymbol{m} = \delta\boldsymbol{w} \times \boldsymbol{m} \quad \text{and} \quad \Delta\boldsymbol{m} = \Delta\boldsymbol{w} \times \boldsymbol{m} \tag{4.66}$$

in terms of the virtual and incremental axial vectors $\delta\boldsymbol{w}$ and $\Delta\boldsymbol{w}$, in analogy to (4.8), with the constraints

$$\delta\boldsymbol{w} \cdot \boldsymbol{m} = 0 \quad \text{and} \quad \Delta\boldsymbol{w} \cdot \boldsymbol{m} = 0 \ . \tag{4.67}$$

These constraints state that the drilling rotations about the axis $\boldsymbol{m}$ must vanish. Thus $\delta\boldsymbol{m}$ and $\Delta\boldsymbol{m}$ are vectors in the tangent space $T_{\boldsymbol{m}}\mathcal{S}^{d-1}$ of the unit sphere $\mathcal{S}^{d-1}$. This property is visualized in Figure 4.4. Introducing the current orthonormal triad

$$\boldsymbol{R} := \{\boldsymbol{a}_1, \boldsymbol{a}_2, \boldsymbol{m}\} \tag{4.68}$$

depicted in Figure 4.4, assembled in the orthogonal tensor $\boldsymbol{R} \in \mathcal{SO}(d)$, we see that the two unit vectors $\boldsymbol{a}_1$ and $\boldsymbol{a}_2$ perpendicular to $\boldsymbol{m}$ span the tangent space $T_{\boldsymbol{m}}\mathcal{S}^{d-1}$. As a consequence, the virtual and incremental axial vectors have the coordinate representation

$$\delta\boldsymbol{w} = \delta\vartheta_1\boldsymbol{a}_1 + \delta\vartheta_2\boldsymbol{a}_2 \quad \text{and} \quad \Delta\boldsymbol{w} = \Delta\vartheta_1\boldsymbol{a}_1 + \Delta\vartheta_2\boldsymbol{a}_2 \tag{4.69}$$

in terms of the two virtual rotations $\delta\vartheta_1, \delta\vartheta_2$ and the two incremental rotations $\Delta\vartheta_1, \Delta\vartheta_2$ around the axes $\boldsymbol{a}_1$ and $\boldsymbol{a}_2$ as indicated in Figure 4.4. Then, insertion of (4.69) into (4.66) gives the matrix representations

$$\boxed{\delta\boldsymbol{m} = [-\boldsymbol{a}_2, +\boldsymbol{a}_1] \cdot \delta\boldsymbol{\vartheta} \quad \text{and} \quad \Delta\boldsymbol{m} = [-\boldsymbol{a}_2, +\boldsymbol{a}_1] \cdot \Delta\boldsymbol{\vartheta} \ ,} \tag{4.70}$$

where the vectors $\delta\boldsymbol{\vartheta} := [\delta\vartheta_1, \ \delta\vartheta_2]$ and $\Delta\boldsymbol{\vartheta} := [\Delta\vartheta_1, \ \Delta\vartheta_2]$ assemble the virtual and incremental rotation degrees. The geometric matrix in (4.70) depends on the current orientation $\boldsymbol{R}$ of the triad defined in (4.68). As a consequence, we need to take into account the linear increment of the variation $\delta\boldsymbol{m}$, which we write in the matrix representation

$$\boxed{\Delta[\delta\boldsymbol{m}] = -\boldsymbol{m}(\delta\boldsymbol{\vartheta} \cdot \Delta\boldsymbol{\vartheta}) \ .} \tag{4.71}$$

Here, we inserted the increments $\Delta\boldsymbol{a}_1 = \Delta\boldsymbol{w} \times \boldsymbol{a}_1 = -\Delta\vartheta_2\boldsymbol{m}$ and $\Delta\boldsymbol{a}_2 = \Delta\boldsymbol{w} \times \boldsymbol{a}_2 = +\Delta\vartheta_1\boldsymbol{m}$. Note carefully, that $\delta\boldsymbol{\vartheta}$ and $\Delta\boldsymbol{\vartheta}$ commute in this expression.

4.4.1.3. Update of Director and Tangent Plane. We have to update in each incremental step the magnetization director $\boldsymbol{m}$ and the tangent plane $T_{\boldsymbol{m}}\mathcal{S}^{d-1}$, represented by the vectors $\boldsymbol{a}_1$ and $\boldsymbol{a}_2$. These objects are assembled in the orthogonal tensor $\boldsymbol{R}$ defined in (4.68). Considering the increment $\Delta\boldsymbol{\vartheta}$ of the incremental degrees to be given, we first compute the incremental axial vector $\Delta\boldsymbol{w}$ from $(4.69)_2$ and then update the rotation via

$$\boldsymbol{R} \Leftarrow (\Delta\boldsymbol{R})\boldsymbol{R} \quad \text{with} \quad \Delta\boldsymbol{R} := \exp[\boldsymbol{1} \times \Delta\boldsymbol{w}] \,. \tag{4.72}$$

Thus the *incremental rotation* of the triad (4.68) is obtained from the exponential map

$$\exp : \begin{cases} Skew(d) \to \mathcal{SO}(d) \\ \Delta\boldsymbol{W} \mapsto \Delta\boldsymbol{R} = \exp[\Delta\boldsymbol{W}] \end{cases} \tag{4.73}$$

forming a skew tensor $\Delta\boldsymbol{W} := \boldsymbol{1} \times \Delta\boldsymbol{w} \in Skew(d)$ with *axial vector* $\Delta\boldsymbol{w}$ of the incremental rotation $\Delta\boldsymbol{R}$. For the Lie group of rotations, the exponential map can be represented in the closed form

$$\Delta\boldsymbol{R} = \boldsymbol{1} + \frac{\sin|\Delta\boldsymbol{w}|}{|\Delta\boldsymbol{w}|}(\boldsymbol{1} \times \Delta\boldsymbol{w}) + \frac{1}{2}\left[\frac{\sin[|\Delta\boldsymbol{w}|/2]}{|\Delta\boldsymbol{w}|/2}\right]^2 (\boldsymbol{1} \times \Delta\boldsymbol{w})^2 \,, \tag{4.74}$$

known as the *Rodrigues representation* of the rotation. Inserting the representation (4.68) into (4.72), we get the closed-form update formula

$$\boxed{\{\boldsymbol{a}_1, \boldsymbol{a}_2, \boldsymbol{m}\} \;\Leftarrow\; \exp[\boldsymbol{1} \times ([\boldsymbol{a}_1, \boldsymbol{a}_2]\Delta\boldsymbol{\vartheta})]\{\boldsymbol{a}_1, \boldsymbol{a}_2, \boldsymbol{m}\}} \tag{4.75}$$

for the triad depicted in Figure 4.4. The proposed updates of the magnetization director and the tangent plane preserves *in each incremental step* of the algorithmic setting the structures of the continuous theory. This property is critical for the subsequent exploitation of an incremental variational principle.

4.4.2. Time-Discrete Incremental Variational Principle

We define the counterpart of the dynamic functional (4.57) in the incremental setting associated with the time internal $[t_n, t_{n+1}]$ by

$$\Pi'^{\tau}_{dyn}(\boldsymbol{u}, \boldsymbol{m}, \widetilde{\phi}) = E' - E'_n + Algo\Big\{ \int_{t_n}^{t_{n+1}} \big[D - L_{\overline{\boldsymbol{\sigma}}} - L_{\overline{\boldsymbol{h}}}\big]\, dt \Big\} \,, \tag{4.76}$$

depending on the current variables $\boldsymbol{\mathfrak{v}}$ defined in $(4.65)_1$. It is based on the energy-enthalpy functional (4.41), the dissipation potential (4.42), the mechanical loading functional (4.17) and the magnetic loading functional (4.24). Here, $E'_n := E'(\boldsymbol{u}_n, \boldsymbol{m}_n, \widetilde{\phi}_n)$ is a constant. Assuming a *linear path* of the state variables in the time increment $[t_n, t_{n+1}]$, we consider an *algorithm Algo* of the form

$$\begin{aligned} \Pi'^{\tau}_{dyn}(\boldsymbol{u}, \boldsymbol{m}, \widetilde{\phi}) = {} & E'(\boldsymbol{u}, \boldsymbol{m}, \widetilde{\phi}) - E'_n + \tau D([\boldsymbol{m} - \boldsymbol{m}_n]/\tau) \\ & - \tau L_{\overline{\boldsymbol{\sigma}}}([\boldsymbol{u} - \boldsymbol{u}_n]/\tau; t) - \tau L_{\overline{\boldsymbol{h}}}([\boldsymbol{m} - \boldsymbol{m}_n]/\tau; t) \end{aligned} \tag{4.77}$$

of (4.76). The insertion of the energy-enthalpy functional (4.41), the dissipation potential (4.42), the mechanical loading functional (4.17), and the magnetic loading functional

(4.24) gives the representation

$$\begin{aligned}\Pi^{\prime\tau}_{dyn} = &\int_{\mathcal{B}} \left\{ \Psi_{mat}(\nabla_s \boldsymbol{u}, \boldsymbol{m}, \nabla \boldsymbol{m}) + \kappa_0 m_s \boldsymbol{m} \cdot \nabla \widetilde{\phi} \right\} dV - \frac{\kappa_0}{2} \int_{\Omega} |\nabla \widetilde{\phi}|^2 \, dV - E'_n \\ &+ \int_{\mathcal{B}} \frac{\eta}{2\tau} |\boldsymbol{m} - \boldsymbol{m}_n|^2 \, dV - \int_{\mathcal{B}} \left\{ \overline{\boldsymbol{\sigma}} : \nabla_s [\boldsymbol{u} - \boldsymbol{u}_n] + \kappa_0 m_s [\boldsymbol{m} - \boldsymbol{m}_n] \cdot \overline{\boldsymbol{h}} \right\} dV \ .\end{aligned} \tag{4.78}$$

Note carefully, that due to this algorithmic assumption, the finite-step-sized rate-type incremental potential is considered to be a functional of the variables $\mathfrak{v}$ defined in $(4.65)_1$ at the current time t_{n+1}. This feature of the finite-step-sized incremental setting marks a formal difference to the continuous incremental functional (4.58) formulated in terms of the rates. The fields in $\mathfrak{v}$ are then determined by the time-discrete *incremental variational principle*

$$\boxed{\{\boldsymbol{u}, \boldsymbol{m}, \widetilde{\phi}\} = \arg \Big\{ \inf_{\boldsymbol{u} \in \mathcal{R}^d} \inf_{\boldsymbol{m} \in \mathcal{S}^{d-1}} \sup_{\widetilde{\phi} \in \mathcal{R}} \Pi^{\prime\tau}_{dyn}(\boldsymbol{u}, \boldsymbol{m}, \widetilde{\phi}) \Big\} \ .} \tag{4.79}$$

Taking into account the geometric structure $(4.66)_1$ of the variation $\delta \boldsymbol{m} \in T_{\boldsymbol{m}} \mathcal{S}^{d-1}$, the variation of the functional (4.78) takes the form

$$\begin{aligned}\delta \Pi^{\prime\tau}_{dyn} = &\int_{\mathcal{B}} - \operatorname{div}[\partial_{\nabla_s \boldsymbol{u}} \Psi_{mat}] \cdot \delta \boldsymbol{u} \, dV \\ &+ \int_{\mathcal{B}} \big(\boldsymbol{m} \times [\delta_{\boldsymbol{m}} \Psi_{mat} - \kappa_0 m_s (\overline{\boldsymbol{h}} - \nabla \widetilde{\phi}) + \frac{\eta}{\tau} (\boldsymbol{m} - \boldsymbol{m}_n)] \big) \cdot \delta \boldsymbol{w} \, dV \\ &+ \int_{\partial \mathcal{B}} \big([\partial_{\nabla_s \boldsymbol{u}} \Psi_{mat} - \overline{\boldsymbol{\sigma}}] \cdot \boldsymbol{n} \big) \cdot \delta \boldsymbol{u} \, dA + \int_{\partial \mathcal{B}_{\mathfrak{h}}} \big(\boldsymbol{m} \times [\partial_{\nabla \boldsymbol{m}} \Psi_{mat} \cdot \boldsymbol{n}] \big) \cdot \delta \boldsymbol{w} \, dA \\ &- \int_{\Omega} \kappa_0 \operatorname{div}[-\nabla \widetilde{\phi} + \hat{m}_s \boldsymbol{m}] \delta \widetilde{\phi} \, dV + \int_{\partial \mathcal{B}} \kappa_0 \big([\![-\nabla \widetilde{\phi} + \hat{m}_s \boldsymbol{m}]\!] \cdot \boldsymbol{n} \big) \delta \widetilde{\phi} \, dA\end{aligned} \tag{4.80}$$

similar to (4.61), however, now for the variations $\{\delta \boldsymbol{u}, \delta \boldsymbol{w}, \delta \widetilde{\phi}\}$ with $\delta \boldsymbol{w} = \boldsymbol{0}$ on $\partial \mathcal{B}_{\boldsymbol{m}}$ and $\delta \widetilde{\phi} = 0$ on $\partial \Omega$. Hence, the Euler equations of the incremental variational principle (4.79) are

$$\left.\begin{aligned} \operatorname{div}[\partial_{\nabla_s \boldsymbol{u}} \Psi_{mat}] &= \boldsymbol{0} \\ \eta \boldsymbol{m} \times \frac{\boldsymbol{m} - \boldsymbol{m}_n}{\tau} + \boldsymbol{m} \times \big[\delta_{\boldsymbol{m}} \Psi_{mat} - \kappa_0 m_s (\overline{\boldsymbol{h}} - \nabla \widetilde{\phi}) \big] &= \boldsymbol{0} \\ \operatorname{div}[-\nabla \widetilde{\phi} + m_s \boldsymbol{m}] &= 0 \end{aligned} \right\} \text{ in } \mathcal{B} \tag{4.81}$$

in the solid domain $\mathcal{B}$, along with the boundary conditions

$$\partial_{\nabla_s \boldsymbol{u}} \Psi_{mat} \cdot \boldsymbol{n} = \overline{\boldsymbol{\sigma}} \cdot \boldsymbol{n} \ \text{ on } \partial \mathcal{B} \quad \text{and} \quad \boldsymbol{m} \times (\partial_{\nabla \boldsymbol{m}} \Psi_{mat} \cdot \boldsymbol{n}) = \boldsymbol{0} \ \text{ on } \partial \mathcal{B}_{\mathfrak{h}} \tag{4.82}$$

the jump condition

$$[\![-\nabla \widetilde{\phi} + \hat{m}_s \boldsymbol{m}]\!] \cdot \boldsymbol{n} = 0 \ \text{ on } \partial \mathcal{B} \tag{4.83}$$

at the interface of the solid domain with the surrounding free space, and the field equation

$$\Delta \widetilde{\phi} = 0 \ \text{ in } \Omega \setminus \mathcal{B} \tag{4.84}$$

in the free space. The Euler equations (4.81)–(4.84) of the incremental variational principle (4.79) are the *time-discrete, algorithmic counterparts* of the Euler equations (4.49)–(4.52) of the rate-type, time-continuous variational principle, when $(4.49)_2$ is replaced for the dynamic problem by (4.62). Note that $(4.81)_2$ is a fully implicit update equation consistent with (4.62), where $\dot{\boldsymbol{m}}$ is replaced by the algorithmic rate $\boldsymbol{r}^\tau := [\boldsymbol{m} - \boldsymbol{m}_n]/\tau$. Taking the cross product of $(4.81)_2$ with the current magnetization director $\boldsymbol{m}$, we obtain the nonlinear update equation

$$\boldsymbol{r}_c^\tau = \frac{1}{\eta}\boldsymbol{m} \times \big(\boldsymbol{m} \times [\delta_{\boldsymbol{m}}\Psi_{mat} - \kappa_0 m_s(\overline{\boldsymbol{h}} - \nabla\widetilde{\phi})]\big) \quad \text{in } \mathcal{B} \ , \tag{4.85}$$

with the geometrically consistent algorithmic expression for the rate of the director

$$\begin{aligned} \boldsymbol{r}_c^\tau := \boldsymbol{p} \cdot \boldsymbol{r}^\tau \quad &\text{with} \quad \boldsymbol{r}^\tau := [\boldsymbol{m} - \boldsymbol{m}_n]/\tau \\ &\text{and} \quad \boldsymbol{p} := \boldsymbol{1} - \boldsymbol{m} \otimes \boldsymbol{m} \ . \end{aligned} \tag{4.86}$$

Equation (4.85) is a variational-based, time-discrete counterpart of the continuous Landau-Lifschitz equation (4.63) based on the algorithmic assumption (4.77) for a potential associated with a finite time increment. Note that the second-order projection tensor $\boldsymbol{p}$ filters out the component of the rate $\boldsymbol{r}^\tau$ perpendicular to $\boldsymbol{m}$, such that we have $\boldsymbol{r}_c^\tau \cdot \boldsymbol{m} = 0$. The projection influences only the viscous term in the evolution equation. This influence increases for increasing difference between $\boldsymbol{m}$ and $\boldsymbol{m}_n$.

4.4.3. Space-Time-Discrete Incremental Variational Principle

The basic difficulty is the construction of a finite element method that preserves the geometric structure $\boldsymbol{m} \in \mathcal{S}^{d-1}$ of the magnetization director, which is the foundation of the incremental variational principle (4.79). In the incremental setting, this is provided by *nonlinear updates* of the form (4.75). In order to preserve this structure in the spatial discretization of the problem, we propose a finite element method that *preserves exactly the constraint* (4.7) *at the nodes of a typical finite element mesh.*

4.4.3.1. Finite Element Discretization. Let $\mathfrak{T}^h$ denote a finite element triangulation of the domain Ω. The index h indicates a typical mesh size based on E^h finite element domains $\Omega_e^h \in \mathfrak{T}^h$ and N^h global nodal points. The first basic step is a standard finite element interpolation of the time-discrete incremental potential (4.78). To this end, we represent the functional (4.78) in the form

$$\Pi_{dyn}'^\tau(\boldsymbol{u}, \boldsymbol{m}, \widetilde{\phi}) = \int_{\mathcal{B}} \pi'^\tau(\mathfrak{c}; \mathfrak{c}_n)\, dV - \frac{\kappa_0}{2}\int_{\Omega} |\nabla\widetilde{\phi}|^2\, dV + C_n \tag{4.87}$$

in terms of the *effective potential density* π'^τ *per unit volume* of the solid domain $\mathcal{B}$ and the additional contribution of the free space. C_n is a constant that assembles contributions at time t_n. The incremental effective potential

$$\begin{aligned} \pi'^\tau(\mathfrak{c}; \mathfrak{c}_n) = \Psi_{mat}(\nabla_s\boldsymbol{u}, \boldsymbol{m}, \nabla\boldsymbol{m}) + \kappa_0 m_s \boldsymbol{m} \cdot \nabla\widetilde{\phi} + \frac{\eta}{2\tau}|\boldsymbol{m} - \boldsymbol{m}_n|^2 \\ - \overline{\boldsymbol{\sigma}} : \nabla_s[\boldsymbol{u} - \boldsymbol{u}_n] - \kappa_0 m_s[\boldsymbol{m} - \boldsymbol{m}_n] \cdot \overline{\boldsymbol{h}} \end{aligned} \tag{4.88}$$

is a function of the objective set of constitutive state variables $\mathfrak{c} := \{\nabla_s\boldsymbol{u}, \boldsymbol{m}, \nabla\boldsymbol{m}, -\nabla\widetilde{\phi}\}$ introduced in (4.27). We then introduce the *nodal variable vector* of the coupled problem

$$\boldsymbol{d} := \mathop{\mathsf{A}}_{I=1}^{N^h} \begin{bmatrix} \boldsymbol{u} \\ \boldsymbol{m} \\ -\widetilde{\phi} \end{bmatrix}_I \in \mathcal{C}_d := (\mathcal{R}^d, \mathcal{S}^{d-1}, \mathcal{R})N^h \ , \tag{4.89}$$

which contains the displacement $\boldsymbol{u} \in \mathcal{R}^d$, the magnetization director $\boldsymbol{m} \in \mathcal{S}^{d-1}$, and the potential $\widetilde{\phi} \in \mathcal{R}$ at the N^h space-discrete nodal points of the finite element mesh. Associated with the triangulation $\mathfrak{T}^h$, we write the finite element interpolations of the constitutive state vector in the compact form

$$\mathfrak{c}^h = \boldsymbol{B}(\boldsymbol{x})\boldsymbol{d} \quad \text{and} \quad \nabla\widetilde{\phi} = \boldsymbol{F}(\boldsymbol{x})\boldsymbol{d} \tag{4.90}$$

in terms of the space-time-discrete nodal variable vector $\boldsymbol{d}$ defined in (6.36). $\boldsymbol{B}$ and $\boldsymbol{F}$ are representations of the global matrices of shape functions for the coupled problem. Clearly, these global arrays are never formulated explicitly, but represent symbolically the interpolations on all finite element domains $\Omega_e^h \in \mathfrak{T}^h$. Note that the global nodal variable vector $\boldsymbol{d}$ is formed from element vectors $\boldsymbol{d}^e$ by a standard finite element assembling procedure. As a consequence, the finite element discretization of the incremental functional (6.37) reads

$$\Pi'^h_{dyn}(\boldsymbol{d}) = \int_{\mathcal{B}} \pi'^{\tau}(\boldsymbol{B}\boldsymbol{d}; \boldsymbol{B}\boldsymbol{d}_n)\, dV - \frac{\kappa_0}{2}\int_{\Omega} |\boldsymbol{F}\boldsymbol{d}|^2\, dV \ . \tag{4.91}$$

Then, a space-time-discrete incremental variational principle of micromagnetics gives at a discrete time the nodal values

$$\boxed{\boldsymbol{d} = \arg\left\{\operatorname*{stat}_{\boldsymbol{d}\in\mathcal{C}_d} \Pi'^h_{dyn}(\boldsymbol{d})\right\}} \tag{4.92}$$

of the coupled problem. Note carefully, that $\boldsymbol{d} \in \mathcal{C}_d$ guarantees the geometric property $\boldsymbol{m} \in \mathcal{S}^{d-1}$ of the magnetization director at the nodal points. Within typical finite element domains, the approximate interpolation (6.38) of the director violates this condition.

4.4.3.2. Variation and Linearization. In order to solve the nonlinear optimization problem (4.92) by a Newton method, we take the variation of the finite element functional (6.39) and consider its linearization. Here, we must account the *geometric structure of the nodal variables* $\boldsymbol{d} \in \mathcal{C}_d$ according to the treatment in Section 4.4.1. To this end, we introduce the *effective virtual and incremental nodal variable vectors*

$$\boldsymbol{\delta} := \operatorname*{A}_{I=1}^{N^h} \begin{bmatrix} \delta\boldsymbol{u} \\ \delta\boldsymbol{\vartheta} \\ -\delta\widetilde{\phi} \end{bmatrix}_I \in \mathcal{R}^{2dN^h} \quad \text{and} \quad \boldsymbol{\Delta} := \operatorname*{A}_{I=1}^{N^h} \begin{bmatrix} \Delta\boldsymbol{u} \\ \Delta\boldsymbol{\vartheta} \\ -\Delta\widetilde{\phi} \end{bmatrix}_I \in \mathcal{R}^{2dN^h} \ . \tag{4.93}$$

Their magnetic slots contain the finite element discretizations of the effective virtual and incremental rotation degrees introduced in (4.70). Taking into account the geometric representations (4.70) and (4.71) of the variation $\delta\boldsymbol{m} \in T_{\boldsymbol{m}}\mathcal{S}^{d-1}$ and the increment $\Delta\boldsymbol{m} \in T_{\boldsymbol{m}}\mathcal{S}^{d-1}$ of the magnetization director, we write the variation and linearization of the nodal variable vector (6.36) in the matrix notation

$$\boxed{\delta\boldsymbol{d} = \boldsymbol{G}\cdot\boldsymbol{\delta} \ , \quad \Delta\boldsymbol{d} = \boldsymbol{G}\cdot\boldsymbol{\Delta} \ , \quad \Delta[\delta\boldsymbol{d}] = \boldsymbol{g}(\boldsymbol{\delta}\cdot\mathbb{G}\cdot\boldsymbol{\Delta})} \tag{4.94}$$

in terms of the symbolic geometric matrices

$$\boldsymbol{G} := \operatorname{diag} \operatorname*{A}_{I=1}^{N^h} \begin{bmatrix} \boldsymbol{1} & & \\ & [-\boldsymbol{a}_2, \ +\boldsymbol{a}_1] & \\ & & 1 \end{bmatrix}_I , \quad \boldsymbol{g} := \operatorname*{A}_{I=1}^{N^h} \begin{bmatrix} \boldsymbol{0} \\ \boldsymbol{m} \\ 0 \end{bmatrix}_I , \quad \mathbb{G} := \operatorname{diag} \operatorname*{A}_{I=1}^{N^h} \begin{bmatrix} \boldsymbol{0} & & \\ & \boldsymbol{1}_{2\times 2} & \\ & & 0 \end{bmatrix}_I \tag{4.95}$$

which extend formally (4.70) and (4.71) to the discrete nodal vectors. With this notation at hand, the necessary condition of the variational principle (4.92) reads

$$\delta\Pi^{\prime h}_{dyn} = \boldsymbol{\delta}^T \cdot \boldsymbol{R} = 0 \quad \forall\ \boldsymbol{\delta} \in \mathcal{R}^{2dN^h} \tag{4.96}$$

in terms of the algebraic finite element residual of the coupled problem

$$\boldsymbol{R} := \int_{\mathcal{B}} (\boldsymbol{BG})^T \cdot \boldsymbol{S}^h \, dV - \kappa_0 \int_{\Omega} (\boldsymbol{FG})^T \cdot (\boldsymbol{Fd}) \, dV \ . \tag{4.97}$$

The linearization of the necessary condition (6.43) reads

$$Lin[\delta\Pi^{\prime h}_{dyn}] := \delta\Pi^{\prime h}_{dyn} + \Delta[\delta\Pi^{\prime h}_{dyn}] = \boldsymbol{\delta}^T[\boldsymbol{R} + \boldsymbol{K}\boldsymbol{\Delta}] \tag{4.98}$$

with the finite element tangent matrix of the coupled problem

$$\boldsymbol{K} := \int_{\mathcal{B}} \left\{ (\boldsymbol{BG})^T \mathbb{C}^h (\boldsymbol{BG}) + [\boldsymbol{S}^h \cdot \boldsymbol{Bg}]\mathbb{G} \right\} dV - \kappa_0 \int_{\Omega} \left\{ (\boldsymbol{FG})^T (\boldsymbol{FG}) + [(\boldsymbol{Fd}) \cdot (\boldsymbol{Fg})]\mathbb{G} \right\} dV \ . \tag{4.99}$$

Observe that the finite element residual and tangent are governed by the *generalized stress* and *tangent arrays*

$$\boldsymbol{S}^h := \partial_{\mathfrak{c}} \pi^{\prime\tau}(\mathfrak{c}^h; \mathfrak{c}^h_n) \quad \text{and} \quad \mathbb{C}^h := \partial^2_{\mathfrak{c}\mathfrak{c}} \pi^{\prime\tau}(\mathfrak{c}^h; \mathfrak{c}^h_n) \ , \tag{4.100}$$

i.e. the first and second derivatives of the incremental effective potential $\pi^{\prime\tau}$ defined in (4.88) by the current constitutive state $\mathfrak{c}^h$. These arrays are a critical ingredient of the proposed variational formulation and make the notation extremely compact. Due to the nonlinear geometric structure $\boldsymbol{m} \in \mathcal{S}^{d-1}$ of the nodal directors, the tangent matrix has an additional geometric term. Observe the *symmetry of the tangent matrix* $\boldsymbol{K}$, induced by the incremental variational structure (4.92) of the coupled three-field problem.

4.4.3.3. Nonlinear Iterative Updates. The necessary condition $\boldsymbol{R} = \boldsymbol{0}$ implied by (6.43) is solved in an iterative manner by a Newton iteration based on the linearization (4.98). Setting $Lin[\delta\Pi^{\prime h}_{dyn}] = 0$ in (4.98) gives the update of the effective incremental nodal variable vector

$$\boldsymbol{\Delta} := \mathop{\mathsf{A}}_{I=1}^{N^h} \begin{bmatrix} \Delta\boldsymbol{u} \\ \Delta\boldsymbol{\vartheta} \\ -\Delta\widetilde{\phi} \end{bmatrix}_I = -\boldsymbol{K}^{-1}\boldsymbol{R} \tag{4.101}$$

in terms of the finite element residual $\boldsymbol{R}$ and tangent $\boldsymbol{K}$ defined in (6.44) and (4.99), respectively. With known effective *incremental* nodal variables $\boldsymbol{\Delta}$, we update the nodal variable vector $\boldsymbol{d}$ by taking into account (4.75), i.e.

$$\boldsymbol{d} := \mathop{\mathsf{A}}_{I=1}^{N^h} \begin{bmatrix} \boldsymbol{u} \\ \boldsymbol{m} \\ -\widetilde{\phi} \end{bmatrix}_I \ \Leftarrow \ \mathop{\mathsf{A}}_{I=1}^{N^h} \begin{bmatrix} \boldsymbol{u} + \Delta\boldsymbol{u} \\ \exp[\,\boldsymbol{1} \times ([\boldsymbol{a}_1, \boldsymbol{a}_2]\Delta\boldsymbol{\vartheta})\,]\boldsymbol{m} \\ -\widetilde{\phi} - \Delta\widetilde{\phi} \end{bmatrix}_I \ . \tag{4.102}$$

Besides the update of the magnetization director $\boldsymbol{m}$, we also need to update the tangent space $T_{\boldsymbol{m}}S^{d-1}$, characterized by the two unit vectors $\boldsymbol{a}_1$ and $\boldsymbol{a}_2$. This is also performed by the exponential update scheme

$$\{\boldsymbol{a}_1, \boldsymbol{a}_2\} \ \Leftarrow \ \exp\left[\boldsymbol{1} \times ([\boldsymbol{a}_1, \boldsymbol{a}_2]\Delta\boldsymbol{\vartheta})\right]\{\boldsymbol{a}_1, \boldsymbol{a}_2\} \ , \tag{4.103}$$

which is in the proposed method performed at each node of the finite element mesh. The sequence (4.101)–(4.103) of the computational steps is repeated until convergence is achieved in the sense $|\boldsymbol{R}| < tol$. The computational procedure preserves the geometric structure $\boldsymbol{m} \in \mathcal{S}^{d-1}$ exactly at the nodal points of the finite element mesh *within each step of an incremental iteration process.*

4.5. FE Discretization of 2D-Problems

4.5.1. Specification of Nodal Variable Vectors

For two-dimensional, plane problems $d = 2$, the virtual and incremental axial vectors in (4.69) for the rotation of the magnetization take the simplified form

$$\delta\boldsymbol{w} = \delta\vartheta_1 \boldsymbol{a}_1 \quad \text{and} \quad \Delta\boldsymbol{w} = \Delta\vartheta_1 \boldsymbol{a}_1 \tag{4.104}$$

in terms of the two virtual and incremental rotations $\delta\vartheta_1$ and $\Delta\vartheta_1$ around the *fixed out-of-plane axis* $\boldsymbol{a}_1$ as depicted in Figure 4.4. Then, the geometric relationships (4.70) and (4.71) read

$$\delta\boldsymbol{m} = -\boldsymbol{a}_2 \delta\vartheta_1 \ , \quad \Delta\boldsymbol{m} = -\boldsymbol{a}_2 \Delta\vartheta_1 \ , \quad \Delta[\delta\boldsymbol{m}] = -\boldsymbol{m}\delta\vartheta_1\Delta\vartheta_1 \ . \tag{4.105}$$

Hence, the *nodal variable vector* $\boldsymbol{d}$ and the *incremental nodal variable vector* $\boldsymbol{\Delta}$ introduced in (6.36) and (6.40) take the specific coordinate form

$$\boldsymbol{d} := \mathop{\mathsf{A}}_{I=1}^{N^h} \begin{bmatrix} u_x \\ u_y \\ m_x \\ m_y \\ -\widetilde{\phi} \end{bmatrix}_I \quad \text{and} \quad \boldsymbol{\Delta} := \mathop{\mathsf{A}}_{I=1}^{N^h} \begin{bmatrix} \Delta u_x \\ \Delta u_y \\ \Delta\vartheta_1 \\ -\Delta\widetilde{\phi} \end{bmatrix}_I \tag{4.106}$$

for coordinates in a fixed Cartesian system $\{\boldsymbol{e}_x, \boldsymbol{e}_y\}$.

4.5.2. Constitutive State, Generalized Stresses and Moduli

The constitutive state vector introduced in (4.27) reads for two-dimensional problems

$$\mathfrak{c} = [u_{x,x}, u_{y,y}, u_{x,y} + u_{y,x}, m_x, m_y, m_{x,x}, m_{x,y}, m_{y,x}, m_{y,y}, -\widetilde{\phi}_{,x}, -\widetilde{\phi}_{,y}]^T \tag{4.107}$$

for coordinates in the Cartesian system $\{\boldsymbol{e}_i\}_{i=1,3}$. Taking into account the incremental potential defined in (4.88), we obtain by exploitation of (4.100) the specific formulations

$$\boldsymbol{S}^h = \begin{bmatrix} \lambda \operatorname{tr}[\nabla_s \boldsymbol{u}]\boldsymbol{1} + 2\mu\nabla_s\boldsymbol{u} - 3\mu E\big(\boldsymbol{m}\otimes\boldsymbol{m} - \frac{1}{3}\boldsymbol{1}\big) - \overline{\boldsymbol{\sigma}} \\ -6\mu E\nabla_s\boldsymbol{u}\cdot\boldsymbol{m} - K\operatorname{tr}[\boldsymbol{m}\otimes\boldsymbol{a}]\boldsymbol{a} + \kappa_0 m_s(\nabla\widetilde{\phi} - \overline{\boldsymbol{h}}) + \frac{\eta}{\tau}(\boldsymbol{m} - \boldsymbol{m}_n) \\ A\nabla\boldsymbol{m} \\ -\kappa_0 m_s \boldsymbol{m} + \kappa_0 \nabla\widetilde{\phi} \end{bmatrix} \tag{4.108}$$

for the *generalized stress array* and

$$\mathbb{C}^h = \begin{bmatrix} \lambda\boldsymbol{1}\otimes\boldsymbol{1} + 2\mu\mathbb{I} & -6\mu E \overset{12}{\operatorname{sym}}[\boldsymbol{m}\otimes\boldsymbol{1}] & \boldsymbol{0} & \boldsymbol{0} \\ & -6\mu E\nabla_s\boldsymbol{u} - K\boldsymbol{a}\otimes\boldsymbol{a} + \frac{\eta}{\tau}\boldsymbol{1} & \boldsymbol{0} & -\kappa_0 m_s \boldsymbol{1} \\ & & A\,\boldsymbol{1}_{4\times 4} & \boldsymbol{0} \\ & & & -\kappa_0\boldsymbol{1} \end{bmatrix} \tag{4.109}$$

for the *generalized tangent array.*

4.5.3. Specification of the Finite Element Matrices

The finite element interpolation matrix for the constitutive state introduced in $(6.38)_1$ has the specific coordinate form

$$\boldsymbol{B} = \mathop{\mathsf{A}}_{I=1}^{N^h} \begin{bmatrix} N_{,x} & & N_{,y} & & & & & & & \\ & N_{,y} & N_{,x} & & & & & & & \\ & & & N & & N_{,x} & N_{,y} & & & \\ & & & & N & & & N_{,x} & N_{,y} & \\ & & & & & & & & & N_{,x} \; N_{,y} \end{bmatrix}_I^T \tag{4.110}$$

in terms of the shape function N_I and their derivatives. The interpolation matrix for the free space introduced in $(6.38)_2$ reads

$$\boldsymbol{F} := \mathop{\mathsf{A}}_{I=1}^{N^h} \begin{bmatrix} 0 & 0 & 0 & 0 & N_{,x} \\ 0 & 0 & 0 & 0 & N_{,y} \end{bmatrix}_I . \tag{4.111}$$

Furthermore, the geometric matrices introduced in (6.42) have the representations

$$\boldsymbol{G} := \operatorname{diag} \mathop{\mathsf{A}}_{I=1}^{N^h} \begin{bmatrix} 1 & & & \\ & 1 & & \\ & & -a_{2x} & \\ & & -a_{2y} & \\ & & & 1 \end{bmatrix}_I , \quad \boldsymbol{g} := \mathop{\mathsf{A}}_{I=1}^{N^h} \begin{bmatrix} 0 \\ 0 \\ m_x \\ m_y \\ 0 \end{bmatrix}_I , \quad \mathbb{G} := \operatorname{diag} \mathop{\mathsf{A}}_{I=1}^{N^h} \begin{bmatrix} 0 & & & \\ & 0 & & \\ & & 1 & \\ & & & 0 \end{bmatrix}_I . \tag{4.112}$$

We may exploit the fact that $\boldsymbol{a}_2$ is a vector perpendicular to the magnetization $\boldsymbol{m}$ by setting $-a_{2x} = -m_y$ and $-a_{2y} = m_x$. its components are represented in terms of the components of the magnetization vector. With the generalized stress and tangent arrays (4.108) and (4.109), the finite element interpolation matrices (4.110)–(4.112), we compute the residual $\boldsymbol{R}$ and $\boldsymbol{K}$ introduced in (6.44) and (4.99), respectively.

4.5.4. Nonlinear Update of Nodal Variables

The increment $\boldsymbol{\Delta}$ of the nodal variables follows then in a typical Newton step of the monolithically coupled problem from (4.101). Then, the nonlinear update of the nodal variables is performed by

$$\mathop{\mathsf{A}}_{I=1}^{N^h} \begin{bmatrix} u_x \\ u_y \\ m_x \\ m_y \\ -\widetilde{\phi} \end{bmatrix}_I \Leftarrow \mathop{\mathsf{A}}_{I=1}^{N^h} \begin{bmatrix} u_x + \Delta u_x \\ u_y + \Delta u_y \\ m_x \cos(\Delta\vartheta) - m_y \sin(\Delta\vartheta) \\ m_x \sin(\Delta\vartheta) + m_y \cos(\Delta\vartheta) \\ -\widetilde{\phi} - \Delta\widetilde{\phi} \end{bmatrix}_I , \tag{4.113}$$

which specifies (4.102) for the two-dimensional problem.

4.6. Selected Initial Boundary Value Problems

In order to demonstrate the modeling capacity of the discussed formulation, we present below some representative simulations. We employ bilinear quad finite elements to discretize the domain. The material in focus will be Permalloy, which is an alloy of 20% Nickel (Ni) and 80% Iron (Fe), and finds wide application in industry as magnetic recording head

Table 4.1: Material parameters of Permalloy used for the numerical examples [41].

No.	Parameter	Name	Value	Unit
1.	λ	Lamé parameter	7.5×10^4	$\mathrm{N/mm^2}$
2.	μ	Lamé parameter	2.6×10^4	$\mathrm{N/mm^2}$
3.	E	Magnetostrictive constant	7.0×10^{-6}	–
4.	K	First anisotropy coefficient	1.0×10^{-3}	$\mathrm{N/mm^2}$
5.	A	Exchange coefficient	2.0×10^{-11}	N
6.	m_s	Saturation magnetization	8.0×10^2	A/mm
7.	η	Damping coefficient	2.0×10^{-1}	$\mathrm{Ns^2/mm^2}$
8.	κ_0	Magnetic permeability	1.3×10^{-6}	$\mathrm{N/A^2}$

sensors. Apart from its importance in practical applications, the low anisotropy exhibited by Permalloy makes it the ideal material to observe the influence of the competing effects, such as magnetostatic energy and mechanical stress in conjunction with sample geometry, on its domain structure. We will look at isothermal strain and stress driven simulations of the material at temperatures below its Curie temperature ($\mathrm{T_c} = 850\mathrm{K}$). The material parameters used in the simulations are listed in Table 4.1.

4.6.1. Example to Demonstrate the Rotation of the Magnetization

The aim of the first example is to demonstrate the *rotation* of the magnetization since this, as mentioned in Section 4.2, is a characteristic feature of the the micro-magnetic problem. We consider a ferromagnetic sample with dimensions $3\mu\mathrm{m} \times 1\mu\mathrm{m}$ and having strong uniaxial anisotropy. In order to show the rotation we have used a relatively coarse structured mesh with 30×10 elements for the discretization of the domain. Note that the material model being dependent on the *gradient of the magnetization* prohibits us from using an arbitrarily coarse mesh to discretize the ferromagnetic body. This is typical of phase-field models which always exhibit *length scale effects*.

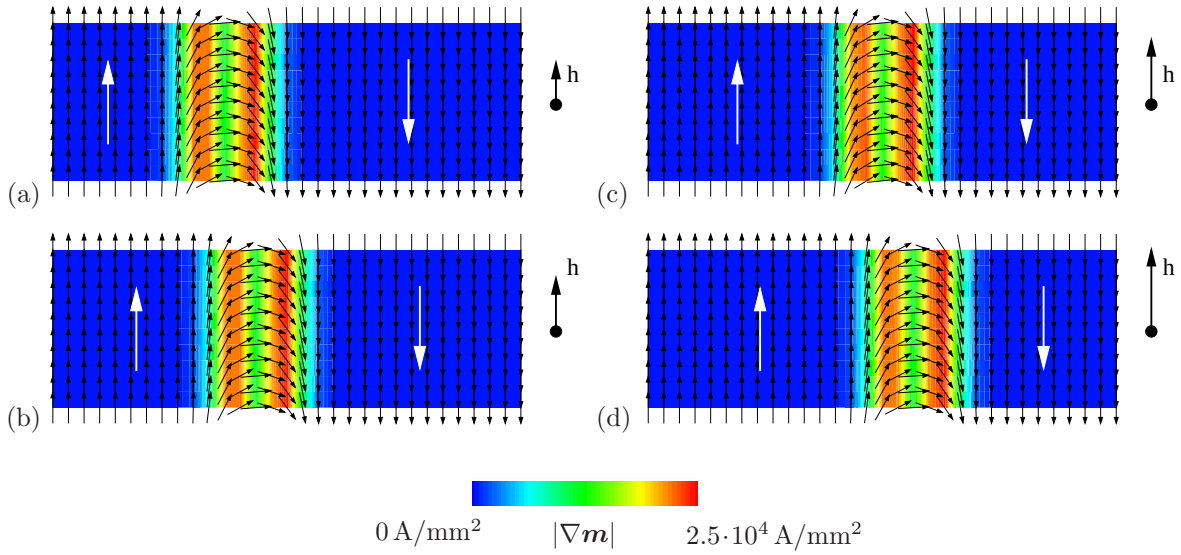

Figure 4.5: Example demonstrating rotation of magnetization. The evolution of the magnetization is governed by the Landau-Lifschitz function. The magnetic domains that result are purely a consequence of the *rotation of the magnetization* as can be observed by focussing on the magnetization vectors within the domain wall in the four snapshots.

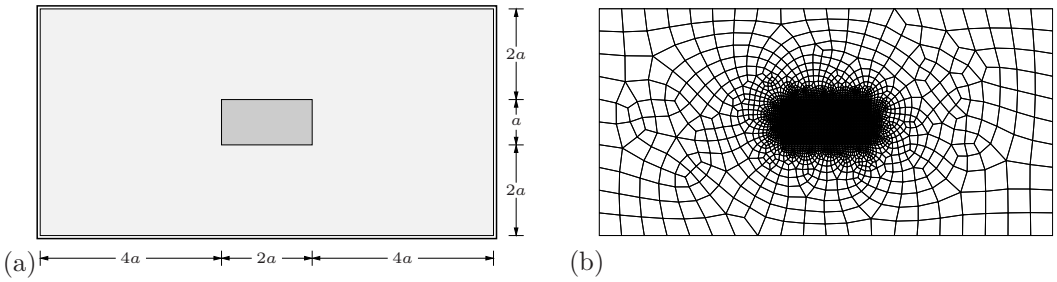

Figure 4.6: (a) Boundary-value-problem and (b) discretization of free space box Ω. The solid part is discretized by a structured mesh with 60×30 quad finite elements while for the surrounding free space, a coarse unstructured mesh is used. Here $a = 100\mu$m.

Figure 4.5(a) shows the initial conditions for the magnetization with the ferromagnetic body containing two magnetic domains, each along the easy directions. The magnetization vector field is shown by the arrows with their midpoints anchored at the nodes. The Euclidean norm of the gradient of this magnetization vector field is plotted in the background in color. The white arrows show the direction of the magnetization in each domain. We initialize the magnetization such that the 180° domain wall is to the left of the center of the sample. When the applied magnetic field $\overline{\boldsymbol{h}}$ is directed upwards, it causes the domain on the left to grow in size at the expense of the other. This *domain growth* is accompanied by the movement of the magnetic domain wall which travels towards the right as shown in the four snapshots of the simulation in Figure 4.5. The objective of this numerical example is to show that the domain wall motion is a result of *rotation* of the magnetization vectors. This evolution of the magnetization vector field is of course governed by the Landau-Lifschitz equation (4.63). Bringing the attention of the reader to this fact is precisely the aim of this example since the description of the rotation is characteristic of the specific discretization and numerical solution approach that has been described in this work.

4.6.2. Formation of Magnetic Domains in Thin Film of Permalloy

For our second example, we consider the initial boundary value problem as shown in Figure 4.6. The entire domain Ω is discretized using 3616 elements out of which, as stated in Figure 4.6, a structured mesh of 1800 elements (60×30 elements) is used to discretize the region occupied by the solid $\mathcal{B}$. The surrounding free space is discretized by a coarse unstructured mesh. We start with a random initial distribution of the magnetic moment over the domain and then observe how it evolves with time under the absence of an applied magnetic field. The material parameters chosen, match those of Permalloy and are stated in Table 4.1.

The simulation results are shown in Figure 4.7 where the magnetic moment and its gradient are depicted at different times. Note that for the purpose of clarity, these are pictures zoomed in to include only the solid body. Starting from Figure 4.7(a), with a completely random configuration, we see the microstructure progressively develop through Figure 4.7(b) and (c) to (d). Figure 4.7(d) shows the final state when the magnetic moment distribution has reached an equilibrium configuration. One can observe the formation of two vortices and a single anti-vortex in between, which forms a single *cross-tie* unit, see Kuepper et al. [96], Miguel et al. [122] for experimental results and Figure 4.9 for a sketch of experimental observation in Rave & Hubert [130].

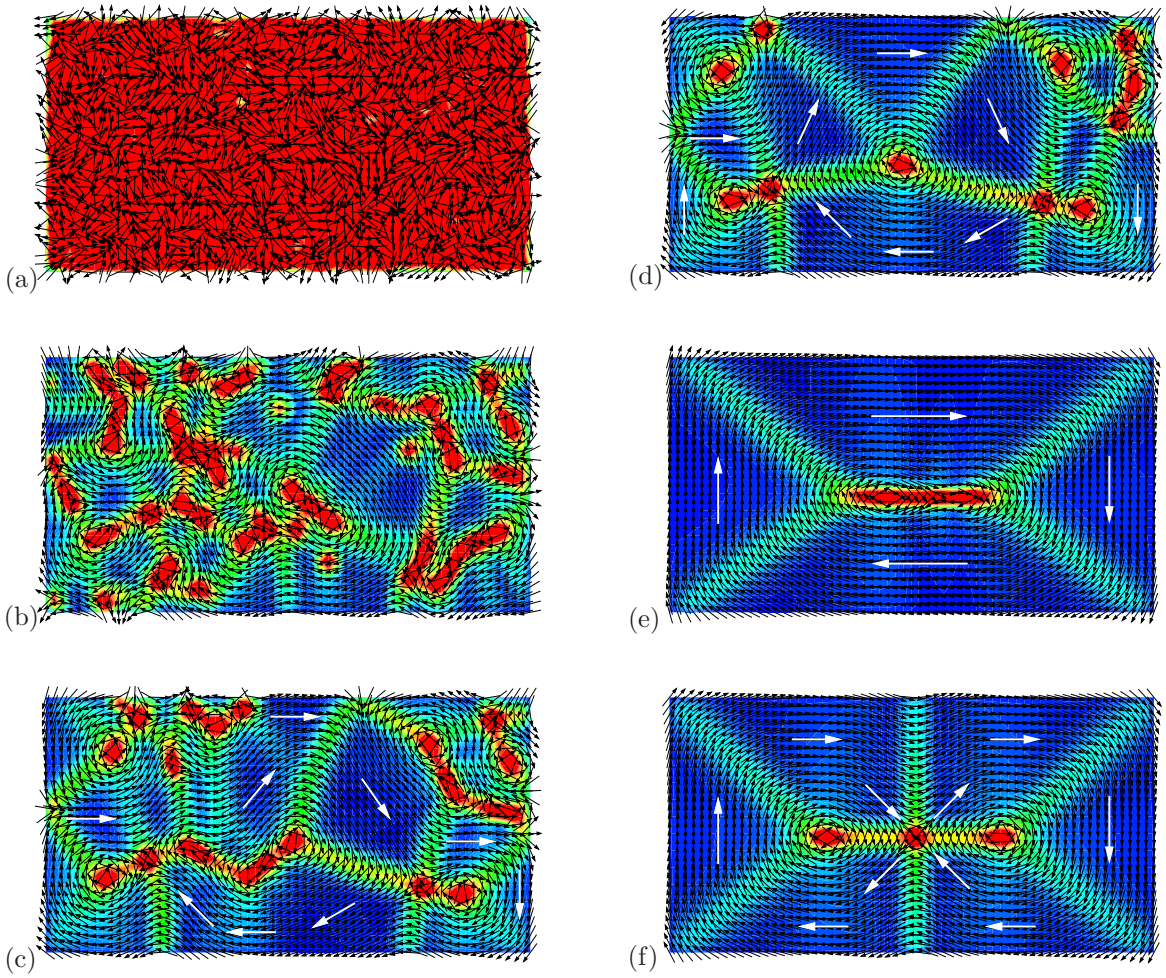

Figure 4.7: Evolution of magnetization in the sample with no applied load. Start with (a) random initial configuration, progressing through (b)–(e) , to reach (f) equilibrium or ground state. Note that magnetic domains can be observed in the final state although the net magnetization of the specimen as a whole is zero. The tendency of the system to reduce the magnetostatic energy, while respecting the constraint on $|\boldsymbol{m}|$, explains the formation of vortices and closure domains with domains pointing even in non-easy directions.

The formation of the specific domain structure cannot be explained by solely considering the competing effects of tendency of the magnetic moment to align in the easy directions (anisotropy energy) and the tendency to reduce domain wall energy, since it would not explain why we have domains in a non-easy direction as seen near the shorter edges of the body. The effect here that is to be considered, is the magnetostatic energy that favors the formation of *closure domains* so that no magnetic poles are formed. This is also a motivating factor to consider the energy stored in the free space since the magnetostatic energy is the only component of the free energy that exists in the free space as well. In order to visualize this, we have presented the final configuration of the magnetization of the body in its free space box in Figure 4.8. Such closure domains in uniaxial materials are typical to materials such as Permalloy where the magnetic anisotropy is very low. The width of the domain walls is related to the exchange coefficient A. From the numerical

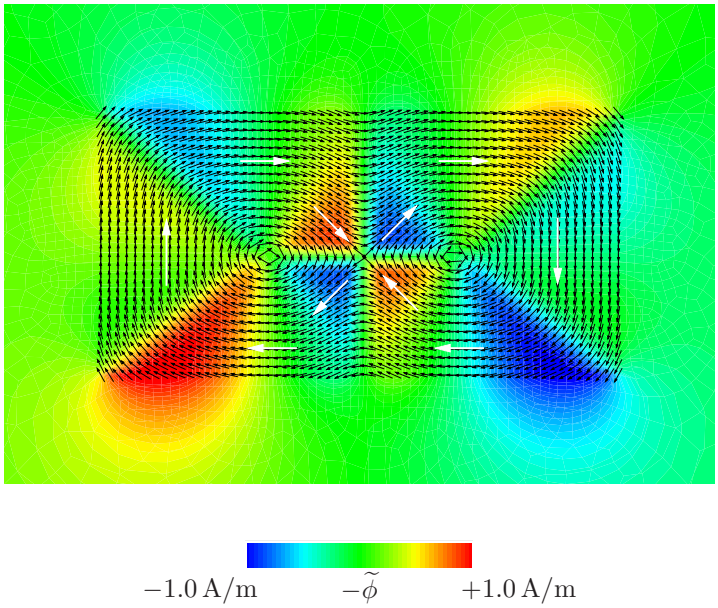

Figure 4.8: Zoomed in picture of the final ground state configuration obtained by relaxing the system. The plot shows the magnetization director vector field $\boldsymbol{m}$ and the associated magnetic potential $\widetilde{\phi}$ of the sample and a part of the adjoining free-space that surrounds it.

perspective however, this material parameter influences the maximum element size that can be used to discretize the body since the mesh must be fine enough to capture the spatial variation of the order parameter, failing which, no walls would be observed. In this example, the edge length of the elements used to discretize the body is

$$h = 1 \times 10^{-6}/30 = 3.3333 \times 10^{-2} \mu\text{m} \ , \tag{4.114}$$

and consequently one observes that the domain walls that are obtained span over at least two or more elements i.e. the width is at least two times h. Although the present simulation starts with a hypothetical initial configuration, its purpose is to arrive at a configuration that is stable and therefore being representative of a realistic microstructure or *ground state* which may serve as a starting point for further simulations. One must make note of the size and geometry dependencies of the ground state configuration that is obtained. Clearly quite different configurations are possible in a sample having a different geometry, say, for example a square which might be expected to have a single vortex. Also, staying with a rectangular shape, one may observe the formation of more than one cross-tie

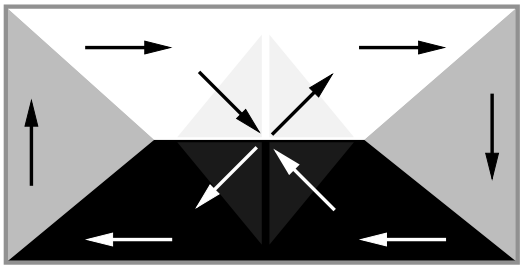

Figure 4.9: Sketch of the contrast image of one of the investigated magnetization patterns for a rectangular thin-film element obtained from Rave & Hubert [130], p. 3887. Such images are obtained by Kerr or Lorentz microscopy and are also captured in the simulation, cf. simulation in Figure 4.7(f).

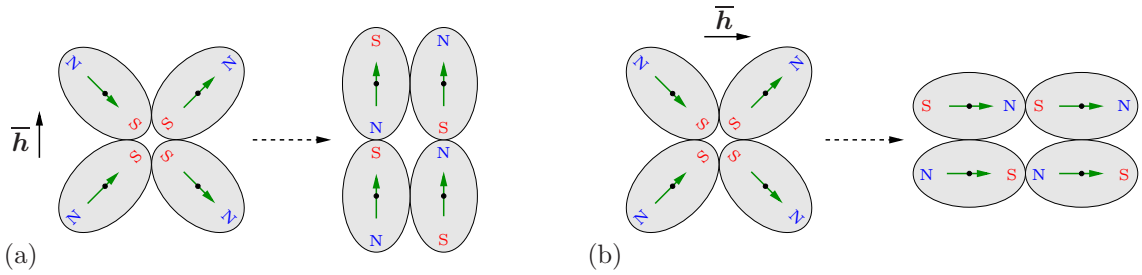

Figure 4.10: Schematic sketch of magnetization of a sample by applying a magnetic field $\bar{\boldsymbol{h}}$. The black dots represent the atomic nucleus, the ellipse represents the electron cloud around it, and the arrows indicate the dipole moment of the atom which is of a fixed magnitude. The application of the magnetic field causes an ordering of the magnetic moments as shown.

units arranged sequentially for longer geometries. For more details on observed magnetic domains and size dependency on ground state configuration, please refer to the works of Hubert & Schäfer [72], Rave & Hubert [130] and Schabes & Bertram [137].

4.6.3. Growth of Magnetic Domains in Thin Permalloy Sample

The following numerical simulation shows domain wall motion in a magnetic field driven process. A simplified sketch of the basic mechanism is shown in Figure 4.10. The initial conditions are taken from the *ground state* (same as in Figure 4.8) which was the result of the first example and is shown again in Figure 4.11(a). An applied magnetic field $\overline{\boldsymbol{h}}$ along the length of the magnetic material and in the direction as shown in the figure, is made to undergo a monotonic increase in magnitude over time. The model parameters are the same as in the previous example since we are dealing with the same material and we use a time step of 1s for the magnetic loading.

Figure 4.11 shows a zoomed in picture of the magnetization director vector field and the associated magnetic potential $\widetilde{\phi}$ in the body and in a part of the free space that surrounds it from initial to final states. One can observe that the domain walls move in such a way so as to accommodate a greater region that has a magnetization in the direction of the applied magnetic field $\overline{\boldsymbol{h}}$. During this movement, it is also of interest to note how the magnetization closer to the domain walls *rotate* into their new positions to occupy another energetically favorable direction. This motion is observed until the domain walls are completely driven out of the body leading to the final state that has the magnetization directed in the direction of the applied magnetic field $\overline{\boldsymbol{h}}$ almost uniformly throughout except at the corners where the magnetization points in a direction so as to reduce the magnetostatic energy. This is the *single domain state* also known as the *flower state* since the magnetization points outwards at the corners like petals, see Schabes & Bertram [137], Hubert & Schäfer [72]. In Figure 4.12 we see the contour plot of the magnetic potential generated by the body's magnetization $\widetilde{\phi}$ in Ω, along with the equipotential lines, which shows quite clearly that the body has been magnetized by the applied magnetic field.

4.6.4. Magnetic Domain Evolution in Stress-Driven Loading

When applying an external stress to a ferromagnetic material, we also observe a change in the magnetic domain structure. In order to show that our formulation captures this effect, we report in Figure 4.14 the simulation results of the application of mechanical stress on the domain $\mathcal{B}$ in a cyclic manner. A simplified sketch of the basic mechanism

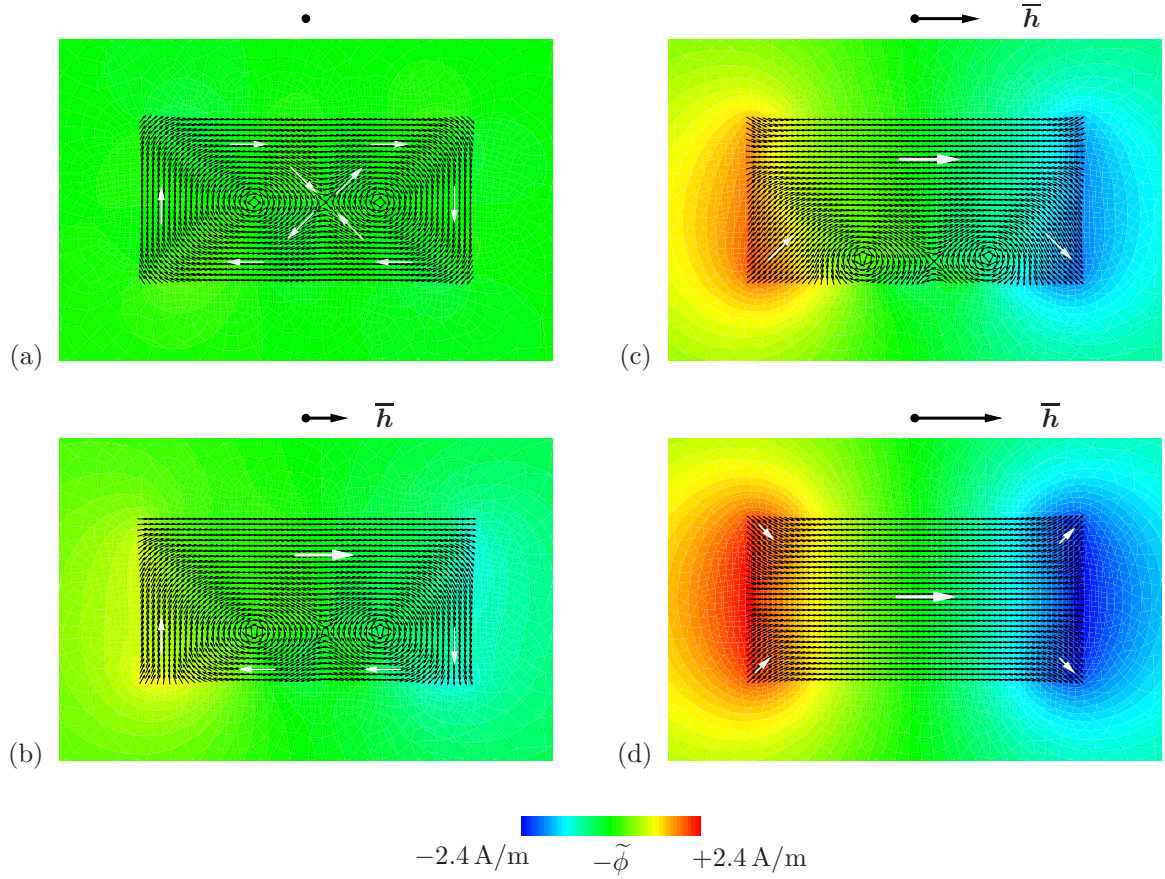

Figure 4.11: The plot shows the magnetization director vector field $\boldsymbol{m}$ and the associated magnetic potential $\widetilde{\phi}$ in a part of the adjoining free space. The final state obtained is called the *flower state* with the specimen almost uniformly magnetized. The magnetization pointing away from the easy-directions at the corners is due to the tendency to reduce magnetostatic energy.

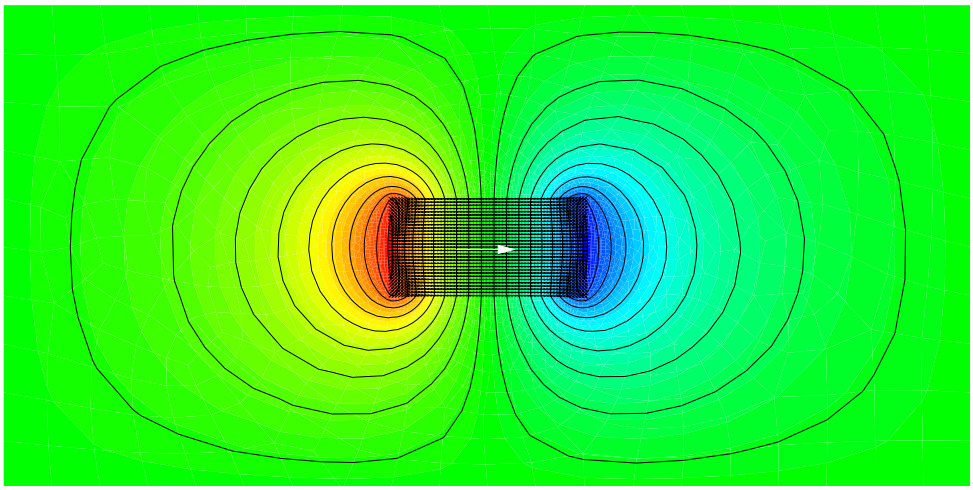

Figure 4.12: Final flower state configuration obtained by starting from the ground state and then applying the magnetic field $\overline{\boldsymbol{h}}$ of increasing magnitude in the horizontal direction. The plot shows the sample with the associated magnetic potential $\widetilde{\phi}$ and its equipotential lines in the free space box Ω.

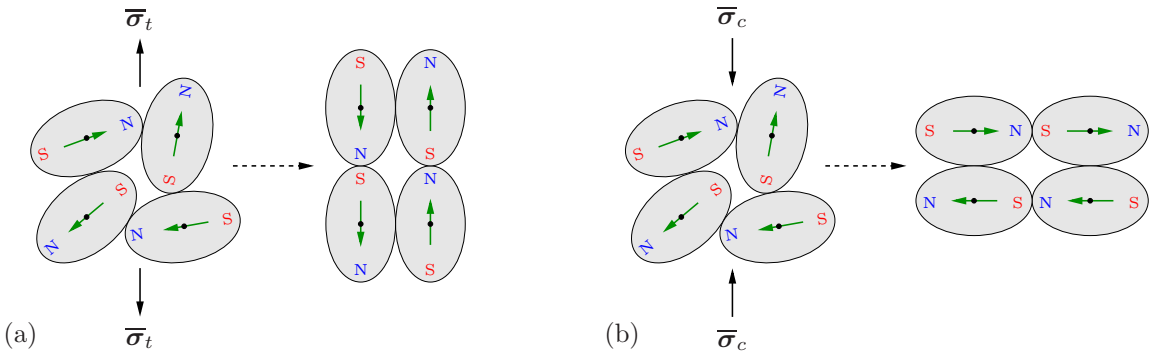

Figure 4.13: Schematic sketch for the effect of stress on magnetic domain structure of a sample. The black dots represent the atomic nucleus, the ellipse represents the electron cloud around it, and the arrows indicate the dipole moment of the atom which is of a fixed magnitude. The application of stress causes an ordering of the magnetic moments as shown for the (a) tensile and (b) compressive cases.

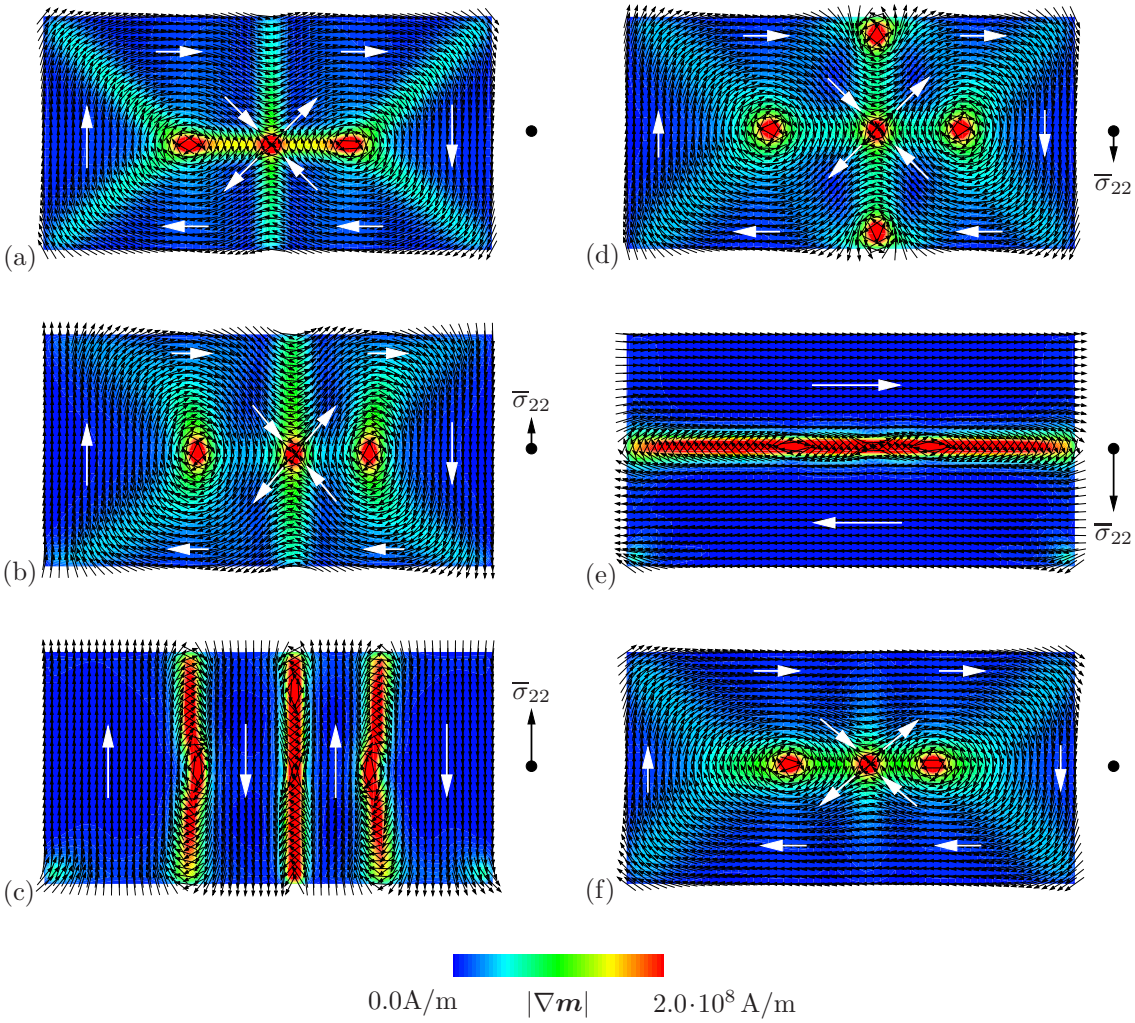

Figure 4.14: Evolution of magnetic domains caused by cyclic tensile and compressive loading. The direction of the magnetization has been indicated within their respective domains. The relative amount of the loading stress $\overline{\sigma}_{22}$ has been plotted adjacent to each snapshot. The snapshots are at times $t = 0s$, $t = 10s$, $t = 20s$, $t = 40s$, $t = 60s$ and $t = 80s$.

is shown in Figure 4.13. Once again Permalloy is the material of choice to observe this effect. The reason lies in the rather low crystal anisotropy and positive magnetostriction of Permalloy.

We start with the same ground state that was obtained as a result of relaxing the random configuration in our second example. We then apply a stress that varies with time also shown in Figure 4.14. In the tensile part of the loading process, we observe that the magnetic domains align in the direction of the load. Starting from the ground state in Figure 4.14(a), we observe that the domains in the direction of the loading are preferred and grow in size gradually from Figure 4.14(a) to Figure 4.14(c).

During the unloading to compression stage one observe that the contrary happens. Firstly we return to a structure similar to the ground state and then we find that the domains that are perpendicular to the loading direction are preferred. Consequently their size grows and we reach the state Figure 4.14(e) which shows that the magnetization in the sample is directed only along the axis perpendicular to the previous case. In this case, these directions coincide with the easy directions of the material.

To summarize, it is important to note that starting from the ground state or demagnetized state, the applied mechanical stress alone is capable of causing domain wall motion only in such a way that ensures zero net magnetization for the whole specimen. This condition is not difficult to meet since there are an infinite number of arrangements of magnetic domains that allow a zero net magnetic moment. Additionally, from the first part of the loading process which involves a tensile load orthogonal to the easy axis, it is apparent that stress alone can create an easy axis of magnetization. The reader is referred to Cullity [28], Chapter 8 for a more complete theoretical background to the effect of stress on magnetization.

5. A Projection Method for Micro-Magneto-Elasticity

In this chapter we present an alternative "divide and conquer" strategy and attack the micro-magneto-elastic problem with an operator split approach. The resulting staggered scheme for solving the coupled problem with geometric constraints, is embedded within a finite element framework. It relies on a post-processing re-normalization step of the magnetization director in order to satisfy the unity constraint. The sub-algorithms of the solution strategy are derived from variational principles and the corresponding potentials are obtained from the original potential in the previous chapter. The use of standard linear updates followed by the re-normalization makes the implementation much easier than the geometrically exact method outlined in the previous chapter and in Miehe & Ethiraj [115]. This is highlighted by the three dimensional simulations in the numerical examples of this chapter. Thus we outline the details related to the implementation and present a comparison of the current method with respect to the geometrically exact method.

5.1. Variational Principles for Micro-Magneto-Elasticity

5.1.1. Variational Formulation for Dynamic Problems

For dynamic problems, which govern the evolution in time of the magnetization in the solid, Miehe & Ethiraj [115] presents a *rate-type variational principle*, that governs the rates $\{\dot{\boldsymbol{u}}, \dot{\boldsymbol{m}}, \dot{\widetilde{\phi}}\}$ at a *given* state $\{\boldsymbol{u}, \boldsymbol{m}, \widetilde{\phi}\}$. This treatment also includes the *kinetics* of the magnetization, which is assumed to be dissipative in nature. It is described by the dissipation potential functional D introduced in (4.43). Based on the energy-enthalpy functional (4.41), the dissipation potential (4.42), the mechanical loading functional (4.17) and the magnetic loading functional (4.24), we define the rate-type *dynamic magneto-elastic potential*

$$\Pi'_{dyn}(\dot{\boldsymbol{u}}, \dot{\boldsymbol{m}}, \dot{\widetilde{\phi}}; t) := \frac{d}{dt} E'(\boldsymbol{u}, \boldsymbol{m}, \widetilde{\phi}) + D(\dot{\boldsymbol{m}}) - L_{\overline{\boldsymbol{\sigma}}}(\dot{\boldsymbol{u}}; t) - L_{\overline{\boldsymbol{h}}}(\dot{\boldsymbol{m}}; t) \tag{5.1}$$

at a given state $\{\boldsymbol{u}, \boldsymbol{m}, \widetilde{\phi}\}$. Note the appearance of the dissipation functional D in the potential. Using integration by parts, the rate functional takes the explicit form

$$\begin{aligned}
\Pi'_{dyn} = &\int_{\mathcal{B}} -\operatorname{div}[\partial_{\nabla_s \boldsymbol{u}} \Psi_{mat}] \cdot \dot{\boldsymbol{u}}\, dV + \int_{\mathcal{B}} \big([\delta_{\boldsymbol{m}} \Psi_{mat} - \kappa_0 m_s (\overline{\boldsymbol{h}} - \nabla \widetilde{\phi})] \cdot \dot{\boldsymbol{m}} + \frac{\eta}{2} \dot{\boldsymbol{m}} \cdot \dot{\boldsymbol{m}} \big)\, dV \\
&+ \int_{\partial\mathcal{B}} \big([\partial_{\nabla_s \boldsymbol{u}} \Psi_{mat} - \overline{\boldsymbol{\sigma}}] \cdot \boldsymbol{n} \big) \cdot \dot{\boldsymbol{u}}\, dA + \int_{\partial\mathcal{B}_{\mathfrak{h}}} (\partial_{\nabla \boldsymbol{m}} \Psi_{mat} \cdot \boldsymbol{n}) \cdot \dot{\boldsymbol{m}}\, dA \\
&- \int_{\Omega} \kappa_0 \operatorname{div}[-\nabla \widetilde{\phi} + \hat{m}_s \boldsymbol{m}] \dot{\widetilde{\phi}}\, dV + \int_{\partial\mathcal{B}} \kappa_0 \big([\![-\nabla \widetilde{\phi} + \hat{m}_s \boldsymbol{m}]\!] \cdot \boldsymbol{n} \big) \dot{\widetilde{\phi}}\, dA \,.
\end{aligned} \tag{5.2}$$

Note that this functional is linear in the rates $\{\dot{\boldsymbol{u}}, \dot{\boldsymbol{m}}, \dot{\widetilde{\phi}}\}$ up to the quadratic term $\eta \dot{\boldsymbol{m}} \cdot \dot{\boldsymbol{m}}/2$, which comes form the dissipation function. We assume that the *rates* of the displacement, the magnetization director, and the magnetic potential at a given state are governed by

the variational principle

$$\boxed{\{\dot{\boldsymbol{u}}, \dot{\boldsymbol{m}}, \dot{\widetilde{\phi}}\} = \arg\Big\{ \inf_{\dot{\boldsymbol{u}}\in\mathcal{R}^d} \inf_{\dot{\boldsymbol{m}}\in T_{\boldsymbol{m}}\mathcal{S}^{d-1}} \sup_{\dot{\widetilde{\phi}}\in\mathcal{R}} \Pi'_{dyn}(\dot{\boldsymbol{u}}, \dot{\boldsymbol{m}}, \dot{\widetilde{\phi}}; t)\Big\} .} \tag{5.3}$$

Note carefully, that this variational principle accounts for the geometric structure of the magnetization. As a consequence of $\boldsymbol{m} \in \mathcal{S}^{d-1}$, we have $\dot{\boldsymbol{m}} \in T_{\boldsymbol{m}}\mathcal{S}^{d-1}$ where $T_{\boldsymbol{m}}\mathcal{S}^{d-1}$ is the *tangent space* of $\mathcal{S}^{d-1}$ at $\boldsymbol{m}$ as depicted in Figure 4.4. As a consequence, we have

$$\delta\dot{\boldsymbol{m}} \;=\; \delta\boldsymbol{\omega} \times \boldsymbol{m} \tag{5.4}$$

for the variation of the rate of the magnetization director at fixed $\boldsymbol{m}$. Then, the necessary condition of the above principle is provided by the variation

$$\begin{aligned}
\delta\Pi'_{dyn} = &\int_{\mathcal{B}} -\operatorname{div}[\partial_{\nabla_s\boldsymbol{u}}\Psi_{mat}]\cdot\delta\dot{\boldsymbol{u}}\,dV + \int_{\mathcal{B}} \big(\boldsymbol{m}\times[\delta_{\boldsymbol{m}}\Psi_{mat} - \kappa_0 m_s(\overline{\boldsymbol{h}} - \nabla\widetilde{\phi}) + \eta\dot{\boldsymbol{m}}]\big)\cdot\delta\boldsymbol{\omega}\,dV \\
&+ \int_{\partial\mathcal{B}} \big([\partial_{\nabla_s\boldsymbol{u}}\Psi_{mat} - \bar{\boldsymbol{\sigma}}]\cdot\boldsymbol{n}\big)\cdot\delta\dot{\boldsymbol{u}}\,dA + \int_{\partial\mathcal{B}_{\mathfrak{h}}} \big[\boldsymbol{m}\times(\partial_{\nabla\boldsymbol{m}}\Psi_{mat}\cdot\boldsymbol{n})\big]\cdot\delta\boldsymbol{\omega}\,dA \\
&- \int_{\Omega} \kappa_0 \operatorname{div}[-\nabla\widetilde{\phi} + \hat{m}_s\boldsymbol{m}]\cdot\delta\dot{\widetilde{\phi}}\,dV + \int_{\partial\mathcal{B}} \kappa_0\big([\![-\nabla\widetilde{\phi} + \hat{m}_s\boldsymbol{m}]\!]\cdot\boldsymbol{n}\big)\delta\dot{\widetilde{\phi}}\,dA
\end{aligned} \tag{5.5}$$

for the virtual fields $\{\delta\dot{\boldsymbol{u}}, \delta\boldsymbol{\omega}, \delta\dot{\widetilde{\phi}}\}$ with $\delta\boldsymbol{\omega} = \boldsymbol{0}$ on $\partial\mathcal{B}_{\boldsymbol{m}}$ and $\delta\dot{\widetilde{\phi}} = 0$ on $\partial\Omega$. Thus, we arrive at the Euler equations

$$\begin{aligned}
\operatorname{div}[\partial_{\nabla_s\boldsymbol{u}}\Psi_{mat}] &= \boldsymbol{0} \quad \text{in } \mathcal{B} \\
\boldsymbol{m}\times[\delta_{\boldsymbol{m}}\Psi_{mat} - \kappa_0 m_s(\overline{\boldsymbol{h}} - \nabla\widetilde{\phi}) + \eta\dot{\boldsymbol{m}}] &= \boldsymbol{0} \quad \text{in } \mathcal{B} \\
\operatorname{div}[-\nabla\widetilde{\phi} + \hat{m}_s\boldsymbol{m}] &= 0 \quad \text{in } \Omega
\end{aligned} \tag{5.6}$$

along with the boundary conditions

$$\partial_{\nabla_s\boldsymbol{u}}\Psi_{mat}\cdot\boldsymbol{n} = \overline{\boldsymbol{\sigma}}\cdot\boldsymbol{n} \;\text{ on } \partial\mathcal{B} \quad \text{and} \quad \partial_{\nabla\boldsymbol{m}}\Psi_{mat}\cdot\boldsymbol{n} = \boldsymbol{0} \;\text{ on } \partial\mathcal{B}_{\mathfrak{h}} \tag{5.7}$$

the jump condition

$$[\![-\nabla\widetilde{\phi} + \hat{m}_s\boldsymbol{m}]\!]\cdot\boldsymbol{n} = 0 \;\text{ on } \partial\mathcal{B} \tag{5.8}$$

at the interface between the solid domain and the surrounding free space, and the field equation

$$\Delta\widetilde{\phi} = 0 \;\text{ in } \Omega\setminus\mathcal{B} \tag{5.9}$$

in the surrounding free space $\Omega\setminus\mathcal{B}$, where $\Delta(\cdot) = \operatorname{div}[\operatorname{grad}[(\cdot)]]$ is the Laplace operator. Here, we introduced the variational or functional derivative of the free energy functions with respect to the magnetization director

$$\delta_{\boldsymbol{m}}\Psi_{mat} := \partial_{\boldsymbol{m}}\Psi_{mat} - \operatorname{div}\left[\partial_{\nabla\boldsymbol{m}}\Psi_{mat}\right] . \tag{5.10}$$

Note that $(4.49)_1$ and $(4.49)_3$ reflect the stress equilibrium equation and the third Maxwell equation. Equation $(4.49)_2$ governs the evolution of the magnetization which *satisfies the*

constraint on the magnetization director a priori. Taking the cross product of $(4.49)_2$ with the vector $\boldsymbol{m}$, we end up with the evolution equation for the magnetization director

$$\dot{\boldsymbol{m}} = \frac{1}{\eta}\boldsymbol{m} \times \left(\boldsymbol{m} \times [\delta_{\boldsymbol{m}}\Psi_{mat} - \kappa_0 m_s(\overline{\boldsymbol{h}} - \nabla\widetilde{\phi})]\right) \text{ in } \mathcal{B} \,. \tag{5.11}$$

This is consistent with the Landau-Lifschitz equation, see Landau & Lifschitz [100]. It contains the damping term of the Landau-Lifschitz-Gilbert equation for non-stationary micromagnetics, see Gilbert [62]. Note that this evolution equations satisfies the constraint $\dot{\boldsymbol{m}} \cdot \boldsymbol{m} = 0$. The boundary value problem of dynamic, quasi-static micromagnetics is governed by equations (5.6)–(5.7), where $(5.6)_2$ is replaced by the Landau-Lifschitz equation (5.11).

5.1.2. Decoupling via Operator Split

The variational statement which was recapped above, was shown to lead to a monolithic solution of the primary variables in our previous work Miehe & Ethiraj [115]. Now an operator split is introduced, where we consider the nonlinear coupled partial differential equations to be split into two groups within a time-interval $[t_n, t_{n+1}]$. This operator split methodology has been already successfully adopted for thermoelastic problems in Simo & Miehe [143] and Miehe [112, 113]. Here we algorithmically decouple the magnetization evolution equation from the other differential equations by first solving for the magnetization keeping the displacement and magnetic potential fixed.

5.1.2.1. Magnetic Predictor. We have the first split or first set of equations in which the rates of the displacements and magnetic potential are frozen, while the time evolution equation for the magnetization is kept "active"

$$\begin{aligned} \dot{\boldsymbol{u}} &= \boldsymbol{0} \quad \text{in } \mathcal{B} \\ \delta_{\boldsymbol{m}_{pre}}\Psi_{mat} - \kappa_0 m_s(\overline{\boldsymbol{h}} - \nabla\widetilde{\phi}) + \eta\dot{\boldsymbol{m}}_{pre} &= \boldsymbol{0} \quad \text{in } \mathcal{B} \\ \dot{\widetilde{\phi}} &= 0 \quad \text{in } \Omega \end{aligned} \tag{5.12}$$

with the boundary condition on $\boldsymbol{m}_{pre}$ corresponding to the *active* differential equation as

$$\partial_{\nabla\boldsymbol{m}}\Psi_{mat} \cdot \boldsymbol{n} = \boldsymbol{0} \;\; \text{on } \partial\mathcal{B}_{\mathfrak{h}} \tag{5.13}$$

Note that the evolution equation $(5.12)_2$ differs from $(4.49)_2$ in that the latter, unlike the former, satisfies the constraint $|\boldsymbol{m}| = 1$ apriori. In order to *correct* this, a projection of the magnetization directors is proposed.

5.1.2.2. Magnetic Corrector. The magnetic corrector step is a *post-processing* step that ensures $\boldsymbol{m} \in \mathcal{S}^{d-1}$. This is done by a projection step on all magnetizations

$$\boldsymbol{m} = f(\boldsymbol{m}_{pre}) := \boldsymbol{m}_{pre}/|\boldsymbol{m}_{pre}| \,. \tag{5.14}$$

With the updated (and normalized) magnetization director, the displacements and magnetic potential need to be obtained. This is solved for in a monolythic manner.

5.1.2.3. Magnetomechanical Corrector. We now consider the second split comprising the mechanical equilibrium and Gauss' Law while the magnetization is frozen at the

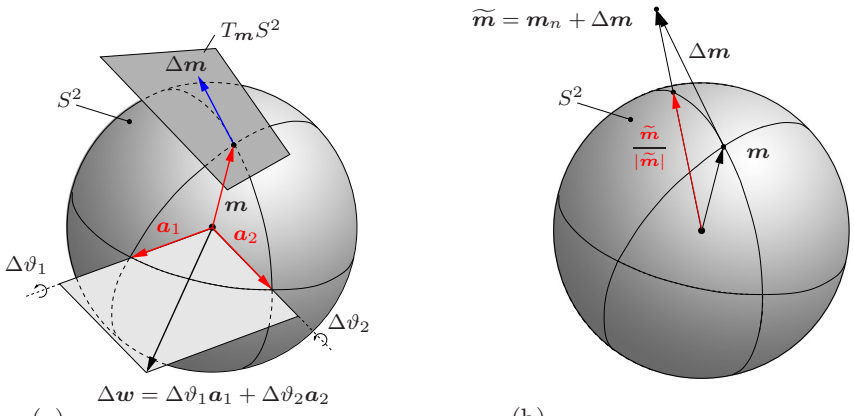

Figure 5.1: Illustration of the update methods for the magnetization director. (a) The exponential update in Miehe & Ethiraj [115] calculates an increment $\Delta\boldsymbol{m}$ that lies in the tangent space defined by $\boldsymbol{a}_1$ and $\boldsymbol{a}_2$. (b) The projection method in the current work provides a substantially simplified alternative to maintain the unity constraint on the magnetization director by employing a post-processing normalization step.

value that is obtained after the magnetic corrector step. Thus,

$$\begin{aligned} \operatorname{div}[\partial_{\nabla_s \boldsymbol{u}} \Psi_{mat}] &= \boldsymbol{0} \quad \text{in } \mathcal{B} \\ \dot{\boldsymbol{m}} &= \boldsymbol{0} \quad \text{in } \mathcal{B} \\ \operatorname{div}[-\nabla\widetilde{\phi} + m_s \boldsymbol{m}] &= 0 \quad \text{in } \mathcal{B} \end{aligned} \tag{5.15}$$

along with the boundary and jump conditions

$$\partial_{\nabla_s \boldsymbol{u}} \Psi_{mat} \cdot \boldsymbol{n} = \overline{\boldsymbol{\sigma}} \cdot \boldsymbol{n} \ \text{ on } \partial\mathcal{B} \quad \text{and} \quad [\![-\nabla\widetilde{\phi} + \hat{m}_s \boldsymbol{m}]\!] \cdot \boldsymbol{n} = 0 \ \text{ on } \partial\mathcal{B} \tag{5.16}$$

respectively. We also include the field equation in the surrounding free space $\Omega \setminus \mathcal{B}$

$$\Delta\widetilde{\phi} = 0 \ \text{ in } \Omega \setminus \mathcal{B} \, . \tag{5.17}$$

In this manner, the coupled differential equations governing the problem have been split into two partitions and one intermediate post-processing operation. This will form the basis of developing incremental variational principles for a staggered solution scheme of the coupled problem.

5.2. Time-Discrete Incremental Variational Formulations

5.2.1. Time-Discrete Field Variables in Incremental Setting

We now outline variational principles for time-discrete problems. To this end, we consider the values of the field variables at the discrete times $0, t_1, \ldots, t_n, t_{n+1}, \ldots, T$ of the process interval $[0, T]$. In order to advance the solution within a typical time step, we focus on the finite time increment $[t_n, t_{n+1}]$, where

$$\tau_{n+1} := t_{n+1} - t_n > 0 \tag{5.18}$$

denotes the step length. In the subsequent treatment, all field variables at time t_n are assumed to be *known*. The goal then is to determine the fields at time t_{n+1} based on variational principles valid for the time increment under consideration. In particular, we

assemble the time-discrete spatial fields (displacement, magnetization, potential) at the discrete times t_n and t_{n+1} in the discrete solution vectors

$$\mathfrak{v}_{n+1} := \{\boldsymbol{u}_{n+1}, \boldsymbol{m}_{n+1}, \widetilde{\phi}_{n+1}\} \quad \text{and} \quad \mathfrak{v}_n := \{\boldsymbol{u}_n, \boldsymbol{m}_n, \widetilde{\phi}_n\} \ . \tag{5.19}$$

In order to obtain a compact notation we drop, in what follows, the subscript $n+1$ and consider all variables without subscript to be evaluated at time t_{n+1}. The link between the variables at the two time-discrete states is obtained in *iterative steps*, which must preserve the *geometric nature* of the variables involved. Here, the particular challenge is to preserve the property $\boldsymbol{m} \in \mathcal{S}^{d-1}$ of the magnetization director. While Miehe & Ethiraj [115] resorted to a nonlinear formulation in order to achieve this, we use here a linear formulation for the updates by taking advantage of an operator split.

We will now obtain a decoupled viewpoint which is contrasted with the subsection above. Furthermore, the constraint $\boldsymbol{m} \in \mathcal{S}^{d-1}$ is treated as a side condition. As a result of the partitioning of the coupled differential equations into the sets (5.12) and (5.15), our overall solution algorithm is composed of two sub-algorithms $ALGO_{\boldsymbol{m}}$ and $ALGO_{\boldsymbol{u}\widetilde{\phi}}$. Thus, within a single time step, we propose a *magnetic predictor-corrector step* $ALGO_{\boldsymbol{m}}$, for the magnetization directors $\boldsymbol{m}$ with *frozen* displacements $\boldsymbol{u}$ and magnetic potential $\widetilde{\phi}$, followed by a *magneto-mechanical corrector step* $ALGO_{\boldsymbol{u}\widetilde{\phi}}$ for displacements $\boldsymbol{u}$ and potential $\widetilde{\phi}$ with *frozen* magnetization director $\boldsymbol{m}$. This is symbolically written as

$$\boxed{ALGO_{tot} = ALGO_{\boldsymbol{u}\widetilde{\phi}} \circ ALGO_{\boldsymbol{m}}} \tag{5.20}$$

Each of these algorithms is shown to have an incremental variational nature and originate from the dynamic potential Π'_{dyn} in (4.57).

5.2.2. Magnetic Predictor-Corrector Algorithm $ALGO_{\boldsymbol{m}}$

The time-discrete incremental potential Π'^{τ}_{pre} for the first sub-problem is obtained by arresting the rates of the displacements $\dot{\boldsymbol{u}} = \boldsymbol{0}$ and magnetic potential $\dot{\widetilde{\phi}} = 0$ in the original potential. Therefore we get the predictor potential

$$\Pi'^{\tau}_{pre}(\boldsymbol{m}_{pre}) = Algo\Big\{ \int_{t_n}^{t_{n+1}} \Pi'_{dyn}(\dot{\boldsymbol{u}} = \boldsymbol{0}, \dot{\boldsymbol{m}}_{pre}, \dot{\widetilde{\phi}} = 0)\, dt \Big\} \ . \tag{5.21}$$

Now with these constraints, we integrate the above expression in the time interval $[t_n, t_{n+1}]$ assuming a *linear path* for the variable $\boldsymbol{m}_{pre}$ to get the potential

$$\Pi'^{\tau}_{pre}(\boldsymbol{m}_{pre}) = E'(\boldsymbol{u}_n, \boldsymbol{m}_{pre}, \widetilde{\phi}_n) - E'_n + \tau D([\boldsymbol{m}_{pre} - \boldsymbol{m}_n]/\tau) - \tau L_{\overline{\boldsymbol{h}}}([\boldsymbol{m}_{pre} - \boldsymbol{m}_n]/\tau) \ . \tag{5.22}$$

Note that $E'(\boldsymbol{u}_n, \boldsymbol{m}, \widetilde{\phi}_n)$ is a functional depending on the magnetization predictor field $\boldsymbol{m}_{pre}$ alone since the other two arguments are already known. Additionally, $E'_n = E'(\boldsymbol{u}_n, \boldsymbol{m}_n, \widetilde{\phi}_n)$ is a constant since it is evaluated on the basis of values at t_n. Insertion of the energy-enthalpy functional (4.41), dissipation functional (4.43), and magnetic loading functional (4.24) yield

$$\begin{aligned} \Pi'^{\tau}_{pre}(\boldsymbol{m}_{pre}) = &\int_{\mathcal{B}} \big(\Psi_{mat} + \kappa_0 m_s \boldsymbol{m}_{pre} \cdot \nabla\widetilde{\phi}_n\big)\, dV - \frac{\kappa_0}{2} \int_{\Omega} |\nabla\widetilde{\phi}_n|^2\, dV - E'_n \\ &+ \int_{\mathcal{B}} \frac{\eta}{2\tau} |\boldsymbol{m}_{pre} - \boldsymbol{m}_n|^2\, dV - \int_{\mathcal{B}} \kappa_0 m_s (\boldsymbol{m}_{pre} - \boldsymbol{m}_n) \cdot \overline{\boldsymbol{h}}\, dV \ . \end{aligned} \tag{5.23}$$

This gives us the potential associated with $ALGO_{\boldsymbol{m}}$. Thus we have the *magnetic predictor* algorithm as

$$ALGO^1_{\boldsymbol{m}} : \Big\{ \ \{\boldsymbol{m}_{pre}\} = \arg\Big\{ \inf_{\boldsymbol{m}_{pre}} \ \Pi'^{\tau}_{pre}(\boldsymbol{m}_{pre})\Big\} \tag{5.24}$$

where the incremental potential for the predictor step is defined in (5.23). Taking the first variation we get

$$\begin{aligned}\delta\Pi'^{\tau}_{pre} = &\int_{\mathcal{B}} [\delta_{\boldsymbol{m}_{pre}}\Psi_{mat} - \kappa_0 m_s(\overline{\boldsymbol{h}} - \nabla\widetilde{\phi}) + \eta[\boldsymbol{m}_{pre} - \boldsymbol{m}_n]/\tau] \cdot \delta\boldsymbol{m}_{pre}\, dV \\ &+ \int_{\partial\mathcal{B}_{\mathfrak{h}}} (\partial_{\nabla\boldsymbol{m}}\Psi_{mat} \cdot \boldsymbol{n}) \cdot \delta\boldsymbol{m}_{pre}\, dA \ .\end{aligned} \tag{5.25}$$

Clearly the necessary condition for the potential to be stationary implies the evolution equation in brackets to be zero together with Neumann type boundary conditions on $\partial\mathcal{B}_{\mathfrak{h}}$.

$$\eta(\boldsymbol{m}_{pre} - \boldsymbol{m}_n)/\tau + \big[\delta_{\boldsymbol{m}_{pre}}\Psi_{mat} - \kappa_0 m_s(\overline{\boldsymbol{h}} - \nabla\widetilde{\phi})\big] = \boldsymbol{0} \text{ in } \mathcal{B} \tag{5.26}$$

in the solid domain $\mathcal{B}$, along with the boundary condition

$$\partial_{\nabla\boldsymbol{m}_{pre}}\Psi_{mat} \cdot \boldsymbol{n} = \boldsymbol{0} \ \text{ on } \partial\mathcal{B}_{\mathfrak{h}} \ . \tag{5.27}$$

Note that (5.26) is a fully implicit update equation but does not obey $\boldsymbol{m}_{pre} \in \mathcal{S}^{d-1}$. We satisfy this by a *post-processing step* in which we project the magnetizations to the unit sphere $\mathcal{S}^{d-1}$ i.e.,

$$ALGO^2_{\boldsymbol{m}} : \{ \ \boldsymbol{m} = \boldsymbol{m}_{pre}/|\boldsymbol{m}_{pre}| \tag{5.28}$$

Thus we have the *magnetic predictor-corrector* algorithm summarized as

$$ALGO_{\boldsymbol{m}} = ALGO^2_{\boldsymbol{m}} \circ ALGO^1_{\boldsymbol{m}} : \begin{cases} \{\boldsymbol{m}_{pre}\} = \arg\Big\{ \inf_{\boldsymbol{m}_{pre}} \ \Pi'^{\tau}_{pre}(\boldsymbol{m}_{pre})\Big\} \\ \boldsymbol{m} = \boldsymbol{m}_{pre}/|\boldsymbol{m}_{pre}| \end{cases} \tag{5.29}$$

where the incremental potential for the predictor step is defined in (5.23). This is followed by the *magneto-mechanical corrector step* described next.

5.2.3. Magneto-Mechanical Corrector Algorithm $ALGO_{\boldsymbol{u}\widetilde{\boldsymbol{\phi}}}$

The output of the magnetization director field in the magnetic predictor step, serves as an input for the *magnetomechanical corrector step* $ALGO_{\boldsymbol{u}\widetilde{\phi}}$. We proceed in a similar manner as before and obtain the incremental potential Π'^{τ}_{cor} for this sub-problem by setting the rate of the magnetization director field to null, i.e. $\dot{\boldsymbol{m}} = \boldsymbol{0}$,

$$\Pi'^{\tau}_{cor}(\boldsymbol{u}, \widetilde{\phi}) = Algo\Big\{ \int_{t_n}^{t_{n+1}} \Pi'_{dyn}(\dot{\boldsymbol{u}}, \dot{\boldsymbol{m}} = \boldsymbol{0}, \dot{\widetilde{\phi}})\, dt \Big\} \ , \tag{5.30}$$

Integrating the expression over the time interval by assumming a linear path for the displacements and magnetic potential,

$$\Pi'^{\tau}_{cor}(\boldsymbol{u}, \widetilde{\phi}) = E'(\boldsymbol{u}, \boldsymbol{m}, \widetilde{\phi},) - E'_{cor} - \tau L_{\overline{\boldsymbol{\sigma}}}([\boldsymbol{u} - \boldsymbol{u}_n]/\tau) \ . \tag{5.31}$$

Note that $E'(\boldsymbol{u}, \boldsymbol{m}, \widetilde{\phi})$ is now a functional depending on the displacement field $\boldsymbol{u}$ and magnetic potential $\widetilde{\phi}$ for a *fixed magnetic director* $\boldsymbol{m}$, while $E'_{cor} = E'(\boldsymbol{u}_n, \boldsymbol{m}, \widetilde{\phi}_n)$ is a constant. Insertion of the energy-enthalpy functional (4.41) and mechanical loading functional (4.17) gives

$$\begin{aligned}\Pi'^{\tau}_{cor}(\boldsymbol{u}, \widetilde{\phi}) = &\int_{\mathcal{B}} \left(\Psi_{mat} + \kappa_0 m_s \boldsymbol{m} \cdot \nabla\widetilde{\phi}\right) dV - \frac{\kappa_0}{2}\int_{\Omega} |\nabla\widetilde{\phi}|^2\, dV - E'_n \\ &- \int_{\mathcal{B}} \overline{\boldsymbol{\sigma}} : \nabla_s[\boldsymbol{u} - \boldsymbol{u}_n] \cdot \overline{\boldsymbol{h}}\, dV\ .\end{aligned} \tag{5.32}$$

This gives us the potential associated with $ALGO_{\boldsymbol{u}\widetilde{\phi}}$. Taking the first variation yields

$$\begin{aligned}\delta\Pi'^{\tau}_{cor} = &\int_{\mathcal{B}} -\operatorname{div}[\partial_{\nabla_s \boldsymbol{u}}\Psi_{mat}] \cdot \delta\boldsymbol{u}\, dV + \int_{\partial\mathcal{B}} \left([\partial_{\nabla_s \boldsymbol{u}}\Psi_{mat} - \bar{\boldsymbol{\sigma}}] \cdot \boldsymbol{n}\right) \cdot \dot{\boldsymbol{u}}\, dA \\ &- \int_{\Omega} \kappa_0 \operatorname{div}[-\nabla\widetilde{\phi} + \hat{m}_s \boldsymbol{m}]\delta\widetilde{\phi}\, dV + \int_{\partial\mathcal{B}} \kappa_0 \left(\llbracket -\nabla\widetilde{\phi} + \hat{m}_s \boldsymbol{m}\rrbracket \cdot \boldsymbol{n}\right)\delta\widetilde{\phi}\, dA\ .\end{aligned} \tag{5.33}$$

Consequently we observe that the necessary condition for the stationarity of the potential Π'^{τ}_{cor} yields the mechanical equilibrium $(4.49)_1$ and the Gauss law $(4.49)_3$ as Euler equations.

$$\left.\begin{aligned}\operatorname{div}[\partial_{\nabla_s \boldsymbol{u}}\Psi_{mat}] &= \boldsymbol{0} \\ \operatorname{div}[-\nabla\widetilde{\phi} + m_s \boldsymbol{m}] &= 0\end{aligned}\right\} \text{ in } \mathcal{B} \tag{5.34}$$

in the solid domain $\mathcal{B}$, along with the boundary and jump conditions

$$\partial_{\nabla_s \boldsymbol{u}}\Psi_{mat} \cdot \boldsymbol{n} = \overline{\boldsymbol{\sigma}} \cdot \boldsymbol{n} \ \text{ on } \partial\mathcal{B} \quad \text{and} \quad \llbracket -\nabla\widetilde{\phi} + \hat{m}_s \boldsymbol{m}\rrbracket \cdot \boldsymbol{n} = 0 \ \text{ on } \partial\mathcal{B} \tag{5.35}$$

and the field equation

$$\Delta\widetilde{\phi} = 0 \ \text{ in } \Omega \setminus \mathcal{B} \tag{5.36}$$

in the free space. These Euler equations of the incremental variational principle are the *time-discrete, algorithmic counterparts* of the corresponding Euler equations of the rate-type, time-continuous variational principle. Thus we have the *magneto-mechanical corrector* for displacements $\boldsymbol{u}$ and potential $\widetilde{\phi}$ with *frozen* magnetization director $\boldsymbol{m}$

$$ALGO_{\boldsymbol{u}\widetilde{\phi}} : \left\{ \{\boldsymbol{u}, \widetilde{\phi}\} = \arg\left\{ \inf_{\boldsymbol{u}} \sup_{\widetilde{\phi}} \ \Pi'^{\tau}_{cor}(\boldsymbol{u}, \widetilde{\phi}) \right\} \right. \tag{5.37}$$

where the incremental potential for the corrector is given by (5.32). This step takes the post-processed magnetization director field as input and solves the mechanical equilibrium and Gauss' Law to deliver the displacements and magnetic potential.

5.3. Space-Time-Discrete Staggered Finite Element Solution

In this section we take a look at finite element implementation of the coupled problem in order to apply the variational principles derived above for solving boundary value problems over a finite domain Ω. Let $\mathfrak{T}^h$ denote a finite element triangulation of the domain Ω. The index h indicates a typical mesh size based on E^h finite element domains $\Omega^h_e \in \mathfrak{T}^h$ and N^h global nodal points.

Box 1: Staggered update scheme $ALGO_{tot} = ALGO_{\boldsymbol{u}\phi} \circ ALGO_{\boldsymbol{m}}$

1. GIVEN $\boldsymbol{d}_n$, the values of the nodal primary variables at t_n
2. Magnetic predictor step $ALGO_{\boldsymbol{m}}$
   - 2.1 Compute the tangent and residuum arrays of the predictor step
   $$\boldsymbol{R}_{\boldsymbol{m}} = \int_{\mathcal{B}} \boldsymbol{B}_{\boldsymbol{m}}^T \boldsymbol{S}_{\boldsymbol{m}}^h \, dV \quad \text{and} \quad \boldsymbol{K}_{\boldsymbol{m}} = \int_{\mathcal{B}} \boldsymbol{B}_{\boldsymbol{m}}^T \mathbb{C}_{\boldsymbol{m}}^h \boldsymbol{B}_{\boldsymbol{m}} \, dV$$
   - 2.2 Compute the update $\boldsymbol{d}_{\boldsymbol{m}} \Leftarrow \boldsymbol{d}_{\boldsymbol{m}} - \boldsymbol{K}_{\boldsymbol{m}}^{-1} \boldsymbol{R}_{\boldsymbol{m}}$
   - 2.3 Project magnetization directors onto unit sphere
   $$\boldsymbol{d}_{\boldsymbol{m}} \Leftarrow \boldsymbol{d}_{\boldsymbol{m}} / |\boldsymbol{d}_{\boldsymbol{m}}|$$
3. Magneto-mechanical corrector $ALGO_{\boldsymbol{u}\widetilde{\phi}}$
   - 3.1 Compute the tangent and residuum arrays of the corrector step
   $$\begin{aligned} \boldsymbol{R}_{\boldsymbol{u}\widetilde{\phi}} &= \int_{\mathcal{B}} \boldsymbol{B}_{\boldsymbol{u}\widetilde{\phi}}^T \boldsymbol{S}_{\boldsymbol{u}\widetilde{\phi}}^h \, dV - \int_{\Omega} \kappa_0 \boldsymbol{F}_{\widetilde{\phi}}^T \boldsymbol{F}_{\widetilde{\phi}} \boldsymbol{d}_{\boldsymbol{u}\widetilde{\phi}} \, dV \\ \boldsymbol{K}_{\boldsymbol{u}\widetilde{\phi}} &= \int_{\mathcal{B}} \boldsymbol{B}_{\boldsymbol{u}\widetilde{\phi}}^T \mathbb{C}_{\boldsymbol{u}\widetilde{\phi}}^h \boldsymbol{B}_{\boldsymbol{u}\widetilde{\phi}} \, dV - \int_{\Omega} \kappa_0 \boldsymbol{F}_{\widetilde{\phi}}^T \boldsymbol{F}_{\widetilde{\phi}} \, dV \end{aligned} \tag{5.38}$$
   - 3.2 Compute the update $\boldsymbol{d}_{\boldsymbol{u}\widetilde{\phi}} \Leftarrow \boldsymbol{d}_{\boldsymbol{u}\widetilde{\phi}} - \boldsymbol{K}_{\boldsymbol{u}\widetilde{\phi}}^{-1} \boldsymbol{R}_{\boldsymbol{u}\phi}$
4. SET $\boldsymbol{d}_n \Leftarrow \boldsymbol{d} = \boldsymbol{d}_{\boldsymbol{m}} \cup \boldsymbol{d}_{\boldsymbol{u}\widetilde{\phi}}$ GOTO 1.

5.3.1. Space-Time Discrete Magnetic Predictor-Corrector

We consider a partition of the state variables as $\mathfrak{c}_{\boldsymbol{m}} = \{\boldsymbol{m}, \nabla \boldsymbol{m}\}$ in terms of which we write the incremental potential

$$\Pi_{pre}^{\prime\tau} = \int_{\mathcal{B}} \pi_{pre}^{\prime\tau}(\mathfrak{c}_{\boldsymbol{m}}) \, dV + C_{pre} \ , \tag{5.39}$$

in terms of the *incremental magnetic predictor potential density per unit volume* of the solid domain $\mathcal{B}$ that reads,

$$\begin{aligned} \pi_{pre}^{\prime\tau}(\mathfrak{c}_{\boldsymbol{m}}) = \Psi_{mat}(\nabla_s \boldsymbol{u}_n, \boldsymbol{m}, \nabla \boldsymbol{m}) + \kappa_0 m_s \boldsymbol{m} \cdot \nabla \widetilde{\phi}_n \\ + \frac{\eta}{2\tau} |\boldsymbol{m} - \boldsymbol{m}_n|^2 - \kappa_0 m_s (\boldsymbol{m} - \boldsymbol{m}_n) \cdot \overline{\boldsymbol{h}} \end{aligned} \tag{5.40}$$

and a constant C_{pre} that includes non-essential contributions at a time t_n. Assuming a triangulation $\mathfrak{T}^h$ of the full domain Ω with N^h nodal points, we consider a magnetic

partition of the primary variables that contains the nodal magnetization directors only

$$\boldsymbol{d}_{\boldsymbol{m}} = \bigwedge_{I=1}^{N^h} [\boldsymbol{m}]_I \ . \tag{5.41}$$

Consequently, we have the finite element interpolation of the constitutive state vector $\boldsymbol{\mathfrak{c}}^h_{\boldsymbol{m}} = \boldsymbol{B}_{\boldsymbol{m}} \boldsymbol{d}_{\boldsymbol{m}}$ in terms of $\boldsymbol{B}_{\boldsymbol{m}}$ which is a symbolic representation of the global matrix of shape functions and its derivatives. We have the space-time-discrete potential,

$$\Pi'^{\tau}_{pre} = \int_{\mathcal{B}} \pi'^{h}_{pre}(\boldsymbol{B}_{\boldsymbol{m}} \boldsymbol{d}_{\boldsymbol{m}}) \, dV + C_{pre} \ . \tag{5.42}$$

Now the variational statement that we need to consider in this step $(5.28)_1$ is written for the space-time-discrete setting as

$$\boxed{\boldsymbol{d}_{\boldsymbol{m}} = \arg \left\{ \underset{\boldsymbol{d}_{\boldsymbol{m}}}{\text{stat}} \ \Pi'^{h}_{pre}(\boldsymbol{d}_{\boldsymbol{m}}) \right\} \ .} \tag{5.43}$$

which is a nonlinear optimization problem that is solved by a Newton-type iterative process. The necessary condition for the above statement is written as

$$\delta \Pi'^{h}_{pre} = \delta \boldsymbol{d}^T_{\boldsymbol{m}} \cdot \boldsymbol{R}_{\boldsymbol{m}} = 0 \qquad \forall \ \delta \boldsymbol{d}^T_{\boldsymbol{m}} \in \mathcal{R}^{d \cdot N^h} \ , \tag{5.44}$$

with $\delta \boldsymbol{d}_{\boldsymbol{m}}$ denoting the variations of the nodal magnetization directors and the algebraic finite element predictor residual of the problem,

$$\boldsymbol{R}_{\boldsymbol{m}} := \int_{\mathcal{B}} \boldsymbol{B}^T_{\boldsymbol{m}} \boldsymbol{S}^h_{\boldsymbol{m}} \, dV \quad \text{with} \quad \boldsymbol{S}^h_{\boldsymbol{m}} := \partial_{\boldsymbol{\mathfrak{c}}_{\boldsymbol{m}}} \pi'^{\tau}_{pre}(\boldsymbol{\mathfrak{c}}^h_{\boldsymbol{m}}) \ . \tag{5.45}$$

The linearization of the necessary condition with $\Delta \boldsymbol{d}_{\boldsymbol{m}}$ denoting the increments of $\boldsymbol{m}$, reads

$$Lin[\delta \Pi'^{h}_{pre}] := \delta \Pi'^{h}_{pre} + \Delta[\delta \Pi'^{h}_{pre}] = \delta \boldsymbol{d}^T_{\boldsymbol{m}} [\boldsymbol{R}_{\boldsymbol{m}} + \boldsymbol{K}_{\boldsymbol{m}} \Delta \boldsymbol{d}_{\boldsymbol{m}}] \tag{5.46}$$

with the finite element tangent matrix of the coupled sub-problem

$$\boldsymbol{K}_{\boldsymbol{m}} := \int_{\mathcal{B}_{\boldsymbol{m}}} \boldsymbol{B}^T \mathbb{C}^h_{\boldsymbol{m}} \boldsymbol{B}_{\boldsymbol{m}} \, dV \quad \text{with} \quad \mathbb{C}^h_{\boldsymbol{m}} := \partial^2_{\boldsymbol{\mathfrak{c}}_{\boldsymbol{m}} \boldsymbol{\mathfrak{c}}_{\boldsymbol{m}}} \pi'^{\tau}_{pre}(\boldsymbol{\mathfrak{c}}^h_{\boldsymbol{m}}) \ . \tag{5.47}$$

With the residuum $\boldsymbol{R}_{\boldsymbol{m}}$ and tangent matrix $\boldsymbol{K}_{\boldsymbol{m}}$ so that we may carry out the update of the magnetization predictor $\boldsymbol{d}_{\boldsymbol{m}} \Leftarrow \boldsymbol{d}_m - \boldsymbol{K}^{-1}_{\boldsymbol{m}} \boldsymbol{R}_{\boldsymbol{m}}$, following which, we have the corrector step as a normalization of the magnetization directors at every node,

$$\boldsymbol{d}_{\boldsymbol{m}} \Leftarrow \boldsymbol{d}_{\boldsymbol{m}} / |\boldsymbol{d}_{\boldsymbol{m}}| \ . \tag{5.48}$$

This sub-algorithm delivers the nodal magnetization directors for the next sub-algorithm.

5.3.2. Space-Time Discrete Magnetomechanical Corrector

We consider a second partition of the state variables as $\mathfrak{c}_{\boldsymbol{u}\widetilde{\phi}} = \{\nabla \boldsymbol{u}, -\nabla\widetilde{\phi}\}$ in terms of which we write the incremental potential

$$\Pi'^{\tau}_{cor} = \int_{\mathcal{B}} \pi'^{\tau}_{cor}(\mathfrak{c}_{\boldsymbol{u}\widetilde{\phi}})\, dV + C_{cor} \ , \tag{5.49}$$

where the *incremental magneto-mechanical corrector potential density per unit volume* of the solid domain $\mathcal{B}$ reads,

$$\pi'^{\tau}_{cor}(\mathfrak{c}_{\boldsymbol{u}\widetilde{\phi}}) = \Psi_{mat}(\nabla_s \boldsymbol{u}, \boldsymbol{m}, \nabla \boldsymbol{m}) + \kappa_0 m_s \boldsymbol{m} \cdot \nabla\widetilde{\phi} - \overline{\boldsymbol{\sigma}} : \nabla_s[\boldsymbol{u} - \boldsymbol{u}_n] \cdot \overline{\boldsymbol{h}} \tag{5.50}$$

and a constant C_{cor} that includes non-essential contributions at a time t_n. Assuming a triangulation $\mathfrak{T}^h$ of the full domain Ω with N^h nodal points, we consider a magneto-mechanical partition of the primary variables that contains the displacement $\boldsymbol{u}$ and the magnetic potential $\widetilde{\phi}$ for this sub-problem

$$\boldsymbol{d}_{\boldsymbol{u}\widetilde{\phi}} = \mathop{\mathsf{A}}_{I=1}^{N^h} \begin{bmatrix} \boldsymbol{u} \\ -\widetilde{\phi} \end{bmatrix}_I^T \ . \tag{5.51}$$

Consequently we have the finite element interpolation of the constitutive state vector for the magnetomechanical corrector step $\mathfrak{c}^h_{\boldsymbol{u}\widetilde{\phi}} = \boldsymbol{B}_{\boldsymbol{u}\widetilde{\phi}} \boldsymbol{d}_{\boldsymbol{u}\widetilde{\phi}}$ in terms of the symbolic matrix representation $\boldsymbol{B}_{\boldsymbol{u}\widetilde{\phi}}$. Furthermore, since the magnetic potential $\widetilde{\phi}$ alone exists in the surrounding free space $\Omega/\mathcal{B}$, we define additionally a matrix $\boldsymbol{F}_{\widetilde{\phi}}$ that extracts only the magnetic field, i.e. $-\nabla\phi^h = \boldsymbol{F}_{\widetilde{\phi}} \boldsymbol{d}_{\boldsymbol{u}\widetilde{\phi}}$. We may therefore write the space-time-discrete potential in terms of the potential density π'^{τ}_{cor} defined above

$$\Pi'^{h}_{cor} = \int_{\mathcal{B}} \pi'^{h}_{cor}(\boldsymbol{B}_{\boldsymbol{u}\widetilde{\phi}} \boldsymbol{d}_{\boldsymbol{u}\widetilde{\phi}})\, dV - \frac{\kappa_0}{2} \int_{\Omega} |\boldsymbol{F}_{\widetilde{\phi}} \boldsymbol{d}_{\boldsymbol{u}\widetilde{\phi}}|^2\, dV \ . \tag{5.52}$$

The variational principle for the second sub-algorithm is then written in the compact notation as

$$\boxed{\boldsymbol{d}_{\boldsymbol{u}\phi} = \arg\left\{ \underset{\boldsymbol{d}_{\boldsymbol{u}\widetilde{\phi}}}{\text{stat}}\ \Pi'^{h}_{cor}(\boldsymbol{d}_{\boldsymbol{u}\widetilde{\phi}}) \right\}} \tag{5.53}$$

which is a coupled nonlinear optimization problem in $\boldsymbol{u}$ and $\widetilde{\phi}$ and is solved by a Newton-type iterative process. The necessary condition for the above statement is written as

$$\delta\Pi'^{h}_{cor} = \delta \boldsymbol{d}^T_{\boldsymbol{u}\widetilde{\phi}} \cdot \boldsymbol{R}_{\boldsymbol{u}\widetilde{\phi}} = 0 \qquad \forall\ \delta \boldsymbol{d}^T_{\boldsymbol{u}\widetilde{\phi}} \in \mathcal{R}^{(d+1)\cdot N^h} \ , \tag{5.54}$$

in terms of the algebraic coupled finite element predictor residual of the problem

$$\boldsymbol{R}_{\boldsymbol{u}\widetilde{\phi}} := \int_{\mathcal{B}} \boldsymbol{B}^T_{\boldsymbol{u}\widetilde{\phi}} \boldsymbol{S}^h_{\boldsymbol{u}\widetilde{\phi}}\, dV - \int_{\Omega} \kappa_0 \boldsymbol{F}^T_{\widetilde{\phi}} \boldsymbol{F}_{\widetilde{\phi}} \boldsymbol{d}_{\boldsymbol{u}\phi}\, dV \quad \text{with} \quad \boldsymbol{S}^h_{\boldsymbol{u}\widetilde{\phi}} := \partial_{\mathfrak{c}_{\boldsymbol{u}\widetilde{\phi}}} \pi'^{\tau}_{cor}(\mathfrak{c}^h_{\boldsymbol{u}\widetilde{\phi}}) \ . \tag{5.55}$$

The linearization of the necessary condition (5.54) reads

$$Lin[\delta\Pi'^{h}_{cor}] := \delta\Pi'^{h}_{cor} + \Delta[\delta\Pi'^{h}_{cor}] = \delta \boldsymbol{d}^T_{\boldsymbol{u}\widetilde{\phi}} [\boldsymbol{R}_{\boldsymbol{u}\widetilde{\phi}} + \boldsymbol{K}_{\boldsymbol{u}\widetilde{\phi}} \Delta \boldsymbol{d}_{\boldsymbol{u}\widetilde{\phi}}] \tag{5.56}$$

with the finite element tangent matrix of the coupled problem

$$\boldsymbol{K}_{\boldsymbol{u}\widetilde{\phi}} := \int_{\mathcal{B}} \boldsymbol{B}^T_{\boldsymbol{u}\widetilde{\phi}} \mathbb{C}^h_{\boldsymbol{u}\widetilde{\phi}} \boldsymbol{B}_{\boldsymbol{u}\widetilde{\phi}}\, dV - \int_{\Omega} \kappa_0 \boldsymbol{F}^T_{\boldsymbol{u}\widetilde{\phi}} \boldsymbol{F}_{\boldsymbol{u}\widetilde{\phi}}\, dV \quad \text{with} \quad \mathbb{C}^h_{\boldsymbol{u}\widetilde{\phi}} := \partial^2_{\mathfrak{c}_{\boldsymbol{u}\widetilde{\phi}}} \pi'^{\tau}_{pre}(\mathfrak{c}^h_{\boldsymbol{u}\widetilde{\phi}}) \,. \quad (5.57)$$

With the residuum $\boldsymbol{R}_{\boldsymbol{u}\widetilde{\phi}}$ and tangent matrix $\boldsymbol{K}_{\boldsymbol{u}\widetilde{\phi}}$ so that we may carry out the update of the displacements and magnetic potential via $\boldsymbol{d}_{\boldsymbol{u}\widetilde{\phi}} \Leftarrow \boldsymbol{d}_{\boldsymbol{u}\widetilde{\phi}} - \boldsymbol{K}^{-1}_{\boldsymbol{u}\widetilde{\phi}} \boldsymbol{R}_{\boldsymbol{u}\widetilde{\phi}}$. With these contributions at hand, we summarize the algorithmic scheme $ALGO_{tot}$ in the Box 1.

5.4. Numerical Results

As already stated, the proposed projection method has the fundamental advantage of being easy to implement, thus enabling a straightforward extension of the computational model from 2D to 3D. This is in sharp contrast to the situation in the geometrically consistent method in Miehe & Ethiraj [115], where the transition from 2D to 3D involves significant increase complexity from the point of view of implementation. The aim of this section is then twofold, *a*) to report 3D results arising from the proposed model, and *b*) to present a comparison of the two methods. This comparison is done for the two-dimensional case.

5.4.1. Formation of Magnetic Domains in Thin Ferromagnetic Film

As we already know, ferromagnetic materials have domain structure even in the *ground state*. Capturing this in our simulations is the first goal since, apart from showing the domain structure, it also provides a starting point for subsequent simulations that are concerned with externally applied loads on the ground state. We consider a domain with dimensions $2\mu m \times 1\mu m \times .02\mu m$ as shown in Figure 5.2. A structured finite element mesh with $60 \times 30 \times 2$ eight-node brick elements is used for the discretization is also seen in Figure 5.2. In order to do this, we begin with a random magnetization director field and let it evolve without applying any external load until it reaches equilibrium. The results of such a simulation is shown in the sequence of plots in Figure 5.3, which shows the vector-field of the magnetization directors at each node and the norm of the gradient of magnetization $|\nabla \boldsymbol{m}|$ as the scalar field for the contour plots. In the final plot of the sequence, one observes uniformly magnetized regions or *magnetic domains* whose

Table 5.1: Material Parameters of Permalloy for the Numerical Examples [41].

Nr.	Parameter	Unit	Name	Value
1.	λ	$\mathrm{N/mm^2}$	Lamé parameter	7.5×10^4
2.	μ	$\mathrm{N/mm^2}$	Lamé parameter	2.6×10^4
3.	E	$\mathrm{N/mm^2}$	Magnetostrictive constant	7.0×10^{-6}
4.	K	$\mathrm{N/mm^2}$	First anisotropy coefficient	1.0×10^{-3}
5.	A	N	Exchange coefficient	2.0×10^{-11}
6.	m_s	A/mm	Saturation magnetization	8.0×10^2
7.	η	$\mathrm{Ns^2/mm^2}$	Damping coefficient	2.0×10^{-1}
8.	κ_0	$\mathrm{N/A^2}$	Magnetic permeability	1.3×10^{-6}

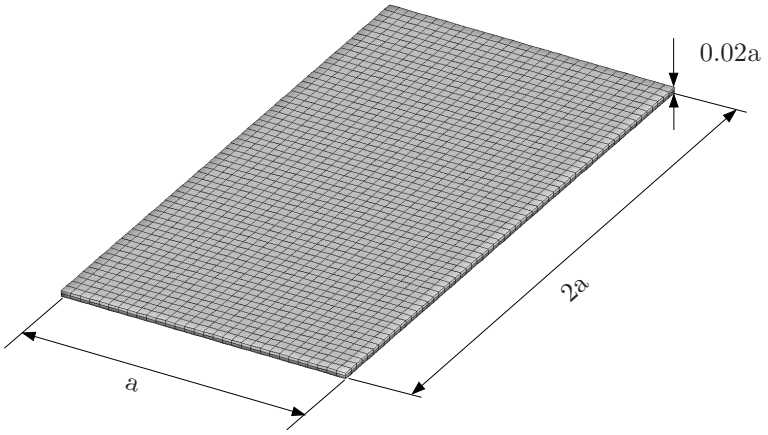

Figure 5.2: Finite element discretization of the three dimensional domain using eight node brick elements with a = 1 μm.

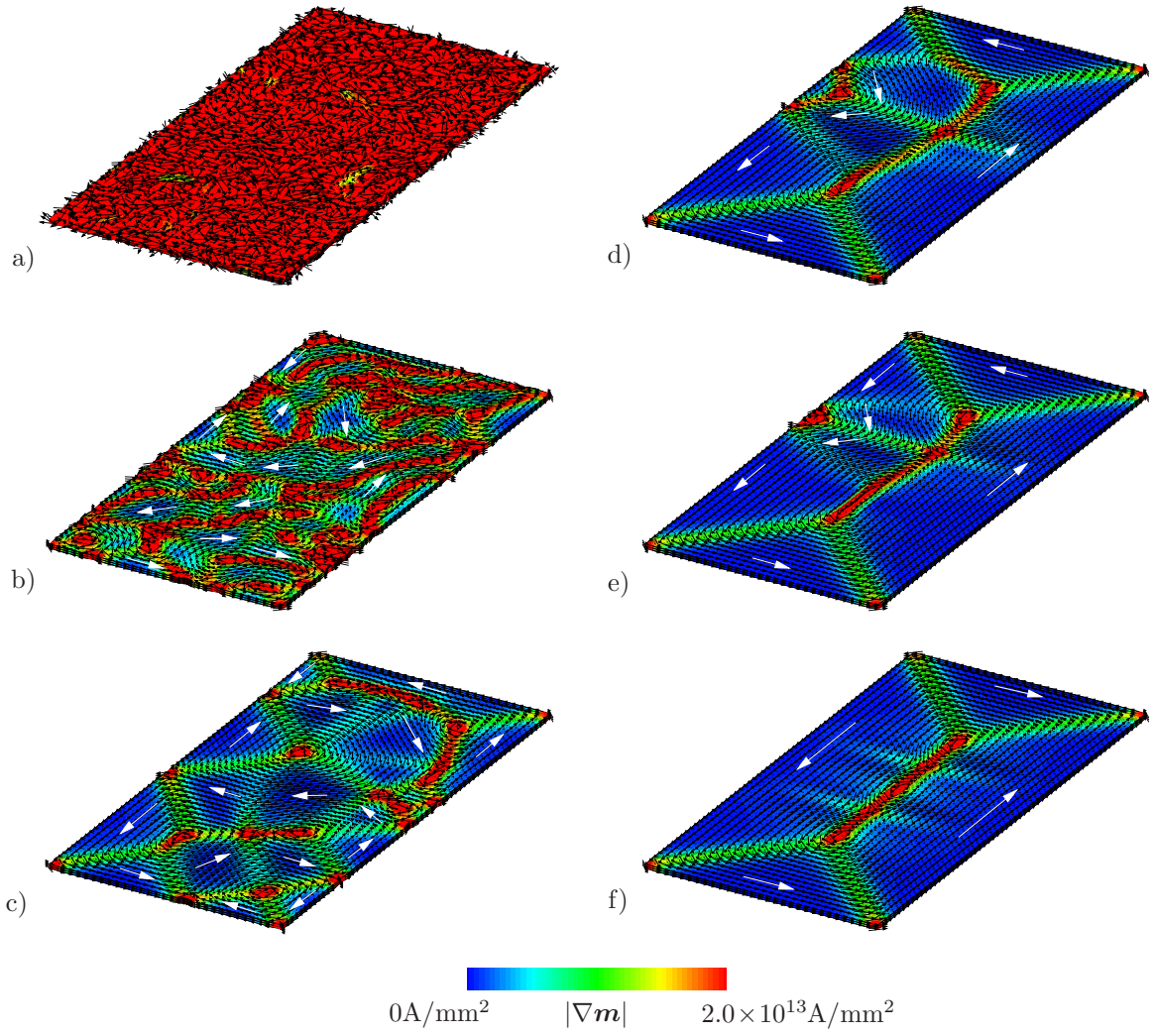

Figure 5.3: Evolution of magnetic domains with $dt = 5\times10^{-6}$s starting from a hypothetical random initial state of magnetization and proceeding towards ground state.

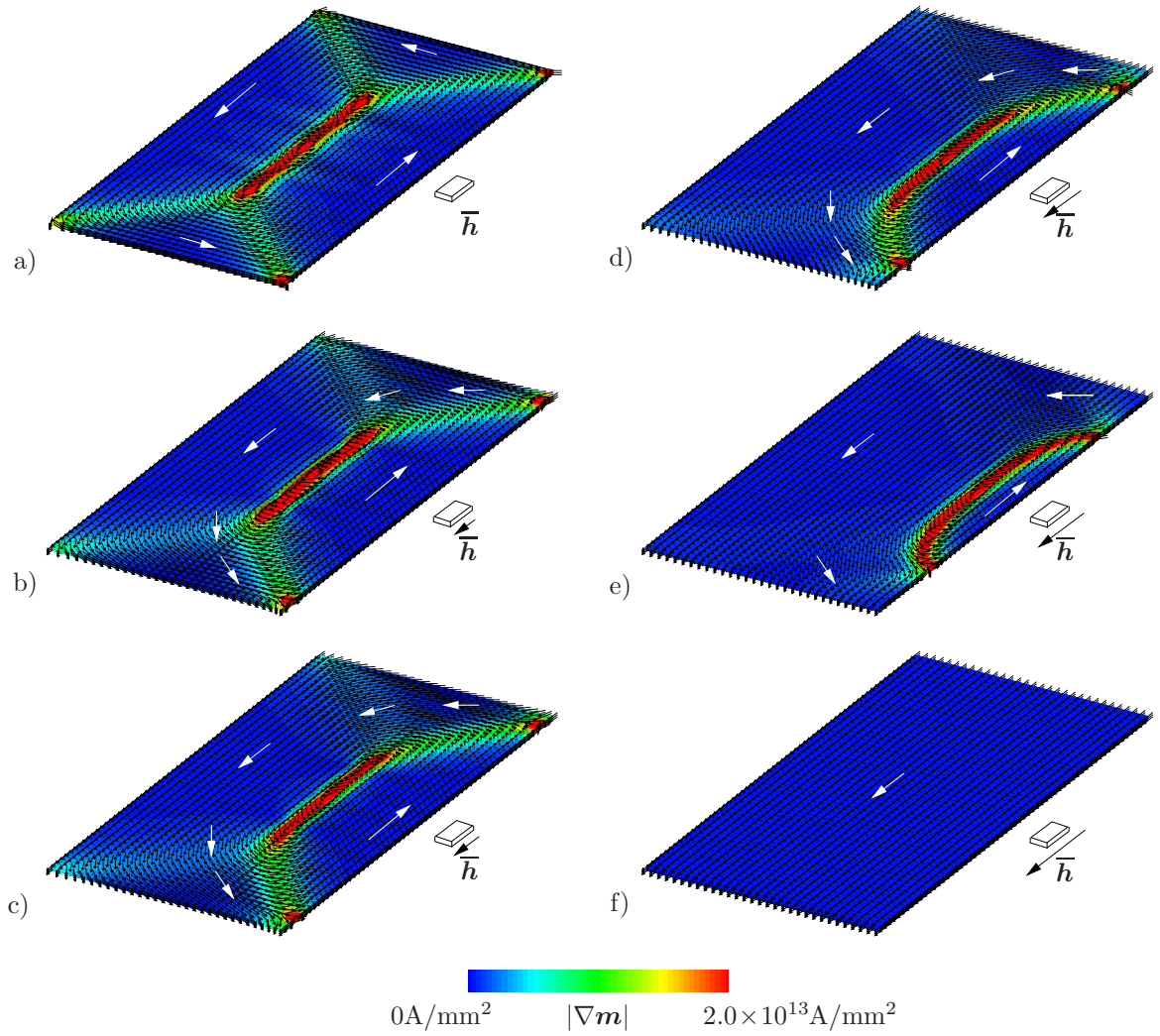

Figure 5.4: Evolution of magnetic domains for $dt = 5 \times 10^{-6}$s starting from a ground state of magnetization with a ramped magnetic field applied as shown in figure.

directions are indicated by the white arrows. These domains are separated by *domain walls*, which are regions where the magnetization directors sharply change thus having high values for $|\nabla \boldsymbol{m}|$. Figure 5.3f is the final equilibrium state or ground state that we are looking for. Thus a hypothetical initial state has been used to obtain a physically meaningful final state that will serve as a good starting point for the next two simulations in Section 5.4.2 and Section 5.4.3, which are concerned with the evolution of the domains with externally applied loads.

5.4.2. Evolution of Magnetic Domains in an Applied Magnetic Field

This example demonstrates the microscale response of a ferromagnetic specimen in an applied magnetic field. Additionally, it highlights the role of the magnetic loading functional $L_{\overline{\boldsymbol{h}}}$, introduced in Section 4.2. While the material parameters and discretization remain unchanged, the initial state used for this simulation is the equilibrium configuration that is delivered by the previous simulation described in Section 5.4.1. With this as starting point, we apply a monotonically increasing magnetic field $\overline{\boldsymbol{h}}$ directed along the longer side of the specimen, as indicated in Figure 5.4. Our focus here, is on the domain wall movement and associated change in domain structure. By observing Figure 5.4,

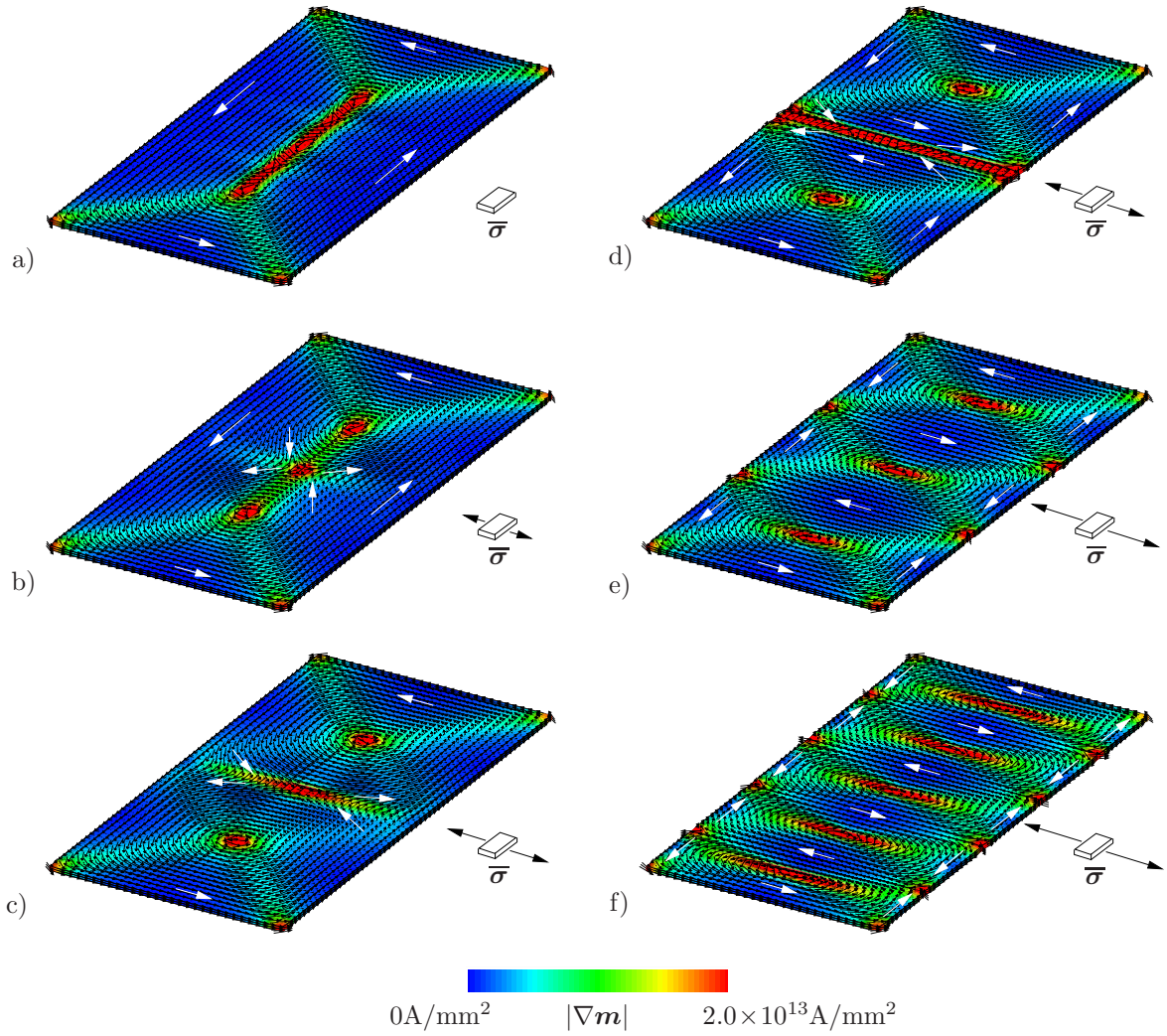

Figure 5.5: Evolution of magnetic domains for $dt = 5\times10^{-6}$s starting from a ground state of magnetization with a ramped stress applied as shown in figure.

it is clear that the applied magnetic field $\overline{\boldsymbol{h}}$, points in along the material's easy-axis of magnetization, since there already exists a domain in this direction in the ground state Figure 5.4a. As a consequence of this external magnetic field, the magnetic domain in the same direction is energetically more favourable, and grows in size at the cost of the other domains. Consequently, as the sequence in Figure 5.4 depicts, the domain wall is driven out completely by rotations of magnetization directors, such that it eventually results in a single-domain, fully magnetized specimen.

5.4.3. Evolution of Magnetic Domains under Applied Mechanical Stress

The effect of applied stress on magnetic properties of a material is a topic of interest, with regard to industrial applications of *magnetostrictive transducers*. Although application of an external mechanical stress $\overline{\boldsymbol{\sigma}}$ to a ferromagnetic material causes no change in net magnetization, it does result in a change in the magnetic domain structure. An applied stress can make a certain set of directions more (or less) favourable than others depending on the orientation of loading as well as the already existing set of easy directions of the material. This would change the overall magnetization properties of the material and is hence an interesting phenomena to capture.

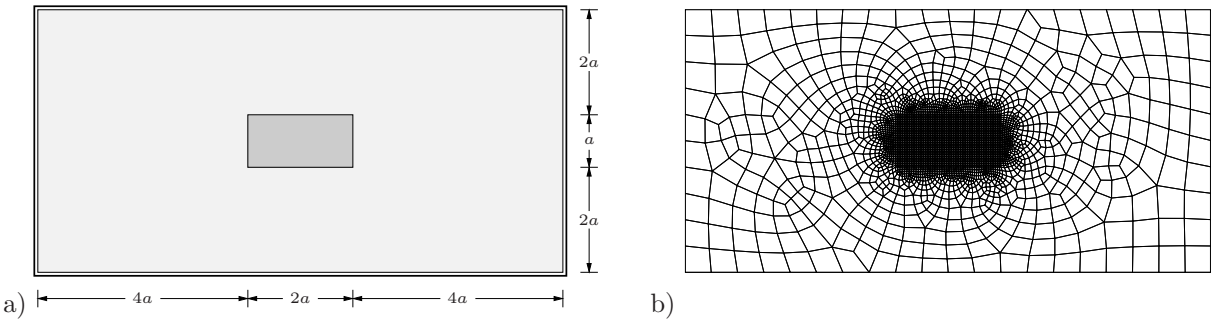

Figure 5.6: a) Two dimensional boundary-value-problem with $a = 1\mu$m. b) Finite Element discretization of the domain consisting of the solid $\mathcal{B}$ (structured, fine mesh) and the free space (unstructured, coarse mesh) $\Omega/\mathcal{B}$ using quad elements.

To show this, we begin with the equilibrium state that resulted from the simulation in Section 5.4.1 and apply a monotonically increasing tensile stress on the specimen in a direction perpendicular to the easy axis. Figure 5.5 shows the loading as well as the resulting reorientation of the magnetic domains. It can be seen that the applied tensile load effectively creates a new easy-axis along the loading direction. This is inferred from the fact that we see an increased number domains being formed in that direction. The final domain structure, consiting of *closure domains* is consistent with the *pole-avoidance principle* [19]. As a final note, the current scenario may be also compared to the ground state in *biaxial materials* which was observed in experiment in the work by Williams [164] and has been discussed in depth in Cullity [28, Ch. 9].

5.4.4. A Comparison of the Two Methods

The final example deals with a comparison of the geometrically exact method in Miehe & Ethiraj [115], with the projection method that has been proposed in this work. To keep it simple and clear, we present this comparison in the context of a two dimensional initial boundary value problem. The geometry and discretization of the domain is shown

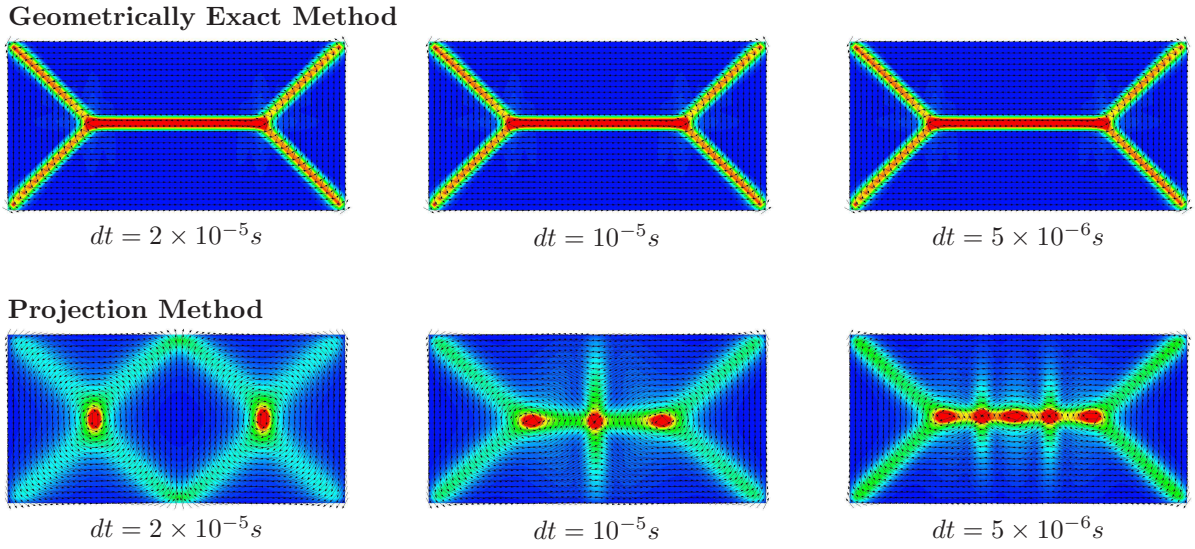

Figure 5.7: Comparison between geometrically exact method and projection method on the basis of final equilibrium configurations obtained.

in Figure 5.6. It consists of a rectangular ferromagnetic domain embedded in free-space or vacuum. The entire domain Ω is discretized using 3616 quad finite elements out of which, a structured mesh of 1800 elements (60×30 elements) is used to discretize the region occupied by the ferromagnetic solid $\mathcal{B}$. The surrounding free space box Ω is discretized by a coarse unstructured mesh. Note that here we have included the free-space surrounding the specimen which was avoided in the three dimensional case due to the complexity in the meshing procedure. For presenting the numerical results however, the surrounding free space has been blanked out so that we may focus on the domain structure within the ferromagnetic sample. We begin, like in Section 5.4.1, with an initial random state of the magnetization director field and allow the system to reach equilibrium under no applied load. This is done for the two methods for three different time-step sizes. The final equilibrium configurations obtained are reported in Figure 5.7.

While the geometrically exact method delivers the Landau state consistently, a dependence on the time-step size is observed in the projection method. Moreover, the results tend closer to those produced by the geometrically exact method on decreasing the time-step size to 5×10^{-6}s. We may conclude that the proposed projection method is easier to implement, however with the disadvantage that a smaller time-step size being needed for the simulation.

6. Magnetoelasticity of MREs

This chapter deals with the modeling of MREs in the magnetoelastic regime. After introducing the basic functionals, we show how the coupled boundary value problem of finite deformation magnetoelasticity can be compactly represented by a *variational principle*. We then show how such a variational principle can be exploited to yield an FE framework for finite deformation magnetoelasticity. After that we present a modular approach for the construction of free energy functions to model MREs. We will then make a particular choice of the free energy function which we shall test against experiment and also implement within the described finite element framework. These numerical results will be presented at the end of the chapter.

6.1. Motivation and Physical Background of MREs

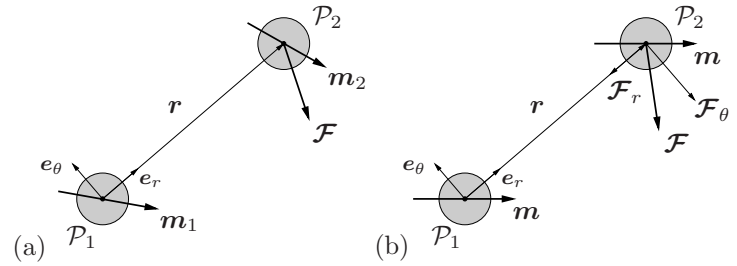

Figure 6.1: Interaction between two magnetic dipoles $\mathcal{P}_1$ and $\mathcal{P}_2$ resulting in a force $\boldsymbol{\mathcal{F}}$ acting on the particle. (a) Arbitrary magnetic moments $\boldsymbol{m}_1$ and $\boldsymbol{m}_2$ and (b) particles magnetized in same direction with magnetic moment $\boldsymbol{m}$.

MREs have iron particles that are embedded in a rubber matrix. An applied magnetic field $\overline{\boldsymbol{h}}$ magnetizes these particles in the same direction. To understand the effect of interactions between these magnetized particles, we assume them to be magnetic dipoles with the magnetic dipole moment being induced by the applied field. The analytical solution for the force $\boldsymbol{\mathcal{F}}$ between two magnetic dipoles with arbitrary magnetic moments $\boldsymbol{m}_1$ and $\boldsymbol{m}_2$ with $\boldsymbol{m}_2$ displaced by $\boldsymbol{r}$ with respect to $\boldsymbol{m}_1$ is well known, see Yung, Landecker & Villani [165], i.e.

$$\boldsymbol{\mathcal{F}} = \frac{3\mu_0}{4\pi r^4}\big[(\boldsymbol{m}_1\cdot\boldsymbol{e}_r)\boldsymbol{m}_2 + (\boldsymbol{m}_2\cdot\boldsymbol{e}_r)\boldsymbol{m}_1 + \big(\boldsymbol{m}_1\cdot\boldsymbol{m}_2 - 5(\boldsymbol{m}_1\cdot\boldsymbol{e}_r)(\boldsymbol{m}_2\cdot\boldsymbol{e}_r)\big)\boldsymbol{e}_r\big] \tag{6.1}$$

where the unit radial director is $\boldsymbol{e}_r = \boldsymbol{r}/r$ with the distance between the dipoles $r = |\boldsymbol{r}|$, see Figure 6.1. $\boldsymbol{\mathcal{F}}$ is the force acting on $\boldsymbol{m}_2$ due to $\boldsymbol{m}_1$. Obviously the force on $\boldsymbol{m}_1$ is the same with the opposite sign. In the present case under consideration, the particles are magnetized in the same direction. Hence, $\boldsymbol{m}_1 = \boldsymbol{m}_2 = \boldsymbol{m}$. Thus, the above equation simplifes to

$$\boldsymbol{\mathcal{F}}(\boldsymbol{r},\boldsymbol{m}) = \frac{3\mu_0}{4\pi r^4}\Big[2(\boldsymbol{m}\cdot\boldsymbol{e}_r)\boldsymbol{m} + \big(\boldsymbol{m}\cdot\boldsymbol{m} - 5(\boldsymbol{m}\cdot\boldsymbol{e}_r)^2\big)\boldsymbol{e}_r\Big]\,. \tag{6.2}$$

To further analyze the equation, we resolve $\boldsymbol{\mathcal{F}}$ in radial and tangential components $\mathcal{F}_r$ and $\mathcal{F}_\theta$, respectively. Therefore, working in polar coordinates with origin at the center of particle $\mathcal{P}_1$ as shown in Figure 6.1, we have

$$\boldsymbol{\mathcal{F}} := \begin{bmatrix}\mathcal{F}_r\\ \mathcal{F}_\theta\end{bmatrix} = \frac{3\mu_0}{4\pi r^4}\begin{bmatrix}\boldsymbol{m}\cdot\boldsymbol{m} - 3(\boldsymbol{m}\cdot\boldsymbol{e}_r)^2\\ 2(\boldsymbol{m}\cdot\boldsymbol{e}_r)(\boldsymbol{m}\cdot\boldsymbol{e}_\theta)\end{bmatrix} \tag{6.3}$$

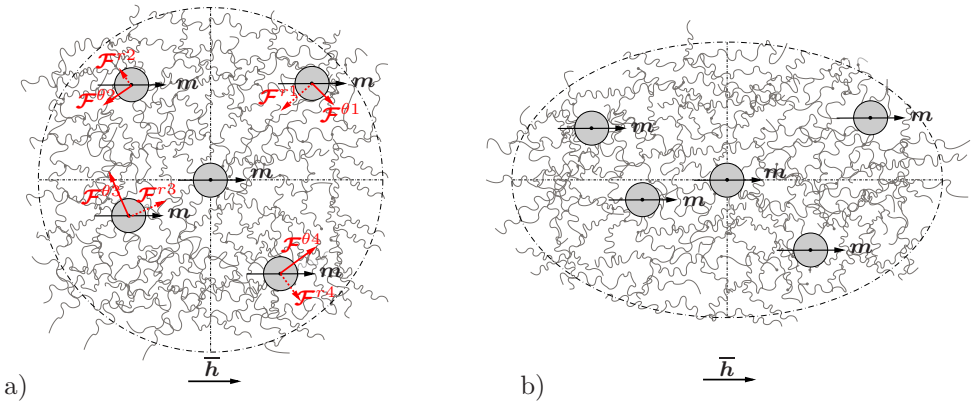

Figure 6.2: Schematic representation of the magnetorheological elastomer at the microscale. a) The tangential components of the dipole-dipole forces always act so as to favour alignment of magnetic particles. b) The tangential components cause a deformation of the entire composite in the direction of the magnetic field.

with the unit tangential director $\boldsymbol{e}_\theta$ perpendicular to $\boldsymbol{e}_r$. In the context of the microsphere model, which is meant to model isochoric deformations, we pay particular attention to the tangential component $\mathcal{F}_\theta$ since it is this component which is responsible for a *change in orientation* of the polymer chains. Furthermore, since the magnetization is a function of the applied magnetic field, we expect an *anisotropy, dependent on the applied magnetic field* $\boldsymbol{h}$. It can be shown that the tangential vector component of the total force, namely $\boldsymbol{\mathcal{F}}_\theta = 2(\boldsymbol{m}\cdot\boldsymbol{e}_r)(\boldsymbol{m}\cdot\boldsymbol{e}_\theta)\boldsymbol{e}_\theta$ always acts in such way so as to *align the magnetic moments* as shown in Figure 6.2. This explanation is consistent with the tendency to afford the path of best conductance to the lines of magnetic force, or alternatively, the tendency of magnetized bodies to align with each other. See also the approach by Borcea & Bruno [9, p.2906]. This microscopic description is the key factor that motivates us to consider a multiplicative split of the deformation gradient into elastic and magnetic parts.

6.2. Basic Functionals of Magnetoelasticity

Let $\Omega_t \subset \mathcal{R}^3$ denote a vacuum free space box and $\mathcal{S} \subset \Omega_t$ be the domain occupied by the deformed material solid, as depicted in Figure 6.3. Ω_t is considered to be large enough such that the magnetic field induced by the magnetization of the body $\mathcal{S}$ is decayed at its surface $\partial\Omega \subset \mathcal{R}^2$. We also denote $\mathcal{B} = \boldsymbol{\varphi}^{-1}(\mathcal{S})$ as the undeformed configuration which occupies the free space box $\Omega = \boldsymbol{\varphi}^{-1}(\Omega_t)$. In what follows, $\nabla(\cdot) := \partial_{\boldsymbol{x}}(\cdot)$ and $\dot{(\cdot)} := \partial_t(\cdot)$ denote the spatial gradient and the time derivative of the field $(\cdot)$, respectively.

6.2.1. Primary Fields: Displacement, Magnetization, Potential

The boundary-value-problem of magneto-mechanics is a coupled multi-field problem. On the mechanical side, the primary variable field is the *deformation map* $\boldsymbol{\varphi}$ of the material point $\boldsymbol{X} \in \mathcal{B}$ at time $t \in \mathcal{T}$. On the magnetic side, the *current magnetization per unit mass* $\boldsymbol{\mu}$ describes the magnetization of the solid material at $\boldsymbol{x} \in \mathcal{S}$ and $t \in \mathcal{T}$, and the magnetic field in the full free space box Ω_t induced by the magnetization $\boldsymbol{\mu}$ is described by a third field, the *magnetostatic potential of the self-field*[6]. Hence, we focus on the three

[6] We will qualify the choice of this particular name later in (6.17).

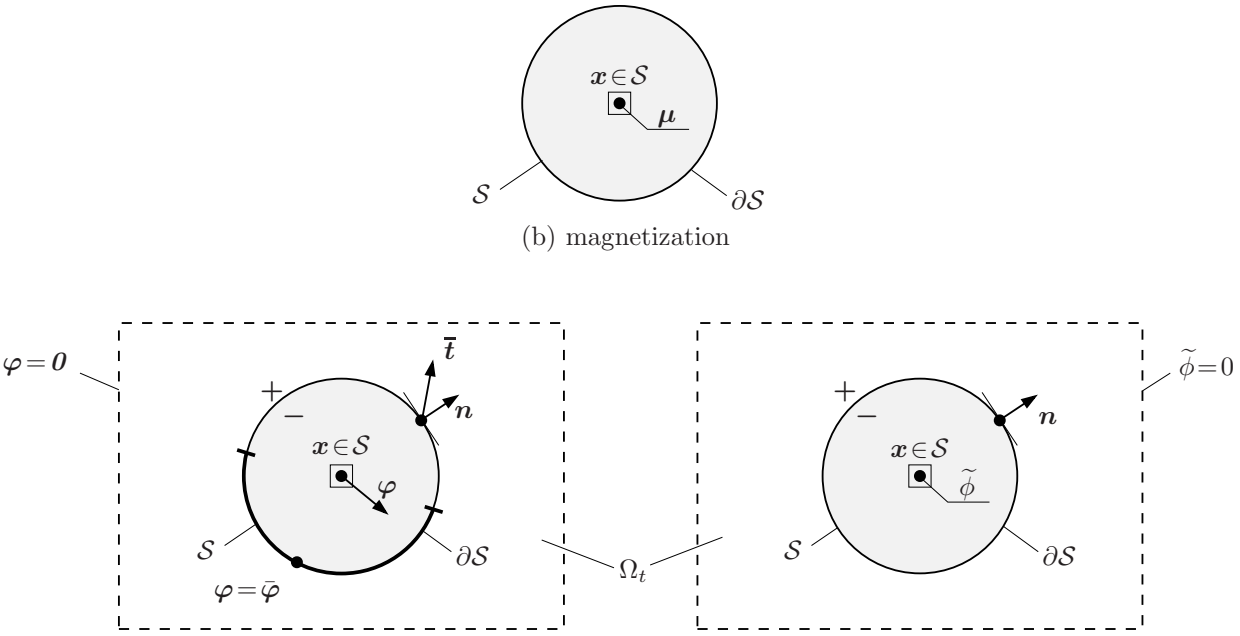

Figure 6.3: Primary variable fields in magnetoelasticity, for a solid $\mathcal{S} \subset \Omega_t$ embedded into a *free space box* $\Omega_t \subset \mathcal{R}^3$. (a) The *deformation map* $\boldsymbol{\varphi}$ defined on Ω with the associated jump conditions on the boundary $\partial\mathcal{S}$. (b) The *magnetization field (per unit mass)* is $\boldsymbol{\mu}$ in $\mathcal{S}$ and has no boundary conditions associated with it. (c) The *magnetostatic potential (of the self-field)* $\widetilde{\phi}$ in Ω_t induced by the magnetization of the solid is continuous across the interface $\partial\mathcal{S}$, and zero on the boundary $\partial\Omega_t$ of the free space box.

primary variable fields

$$\boldsymbol{\varphi} : \begin{cases} \Omega \times \mathcal{T} \to \mathcal{R}^3 \\ (\boldsymbol{X}, t) \mapsto \boldsymbol{x} = \boldsymbol{\varphi}(\boldsymbol{X}, t) \end{cases}, \quad \boldsymbol{\mu} : \begin{cases} \mathcal{S} \times \mathcal{T} \to \mathcal{R}^3 \\ (\boldsymbol{x}, t) \mapsto \boldsymbol{\mu}(\boldsymbol{x}, t) \end{cases} \text{and} \quad \widetilde{\phi} : \begin{cases} \Omega_t \times \mathcal{T} \to \mathcal{R} \\ (\boldsymbol{x}, t) \mapsto \widetilde{\phi}(\boldsymbol{x}, t) \end{cases}. \tag{6.4}$$

The potential $\widetilde{\phi}$ is assumed to be continuous across the interface $\partial\mathcal{S}$ between the solid domain $\mathcal{S}$ and the surrounding free space $\Omega_t \setminus \mathcal{S}$, i.e.

$$[\![\widetilde{\phi}]\!] = 0 \quad \text{on } \partial\mathcal{S} \ , \tag{6.5}$$

where $[\![(\cdot)]\!] := (\cdot)_+ - (\cdot)_-$ denotes jump between the sides $\partial\mathcal{S}_+$ and $\partial\mathcal{S}_-$ of the interface as depicted in Figure 6.3. The gradients of the deformation map $\boldsymbol{\varphi}$ and the potential $\widetilde{\phi}$ define $\boldsymbol{F}$, the deformation gradient tensor, and $\widetilde{\boldsymbol{h}}$, the magnetic field vector induced by the magnetization[6]

$$\boldsymbol{F} := \nabla_{\boldsymbol{X}} \boldsymbol{\varphi} \quad \text{and} \quad \widetilde{\boldsymbol{h}} := -\nabla_{\boldsymbol{x}} \widetilde{\phi} \ , \tag{6.6}$$

respectively. These definitions satisfy automatically the *deformation compatibility* $\mathrm{Curl}[\boldsymbol{F}] = \boldsymbol{0}$ in $\mathcal{B} = \boldsymbol{\varphi}^{-1}(\mathcal{S})$ and *Amperes's law*, the fourth Maxwell equation, $\mathrm{curl}[\widetilde{\boldsymbol{h}}] = \boldsymbol{0}$ in Ω_t for the quasi-static problem under consideration.

6.2.2. Energy-Enthalpy Functional of Magneto-Elasticity

We begin with the *free energy density per unit mass* $\psi(\boldsymbol{F}, \boldsymbol{\mu}, \widetilde{\boldsymbol{b}})$ of the non-polarizable magnetoactive elastomer occupying a region $\mathcal{S}$ embedded in the free space box Ω_t. Since

this function includes the contributions for the material as well as vacuum (or free space), we have

$$\rho\psi(\boldsymbol{F},\boldsymbol{\mu},\widetilde{\boldsymbol{b}}) = \rho\psi_{mat}(\boldsymbol{F},\boldsymbol{\mu}) + \psi_{vac}(\boldsymbol{\mu},\widetilde{\boldsymbol{b}}) \tag{6.7}$$

where ρ is the density of the material. The magnetic induction induced by the magnetized body $\widetilde{\boldsymbol{b}}$, the magnetic field of the magnetized body $\widetilde{\boldsymbol{h}}$ (also called the *demagnetization field* or *the self-field*, see ERICKSEN [51] and STEIGMANN [148]) and the magnetization per unit mass $\boldsymbol{\mu}$ are connected by the universal relation[7]

$$\widetilde{\boldsymbol{b}} = \mu_0(\widetilde{\boldsymbol{h}} + \rho\boldsymbol{\mu}) \quad \text{in } \Omega_t \tag{6.8}$$

If we consider $\widetilde{\boldsymbol{h}} = \hat{\boldsymbol{h}}(\boldsymbol{\mu},\widetilde{\boldsymbol{b}})$, the vacuum free energy density per unit current volume is

$$\psi_{vac}(\boldsymbol{\mu},\widetilde{\boldsymbol{b}}) = \frac{\mu_0}{2}\hat{\boldsymbol{h}}\cdot\hat{\boldsymbol{h}} = \frac{1}{2\mu_0}(\widetilde{\boldsymbol{b}} - \mu_0\rho\boldsymbol{\mu})\cdot(\widetilde{\boldsymbol{b}} - \mu_0\rho\boldsymbol{\mu}) \tag{6.9}$$

We obtain the mixed energy-enthalpy function by the partial Legendre transformation

$$\rho\psi'(\boldsymbol{F},\boldsymbol{\mu},\widetilde{\boldsymbol{h}}) = \inf_{\widetilde{\boldsymbol{b}}}\left[\rho\psi(\boldsymbol{F},\boldsymbol{\mu},\widetilde{\boldsymbol{b}}) - \widetilde{\boldsymbol{h}}\cdot\widetilde{\boldsymbol{b}}\right] \tag{6.10}$$

with respect to the magnetic (induction) slot. This transformation affects only the free space part ψ_{vac} of the free energy. The necessary condition of (6.10) gives (6.8). Using this as an elimination equation for $\widetilde{\boldsymbol{b}}$, we get from (6.10) the energy-enthalpy function

$$\rho\psi'(\boldsymbol{F},\boldsymbol{\mu},\widetilde{\boldsymbol{h}}) = \rho\psi_{mat}(\boldsymbol{F},\boldsymbol{\mu}) - \frac{\mu_0}{2}\widetilde{\boldsymbol{h}}\cdot\widetilde{\boldsymbol{h}} - \mu_0\rho\boldsymbol{\mu}\cdot\widetilde{\boldsymbol{h}}\ , \tag{6.11}$$

which includes the free energy density ψ_{mat} of the solid material. With this function at hand, we finally obtain the *energy-enthalpy functional* of the magnetized solid $\mathcal{S}$ embedded in the free space box Ω_t

$$E'(\boldsymbol{\varphi},\boldsymbol{\mu},\widetilde{\phi}) = \int_{\mathcal{S}} \rho[\psi_{mat}(\nabla_{\boldsymbol{X}}\boldsymbol{\varphi},\boldsymbol{\mu}) + \mu_0\boldsymbol{\mu}\cdot\nabla_{\boldsymbol{x}}\widetilde{\phi}]\,dv - \frac{\mu_0}{2}\int_{\Omega_t}|\nabla_{\boldsymbol{x}}\widetilde{\phi}|^2\,dv\ . \tag{6.12}$$

6.2.3. Loading Functional of Magneto-Elasticity

Here we specify the potential of the external loads Π^{ext}. For defining this potential, we consider a *prescribed body force density per unit mass* $\overline{\boldsymbol{\gamma}}$, a *prescribed traction per unit current area* $\overline{\boldsymbol{t}}$, and a *prescribed applied magnetic field* $\overline{\boldsymbol{h}}$. Thus, we have

$$\Pi^{ext}(\boldsymbol{\varphi},\boldsymbol{\mu}) = \int_{\mathcal{S}}(\rho\overline{\boldsymbol{\gamma}}\cdot\boldsymbol{\varphi} + \mu_0\rho\boldsymbol{\mu}\cdot\overline{\boldsymbol{h}})\,dv + \int_{\partial\mathcal{S}_t}\overline{\boldsymbol{t}}\cdot\boldsymbol{\varphi}\,da\ , \tag{6.13}$$

While the prescribed body force $\overline{\boldsymbol{\gamma}}$ and the traction $\overline{\boldsymbol{t}}$ on the boundary $\partial\mathcal{S}_t$ are taken as fixed functions of the material coordinates or "dead loads," the applied magnetic field $\overline{\boldsymbol{h}}$ is treated slightly differently[8] in order to allow us to simulate the applications considered

[7] We have used the fact that the applied magnetic field $\overline{\boldsymbol{h}}$ results in the induction $\overline{\boldsymbol{b}} = \mu_0\overline{\boldsymbol{h}}$.

[8] Physically, this field represents the field created by another magnetized body or a current carrying coil [51]

here. We assume that the $\overline{\boldsymbol{h}}$ dependence on the material coordinates $\boldsymbol{X}$ is described via a constant vector $\overline{\boldsymbol{H}}$ and the deformation $\boldsymbol{F}$ of the body $\mathcal{B}$ only. With regard to applications of interest here, this will give rise to two cases of interest namely[9]

1. $\overline{\boldsymbol{h}}$ is a uniform field similar to the dead load $\boldsymbol{\gamma}$, hence $\overline{\boldsymbol{h}}=\overline{\boldsymbol{H}}$ and
2. $\overline{\boldsymbol{h}}$ deforms with the body, as in the case of the finger actuator where $\overline{\boldsymbol{h}}=\boldsymbol{F}\overline{\boldsymbol{H}}$.

6.3. Variational Principle for Stationary Problems

6.3.1. The Variational Statement

We define a global variational principle, that governs the boundary-value-problem of finite deformation magneto-mechanics

$$\boxed{\{\boldsymbol{\varphi},\boldsymbol{\mu},\widetilde{\phi}\}=\arg\Big\{\inf_{\boldsymbol{\varphi}\in\mathcal{R}^3}\inf_{\boldsymbol{\mu}\in\mathcal{R}^3}\sup_{\widetilde{\phi}\in\mathcal{R}}\Pi'_{stat}(\boldsymbol{\varphi},\boldsymbol{\mu},\widetilde{\phi};t)\Big\}\ .} \tag{6.14}$$

Here the *stationary magneto-elastic potential* Π'_{stat} is constructed from the energy-enthalpy functional and the potential due to applied loads as

$$\Pi'_{stat}(\boldsymbol{\varphi},\boldsymbol{\mu},\widetilde{\phi}):=E'(\boldsymbol{\varphi},\boldsymbol{\mu},\widetilde{\phi})-\Pi^{ext}(\boldsymbol{\varphi},\boldsymbol{\mu})\ . \tag{6.15}$$

Thus the total potential reads

$$\begin{aligned}\Pi'_{stat}(\boldsymbol{\varphi},\boldsymbol{\mu},\widetilde{\phi})=&\int_{\mathcal{S}}\rho\big[\psi_{mat}(\nabla_{\boldsymbol{X}}\boldsymbol{\varphi},\boldsymbol{\mu})+\mu_0\boldsymbol{\mu}\cdot\nabla_{\boldsymbol{x}}\widetilde{\phi}-\mu_0\boldsymbol{\mu}\cdot\overline{\boldsymbol{h}}-\overline{\boldsymbol{\gamma}}\cdot\boldsymbol{\varphi}\big]\,dv\\&-\int_{\partial\mathcal{S}_t}\overline{\boldsymbol{t}}\cdot\boldsymbol{\varphi}\,da-\frac{\mu_0}{2}\int_{\Omega}|\nabla_{\boldsymbol{x}}\widetilde{\phi}|^2\,dv\ ,\end{aligned} \tag{6.16}$$

Optimizing the functional (6.16) with respect to the magnetic potential $\widetilde{\phi}$, we obtain

$$\mu_0\,\mathrm{div}[-\nabla_{\boldsymbol{x}}\widetilde{\phi}+\rho\boldsymbol{\mu}]=0\ , \tag{6.17}$$

which is the Gauss law of magnetism. For a given $\boldsymbol{\mu}$, the above equation shows that the potential $\widetilde{\phi}$ is *induced by the magnetization*. This qualifies the name chosen for $\widetilde{\phi}$ and $\widetilde{\boldsymbol{h}}$. As shown by James & Kinderlehrer [80] p.220 and [81] p.246. we can use (6.17) to get the condition

$$\int_{\mathcal{S}}\rho\boldsymbol{\mu}\cdot\nabla_{\boldsymbol{x}}\widetilde{\phi}\,dv=\int_{\Omega}|\nabla_{\boldsymbol{x}}\widetilde{\phi}|^2\,dv\ . \tag{6.18}$$

See also the "companion theorem" in Brown [19] p.58 for more details. Substituting this result and using $\widetilde{\boldsymbol{h}}=-\nabla_{\boldsymbol{x}}\widetilde{\phi}$ into (6.16) yields the functional

$$\hat{\Pi}(\boldsymbol{\varphi},\boldsymbol{\mu})=\int_{\mathcal{S}}\rho[\psi_{mat}(\nabla_{\boldsymbol{X}}\boldsymbol{\varphi},\boldsymbol{\mu})-\mu_0\boldsymbol{\mu}\cdot\overline{\boldsymbol{h}}-\overline{\boldsymbol{\gamma}}\cdot\boldsymbol{\varphi}]\,dv-\int_{\partial\mathcal{S}_t}\overline{\boldsymbol{t}}\cdot\boldsymbol{\varphi}\,da+\frac{\mu_0}{2}\int_{\Omega}\widetilde{\boldsymbol{h}}\cdot\widetilde{\boldsymbol{h}}\,dv \tag{6.19}$$

[9] Thus, we can account for the viewpoints of Steigmann [148] and Ericksen [51] on the field $\overline{\boldsymbol{h}}$. Additionally, as will be seen later, we will be able to inculde a stress contribution of the applied field into the Maxwell stress rather than have it as a body force.

which coincides with the potential energy expression in KANKANALA & TRIANTAFYLLIDIS [88] p.2886 and [89] p.1149 (excluding the energy of the applied field, which being constant, is not considered in their subsequent treatment anyway). This functional is used in [88] as a starting point, to derive alternative global functionals for variational principles governing the magneto-elastic response of MREs[10]. If we make the opposite substitution, we obtain the following expression

$$\tilde{\Pi}(\boldsymbol{\varphi},\boldsymbol{\mu}) = \int_{\mathcal{S}} \rho[\psi_{mat}(\nabla_{\boldsymbol{X}}\boldsymbol{\varphi},\boldsymbol{\mu}) - \frac{\mu_0}{2}\boldsymbol{\mu}\cdot\widetilde{\boldsymbol{h}} - \mu_0\boldsymbol{\mu}\cdot\overline{\boldsymbol{h}} - \overline{\boldsymbol{\gamma}}\cdot\boldsymbol{\varphi}]\,dv + \int_{\partial\mathcal{S}_t}\overline{\boldsymbol{t}}\cdot\boldsymbol{\varphi}\,da\ . \tag{6.20}$$

This expression appears as the quantity to be minimized in BROWN [21] p.73–74 (here however, we ignore exchange effects and hence have no dependence on the gradient of the magnetization), in which we can identify the second term in the first integral as the *magnetostatic energy of the self-field* or the *demagnetization energy*. The third term is the *Zeeman energy*.

6.3.2. Euler-Lagrange Equations in Reference Configuration

Since we are concerned with finite element implementation, we will now go over to the more amenable reference configuration. Using the appropriate pull-back operations we get the potential governing the boundary-value-problem of finite deformation magnetoelasticity in the Lagrangian setting. See TOUPIN [156] p.880–881 for an account on this point. Thus,

$$\widetilde{\phi}(\boldsymbol{X}) = \widetilde{\phi}(\boldsymbol{\varphi}(\boldsymbol{X})),\quad \boldsymbol{\mu}(\boldsymbol{X}) = \boldsymbol{\mu}(\boldsymbol{\varphi}(\boldsymbol{X})),\quad \overline{\boldsymbol{h}}(\boldsymbol{X}) = \overline{\boldsymbol{h}}(\boldsymbol{\varphi}(\boldsymbol{X}))\ , \tag{6.21}$$

in Ω. Note that $\boldsymbol{\mu} = \boldsymbol{0}$ outside the body. If we denote $\mathcal{B}$ as the reference configuration of the body, ie. $\mathcal{B}=\boldsymbol{\varphi}^{-1}(\mathcal{S})$, we can now rewrite the variational potential (6.16)

$$\begin{aligned}\Pi'_{stat}(\boldsymbol{\varphi},\boldsymbol{\mu},\widetilde{\phi}) = &\int_{\mathcal{B}}\rho_0\big[\Psi_{mat}(\boldsymbol{F},\boldsymbol{\mu}) - \mu_0\boldsymbol{\mu}\cdot(\boldsymbol{F}^{-T}\widetilde{\boldsymbol{H}}) - \mu_0\boldsymbol{\mu}\cdot\overline{\boldsymbol{h}} - \overline{\boldsymbol{\gamma}}\cdot\boldsymbol{\varphi}\big]\,dV\\ &- \int_{\partial\mathcal{S}_t}\overline{\boldsymbol{t}}\cdot\boldsymbol{\varphi}\,da - \frac{\mu_0}{2}\int_{\Omega} J\big|\boldsymbol{F}^{-T}\widetilde{\boldsymbol{H}}\big|^2\,dV\end{aligned} \tag{6.22}$$

where we have used $\boldsymbol{F} = \nabla_{\boldsymbol{X}}\boldsymbol{\varphi}$ and $\widetilde{\boldsymbol{H}} = -\nabla_{\boldsymbol{X}}\widetilde{\phi}$ for brevity. The necessary condition of the variational statement is that the first variation of (6.22) should be zero. Thus, taking the first variation and using the divergence theorem we then get

$$\begin{aligned}\delta\Pi'_{stat} = &-\int_{\mathcal{B}}(\mathrm{Div}\,\boldsymbol{P} + \rho_0\overline{\boldsymbol{\gamma}})\cdot\delta\boldsymbol{\varphi}\,dV + \int_{\partial\mathcal{B}_t}\big\{[\![\boldsymbol{P}]\!]\cdot\boldsymbol{N} - \overline{\boldsymbol{t}}\big\}\cdot\delta\boldsymbol{\varphi}\,dA\\ &+\int_{\mathcal{B}}\rho_0(\partial_{\boldsymbol{\mu}}\Psi_{mat} - \mu_0\boldsymbol{h})\cdot\delta\boldsymbol{\mu}\,dV - \int_{\Omega}\mathrm{Div}\,\widetilde{\boldsymbol{B}}\ \delta\widetilde{\phi}\,dV + \int_{\partial\mathcal{B}}[\![\widetilde{\boldsymbol{B}}]\!]\cdot\boldsymbol{N}\delta\widetilde{\phi}\,dA\end{aligned} \tag{6.23}$$

for the virtual fields $\{\delta\boldsymbol{\varphi},\delta\boldsymbol{\mu},\delta\widetilde{\phi}\}$ with $\delta\boldsymbol{\mu}=\boldsymbol{0}$ on $\Omega\setminus\mathcal{B}$ and $\delta\widetilde{\phi}=0$ on $\partial\Omega$. The above expression makes use of the following identifications. The *total* first Piola-Kirchhoff stress is the sum of a mechanical part and non-mechanical part

$$\boldsymbol{P} := \rho_0\partial_{\boldsymbol{F}}\Psi_{mat} + \boldsymbol{P}_{Max}\ , \tag{6.24}$$

[10]The focus in [88] being magnetoelastic stability problems, obliges them to consider, in detail, only those functionals that lead to minimization problems. We do not have this constraint here.

where $\boldsymbol{P}_{Max}$, is the Maxwell stress tensor (for this formulation) and is given by

$$\boldsymbol{P}_{Max} := \boldsymbol{F}^{-T}\widetilde{\boldsymbol{H}} \otimes \widetilde{\boldsymbol{B}} - \frac{\mu_0}{2} J\boldsymbol{C}^{-1} : (\widetilde{\boldsymbol{H}} \otimes \widetilde{\boldsymbol{H}})\boldsymbol{F}^{-T} + \rho_0\mu_0\boldsymbol{\mu} \cdot \partial_{\boldsymbol{F}}\overline{\boldsymbol{h}} \ . \tag{6.25}$$

That expression is derived assuming that the applied magnetic field $\overline{\boldsymbol{h}}$ depends on the material coordinates via the deformation gradient only and also makes use of the induced magnetic induction in the Lagrangian configuration

$$\widetilde{\boldsymbol{B}} := \mu_0(J\boldsymbol{C}^{-1}\widetilde{\boldsymbol{H}} + \rho_0\boldsymbol{F}^{-1}\boldsymbol{\mu}) \ . \tag{6.26}$$

If we denote the (Eulerian) total Maxwellian magnetic field $\boldsymbol{h}$ is denoted by

$$\boldsymbol{h} := \overline{\boldsymbol{h}} + \boldsymbol{F}^{-T}\widetilde{\boldsymbol{H}} \ , \tag{6.27}$$

we can now exploit the independence and arbitrariness of the variations of the primary variables, to get the following balance equations as the Euler equations

$$\left.\begin{aligned} \operatorname{Div}\boldsymbol{P} + \rho_0\overline{\boldsymbol{\gamma}} &= \boldsymbol{0} \\ \partial_{\boldsymbol{\mu}}\Psi_{mat} - \mu_0\boldsymbol{h} &= \boldsymbol{0} \\ \operatorname{Div}\widetilde{\boldsymbol{B}} &= 0 \end{aligned}\right\} \text{ in } \mathcal{B} \tag{6.28}$$

along with the boundary condition and jump condition at the interface between the solid and the surrounding free space

$$[\![\boldsymbol{P}]\!] \cdot \boldsymbol{N} = \overline{\boldsymbol{t}} \ \text{ on } \partial\mathcal{B}_t \quad \text{and} \quad [\![\widetilde{\boldsymbol{B}}]\!] \cdot \boldsymbol{N} = 0 \ \text{ on } \partial\mathcal{B} \tag{6.29}$$

respectively. Additionally, in the surrounding free space we have the the field equations

$$\operatorname{Div}[J\boldsymbol{C}^{-1}\widetilde{\boldsymbol{H}}] = 0 \quad \text{and} \quad \operatorname{Div}\boldsymbol{P}_{Max} = \boldsymbol{0} \ \text{ in } \Omega \setminus \mathcal{B} \tag{6.30}$$

6.4. Finite Element Implementation of the Coupled Problem

We now consider aspects of computational implementation of the variational principle. For notational convenience, we will focus on pure Dirichlet problems. We introduce the local energy-enthalpy function

$$\pi = \rho_0\big[\Psi_{mat} - \mu_0\boldsymbol{\mu}\cdot(\boldsymbol{F}^{-T}\widetilde{\boldsymbol{H}}) - \mu_0\boldsymbol{\mu}\cdot\overline{\boldsymbol{h}} - \overline{\boldsymbol{\gamma}}\cdot\boldsymbol{\varphi}\big] - \frac{\mu_0}{2}J\big|\boldsymbol{F}^{-T}\widetilde{\boldsymbol{H}}\big|^2 \tag{6.31}$$

Taking advantage of the fact that the Euler equation $(6.28)_2$ is of local character, we solve for the corresponding variable $\boldsymbol{\mu}$ locally[11]. Thus the the subproblem

$$\boxed{(L): \quad \{\boldsymbol{\mu}\} = \arg\Big\{\inf_{\boldsymbol{\mu}} \ \Pi'_{stat}(\boldsymbol{\varphi}, \boldsymbol{\mu}, \widetilde{\phi})\Big\}} \tag{6.32}$$

[11]This will cause a substantial reduction in the memory requirements but should be expected to cause an increase in computation time (time-memory tradeoff). Hence this approach should be followed for large problems where memory resources are a limiting factor. In case one does not have this constraint, there is no need to solve for $\boldsymbol{\mu}$ locally and it may be retained as a global variable.

is considered at a local level, while simultaneously, the other primary variables $\boldsymbol{\varphi}$ and $\widetilde{\phi}$ are solved for by resorting to the finite element machinery that will be described shortly. Note that (6.32) implies

$$\mathbb{r}_{\boldsymbol{\mu}} := \partial_{\boldsymbol{\mu}}\pi = \partial_{\boldsymbol{\mu}}\Psi_{mat} - \mu_0 \boldsymbol{h} = 0 \ , \tag{6.33}$$

which is solved for $\boldsymbol{\mu}$ at each Gauss point. Since this is a nonlinear equation, we solve this iteratively via a local Newton update in the usual manner

$$\boldsymbol{\mu} \Leftarrow \boldsymbol{\mu} - \mathbb{c}_{\boldsymbol{\mu}}^{-1}\mathbb{r}_{\boldsymbol{\mu}} \quad \text{with} \quad \mathbb{c}_{\boldsymbol{\mu}} := \partial_{\boldsymbol{\mu}\boldsymbol{\mu}}\pi \ , \tag{6.34}$$

until convergence $|\mathbb{r}_{\boldsymbol{\mu}}| < tol$, where tol is a given tolerance value.

We now describe the simultaneous finite element solution for the other primary variables $\boldsymbol{\varphi}$ and $\widetilde{\phi}$ using a compact notation that is suitable for concise implementation. The global part of the problem (G) to be solved here is

$$\boxed{(G): \quad \{\boldsymbol{\varphi}, \widetilde{\phi}\} = \arg\Big\{ \inf_{\boldsymbol{\varphi}} \sup_{\widetilde{\phi}} \ \Pi'_{stat}(\boldsymbol{\varphi}, \boldsymbol{\mu}, \widetilde{\phi}) \Big\} \ .} \tag{6.35}$$

We consider the spatial discretization of the coupled problem by a finite element method. Let $\mathfrak{T}^h$ denote a finite element triangulation of the domain $\mathcal{B}$. The index h indicates a typical mesh size based on E^h finite element domains $\mathcal{B}_e^h \in \mathfrak{T}^h$ and N^h global nodes. The *global nodal degrees of freedom* are the deformation map and the magnetic potential at a typical nodal point of the finite element mesh.

$$\mathfrak{d} := [\boldsymbol{\varphi}, -\widetilde{\phi}]^T \in \mathcal{R}^{(d+1)N^h} \tag{6.36}$$

The constitutive state variables for the coupled magneto-mechanical problem form the *generalized gradient field* $\mathfrak{F} := \{\nabla\boldsymbol{\varphi}, \nabla\widetilde{\phi}\}$. Explicitly, we get the discrete global strain-like vector

$$\mathfrak{F}^h = \mathfrak{B}(\boldsymbol{X})\mathfrak{d} \tag{6.37}$$

$\mathfrak{B}$ is a symbolic representation of the global matrices of shape functions for the coupled problem. Clearly, these global arrays are never formulated explicitly, but represent symbolically the interpolations on all finite element domains $\mathcal{B}_e^h \in \mathfrak{T}^h$. Note that the global nodal variable vector $\mathfrak{d}$ is formed from element vectors $\mathfrak{d}^e$ by a standard finite element assembling procedure. For three-dimensional problems $d = 3$, the generalized displacement vector in (6.36) at the node I is

$$\mathfrak{d}_I = [\varphi_1, \varphi_2, \varphi_3, -\widetilde{\phi}\,]_I^T \ . \tag{6.38}$$

Associated with node I of a standard finite element e, the finite element interpolation matrix for the constitutive state in (6.37) has the form

$$\mathfrak{B}_I^e = \begin{bmatrix} N_{,X} & & & N_{,Y} & & & N_{,Z} & & \\ & N_{,Y} & & & N_{,X} & N_{,Z} & & & \\ & & N_{,Z} & & & & N_{,Y} & N_{,X} & \\ & & & & & & & & N_{,X}\ N_{,Y}\ N_{,Z} \end{bmatrix}_I^T \tag{6.39}$$

in terms of the shape functions N_I and their material derivatives. With the generalized displacement (6.36) and the constitutive state fields (6.37), we write the finite element discretization of the potential Π_{stat} as

$$\Pi^h(\mathfrak{d}) = \int_{\mathcal{B}^h} \pi(\mathfrak{B}\mathfrak{d})\, dV \ , \tag{6.40}$$

where we drop the subscript *stat* but use the superscript h to denote a spatial discretization. Then, the finite-step-sized discrete stationary principle

$$\boxed{\mathfrak{d} = \arg\left\{\operatorname*{stat}_{\mathfrak{d}} \Pi^h(\mathfrak{d})\right\}} \tag{6.41}$$

determines the nodal variables $\mathfrak{d}$ of the finite element mesh. The necessary condition of the discrete variational problem in terms of the generalized stress array $\mathfrak{S}^h$ reads

$$\Pi^h_{,\mathfrak{d}} := \operatorname*{A}_{e=1}^{N^h} \left\{ \int_{\mathcal{B}^e} \mathfrak{B}^{eT}[\mathfrak{S}^h]\, dV \right\} = \boldsymbol{0} \quad \text{with} \quad \mathfrak{S}^h := \partial_{\mathfrak{F}}\pi = [\partial_{\boldsymbol{F}}\pi, \partial_{\widetilde{\boldsymbol{H}}}\pi]^T \tag{6.42}$$

and provides a nonlinear algebraic system for the determination of the nodal variables $\mathfrak{d}$. For smooth problems, a standard Newton-type iteration of the nonlinear algebraic system (6.42) updates the generalized displacements by the algorithm

$$\mathfrak{d} \Leftarrow \mathfrak{d} - [\Pi^h_{,\mathfrak{d}\mathfrak{d}}]^{-1}[\Pi^h_{,\mathfrak{d}}] \tag{6.43}$$

in terms of the monolithic tangent matrix of the coupled problem

$$\Pi^h_{,\mathfrak{d}\mathfrak{d}} := \operatorname*{A}_{e=1}^{N^h} \left\{ \int_{\mathcal{B}^e} \mathfrak{B}^{eT}[\partial^2_{\mathfrak{F}\mathfrak{F}}\pi]\mathfrak{B}^e\, dV \right\} . \tag{6.44}$$

Observe the *symmetry of the tangent matrix* $\Pi^h_{,\mathfrak{d}\mathfrak{d}}$ induced by the variational structure of the coupled two-field problem. The update (6.43) is performed until convergence is achieved in the sense $\|\Pi^h_{,\mathfrak{d}}\| < tol$. Observe further that the finite element tangent is governed by the *generalized tangent arrays*

$$\mathfrak{C}^h := \begin{bmatrix} (\partial^2_{\boldsymbol{F}\boldsymbol{F}}\pi - \partial^2_{\boldsymbol{F}\boldsymbol{\mu}}\pi\ \mathbb{c}^{-1}_{\boldsymbol{\mu}\boldsymbol{\mu}}\ \partial^2_{\boldsymbol{\mu}\boldsymbol{F}}\pi) & (\partial^2_{\boldsymbol{F}\widetilde{\boldsymbol{H}}}\pi - \partial^2_{\boldsymbol{F}\boldsymbol{\mu}}\pi\ \mathbb{c}^{-1}_{\boldsymbol{\mu}\boldsymbol{\mu}}\ \partial^2_{\boldsymbol{\mu}\widetilde{\boldsymbol{H}}}\pi) \\ (\partial^2_{\widetilde{\boldsymbol{H}}\boldsymbol{F}}\pi - \partial^2_{\widetilde{\boldsymbol{H}}\boldsymbol{\mu}}\pi\ \mathbb{c}^{-1}_{\boldsymbol{\mu}\boldsymbol{\mu}}\ \partial^2_{\boldsymbol{\mu}\boldsymbol{F}}\pi) & (\partial^2_{\widetilde{\boldsymbol{H}}\widetilde{\boldsymbol{H}}}\pi - \partial^2_{\widetilde{\boldsymbol{H}}\boldsymbol{\mu}}\pi\ \mathbb{c}^{-1}_{\boldsymbol{\mu}\boldsymbol{\mu}}\ \partial^2_{\boldsymbol{\mu}\widetilde{\boldsymbol{H}}}\pi) \end{bmatrix} \tag{6.45}$$

i.e. the first and second derivatives of the enthalpy density function π defined in (6.40) by the discretized constitutive state vector $\mathfrak{F}^h$. These arrays are a critical ingredient of the proposed variational formulation and make the notation extremely compact.

6.5. Properties of the Free Energy Function

6.5.1. Objectivity

Objectivity is explored by studying the effect of a rigid body motion superimposed on the deformed configuration. In our case it will be sufficient to study the objectivity of the function ψ_{mat} by imposing a rigid body motion of the form $\boldsymbol{\varphi}^+ = \boldsymbol{Q}(t)\boldsymbol{\varphi} + \boldsymbol{c}(t)$ where $\boldsymbol{Q}$ is a *proper rotation* and $\boldsymbol{c}(t)$ is a rigid body translation. In other words

$$\Psi_{mat}(\boldsymbol{Q}\boldsymbol{F}, \boldsymbol{Q}\boldsymbol{\mu}) \stackrel{!}{=} \Psi_{mat}(\boldsymbol{F}, \boldsymbol{\mu}) \quad \forall\, \boldsymbol{Q} \in \mathcal{SO}(3) \tag{6.46}$$

6.5.2. Material Symmetry

The principle of material symmetry states that locally the free energy-enthalpy function ought to be invariant with respect to rotations $\boldsymbol{Q}$ superimposed onto the open neighborhood $\mathcal{N}_X \subset \mathcal{B}$ of a material point $\boldsymbol{X}$ in the reference configuration, in case these rotations are elements of the appropriate *material symmetry group* $\mathcal{G} \subset \mathcal{SO}(3)$. Or in other words, a magnetomechanical experiment involving the considered material should make no distinction between symmetry-related reference states. For the objective reduced form of the free energy-enthalpy function this requirement is mathematically expressed as

$$\Psi_{mat}(\boldsymbol{F}\boldsymbol{Q}, \boldsymbol{\mu}) \stackrel{!}{=} \hat{\Psi}_{mat}(\boldsymbol{F}, \boldsymbol{\mu}) \ , \quad \forall\, \boldsymbol{Q} \in \mathcal{G} \subset \mathcal{SO}(3) \ . \tag{6.47}$$

Note that for a isotropic MREs considered here, the symmetry group is identical to the set of all rotations, i.e. $\mathcal{G} \equiv \mathcal{SO}(3)$.

6.5.3. Magnetic Symmetry

This is an additional symmetry constraint arising due to the dependence of Ψ_{mat} on $\boldsymbol{\mu}$. For our purposes, it implies that the state of the material remains unchanged on reversal of the magnetization direction[12]. Thus we have

$$\Psi_{mat}(\boldsymbol{F}, -\boldsymbol{\mu}) \stackrel{!}{=} \Psi_{mat}(\boldsymbol{F}, \boldsymbol{\mu}) \ . \tag{6.48}$$

6.5.4. Invariants

Assuming that the material is isotropic, the combination of requirements in (6.46), (6.47) and (6.48) imply that the free energy is a function of six invariants

$$\begin{aligned} &I_1 := \operatorname{tr} \boldsymbol{C}, \quad I_2 := \tfrac{1}{2}\left[(\operatorname{tr} \boldsymbol{C})^2 - \operatorname{tr}(\boldsymbol{C}^2)\right], \quad I_3 := \det \boldsymbol{C}, \\ &I_4 := \boldsymbol{\mu} \cdot \boldsymbol{\mu}, \quad I_5 := (\boldsymbol{F}^T\boldsymbol{\mu}) \cdot (\boldsymbol{F}^T\boldsymbol{\mu}), \quad I_6 := \boldsymbol{C} : [(\boldsymbol{F}^T\boldsymbol{\mu}) \otimes (\boldsymbol{F}^T\boldsymbol{\mu})] \end{aligned} \tag{6.49}$$

The discussion on the constitutive framework below will present suitable candidates for the free energy function that satisfy the requirements above.

6.6. Constitutive Framework Modeling MREs

In the previous chapter, we outlined the variational machinery required to set up the FEM framework for magnetomechanically coupled boundary value problems. With that background, we now present the building blocks for the construction of the constitutive model for the magnetoelastic response of MREs. We will use a multiplicative split of the deformation gradient into a prescribed magnetostrictive deformation and a stress producing part. In this respect, we outline a general structure that includes three alternatives for the split. This approach enables the modular incorporation of a range of existing mechanical, and magnetostatic models. These mechanical network kernels may have statistically-based free energies for polymer networks, such as outlined in Treloar [158], Flory [59], Arruda & Boyce [1], Boyce & Arruda [13] and Miehe, Göktepe & Lulei [118], and are included without any change. Although we show how existing statistical models may be used to construct the free energy, one may even use purely phenomenological models.

[12] Note that this constraint does not apply to piezomagnetic materials, see Dzyaloshinsky [47, 48] and Tavger & Zaitsev [150] and references cited therein.

6.6.1. Ingredient 1: Additive Split of Energy-Enthalpy Density

First we assume an additive decomposition of the total enthalpy function into a *mechanical part* and a *magnetostatic part*,

$$\hat{\Psi}_{mat}(\boldsymbol{F}, \boldsymbol{\mu}) = \hat{\Psi}_{mag}(\boldsymbol{\mu}) + \hat{\Psi}_{mec}(\boldsymbol{F}, \boldsymbol{\mu}) \tag{6.50}$$

The first part $\hat{\Psi}_{mag}$ is a purely magnetic contribution to capture the (magnetic) energy stored in the rigid magnetic particles alone. Thus, this term would be the only energy contribution for a rigid magnetizable body. We show how this may be obtained from statistical models for magnetic materials. The second part $\hat{\Psi}_{mec}$ includes the energetic contribution due to the deformable composite. Thus, this part accounts for the magnetomechanical contribution ie. pure mechanical contributions as well as magnetostriction. We are aided by micro-mechanically-based theories of statistical mechanics of polymers to construct this function. Additionally, a *multiplicative magnetomechanical split of the deformation gradient* will account for the magnetostriction. Since we focus on *homogeneous material models*, we have dropped the dependence on $\boldsymbol{X}$.

6.6.2. Ingredient 2: Energy of the Magnetic State

This function models the magnetic energy stored in the material by virtue of its magnetization alone and hence will be zero in the free space (since the magnetization is zero outside the body). The contribution from the body $\mathcal{B}$ is governed entirely by the rigid, magnetic carbonyl iron particles. Keeping in mind that we are using homogeneous models, we outline two micromechanically motivated approaches to identify suitable functions for $\hat{\Psi}_{mag}(\boldsymbol{\mu})$.

6.6.2.1. Phenomenological Description of the Magnetic State. From the experimentally obtained $m-h$ characteristics in Kallio [87], Diguet et al. [36, 37], Kankanala & Triantafyllidis [89] and Danas, Kankanala & Triantafyllidis [30], it is clear that the magnetization of the magnetic material increases with the applied magnetic field, and approaches a saturation value for higher magnetic fields. There is a reasonable micromechanical explanation for this. In an absence of an applied field, the magnetic moments are arranged in such a manner that the overall magnetization is zero (in fact, the iron particles will have multiple domains that cancel out). With an increasing magnetic field, the dipole moments of the iron particles gradually reorient themselves in the direction of the applied magnetic field in order to lower their potential energy. This continues until all magnetic moments have been aligned. After that, an increase in the applied magnetic field will cause no further increase of the magnetization since the dipole moment of each atom is of fixed magnitude, see Miehe & Ethiraj [115] for computational models and simulations of the magnetization mechanism in ferromagnetics. Thus, for low magnetic fields, where the saturation values are not reached, any convex function of the magnetization, such as that from a simple theory of paramagnetism, would be adequate e.g.

$$\hat{\Psi}_{mag} := \frac{C_m}{2}\boldsymbol{\mu}\cdot\boldsymbol{\mu}\ , \tag{6.51}$$

where C_m is a material parameter that is temperature dependent and $C_m > \mu_0$, see Ericksen [50] p.40. We will call C_m as the paramagnetic coefficient. However, saturation effects observed for higher magnetic fields, prompts the use of energy functions, whose

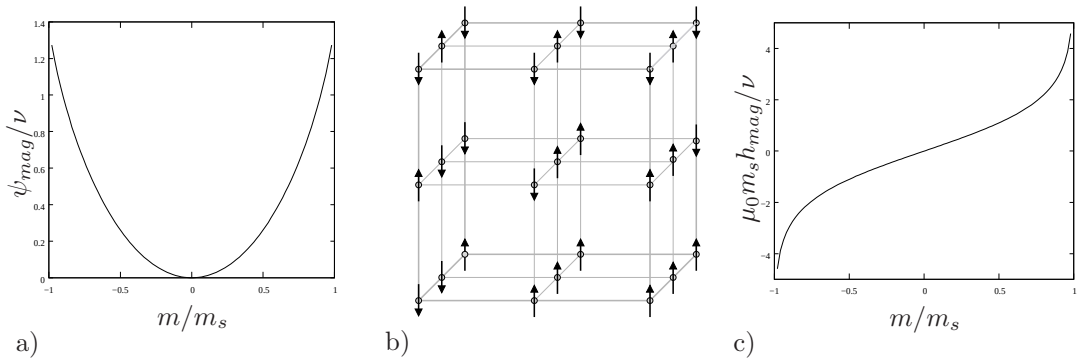

Figure 6.4: a) Normalized local magnetization energy as specified by (6.54) obtained from statistics of b) an Ising lattice with lattice sites having spins pointing up or down only. c) Its derivative with $\mu_0 h_{mag} = \partial_m \psi'_{mag}$ is an inverse saturation function. Here $\nu := \bar{n}k\theta/2$.

derivative yields inverse saturation type functions e.g. the inverse Langevin function or others, to capture the $m-h$ curve. As an example, the pure magnetic part of the free energy expression in Kankanala & Triantafyllidis [88] is

$$\hat{\Psi}_{mag} := C_{01}\frac{\boldsymbol{\mu}\cdot\boldsymbol{\mu}}{(M_s)^2} + C^*_{01}\left[\cosh\left(\frac{\boldsymbol{\mu}\cdot\boldsymbol{\mu}}{(M_s)^2}\right)\right] \tag{6.52}$$

The first derivative of this function with respect to the magnetization $\boldsymbol{\mu}$, yields the desired inverse saturation response. The values of the material parameters $C_{01}, C*_{01}$ and saturation magnetization M_s are then fitted to experiments. A similar strategy has been employed in Kankanala & Triantafyllidis [89] [13]. We also refer the reader to other phenomenological approaches for this term in Ponte Castaneda et al. [128, 60, 61], Bustamante, Dorfmann & Ogden [25] that employ formulations in terms of the total magnetic induction and total magnetic field, without having the magnetization explicitly as a field variable.

6.6.2.2. Statistical Treatment of the Magnetic State. One usually refers to an Ising model for a statistical treatment of magnetic response of materials[14]. However, Ising models give only a one dimensional response since the spins at the lattices are constrained to be "up" or "down" only. We therefore need to integrate this response over all orientations to get a three dimensional response function. We refer to the results of the Ising model presented in Smith et al. [144, 146] and assume that the exchange energy is negligible. This is consistent with our modeling approach adopted so far since we exclude exchange effects for such dilute specimens. Here, we have $\bar{n}$ dipoles per unit mass, the temperature is θ, k is the Boltzmann's constant, m is the magnetization per unit mass of the lattice, and m_s is the lattice saturation magnetization per unit mass. The free energy per unit mass of *of a system* as

$$\psi_{mag} = -\theta s \quad \text{with} \quad s = k\bar{n}\,\ln[W] \tag{6.53}$$

where W is the number of ways the spins of the lattice can be arranged in order to yield a magnetization m. If we consider a lattice of having N_+ spins upwards and N_-

[13] Danas & Triantafyllidis [29] include an additional contribution due to anisotropy caused by the existence of aligned chains of iron particles.

[14] Griffiths [66, 67] shows that the free energy of such a Ising models is extensive (proportional to the number of particles) and convex in the magnetization.

spins downwards, we can equate the problem of finding W, to finding the number of arrangements of N_+ moments on a N sites. This gives us $W = \binom{N}{N_+}$. Using this along with the Striling's approximation for factorials $\ln x! = x\,\ln x - x$, gives the free energy per unit mass as

$$\psi_{mag}(m) = \frac{\bar{n}k\theta}{2}\left[\frac{m}{m_s}\,\ln\left(\frac{1+m/m_s}{1-m/m_s}\right) + \ln\left(1-\left(\frac{m}{m_s}\right)^2\right)\right] \tag{6.54}$$

We plot the function for such cases in Figure 6.4. Following Smith et al. [144, 146] we can use a truncated series expansion as an approximation for the energy function (6.54). Thus, excluding non-essential constants,

$$\psi_{mag}(m) \approx \bar{n}k\theta\left[\left(\frac{m}{m_s}\right)^2 + \frac{5}{12}\left(\frac{m}{m_s}\right)^4\right] \tag{6.55}$$

for a Taylor series expansion of (6.54) upto quartic terms in m. This expression is more suitable for efficient numerical implementation since it avoid the logarithmic evaluations of (6.54). Note that an expansion upto the quadratic term only, would yield the simple paramagnetic expression of (6.51). The question remains on how to relate the Ising magnetization m and energy ψ_{mag} to the the (macroscopic) magnetization model. This is realised by a homogenization procedure over all orientations. The macro-magnetization component $\bar{m}$ in any direction is given in terms of the Eulerian unit vector $\boldsymbol{v}$ in that direction as

$$\bar{m} := \boldsymbol{\mu}\cdot\boldsymbol{v} \tag{6.56}$$

Under an affine relationship, the micro- and macro-magnetization components are identical and hence

$$\hat{\Psi}_{mag}(\boldsymbol{\mu}) := \frac{1}{|\mathcal{S}|}\int_{\mathcal{S}} \psi_{mag}(m)\,dA \quad \text{with} \quad m = \bar{m}\ . \tag{6.57}$$

More generally however, we allow the micro-magnetization to be different from the macro-magnetization. This is assumption is in line with micromagnetic simulations such as in Miehe & Ethiraj [115]. The micro-magnetization components, denoted by m are allowed to fluctuate around the macro-magnetization values and hence written in terms of a scalar fluctuation field defined f over a unit sphere $\mathcal{S}$. Hence,

$$m := \bar{m}f\ . \tag{6.58}$$

Although fluctuations are permitted, they are constrained by the condition

$$\langle m\rangle_q = \langle m\rangle_q \tag{6.59}$$

in terms of the $q-$root averaging operator which is defined for any scalar variable v as

$$\langle v\rangle_q = \sqrt[q]{\langle v\rangle_q} := \left[\tfrac{1}{|\mathcal{S}|}\int_{\mathcal{S}} v^q\,dA\right]^{1/q} \tag{6.60}$$

While q is treated as a parameter of the magnetization response, the fluctuation field f is determined by a *principle of minimum averaged free energy*. Thus, the macroscopic pure magnetization energy is obtained as

$$\Psi_{mag} = \sup_{\kappa} \inf_{f} \{ \langle \psi_{mag}(\bar{m} f) \rangle - \kappa (\langle \bar{m} f \rangle_q - \langle \bar{m} \rangle_q) \} \tag{6.61}$$

where κ is a Lagrange multiplier to enforce the incompressibility constraint. The necessary condition for this saddle point problem may be written as

$$\psi_{mag}(m) (\langle m \rangle_p)^{q-1} (\bar{m} f)^{1-q} = \kappa \tag{6.62}$$

A *non-trivial solution* of this equation for non-zero fluctuations f is obtained when $m = \bar{m} f$ is constant on the unit sphere $\mathcal{S}$. In this case,

$$m = \langle \bar{m} \rangle_q \quad \Rightarrow \quad \Psi_{mag}(\boldsymbol{\mu}) = \psi_{mag}(m) \tag{6.63}$$

thus relating the micro- and macro-magnetization components and energy contributions. Note that q should not be an odd number, see Menzel et al. [151]. For the special case with $q = 2$, we get

$$m = \langle \bar{m} \rangle_2 = \sqrt{\boldsymbol{\mu} \cdot \boldsymbol{\mu} / 3} \tag{6.64}$$

6.6.3. Ingredient 3: Volumetric-Isochoric Split of Local Deformation

Magnetoactive elastomers undergo nearly incompressible deformations. We account for this aspect by applying a penalty method that ensures the incompressibility constraint $J \approx 1$. In the constitutive model, it motivates a multiplicative split of the deformation map $\boldsymbol{F}$, defining its *isochoric part*

$$\bar{\boldsymbol{F}} := J^{-1/3} \boldsymbol{F} \tag{6.65}$$

and its *volumetric part* $J := \det[\boldsymbol{F}]$. As a consequence, the *mechanical contribution* to the enthalpy function is assumed to decompose into a volumetric contribution and an isochoric part,

$$\hat{\Psi}_{mec}(\boldsymbol{F}, \boldsymbol{\mu}) = U(J) + \bar{\Psi}_{mec}(\bar{\boldsymbol{F}}, \boldsymbol{\mu}) \tag{6.66}$$

that includes a magnetostatic expansion as explained below. The volumetric contribution U is considered as a penalty function which approximately enforces the incompressibility constraint. The above additive split induces a decomposition of the stresses into spherical and deviatoric parts, where only the latter is considered to be of physical relevance.

6.6.4. Ingredient 4: Magnetostrictive Deformation

We assume a multiplicative split of the total deformation gradient into *stress-free (magnetostrictive)* and *stress-producing* parts. The former, denoted by $\bar{\boldsymbol{\mathcal{E}}}$ is assumed to be a *volume-preserving spatial stretch tensor*, dependent on the current magnetization $\boldsymbol{\mu}$. A simple example construction is as follows. Consider the stretch tensor

$$\boldsymbol{\mathcal{E}}^{-1}(\boldsymbol{\mu}) := \boldsymbol{1} + c \boldsymbol{\mu} \otimes \boldsymbol{\mu} \ , \tag{6.67}$$

which is dependent on the magnetostrictive coefficient c and describes a magnetostrictive deformation aligned with the magnetization. The determinant of this tensor is $J_\mu :=$

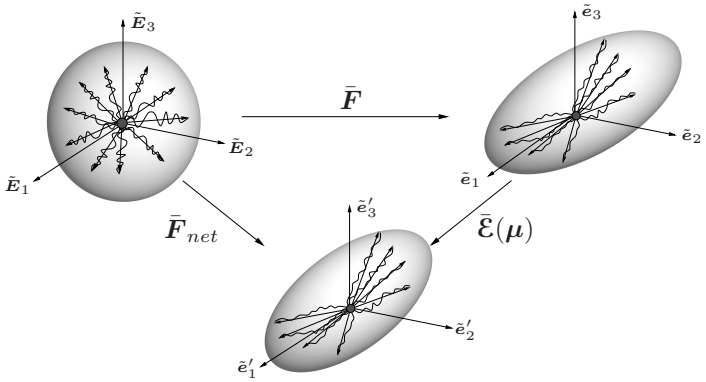

Figure 6.5: Multiplicative decomposition of isochoric part of deformation gradient into network contribution $\bar{\boldsymbol{F}}_{net}$ and local magnetically-induced deformation $\bar{\boldsymbol{\mathcal{E}}}$. We consider a *left multiplicative decomposition* $\bar{\boldsymbol{F}}_{net} = \bar{\boldsymbol{\mathcal{E}}}(\boldsymbol{\mu})\bar{\boldsymbol{F}}$.

$\det[\boldsymbol{\mathcal{E}}^{-1}] = 1 + c|\boldsymbol{\mu}|^2 > 0$. Note that the above deformation $\boldsymbol{\mathcal{E}}^{-1}$ does not preserve the volume of the polymer network. The desired *isochoric stretch mode* is obtained as the isochoric part of (7.42), governed by the multiplicative definition $\bar{\boldsymbol{\mathcal{E}}}^{-1} := J_\mu^{-1/3}\boldsymbol{\mathcal{E}}^{-1}$. Taking into account the inverse of the sum of two square matrices, see e.g. MILLER [123], we obtain a closed-form kinematic assumption for the *inverse isochoric stretch* associated with the spatial magnetization

$$\bar{\boldsymbol{\mathcal{E}}}(\boldsymbol{\mu}) = J_\mu^{1/3}\left[\boldsymbol{1} - \frac{c}{J_\mu}\boldsymbol{\mu}\otimes\boldsymbol{\mu}\right] . \tag{6.68}$$

It is used in the subsequent treatment as a part of the constitutive structure. Thus we can define the *elastic network deformation* $\bar{\boldsymbol{F}}_{net}$

$$\bar{\boldsymbol{F}}_{net} := \bar{\boldsymbol{\mathcal{E}}}\bar{\boldsymbol{F}} \tag{6.69}$$

6.6.5. Ingredient 5: Local Isochoric Mechanical Network Kernel

An important aspect of this modular constitutive structure of magneto-elasticity, is that it allows to include micromechanically-based network models for polymers without any change. This *micromechanical kernel* is assumed to define the energy $\bar{\Psi}_{mec}$ in (7.41) by the constitutive assumption

$$\bar{\Psi}_{mec}(\bar{\boldsymbol{F}}, \boldsymbol{\mu}) = \bar{\Psi}_{net}(\bar{\boldsymbol{F}}_{net}) \tag{6.70}$$

in terms of the *elastic network storage function* $\bar{\Psi}_{net}$. This function is taken from existing statistical approaches to finite elasticity of crosslinked polymer networks. We consider closed-form representations in that are described below, In classical entropic elasticity of polymer networks, the entropy s of a single polymer chain is governed by Boltzmann's equation. Hence, the free energy of a chain is

$$\psi^e = -\theta s \quad \text{with} \quad s = k\ln p\ , \tag{6.71}$$

where p is the probability density that describes the free chain response. k is the Boltzmann constant and $\theta > 0$ the absolute temperature. Now consider a single polymer consisting of N segments of equal length l as depicted in Figure 6.6a. The classical Gaussian statistics derived by KUHN [97, 98] considers the unconstrained chain with end-to-end

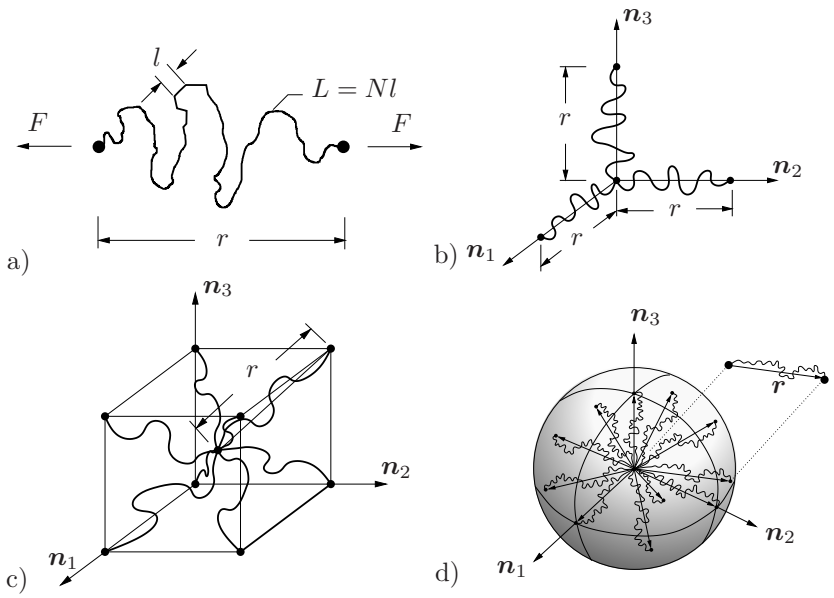

Figure 6.6: Network models for rubbery polymers. a) *Single chain* with N segments of length l, end-to-end distance r and contour length $L = Nl$. b) *Three-chain model*: Chains in principal stretch directions $\boldsymbol{n}_i$. c) *Eight-chain model*: Chains placed along the space-diagonals of a cube, all undergoing the same stretch. d) *Microsphere model*: Chain orintation continuum with directors $\boldsymbol{r}$, stretch fluctuation determined by a principle of minimum averaged energy.

distance $r := |\boldsymbol{r}| \ll L$ much smaller than the contour length $L := Nl$, i.e. moderate deformations of the chain. Here, the probability density per unit volume of a randomly jointed chain characterized by the end-to-end vector $\boldsymbol{r}$ has the form

$$p(\boldsymbol{r}) = p_0 \exp\big[-\tfrac{3}{2}\lambda^2\big] \quad \text{with} \quad p_0 := \big(\tfrac{3}{2}Nl^2\pi\big)^{3/2} , \tag{6.72}$$

see TRELOAR [158, p.47], in terms of the stretch $\lambda := r/r_0 \in [0, \sqrt{N})$. Here, $r_0 := \sqrt{N}l$ is the random-walk mean-square distance of a chain. Insertion of (6.72) into (6.71) gives the *free energy of the chain*

$$\psi^e(\lambda) = \frac{3}{2}k\theta\lambda^2 \tag{6.73}$$

as a function of the stretch λ. The simplest *network model* that links the response of a single polymer chain to the macroscopic deformation of a continuum is the *three-chain model*, which can be traced back to KUHN & GRÜN [99] and JAMES & GUTH [79]. It considers a network of n chains per unit volume and links the microscopic stretch λ of a single strain embedded in the continuum by an *affine deformation assumption* to the three macroscopic elastic principal stretches $\{\lambda_i\}_{i=1,3}$, obtained by the singular value decomposition of the (isochoric) elastic deformation map of multiplicative magneto-mechanics defined in (7.44), i.e.

$$\bar{\boldsymbol{F}}_{net} = \sum_{i=1}^{3} \lambda_i \boldsymbol{n}_i \otimes \boldsymbol{N}_i \quad \text{with} \quad \det[\bar{\boldsymbol{F}}_{net}] = 1 \ . \tag{6.74}$$

The elastic free energy of the network is constructed by taking the arithmetic average of *three representative chain energies* aligned with the macroscopic principal stretch directions as depicted in Figure 6.6b, i.e.

$$\bar{\Psi}^e_{net} = n\langle\psi\rangle \quad \text{with} \quad \langle\psi^e\rangle := \tfrac{1}{3}\left[\psi^e(\lambda_1) + \psi^e(\lambda_2) + \psi^e(\lambda_3)\right] . \tag{6.75}$$

Insertion of (6.73) into (6.75) and taking into account $\mathrm{tr}[\bar{\boldsymbol{F}}_{net}^T \boldsymbol{g} \bar{\boldsymbol{F}}_{net}^T] = \lambda_1^2 + \lambda_2^2 + \lambda_3^2$ finally gives the classical closed-form *elastic free energy function* of the polymer network

$$\bar{\Psi}_{net}^e(\bar{\boldsymbol{F}}_{net}) = \frac{\mu}{2}\,\mathrm{tr}[\bar{\boldsymbol{F}}_{net}^T \boldsymbol{g} \bar{\boldsymbol{F}}_{net}] \quad \text{with} \quad \mu := nk\theta \tag{6.76}$$

In continuum mechanics, this energy function is known as the Neo-Hookean free energy, which has through the above treatment a well-defined micromechanically motivated *network stiffness* μ. More advanced network theories of rubbery polymers applicable to large deformations replace the Gaussian statistics by the *inverse Langevin statistics*, developed by Kuhn & Grün [99] and James & Guth [79], which takes account for the finite extensibility of the chain. It results in the free energy of a single chain

$$\psi^e(\lambda) = Nk\theta(\lambda_r \mathcal{L}^{-1}(\lambda_r) + \ln \frac{\mathcal{L}^{-1}(\lambda_r)}{\sinh \mathcal{L}^{-1}(\lambda_r)}) \;, \tag{6.77}$$

which advances (6.73) for end-to-end distances r up to the limiting value L. Here, $\mathcal{L}(x) = \coth x - 1/x$ is the well-known Langevin function, see Treloar [158, p.103], and $\lambda_r := r/L = \lambda/\sqrt{N} \in [0, 1)$ the relative stretch. Furthermore, the restrictive affine deformation assumption can be relaxed by more advanced network models, such as the *non-affine microsphere network model* developed in Miehe, Göktepe & Lulei [118], that links by a particular homogenization method on the unit sphere $\mathcal{S} \subset \mathcal{R}^2$ depicted in Figure 6.6d the micro-stretch λ of the single chain to the macroscopic deformation gradient (6.74) by the p-root average of the macroscopic stretch

$$\langle \bar{\lambda} \rangle_p := \Big[\tfrac{1}{|\mathcal{S}|} \int_{\mathcal{S}} \bar{\lambda}^p \, dA \Big]^{1/p} \quad \text{with} \quad \bar{\lambda} := |\bar{\boldsymbol{F}}_{net} \boldsymbol{r}| \;, \tag{6.78}$$

where $\boldsymbol{r}$ is the unit director to the surface of the sphere. The elastic free energy of the non-affine network model is derived as

$$\bar{\Psi}_{net}^e(\bar{\boldsymbol{F}}_{net}) = n\psi^e(\langle \bar{\lambda} \rangle_p) \;. \tag{6.79}$$

This function describes the idealized network with free fluctuation of the chains between the cross-links of the network. An additional free energy representing the energy due to interaction of chain is added. The model is based on five physically motivated material parameters and shows excellent fits to multi-dimensional experimental results, as demonstrated in Figure 6.7. We refer to Miehe, Göktepe & Lulei [118] for more details. $p > 0$ in (6.78) is a material parameter. For $p = 2$, the microsphere model degenerates to the *eight-chain model* proposed by Arruda & Boyce [1] and visualized in Figure 6.6c,

$$\bar{\Psi}_{net}^e(\bar{\boldsymbol{F}}_{net}) = n\psi^e(\langle \bar{\lambda} \rangle_2) \quad \text{with} \quad \langle \bar{\lambda} \rangle_2 = \sqrt{\mathrm{tr}[\bar{\boldsymbol{F}}_{net}^T \boldsymbol{g} \bar{\boldsymbol{F}}_{net}]/3} \;, \tag{6.80}$$

which is simpler due to its closed-form relationship to the invariant $\mathrm{tr}[\bar{\boldsymbol{F}}_{net}^T \boldsymbol{g} \bar{\boldsymbol{F}}_{net}]$ of $\bar{\boldsymbol{F}}_{net}$ but of limited fitting capability. This summarizes our overview about physically motivated network models of rubber-like polymers. Further details can be found in the textbooks Treloar [158], Flory [59] and Doi & Edwards [40], as well as in the papers Boyce & Arruda [13] and Miehe, Göktepe & Lulei [118].

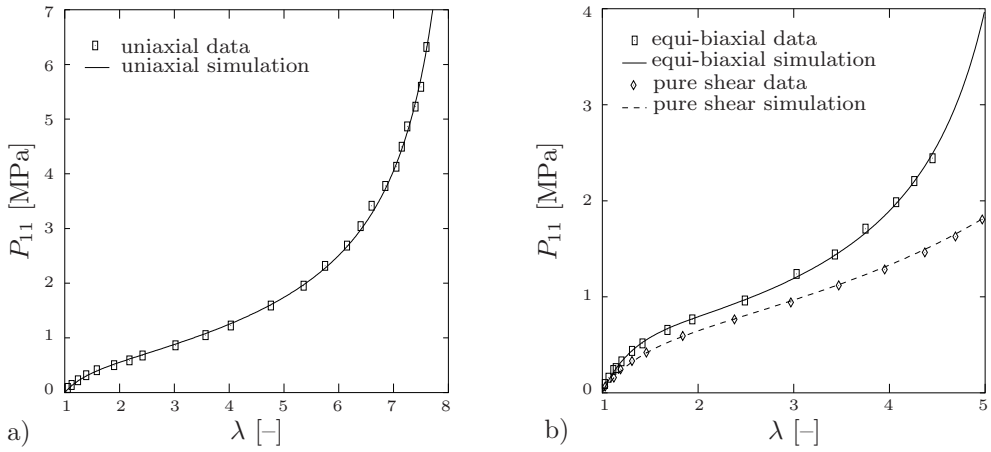

Figure 6.7: Performance of the non-affine microsphere model developed in MIEHE, GÖKTEPE & LULEI [118]. Fit of multi-dimensional test date from TRELOAR [157] with five micromechanically motivated material parameters $\mu = 0.292\,\text{MPa}, N = 22.01, p = 1.472, U = 0.744, q = 0.1086$. a) Uniaxial deformation and b) equi-biaxial and pure shear deformation.

6.7. The Stress and Magnetic Induction

With the structure of the energy-enthalpy function at hand, the material stresses take the form

$$\boxed{\boldsymbol{P} = U' J \boldsymbol{F}^{-T} + \bar{\boldsymbol{P}}^{e}_{net} : \mathbb{D} + \boldsymbol{P}_{Max}} \tag{6.81}$$

in terms of the penalty-type elastic pressure contribution, a deviatoric contribution due to the network deformation and a Maxwell-type magnetostatic contribution. The second term on the RHS of (6.81) includes the material deviatoric projection tensor defined as

$$\mathbb{D} := \partial_{\boldsymbol{F}} \bar{\boldsymbol{F}}_{net} = J^{-1/3} \bar{\mathfrak{E}} [\mathbb{I} - \tfrac{1}{3} \boldsymbol{F} \otimes \boldsymbol{F}^{-T}] \tag{6.82}$$

in terms of the fourth-order identity tensor $\mathbb{I}_{ijkl} = \delta_{ik}\delta_{jl}$. For our computations, the isochoric stress kernel $\bar{\boldsymbol{P}}_{net}$ is taken from the microsphere model of rubber elasticity and is explicitly written as

$$\bar{\boldsymbol{P}}^{e}_{net} := \partial_{\bar{\boldsymbol{F}}_{net}} \bar{\Psi}_{net}(\bar{\boldsymbol{F}}_{net}) = n \psi^{e\prime} \langle \bar{\lambda} \rangle_p^{1-p} \langle \bar{\lambda}^{p-2} \boldsymbol{t} \otimes \boldsymbol{r} \rangle \ . \tag{6.83}$$

with the Eulerian orientation vectors $\boldsymbol{t}$ related to their Lagrangian counterparts via $\boldsymbol{t} = \bar{\boldsymbol{F}}_{net} \boldsymbol{r}$. For brevity, we have not repeated the *tube* contributions of MIEHE, GÖKTEPE & LULEI [118] but they may be easily included into the model. The Lagrangian magnetic induction $\widetilde{\boldsymbol{B}}$ was already obtained in $(6.26)_2$ and is repeated here for convenience

$$\boxed{\widetilde{\boldsymbol{B}} = \mu_0 (J \boldsymbol{C}^{-1} \widetilde{\boldsymbol{H}} + \rho_0 \boldsymbol{F}^{-1} \boldsymbol{\mu})} \tag{6.84}$$

In a similar fashion, to the stress variables above the total Maxwellian magnetic field $\boldsymbol{h}$ appears as a conjugate to the magnetization $\boldsymbol{\mu}$ and the local balance of magnetomechanical microtractions may be written as

$$\boxed{\mu_0 \boldsymbol{h} = \mu_0 \boldsymbol{h}_{mag} + \bar{\boldsymbol{P}}_{net} : \mathbb{G} \ .} \tag{6.85}$$

The first term comes from the contribution of the pure magnetic response and hence $\mu_0 \boldsymbol{h}_{mag} = \partial_{\boldsymbol{\mu}} \hat{\Psi}_{mag}$ depends on the model chosen for rigid magnetic response. The second term on the RHS of (6.85) arises due to the magnetostriction and includes the tensor

$$\mathbb{G}_{ijk} := \left[\partial_{\boldsymbol{\mu}} \bar{\boldsymbol{F}}_{net}\right]_{ijk} = cD^{-2/3}\left[\frac{2}{3}\mu_k \delta_{ia} - \mu_a \delta_{ik} - \mu_i \delta_{ak} + \frac{4c}{3}\frac{\mu_i \mu_a \mu_k}{D}\right] \bar{F}_{aj} \ . \quad (6.86)$$

Note that the constitutive equations (6.81), (6.84) and (6.85) highlight the modularity of the presented approach since everything is explicitly specified except the *pure magnetic kernel* $\mu_0 \boldsymbol{h}_{mag}$ and the *stress kernel* $\bar{\boldsymbol{P}}_{net}$ *in the isochoric elastic deformation space*. This allows to include a variety of micromechanically based magnetic response functions and, more importantly, all elastic network models for polymers.

6.8. Coupled Tangent Moduli for FEM Implementation

The computation of the tangent moduli needed for Newton-type solvers needs a further derivative of the above outlined constitutive functions for the stresses and the magnetic induction. Due to the multiplicative split, these derivatives are demanding. Following Miehe [114], we compute the moduli numerically. We breifly outline the approach here but refer the reader to the original work for full details.

In order to get a compact formulation, we assemble the magneto-mechanical variables in arrays, such that

$$\mathfrak{S} := \begin{bmatrix} \boldsymbol{P} \\ -\widetilde{\boldsymbol{B}} \end{bmatrix} \quad \text{and} \quad \mathfrak{F} := \begin{bmatrix} \boldsymbol{F} \\ \widetilde{\boldsymbol{H}} \end{bmatrix} \quad (6.87)$$

denote material generalized stresses and deformations. The sensitivity of the generalized stress with respect to the generalized deformation defines the *material moduli* that we assemble in a *material magneto-mechanical coupling array*

$$\mathfrak{A} := \begin{bmatrix} \mathbb{C} & \mathbb{E} \\ \mathbb{E}^T & \mathbb{M} \end{bmatrix} . \quad (6.88)$$

They determine the sensitivity $\Delta\mathfrak{S}$ of the generalized stress array with respect to the generalized deformation increment $\Delta\mathfrak{F}$ according to $\Delta\mathfrak{S} = \mathfrak{A} \cdot \Delta\mathfrak{F}$. Let the generalized stresses and deformation be rearranged in vector arrays, such that $\mathfrak{S} = \mathfrak{S}_I$ and $\mathfrak{F} = \mathfrak{F}_I$ for $I = 1, 12$. In order to determine a numerical approximation of the tangent matrix, assume a perturbation of a given generalized strain $\mathfrak{F}$ in the form

$$\mathfrak{F}^{\epsilon}_{(I)} := \mathfrak{F} + \epsilon \mathfrak{E}_{(I)} \ , \quad (6.89)$$

where $\{\mathfrak{E}_{(I)}\}_{I=1,12}$ are base vectors which span the $\mathcal{R}^{12}$. Based on this perturbation, define the columns of the magneto-mechanical coupling array by the difference of perturbed generalized stresses relative to the current state

$$\mathfrak{A}_{I(J)} \approx \frac{1}{\epsilon}\left[\hat{\mathfrak{S}}_I(\mathfrak{F} + \epsilon \mathfrak{E}_{(J)}) - \hat{\mathfrak{S}}_I(\mathfrak{F})\right] \quad (6.90)$$

for $J = 1, 12$. This needs for twelve additional evaluations of the generalized stress for perturbed generalized deformations, governed by the material constitutive functions (6.81) and (6.84).

6.9. Numerical Examples

6.9.1. Saturation Effect in Magnetostriction

This example demonstrates that (*i*) the model captures the *saturation effect in the magnetostrictive deformation* and (*ii*) that this saturation is *due to the saturation in the magnetization response*. These points are important since (i) these characteristics are consistent with the micromechanics of MREs and (*ii*) the presented calculation highlights a qualitative difference with respect to other formulations which do not use the magnetization as a primary variable. Such formulations find it necessary to employ two saturation functions, one for the magnetic response and one for the magnetomechanical response which often yield unwieldy expressions for the energy without any micromechanical basis. The presented model does not have this drawback.

We will consider the case of magnetically-induced stress-free (up to the Maxwell stress) deformations of the MRE material. We will not solve a boundary value problem but look at the expressions corresponding to one material point of the continuum. The focus will be on showing the effect of the total magnetic field $\mu_0 \boldsymbol{h}$ on the magnetostrictive deformation. For stress-free deformations we have $\bar{\boldsymbol{F}}_{net} = \boldsymbol{1}$. This means that, due to the multiplicative split (7.42), we have $\bar{\boldsymbol{F}} = \bar{\boldsymbol{\mathcal{E}}}^{-1}$. We will consider a one-dimensional homogeneous loading case where

$$\boldsymbol{h} := \begin{bmatrix} h \\ 0 \\ 0 \end{bmatrix} \quad , \quad \boldsymbol{\mu} := \begin{bmatrix} m \\ 0 \\ 0 \end{bmatrix} \quad \text{and} \quad \bar{\boldsymbol{\mathcal{E}}}^{-1} := \frac{1}{(1+\lambda_{\mathcal{E}^{-1}})^{1/3}} \begin{bmatrix} 1+\lambda_{\mathcal{E}^{-1}} & 0 & 0 \\ 0 & 1 & 0 \\ 0 & 0 & 1 \end{bmatrix} \tag{6.91}$$

Using the expression $\boldsymbol{\mathcal{E}}^{-1} := \boldsymbol{1} + c\boldsymbol{\mu} \otimes \boldsymbol{\mu}$ for the magnetostrictive stretch, we can easily show that $\lambda_{\mathcal{E}^{-1}} = c\ m^2$. For the pure magnetic energy expression Ψ_{mag} we will use the expression (6.54) that originates from the Ising model. Since $\bar{\boldsymbol{P}}_{net} = \boldsymbol{0}$, the expression (6.85) relating the magnetic field to the magnetization reduces to $\mu_0 \boldsymbol{h} = \partial_{\boldsymbol{\mu}} \hat{\Psi}_{mag}$. In one dimension we assume the relation (6.57) which allows us to use the local magnetization as $m = (\boldsymbol{\mu} \cdot \boldsymbol{\mu})^{1/2}$ and hence,

$$\mu_0 h = \partial_m \psi_{mag} = \beta \tanh^{-1}(m/m_s) \quad \text{with} \quad \beta = \bar{n} k \theta / m_s \tag{6.92}$$

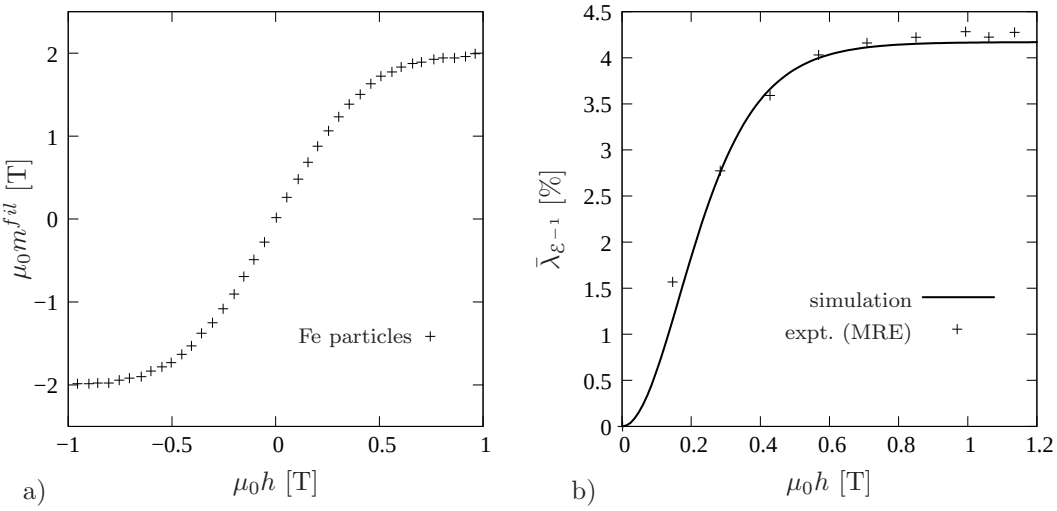

Figure 6.8: a) Experimentally determined magnetization characteristic of filler particles indicates a saturation magnetization of 2.08 T. Using this data to estimate m_s for the sample, we are able to get a good fit $c =$ and $\beta =$.

from which it now follows that the stretch saturates with an increasing magnetic field h

$$\lambda_{\mathcal{E}^{-1}} = c\,[m_s \tanh(\mu_0 h/\beta)]^2\ . \tag{6.93}$$

We may apply these calculations to find an approximate fit against a real material. In doing this, we ignore the influence of shape effects and the Maxwell stress on the specimen undergoing a homogeneous loading. The data is obtained from the experiments by Diguet [36] on isotropic MREs. The magnetization characteristic or $m-h$ curve for the filler particles (98.7% iron) are shown in Figure 6.8a. From this, it is possible to identify the saturation magnetization of the filler particles as $\mu_0 m_s^{fil} = 2.08\text{T}$. Since the MRE has a 30% volume fraction of iron, we can estimate the saturation magnetization of the MRE as $\mu_0 m_s = 2.08\text{T} \times 0.3 = 0.62\text{T}$ and hence $m_s = 1.66 \times 10^6$ A/m for the MRE.

The magnetostriction curve Figure 6.8b shows that the strains are small and hence we can approximate the isochoric magnetostrictive stretch as

$$\bar{\lambda}_{\mathcal{E}^{-1}} = (1 + \lambda_{\boldsymbol{\mathcal{E}}^{-1}})^{2/3} - 1 \approx 2/3\lambda_{\mathcal{E}^{-1}} \tag{6.94}$$

Using the magnetostriction curve, in Figure 6.8b, we can then identify the parameters c and β using (6.92) and (6.93) as $c = 2.5725 \times 10^{-11}$ m^2/A^2 and $\beta = 2.83 \times 10^{-7}$ A^2/(T·m^2). The response of the model has also been plotted and it is seen that it shows a good qualitative fit with the experimental curve.

In the examples that follow, we demonstrate the capability of the full modeling framework. As a micromechanical network kernel, we choose the microsphere model of Miehe, Göktepe & Lulei [118]. Unless mentioned otherwise, for the pure magnetic response we use the simple paramagnetic expression $\Psi_{mag} = \frac{C_m}{2}\boldsymbol{\mu}\cdot\boldsymbol{\mu}$. The structural model employs eight-node brick finite elements for the space discretization. The degrees of freedom at the nodes are the displacements $\boldsymbol{u} = \boldsymbol{\varphi} - \boldsymbol{X}$ and magnetic potential $\widetilde{\phi}$. The material parameters used in for the simulations of the boundary value problems are given in the tables. Note that the parameters used for the simulations of boundary value problems are purely academic and are not intended to correspond to any specific material since our main focus is to show the capability of the proposed finite deformation framework.

6.9.2. Spherical Magnetorheological Elastomer Sample in Free Space

In this example we consider a spherical sample of an MR elastomer under the action of a uniform magnetic field. The motivation for the example comes from Diguet [36] where the snapshot of a deformed spherical MRE sample in a uniform magnetic field. The geometry and boundary conditions of the problem is shown in Figure 6.9a. Clearly we have taken advantage of the symmetry of the problem, by considering only $1/4^{\text{th}}$ of the

Table 6.1: Magneto-Elastic Material Parameters for MRE in Free Space.

No.	Parameter	Name	MRE	Free Space	Unit
1.	κ	Bulk modulus	6.00×10^2	6.00×10^{-3}	N/mm^2
2.	μ	Shear modulus	2.07×10^{-1}	2.07×10^{-6}	N/mm^2
3.	N	Number of chain segments	4.31	4.31	–
4.	p	Non-affine averaging parameter	6.22	6.22	–
5.	c	Magnetostrictive coefficient	5.00	0.00	mm^2/A^2
6.	C_m	Paramagnetic coefficient	125.66	0.00	N/A^2

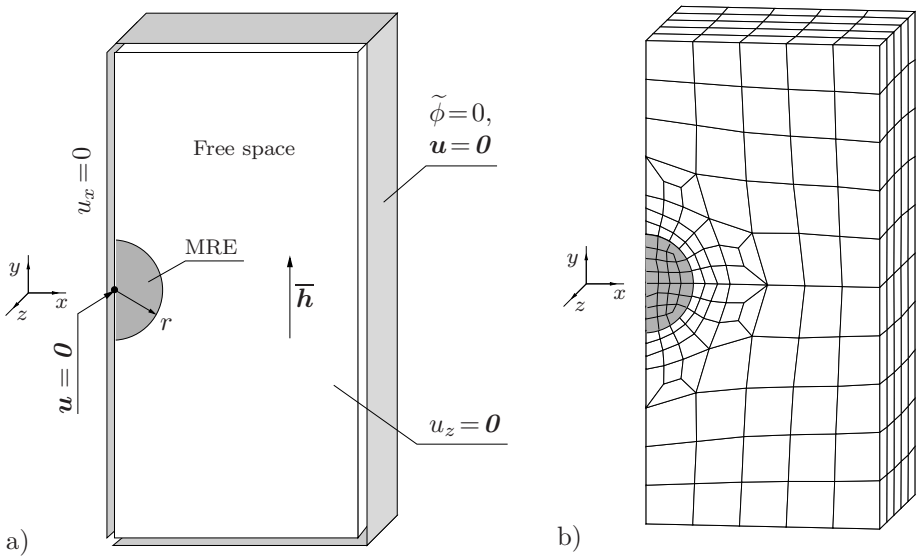

Figure 6.9: Stiff inclusion in magneto-rheological elastomer (MRE) matrix. Description of the a) boundary value problem, boundary conditions, and b) finite element mesh. Discretization with 560 elements in matrix material and 54 elements in stiff inclusion. Cube dimensions 100 mm $\times$ 50 mm and inclusion of radius $r = 10$mm.

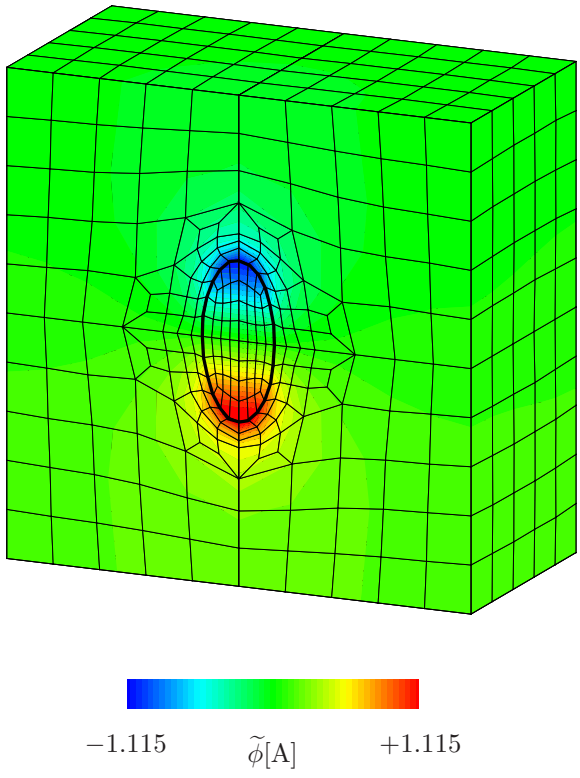

Figure 6.10: Deformed spherical MRE specimen in a constant applied magnetic field $\overline{\boldsymbol{h}} = 5 \times 10^7$ A/m. The plotted contour in color is the magnetic potential of the self-field $\widetilde{\phi}$.

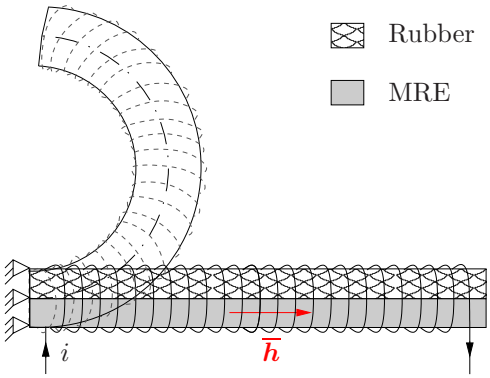

Figure 6.11: Sketch of the construction and working of the bimorph finger actuator. The current i creates a magnetic field $\overline{\boldsymbol{h}}$ along the length of the actuator which results in a curling action. The idea was inspired by the construction of the magnetic potentiometer in CHATTOCK [26].

full geometry which reduces computational time as well as memory requirements. The outer box represents free space and hence the magnetic potential of the self field $\widetilde{\phi}$ and the displacements $\boldsymbol{u}$ are fixed to zero at the outer surface. The magnetization degrees of freedom have also been set to zero in the free-space. The remaining boundary conditions are specified in order to be consistent with the symmetry requirements of the problem. Additionally, as indicated we fix all the displacement components of the node at the center of the sphere in order to arrest rigid body translations. The direction of the the applied magnetic field $\overline{\boldsymbol{h}}$ is also indicated in the figure.

The mesh used for the finite element discretization is shown in Figure 6.9b. There are a total of 614 elements (and 844 nodes) is used in the discretization. Out of these, 54 elements are in the inclusion. The material parameters used for this simulation are in Table 6.1. The free space region is modeled as a material with low stiffness and pure magnetic coefficients, and zero magnetostrictive coefficent. For the chosen material parameters (these are not assumed to correspond to a real material), Figure 6.10 shows the deformed mesh with the contours of the magnetic potential of the self-field $\widetilde{\phi}$ for an applied magnetic field $\overline{\boldsymbol{h}} = 5 \times 10^7$ A/m. The self field $\widetilde{\boldsymbol{h}}$, and hence the magnetization, was of uniform value within the deformed body, which is also verifiable by the uniform and gradual change in the self-field within the specimen along the direction of the applied magnetic field.

Table 6.2: Magneto-Elastic Material Parameters for the Finger Actuator.

No.	Parameter	Name	MRE	Inclusion	Unit
1.	κ	Bulk modulus	6.00×10^2	6.00×10^4	N/mm^2
2.	μ	Shear modulus	2.07×10^{-1}	2.07×10^1	N/mm^2
3.	N	Number of chain segments	4.31	4.31	–
4.	p	Non-affine averaging parameter	6.22	6.22	–
5.	c	Magnetostrictive coefficient	5.00	0.00	mm^2/A^2
6.	C_m	Paramagnetic coefficient	62.83	0.00	N/A^2

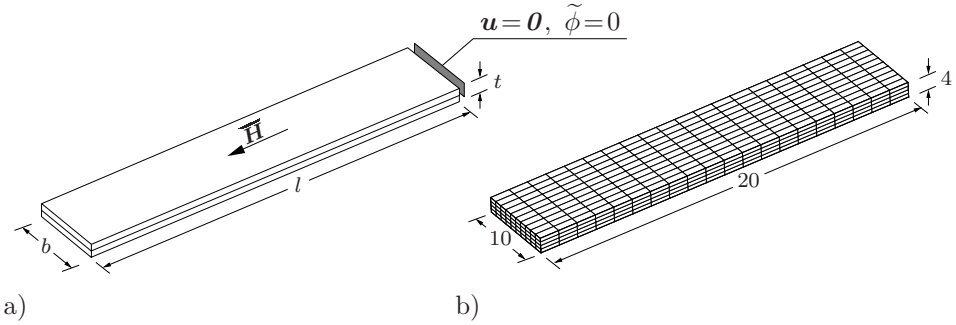

Figure 6.12: Boundary value problem definition for finger actuator using bi-material strip. The strip at the bottom is the MRE material, which extends in the direction of the magnetic field, while the strip above it, is a polymer that does not deform in a magnetic field. a) Dimensions $l = 10$ mm, $b = 2$ mm, and $t = 0.8$ mm of the strip and boundary conditions defining the problem. b) Finite element mesh with number of elements per edge indicated.

6.9.3. MRE for a Finger Actuator

We now look at a problem that not only presents a possible application, but also demonstrates the cabability of the proposed model with respect to large deformations and rotations. The inspiration for this application comes from the design of a magnetic potentiometer which was originally constructed to measure magnetic fields, see Chattock [26]. Although the magnetic potentiometer has a completely different purpose, the idea of a flexible solenoidal winding is used here. As Figure 6.11 shows, the finger actuator consists of two polymer strips glued together. While one of the materials is magnetostrictive, the does not have any inherent coupling with the magnetic field. A magnetic field applied parallel to the long axis will thus cause the MRE material to lengthen while the other strip will not be directly affected. This causes a *differential elongation* between the two layers under the action of a magnetic field and thus cause a curling action in the bimaterial strip with the magnetoactive material (MRE) to be in the convex (outer) side. In order to apply the magnetic field $\overline{\boldsymbol{h}}$ in this required manner ie. along the axis, a solenoidal winding carrying current could be used which deforms along with the bimorphic finger.

In order to simulate this device, we consider two strips having the dimensions $l = 10$ mm, $b = 2$ mm and $t = 0.2$ mm each as shown in Figure 6.12. 800 brick elements are

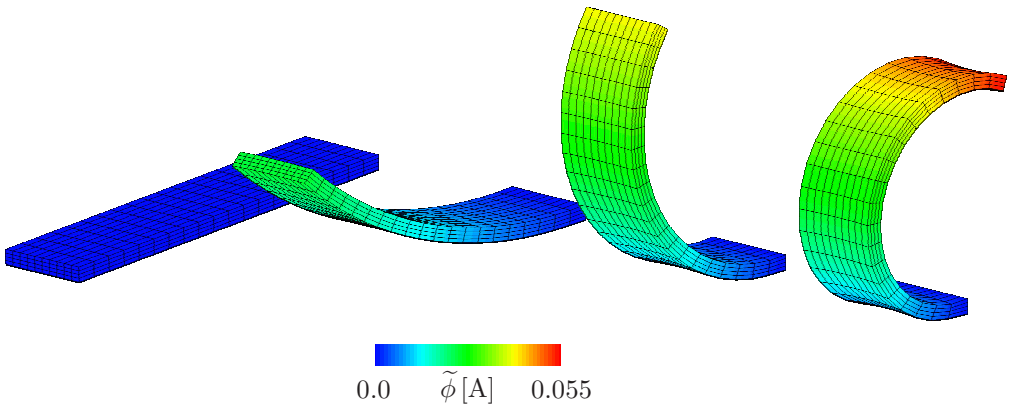

Figure 6.13: Magnetic field-induced deformation of a bi-material finger actuator. The magnetically induced differential extension along the thickness direction causes the assembly progressively curl up with an increasing magnetic field.

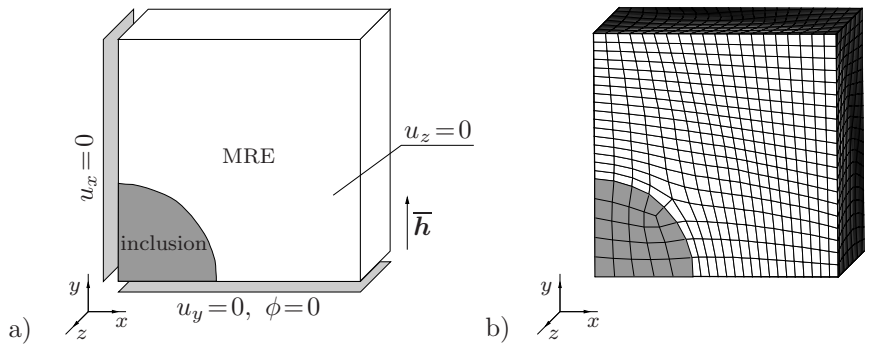

Figure 6.14: Stiff inclusion in magneto-rheological elastomer (MRE) matrix. Description of the a) boundary value problem, boundary conditions, and b) finite element mesh. Discretization with 7985 elements in matrix material and 111 elements in stiff inclusion. Cube of side length $l = 50$mm and inclusion of radius $r = 20$mm.

used to discretize the geometry. Note that we have not discretized the free space in this example. As shown, one face (perpendicular to the applied field) has all displacements as well as magnetic potential $\widetilde{\phi}$ fixed to zero while the opposite face is left free. In order to simulate the loading by the applied magnetic field, we use the relation $\overline{\boldsymbol{h}} = \boldsymbol{F}\overline{\boldsymbol{H}}$, where $\overline{\boldsymbol{H}}$ is a prescribed vector parallel to the longer edge of the assembly. As a result, we have a *deformation dependent load*. The material parameters for the simulation are shown in Table 6.2. The finger-like curling action is shown in the sequence in Figure 6.13 for a increasing magnetic fields up to $\overline{\boldsymbol{h}} = 3.3 \times 10^6$A/m.

6.9.4. Inhomogeneous Large Magnetically-Induced Strains in MRE

Table 6.3: Magneto-Elastic Material Parameters for Block with an Inclusion.

No.	Parameter	Name	Matrix	Inclusion	Unit
1.	κ	Bulk modulus	6.00×10^2	6.00×10^4	N/mm^2
2.	μ	Shear modulus	2.07×10^{-1}	2.07×10^1	N/mm^2
3.	N	Number of chain segments	4.31	4.31	–
4.	p	Non-affine averaging parameter	6.22	6.22	–
5.	c	Magnetostrictive coefficient	1.00×10^{-1}	0.00	mm^2/A^2
6.	C_m	Paramagnetic coefficient	12.57	12.57	N/A^2

In this example we consider a block of the MR elastomer with a stiff inclusion. We simulate the deformation of the body when it is placed in a magnetic field applied in direction parallel to one of the edges. The geometry, mesh, and boundary conditions which define the boundary value problem are shown in Figure 6.14. Due to the symmetry of the problem, we may consider only $1/8^{\text{th}}$ of the full geometry which reduces computational time as well as memory requirements. The material parameters for this simulation are in Table 6.3 and a fine mesh of 8096 elements is used in the discretization. The inclusion in the matrix has a considerably higher stiffness compared to the matrix surrounding it. Additionally, there is no coupling present between mechanical and magnetic degrees of freedom in the inclusion. In Figure 6.15, we see the deformed mesh with the contours of the $z-$component of the displacement shown in color. The applied potential difference is monotonically increased and the series of pictures from a) to f) show that a stronger magnetic field causes a greater deformation. The deformation in the matrix near the stiff

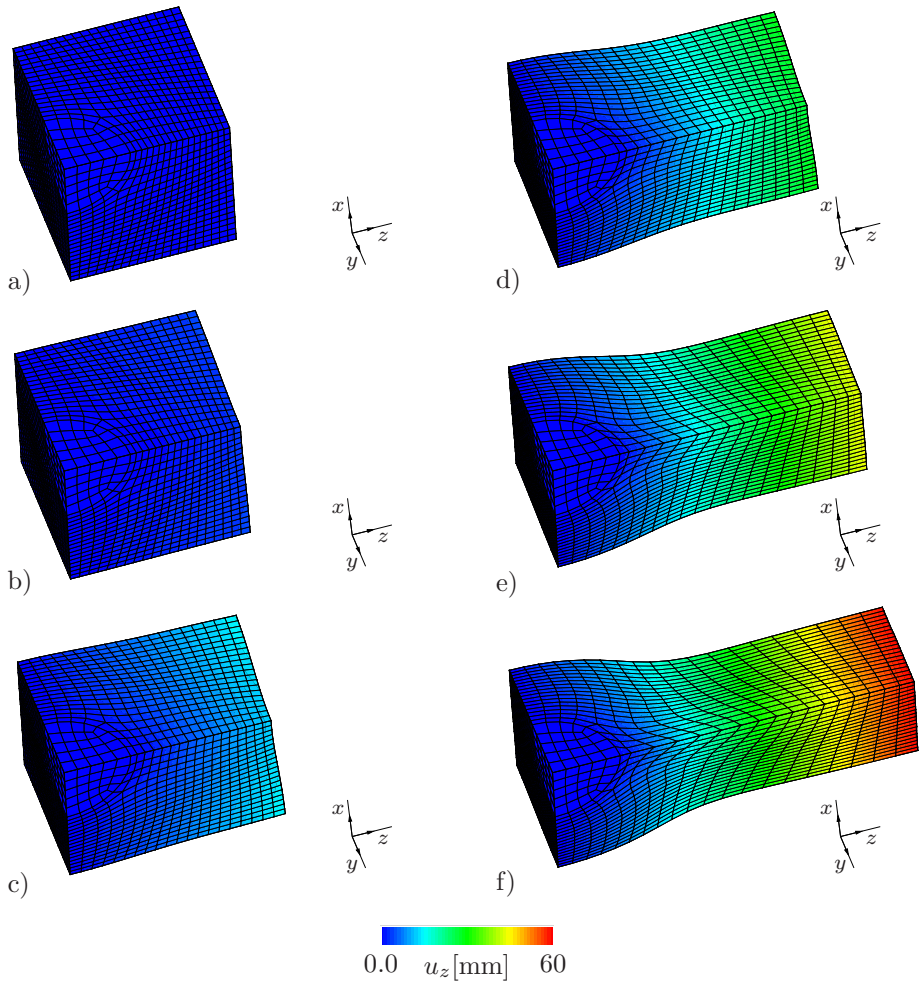

Figure 6.15: Deformed geometry for increasing magnetic potential difference. The deformation near the stiff spherical inclusion is inhomogeneous and it becomes uniform away from it as seen by the contour plot in color of the displacement component u_z.

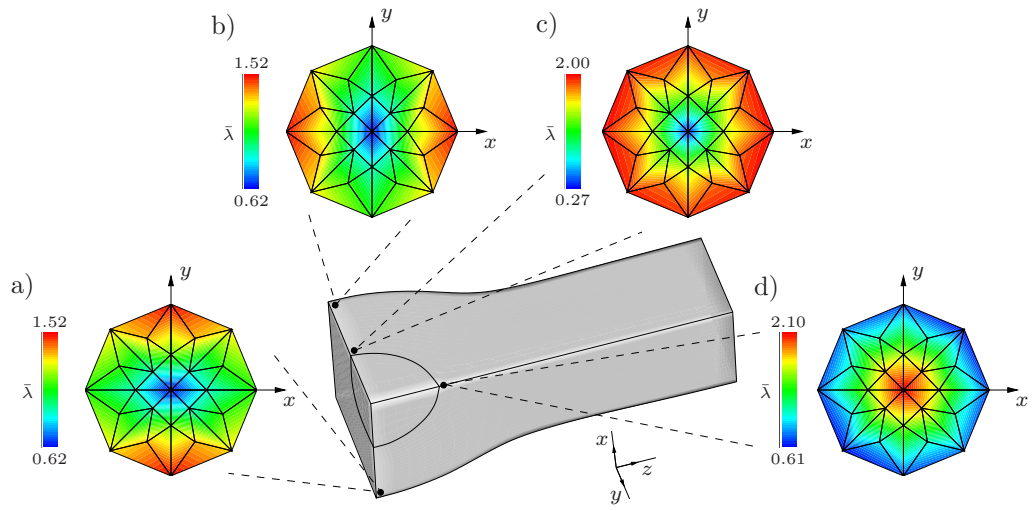

Figure 6.16: Deformed geometry for increasing magnetic potential difference. The stiff spherical inclusion causes an inhomogeneous deformation. Pole figures indicate the stretch $\bar{\lambda}$ at chosen points.

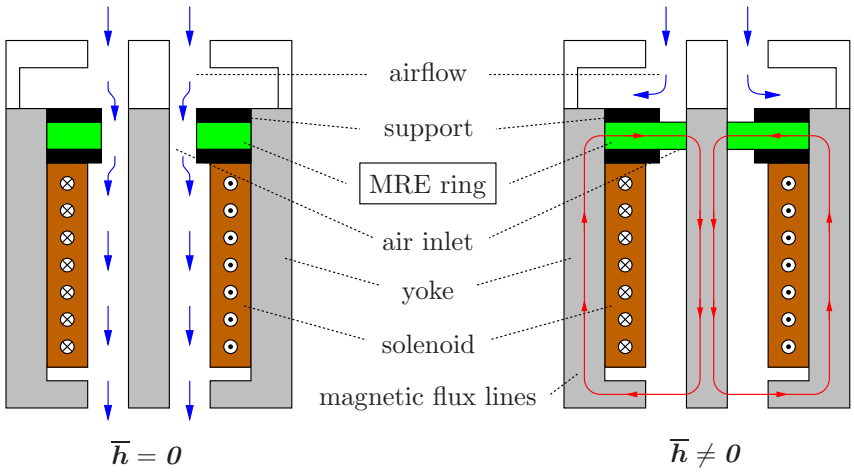

Figure 6.17: Schematic diagram of valve with MRE ring as active component adapted from Böse, Rabindranath & Ehrlich [12]. The solenoid creates a magnetic field (shown in red, right figure) that acts in a radial direction within the MRE ring thus deforming it and hence causing the air inlet to close.

inclusion shows some inhomogeneity where as it is mostly homogeneous away from the inclusion. These pole projections in Figure 6.16 give a view of the deformation $\bar{\boldsymbol{F}}_{net}$ at the chosen material points. All points on or near the symmetry axes experience anisotropic deformations. Points a), b) and c) are close to the xy-plane. Out of these, a) and b) are close to the outer surface and hence it is reasonable to expect no stretch in the thickness direction of the body. Point c) however is an internal point quite close to the rigid inclusion. As a result, it experiences a stretch in all directions in the xy-plane. The inclusion constrains stretches in the z-direction. Point d) is also an internal point close to the inclusion, but chosen on the z-axis. Since a magnetic field essentially causes a deformation in a direction parallel to itself (z-axis), the point d) shows a stretch in the z-direction. Note that the inclusion cannot constrain the stretch in the z-direction for this point.

6.9.5. Magnetorheological Elastomer as Actuator in Valve

Table 6.4: Magneto-Elastic Material Parameters for Valve.

No.	Parameter	Name	Matrix	Unit
1.	κ	Bulk modulus	6.00×10^{2}	$\mathrm{N/mm^2}$
2.	μ	Shear modulus	2.07×10^{-1}	$\mathrm{N/mm^2}$
3.	N	Number of chain segments	4.31	–
4.	p	Non-affine averaging parameter	6.22	–
5.	c	Magnetostrictive coefficient	5.00×10^{-1}	$\mathrm{mm^2/A^2}$
6.	C_m	Paramagnetic coefficient	1.26×10^{3}	$\mathrm{N/A^2}$

This example takes a look at a practical application of soft MR elastomers presented in the work Böse, Rabindranath & Ehrlich [12], which explores the actuation behavior of soft silicone-based magnetorheological elastomers in magnetic fields, and demonstrates the use of such materials as the active element in a valve. A schematic diagram of the working of the component is revealed in Figure 6.17. The basic idea is that a radial magnetic field is used to deform the MRE ring thereby opening or closing the axisymmetric inlet, see

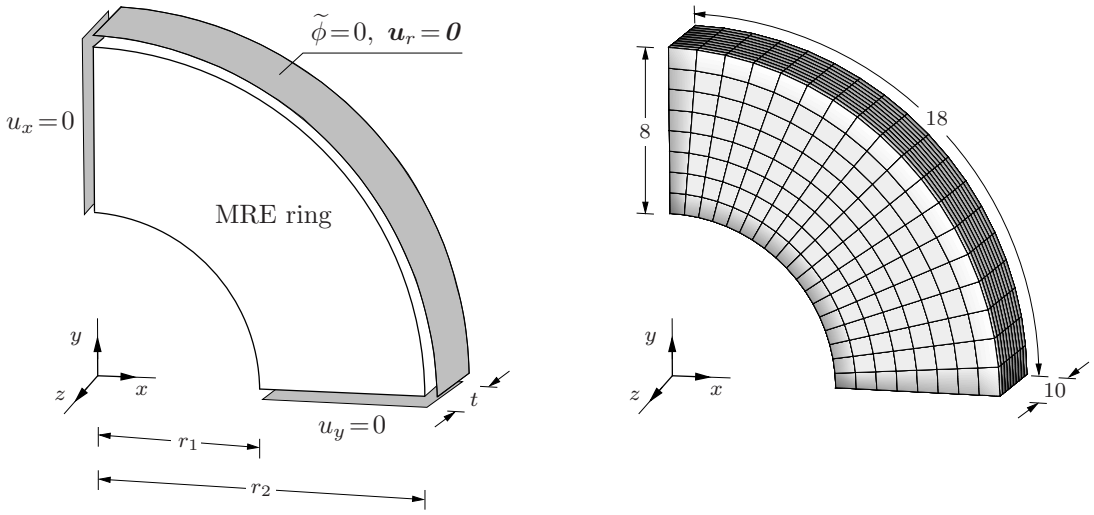

Figure 6.18: MRE ring as active component in a valve. Dimensions and boundary value problem definition with associated discretization of the geometry. A radial magnetic field $\overline{\boldsymbol{h}}$ as given in (6.95) is assumed to act between the inner ($r_1 =$ 5mm) and outer ($r_2 = 10$mm) surfaces throughout the thickness ($t = 3$mm).

Figure 6.17. Additionally the size of the inlet maybe controlled thus allowing it to work as a proportional valve as it regulates the flow of air through it [12].

We are interested in modeling the active element of this component namely, the MRE ring. Due to symmetry considerations we need to discretize only $1/4^{\text{th}}$ of the geometry and apply the appropriate boundary conditions that enforce this symmetry. Thus the boundary value problem definition is shown in Figure 6.18 where it is clear that the mechanical boundary conditions enforce the symmetry of the problem. The material parameters used correspond to those used for the matrix in Table 6.4. 1440 brick elements have been used to discretize the quarter of the valve geometry and the results are presented by mirroring on the xz- and yz-planes. As indicated in the caption, a radial magnetic

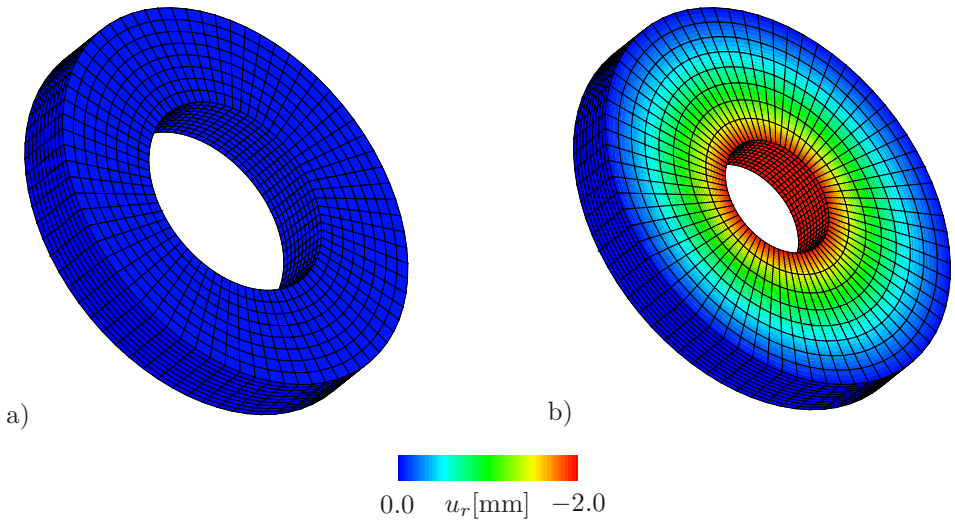

Figure 6.19: Deformation of MRE ring in radial magnetic field. Valve ring deforms and closes the air inlet. a) Initial configuration for $\overline{H} = \boldsymbol{0}$ and b) final configuration for $\overline{H} = 1.05 \times 10^6$ A/m. The contour plot shows the radial component of the displacement.

field is applied to induce actuation. For the sake of simplicity, we take an artificial $\overline{\boldsymbol{h}}$ of constant magnitude in the radial direction and dependent on material coordinates only. Therefore, in terms of a prescribed magnitude $\overline{H}$, we have

$$\overline{\boldsymbol{h}} := \overline{H} \begin{bmatrix} X/\sqrt{X^2+Y^2} \\ Y/\sqrt{X^2+Y^2} \\ 0 \end{bmatrix} . \tag{6.95}$$

This magnetic field causes the material to expand radially inwards and as a result, the inner diameter is reduced. Figure 6.19 shows the deformed MRE ring with the radial component of the displacement u_r as the contour plot corresponding to the state when the applied magnetic field is $\overline{H} = 2.5 \times 10^7 \mathrm{A/m}$.

7. Magneto-Viscoelasticity of MREs

In this chapter we extend the framework presented in the previous chapter to include inelastic effects. In particular we consider the case of viscoelasticity that arises due to the matrix. We will present the variational principle for magneto-viscoelasticity and then, after discussing its finite element implementation, we will show the construction of the material model by extending the framework that we have already established in the previous chapter. Finally, we will present some numerical results that highlight the salient features of the fully coupled model framework.

7.1. Primary Variables for Magneto-Viscoelasticity

In line with the Lagrangian setting of the previous chapter, we have $\Omega \subset \mathcal{R}^3$ as a vacuum free space box and $\mathcal{B} \subset \Omega$ be the undeformed material configuration of the solid. Ω is considered to be large enough such that the magnetic field induced by the magnetization of the body is decayed at its surface $\partial\Omega \subset \mathcal{R}^2$. We study the magnetomechanical response of the body under quasi-static, magneto-mechanical loading in the range $\mathcal{T} \subset \mathcal{R}$ of time. In what follows, $\nabla(\cdot) := \partial_{\boldsymbol{x}}(\cdot)$ and $\dot{(\cdot)} := \partial_t(\cdot)$ denote the spatial gradient and the time derivative of the field $(\cdot)$, respectively. The primary variables defined over the full domain Ω are the *deformation map* $\boldsymbol{\varphi}$ and the *magnetostatic potential of the self-field* $\widetilde{\phi}$

$$\boldsymbol{\varphi} : \begin{cases} \Omega \times \mathcal{T} \to \mathcal{R}^3 \\ (\boldsymbol{X}, t) \mapsto \boldsymbol{x} = \boldsymbol{\varphi}(\boldsymbol{X}, t) \end{cases}, \quad \widetilde{\phi} : \begin{cases} \Omega \times \mathcal{T} \to \mathcal{R} \\ (\boldsymbol{X}, t) \mapsto \widetilde{\phi}(\boldsymbol{X}, t) \end{cases}. \tag{7.1}$$

On the body $\mathcal{B}$ alone, we have the *current magnetization per unit mass* $\boldsymbol{\mu}$.

$$\boldsymbol{\mu} : \begin{cases} \mathcal{B} \times \mathcal{T} \to \mathcal{R}^3 \\ (\boldsymbol{X}, t) \mapsto \boldsymbol{\mu}(\boldsymbol{X}, t) \end{cases}. \tag{7.2}$$

We additionally have a *set of internal variables* $\boldsymbol{\mathcal{I}}$ to describe viscous structural changes. The potential $\widetilde{\phi}$ is assumed to be continuous across the interface $\partial\mathcal{B}$ between the solid domain $\mathcal{B}$ and the surrounding free space $\Omega \setminus \mathcal{B}$, i.e. $[\![\widetilde{\phi}]\!] = 0$ on $\partial\mathcal{B}$. where $[\![(\cdot)]\!] := (\cdot)_+ - (\cdot)_-$ denotes jump between the sides $\partial\mathcal{B}_+$ and $\partial\mathcal{B}_-$ of the interface.

7.2. Variational Principle for Rate-Dependent Problems

We begin by stating the rate-type variational principle for viscoelasticity of MREs. We will work directly in the Lagrangian setting since it is more suited for FEM implementation. Thus, the rate-type variational principle defining the magneto-viscoelastic boundary-value-problem is stated as

$$\boxed{\{\dot{\boldsymbol{\varphi}}, \dot{\boldsymbol{\mu}}, \dot{\widetilde{\phi}}, \dot{\boldsymbol{\mathcal{I}}}\} = \arg\Big\{ \inf_{\dot{\boldsymbol{\varphi}}} \inf_{\dot{\boldsymbol{\mu}}} \sup_{\dot{\widetilde{\phi}}} \inf_{\dot{\boldsymbol{\mathcal{I}}}} \; \Pi'_{rate}(\dot{\boldsymbol{\varphi}}, \dot{\boldsymbol{\mu}}, \dot{\widetilde{\phi}}, \dot{\boldsymbol{\mathcal{I}}}; t) \Big\}} \tag{7.3}$$

at a given global state $\{\boldsymbol{\varphi}, \boldsymbol{\mu}, \widetilde{\phi}, \boldsymbol{\mathcal{I}}\}$. Here Π'_{rate} is constructed from the energy-enthalpy functional, and the magneto-mechanical potential of the external loads. Thus we have the *magneto-viscoelastic rate potential*

$$\Pi'_{rate}(\dot{\boldsymbol{\varphi}}, \dot{\boldsymbol{\mu}}, \dot{\widetilde{\phi}}, \dot{\boldsymbol{\mathcal{I}}}; t) := \frac{d}{dt} E'(\boldsymbol{\varphi}, \boldsymbol{\mu}, \widetilde{\phi}, \boldsymbol{\mathcal{I}}) + D(\dot{\boldsymbol{\mathcal{I}}}) - \Pi_{ext}(\dot{\boldsymbol{\varphi}}, \dot{\boldsymbol{\mu}}; t) \,. \tag{7.4}$$

The energy-enthalpy functional E' is written as

$$E' = \int_{\mathcal{B}} \rho_0[\Psi_{mat}(\boldsymbol{F}, \boldsymbol{\mu}, \boldsymbol{\mathcal{I}}) + \mu_0 \boldsymbol{\mu} \cdot (\boldsymbol{F}^{-T} \nabla_{\boldsymbol{X}} \widetilde{\phi})] \, dV - \frac{\mu_0}{2} \int_{\Omega} J \big| (\nabla_{\boldsymbol{X}} \boldsymbol{\varphi})^{-T} \, \nabla_{\boldsymbol{X}} \widetilde{\phi} \big|^2 \, dV \ , \quad (7.5)$$

where the free energy function Ψ_{mat} is constructed as described in a later section.

The dissipation functional D depends on the viscous strain-like (internal) variables $\boldsymbol{\mathcal{I}}$. It is defined in terms of the *dissipation potential* Φ which will be specified in the section dealing with the constitutive model. Thus,

$$D(\dot{\boldsymbol{\mathcal{I}}}) = \int_{\mathcal{B}} \Phi(\dot{\boldsymbol{\mathcal{I}}}) \, dV \ . \quad (7.6)$$

For simplicity, the external loading functional is taken for "dead" loads only and is

$$\Pi_{ext}(\dot{\boldsymbol{\varphi}}, \dot{\boldsymbol{\mu}}) = \int_{\mathcal{B}} \rho_0(\overline{\boldsymbol{\gamma}} \cdot \dot{\boldsymbol{\varphi}} + \mu_0 \overline{\boldsymbol{h}} \cdot \dot{\boldsymbol{\mu}}) \, dV + \int_{\partial \mathcal{S}_t} \overline{\boldsymbol{t}} \cdot \dot{\boldsymbol{\varphi}} \, da \ , \quad (7.7)$$

in which we have a *prescribed body force density per unit mass* $\overline{\boldsymbol{\gamma}}$, a *prescribed traction per unit current area* $\overline{\boldsymbol{t}}$, and a *prescribed applied magnetic field* $\overline{\boldsymbol{h}}$. Therefore, the rate dependent functional takes the form

$$\begin{aligned} \Pi'_{rate} = &- \int_{\mathcal{B}} (\operatorname{Div} \boldsymbol{P} + \rho_0 \overline{\boldsymbol{\gamma}}) \cdot \dot{\boldsymbol{\varphi}} \, dV + \int_{\partial \mathcal{B}_t} \big([\![\boldsymbol{P}]\!] \cdot \boldsymbol{N} - \overline{\boldsymbol{t}} \big) \cdot \dot{\boldsymbol{\varphi}} \, dA + \int_{\mathcal{B}} (\partial_{\boldsymbol{\mathcal{I}}} \Psi_{mat} \cdot \dot{\boldsymbol{\mathcal{I}}} + \Phi) \, dV \\ &+ \int_{\mathcal{B}} (\partial_{\boldsymbol{\mu}} \Psi_{mat} - \mu_0 \boldsymbol{h}) \cdot \dot{\boldsymbol{\mu}} \, dV - \int_{\Omega} \operatorname{Div} \widetilde{\boldsymbol{B}} \ \dot{\widetilde{\phi}} \, dV + \int_{\partial \mathcal{B}} [\![\widetilde{\boldsymbol{B}}]\!] \cdot \boldsymbol{N} \ \dot{\widetilde{\phi}} \, dA \end{aligned} \quad (7.8)$$

The first variation yields

$$\begin{aligned} \delta \Pi'_{rate} = &- \int_{\mathcal{B}} (\operatorname{Div} \boldsymbol{P} + \rho_0 \overline{\boldsymbol{\gamma}}) \cdot \delta \dot{\boldsymbol{\varphi}} \, dV + \int_{\partial \mathcal{B}_t} ([\![\boldsymbol{P}]\!] \cdot \boldsymbol{N} - \overline{\boldsymbol{t}}) \cdot \delta \dot{\boldsymbol{\varphi}} \, dA + \int_{\mathcal{B}} (\partial_{\boldsymbol{\mathcal{I}}} \Psi_{mat} + \partial_{\dot{\boldsymbol{\mathcal{I}}}} \Phi) \cdot \delta \dot{\boldsymbol{\mathcal{I}}} \, dV \\ &+ \int_{\mathcal{B}} (\partial_{\boldsymbol{\mu}} \Psi_{mat} - \mu_0 \boldsymbol{h}) \cdot \delta \dot{\boldsymbol{\mu}} \, dV - \int_{\Omega} \operatorname{Div} \widetilde{\boldsymbol{B}} \ \delta \dot{\widetilde{\phi}} \, dV + \int_{\partial \mathcal{B}} [\![\widetilde{\boldsymbol{B}}]\!] \cdot \boldsymbol{N} \ \delta \dot{\widetilde{\phi}} \, dA \end{aligned} \quad (7.9)$$

for the virtual fields $\{\delta \dot{\boldsymbol{\varphi}}, \delta \dot{\boldsymbol{\mu}}, \delta \dot{\widetilde{\phi}}, \delta \dot{\boldsymbol{\mathcal{I}}}\}$ with $\delta \boldsymbol{\mu} = \boldsymbol{0}$ on $\Omega \setminus \mathcal{B}$, $\delta \boldsymbol{\mathcal{I}} = \boldsymbol{0}$ on $\Omega \setminus \mathcal{B}$ and $\delta \widetilde{\phi} = 0$ on $\partial \Omega$. The above expression makes use of the following identifications. The *total* first Piola-Kirchhoff stress is the sum of a mechanical part and non-mechanical part

$$\boldsymbol{P} := \rho_0 \partial_{\boldsymbol{F}} \Psi_{mat} + \boldsymbol{P}_{Max} \ , \quad (7.10)$$

where $\boldsymbol{P}_{Max}$, is the Maxwell stress tensor (for this formulation) and is given by

$$\boldsymbol{P}_{Max} := \boldsymbol{F}^{-T} \widetilde{\boldsymbol{H}} \otimes \widetilde{\boldsymbol{B}} - \frac{\mu_0}{2} J \boldsymbol{C}^{-1} : (\widetilde{\boldsymbol{H}} \otimes \widetilde{\boldsymbol{H}}) \boldsymbol{F}^{-T} \ . \quad (7.11)$$

That expression is derived assuming that the applied magnetic field $\overline{\boldsymbol{h}}$ depends on the material coordinates via the deformation gradient only and also makes use of the induced magnetic induction in the Lagrangian configuration

$$\widetilde{\boldsymbol{B}} := \mu_0(J\boldsymbol{C}^{-1}\widetilde{\boldsymbol{H}} + \rho_0\boldsymbol{F}^{-1}\boldsymbol{\mu}) \ . \tag{7.12}$$

Additionally, if we denote the (Eulerian) total Maxwellian magnetic field $\boldsymbol{h}$ is denoted by

$$\boldsymbol{h} := \overline{\boldsymbol{h}} + \boldsymbol{F}^{-T}\widetilde{\boldsymbol{H}} \ , \tag{7.13}$$

We can now exploit the independence and arbitrariness of the variations of the primary variables, to get the following balance equations as the Euler equations

$$\left.\begin{aligned} \operatorname{Div}\boldsymbol{P} + \rho_0\overline{\boldsymbol{\gamma}} &= \boldsymbol{0} \\ \partial_{\boldsymbol{\mu}}\Psi_{mat} - \mu_0\boldsymbol{h} &= \boldsymbol{0} \\ \operatorname{Div}\widetilde{\boldsymbol{B}} &= 0 \\ \partial_{\boldsymbol{\mathcal{I}}}\Psi_{mat} + \partial_{\dot{\boldsymbol{\mathcal{I}}}}\Phi &= \boldsymbol{0} \end{aligned}\right\} \text{ in } \mathcal{B} \tag{7.14}$$

along with the boundary condition and jump condition at the interface between the solid and the surrounding free space

$$[\![\boldsymbol{P}]\!]\cdot\boldsymbol{N} = \overline{\boldsymbol{t}} \ \text{ on } \partial\mathcal{B}_t \quad \text{and} \quad [\![\widetilde{\boldsymbol{B}}]\!]\cdot\boldsymbol{N} = 0 \ \text{ on } \partial\mathcal{B} \tag{7.15}$$

respectively. Additionally, in the surrounding free space we have the the field equations

$$\operatorname{Div}[J\boldsymbol{C}^{-1}\widetilde{\boldsymbol{H}}] = 0 \quad \text{and} \quad \operatorname{Div}\boldsymbol{P}_{Max} = \boldsymbol{0} \ \text{ in } \Omega\setminus\mathcal{B} \ . \tag{7.16}$$

7.3. Time-Discrete Incremental Variational Principle

We now outline variational principles for time-discrete problems. To this end, we consider time-discrete solutions of the field variables at the discrete times $0, t_1, t_2, \ldots, t_n, t_{n+1}, \ldots, T$ of the process interval $[0, T]$. In order to advance the solution within a typical time step, we focus on the finite time increment $[t_n, t_{n+1}]$, where

$$\tau_{n+1} := t_{n+1} - t_n > 0 \tag{7.17}$$

denotes the step length. In the subsequent treatment, all field variables at time t_n are assumed to be *known*. The goal then is to determine the fields at time t_{n+1} based on variational principles valid for the time increment under consideration. In particular, we assemble the time-discrete spatial fields (displacement, magnetization, potential) at the discrete times t_n and t_{n+1} in the discrete solution vectors

$$\mathfrak{v}_{n+1} := \{\boldsymbol{\varphi}_{n+1}, \boldsymbol{\mu}_{n+1}, \widetilde{\phi}_{n+1}, \boldsymbol{\mathcal{I}}_{n+1}\} \quad \text{and} \quad \mathfrak{v}_n := \{\boldsymbol{\varphi}_n, \boldsymbol{\mu}_n, \widetilde{\phi}_n, \boldsymbol{\mathcal{I}}_n\} \ . \tag{7.18}$$

In order to obtain a compact notation, we drop in what follows the subscript $n+1$ and consider all variables without subscript to be evaluated at time t_{n+1}. The link between the variables at the two time-discrete states is obtained in *iterative steps*, which must preserve the geometric nature of the variables involved. To this end, we first outline the variation, the linearization and the update equation of the magnetization director within an incremental setting.

We define the counterpart of the dynamic functional (7.4) in the incremental setting associated with the time internal $[t_n, t_{n+1}]$ by

$$\Pi'^{\tau}_{inc}(\boldsymbol{\varphi}, \boldsymbol{\mu}, \widetilde{\phi}) = E' - E'_n + Algo\Big\{ \int_{t_n}^{t_{n+1}} \big[D - \Pi_{ext}\big]\, dt \Big\} , \tag{7.19}$$

depending on the current variables $\mathfrak{v}$ defined in $(7.18)_1$. It is based on the energy-enthalpy functional (7.5), the dissipation functional (7.6), the potential due to external loads (7.7). Here, $E'_n := E'(\boldsymbol{\varphi}_n, \boldsymbol{\mu}_n, \widetilde{\phi}_n)$ is a constant. Assuming a *linear path* of the state variables in the time increment $[t_n, t_{n+1}]$, we consider an *algorithm Algo* of the form

$$\Pi'^{\tau}_{inc}(\boldsymbol{\varphi}, \boldsymbol{\mu}, \widetilde{\phi}) = E'(\boldsymbol{\varphi}, \boldsymbol{\mu}, \widetilde{\phi}) - E'_n + \tau D(\frac{\boldsymbol{\mathcal{I}} - \boldsymbol{\mathcal{I}}_n}{\tau}; t) - \tau \Pi_{ext}(\frac{\boldsymbol{\varphi} - \boldsymbol{\varphi}_n}{\tau}, \frac{\boldsymbol{\mu} - \boldsymbol{\mu}_n}{\tau}; t) \tag{7.20}$$

of (7.19). The insertion of the energy-enthalpy functional (7.5), the dissipation functional (7.6), and the external loading functional (7.7) gives the representation

$$\begin{aligned} \Pi'^{\tau}_{inc} = & \int_{\mathcal{B}} \big\{ \Psi_{mat} + \kappa_0 m_s \boldsymbol{\mu} \cdot \nabla \widetilde{\phi} \big\}\, dV - \frac{\kappa_0}{2} \int_{\Omega} |\nabla \widetilde{\phi}|^2\, dV - E'_n + \int_{\mathcal{B}} \tau \boldsymbol{\Phi}\Big(\frac{\boldsymbol{\mathcal{I}} - \boldsymbol{\mathcal{I}}_n}{\tau}\Big) \\ & - \int_{\mathcal{B}} \rho_0 [\overline{\boldsymbol{\gamma}} \cdot (\boldsymbol{\varphi} - \boldsymbol{\varphi}_n) + \mu_0 \overline{\boldsymbol{h}} \cdot (\boldsymbol{\mu} - \boldsymbol{\mu}_n)]\, dV - \int_{\partial \mathcal{B}_t} \overline{\boldsymbol{t}} \cdot (\boldsymbol{\varphi} - \boldsymbol{\varphi}_n)\, dA \ . \end{aligned} \tag{7.21}$$

Note carefully, that due to this algorithmic assumption, the finite-step-sized rate-type incremental potential is considered to be a functional of the variables $\mathfrak{v}$ defined in $(7.18)_1$ at the current time t_{n+1}. This feature of the finite-step-sized incremental setting marks a formal difference to the continuous incremental functional (7.8) formulated in terms of the rates. The fields in $\mathfrak{v}$ are then determined by the time-discrete *incremental variational principle*

$$\boxed{\{\boldsymbol{\varphi}, \boldsymbol{\mu}, \widetilde{\phi}, \boldsymbol{\mathcal{I}}\} = \arg \Big\{ \inf_{\boldsymbol{\varphi}} \inf_{\boldsymbol{\mu}} \sup_{\widetilde{\phi}} \inf_{\boldsymbol{\mathcal{I}}} \Pi'^{\tau}_{inc}(\boldsymbol{\varphi}, \boldsymbol{\mu}, \widetilde{\phi}, \boldsymbol{\mathcal{I}}; t) \Big\} \ .} \tag{7.22}$$

The Euler equations and are the time discrete versions of (7.14) that come from the the original rate-type principle. They will not be repeated here since they will be apparent from the algorithmic exploitation that follows now.

7.4. Finite Element Implementation of the Coupled Problem

We now consider aspects of computational implementation of the variational principle. For notational convenience, we will focus on pure Dirichlet problems. We introduce the local energy-enthalpy function

$$\pi = \rho_0 \big[\Psi_{mat} - \mu_0 \boldsymbol{\mu} \cdot (\boldsymbol{F}^{-T} \widetilde{\boldsymbol{H}}) - \mu_0 \boldsymbol{\mu} \cdot \overline{\boldsymbol{h}} - \overline{\boldsymbol{\gamma}} \cdot \boldsymbol{\varphi}\big] - \frac{\mu_0}{2} J \big|\boldsymbol{F}^{-T} \widetilde{\boldsymbol{H}}\big|^2 + \tau \boldsymbol{\Phi}\Big(\frac{\boldsymbol{\mathcal{I}} - \boldsymbol{\mathcal{I}}_n}{\tau}\Big) \tag{7.23}$$

Taking advantage of the fact that the Euler equations $(7.14)_2$ and $(7.14)_4$ are of local character, we solve for the corresponding variable $\boldsymbol{\mu}$ locally. Thus the subproblem

$$\boxed{(L): \quad \{\boldsymbol{\mu}, \boldsymbol{\mathcal{I}}\} = \arg \Big\{ \inf_{\boldsymbol{\mu}} \ \Pi'^{\tau}_{inc}(\boldsymbol{\varphi}, \boldsymbol{\mu}, \widetilde{\phi}, \boldsymbol{\mathcal{I}}, t) \Big\}} \tag{7.24}$$

is considerd at a local level, while simultaneously, the other primary variables $\boldsymbol{\varphi}$ and $\widetilde{\phi}$ are solved for by resorting to the finite element machinery that will be described shortly. For a compact notation, we denote $\mathfrak{Q} := \{\boldsymbol{\mu}, \boldsymbol{\mathcal{I}}\}$ Note that (7.24) implies

$$\mathbb{r}_{loc} := \partial_{\mathfrak{Q}}\pi := \begin{bmatrix} \partial_{\boldsymbol{\mu}}\pi \\ \partial_{\boldsymbol{\mathcal{I}}}\pi \end{bmatrix} = \begin{bmatrix} \partial_{\boldsymbol{\mu}}\Psi_{mat} - \mu_0 \boldsymbol{h} \\ \partial_{\boldsymbol{\mathcal{I}}}\Psi_{mat} + \tau \partial_{\boldsymbol{\mathcal{I}}}\Phi \end{bmatrix} \stackrel{!}{=} \boldsymbol{0} \ , \tag{7.25}$$

which is solved for $\boldsymbol{\mu}$ and $\boldsymbol{\mathcal{I}}$ at each Gauss point. Thus we get an update equation for the internal variables $\boldsymbol{\mathcal{I}}$. Since this is a nonlinear equation, we solve this iteratively via a local Newton update in the usual manner

$$\mathfrak{Q} \Leftarrow \mathfrak{Q} - \mathbb{c}_{loc}^{-1}\mathbb{r}_{loc} \quad \text{with} \quad \mathbb{c}_{loc} := \partial_{\mathfrak{Q}\mathfrak{Q}}\pi \ , \tag{7.26}$$

until convergence $|\mathbb{r}_{loc}| < tol$, where tol is a given tolerance value.

The simultaneous finite element solution for the other primary variables $\boldsymbol{\varphi}$ and $\widetilde{\phi}$ proceeds in a similar manner as the previous chapter by using a compact notation that is suitable for concise implementation. The global part of the problem (G) to be solved here is

$$\boxed{(G): \quad \{\boldsymbol{\varphi}, \widetilde{\phi}\} = \arg\Big\{ \inf_{\boldsymbol{\varphi}} \sup_{\widetilde{\phi}} \ \Pi_{inc}^{\prime\tau}(\boldsymbol{\varphi}, \boldsymbol{\mu}, \widetilde{\phi}, \boldsymbol{\mathcal{I}}, t) \Big\} \ .} \tag{7.27}$$

We consider the spatial discretization of the coupled problem by a finite element method. Let $\mathfrak{T}^h$ denote a finite element triangulation of the domain Ω. The index h indicates a typical mesh size based on E^h finite element domains $\mathcal{B}_e^h \in \mathfrak{T}^h$ and N^h global nodes. The *global nodal degrees of freedom* are the deformation map and the magnetic potential at a typical nodal point of the finite element mesh.

$$\mathfrak{d} := [\boldsymbol{\varphi}, -\widetilde{\phi}]^T \in \mathcal{R}^{(d+1)N^h} \tag{7.28}$$

The constitutive state variables for the coupled magneto-mechanical problem form the *generalized gradient field* $\mathfrak{F} := \{\nabla\boldsymbol{\varphi}, \nabla\widetilde{\phi}\}$. Explicitly, we get the discrete global strain-like vector

$$\mathfrak{F}^h = \mathfrak{B}(\boldsymbol{X})\mathfrak{d} \tag{7.29}$$

$\mathfrak{B}$ is a symbolic representation of the global matrices of shape functions for the coupled problem. Clearly, these global arrays are never formulated explicitly, but represent symbolically the interpolations on all finite element domains $\mathcal{B}_e^h \in \mathfrak{T}^h$. Note that the global nodal variable vector $\mathfrak{d}$ is formed from element vectors $\mathfrak{d}^e$ by a standard finite element assembling procedure. For three-dimensional problems $d = 3$, the generalized displacement vector in (6.36) at the node I is

$$\mathfrak{d}_I = [\varphi_1, \varphi_2, \varphi_3, -\widetilde{\phi}\,]_I^T \ . \tag{7.30}$$

Associated with node I of a standard finite element e, the finite element interpolation matrix for the constitutive state in (6.37) has the form

$$\mathfrak{B}_I^e = \begin{bmatrix} N_{,X} & & & N_{,Y} & & & N_{,Z} & & \\ & N_{,Y} & & & N_{,X} & N_{,Z} & & & \\ & & N_{,Z} & & & & N_{,Y} & N_{,X} & \\ & & & & & & & & N_{,X}\ N_{,Y}\ N_{,Z} \end{bmatrix}_I^T \tag{7.31}$$

in terms of the shape functions N_I and their material derivatives. With the generalized displacement (7.28) and the constitutive state fields (7.29), we write the finite element discretization of the potential Π_{inc} as

$$\Pi^h(\mathfrak{d}) = \int_{\mathcal{B}^h} \pi(\mathfrak{B}\mathfrak{d})\, dV \ , \tag{7.32}$$

where we drop the subscript *stat* but use the superscript h to denote a spatial discretization. Then, the finite-step-sized discrete stationary principle

$$\boxed{\mathfrak{d} = \arg\left\{\operatorname*{stat}_{\mathfrak{d}} \Pi^h(\mathfrak{d})\right\}} \tag{7.33}$$

determines the nodal variables $\mathfrak{d}$ of the finite element mesh. The necessary condition of the discrete variational problem in terms of the generalized stress array $\mathfrak{S}^h$ reads

$$\Pi^h_{,\mathfrak{d}} := \mathop{\mathsf{A}}_{e=1}^{N^h} \Big\{ \int_{\mathcal{B}^e} \mathfrak{B}^{eT}[\mathfrak{S}^h]\, dV \Big\} = \boldsymbol{0} \quad \text{with} \quad \mathfrak{S}^h := \partial_{\mathfrak{F}}\pi = [\partial_{\boldsymbol{F}}\pi, \partial_{\widetilde{\boldsymbol{H}}}\pi]^T \tag{7.34}$$

and provides a nonlinear algebraic system for the determination of the nodal variables $\mathfrak{d}$. For smooth problems, a standard Newton-type iteration of the nonlinear algebraic system (7.34) updates the generalized displacements by the algorithm

$$\mathfrak{d} \Leftarrow \mathfrak{d} - [\Pi^h_{,\mathfrak{d}\mathfrak{d}}]^{-1}[\Pi^h_{,\mathfrak{d}}] \tag{7.35}$$

in terms of the monolithic tangent matrix of the coupled problem

$$\Pi^h_{,\mathfrak{d}\mathfrak{d}} := \mathop{\mathsf{A}}_{e=1}^{N^h} \Big\{ \int_{\mathcal{B}^e} \mathfrak{B}^{eT}[\partial^2_{\mathfrak{F}\mathfrak{F}}\pi]\mathfrak{B}^e\, dV \Big\} \ . \tag{7.36}$$

Observe the *symmetry of the tangent matrix* $\Pi^h_{,\mathfrak{d}\mathfrak{d}}$ induced by the variational structure of the coupled two-field problem. The update (7.35) is performed until convergence is achieved in the sense $\|\Pi^h_{,\mathfrak{d}}\| < tol$. Observe further that the finite element residual and tangent are governed by the *generalized tangent array* $\mathfrak{C}^h := \partial^2_{\mathfrak{F}\mathfrak{F}}\pi$, which is

$$\mathfrak{C}^h := \begin{bmatrix} (\partial^2_{\boldsymbol{F}\boldsymbol{F}}\pi - \partial^2_{\boldsymbol{F}\mathfrak{Q}}\pi : \mathbb{c}^{-1}_{loc} : \partial^2_{\mathfrak{Q}\boldsymbol{F}}\pi) & (\partial^2_{\boldsymbol{F}\widetilde{\boldsymbol{H}}}\pi - \partial^2_{\boldsymbol{F}\mathfrak{Q}}\pi : \mathbb{c}^{-1}_{loc} : \partial^2_{\mathfrak{Q}\widetilde{\boldsymbol{H}}}\pi) \\ (\partial^2_{\widetilde{\boldsymbol{H}}\boldsymbol{F}}\pi - \partial^2_{\widetilde{\boldsymbol{H}}\mathfrak{Q}}\pi : \mathbb{c}^{-1}_{loc} : \partial^2_{\mathfrak{Q}\boldsymbol{F}}\pi) & (\partial^2_{\widetilde{\boldsymbol{H}}\widetilde{\boldsymbol{H}}}\pi - \partial^2_{\widetilde{\boldsymbol{H}}\mathfrak{Q}}\pi : \mathbb{c}^{-1}_{loc} : \partial^2_{\mathfrak{Q}\widetilde{\boldsymbol{H}}}\pi) \end{bmatrix} \tag{7.37}$$

These arrays are a critical ingredient of the proposed variational formulation and make the notation extremely compact.

7.5. Constitutive Ingredients for Constructing the Model

Here we describe the construction of the constitutive ingredients Ψ_{mat} and Φ_{mat} in a modular manner. Since many of the contributions are repeated from the previous chapter, we will only state these contributions and allow ourselves a longer discusison for the newer ingredients.

7.5.1. Ingredient 1: Additive Split of Energy-Enthalpy Density

We assume an additive decomposition of the total enthalpy function into a *mechanical part* and a *magnetostatic part*,

$$\hat{\Psi}_{mat}(\boldsymbol{F}, \boldsymbol{\mu}) = \hat{\Psi}_{mag}(\boldsymbol{\mu}) + \hat{\Psi}_{mec}(\boldsymbol{F}, \boldsymbol{\mu}) \tag{7.38}$$

The mechanical part $\hat{\Psi}_{mec}$ will now contain viscoelastic contributions. This will be described in detail shortly.

7.5.2. Ingredient 2: Energy of the Magnetic State

For the purposes of the simulations in this chapter we resort to the simple paramagnetic expression for the energy of the magnetic state. Thus

$$\hat{\Psi}_{mag}(\boldsymbol{\mu}) := \frac{C_m}{2}\boldsymbol{\mu} \cdot \boldsymbol{\mu} \tag{7.39}$$

For a detailed discussion of micromechanically motivated models, we refer the reader to Ingredient 2 of the constitutive framework of the previous chapter.

7.5.3. Ingredient 3: Volumetric-Isochoric Split of Local Deformation

As before, the due to the incompressibility of the rubber matrix and iron particles, we expect magnetoactive elastomers undergo nearly incompressible deformations. This is accounted for, by applying a penalty method that ensures the incompressibility constraint $J \approx 1$. In the constitutive model, it motivates a multiplicative split of the deformation map $\boldsymbol{F}$, defining its *isochoric part*

$$\bar{\boldsymbol{F}} := J^{-1/3}\boldsymbol{F} \tag{7.40}$$

and its *volumetric part* $J := \det[\boldsymbol{F}]$. As a consequence, the *mechanical contribution* to the enthalpy function is assumed to decompose into a volumetric contribution and an isochoric part,

$$\hat{\Psi}_{mec}(\boldsymbol{F}, \boldsymbol{\mu}) = U(J) + \bar{\Psi}_{mec}(\bar{\boldsymbol{F}}, \boldsymbol{\mu}) \tag{7.41}$$

that includes a magnetostatic expansion as explained below. The volumetric contribution U is considered as a penalty function which approximately enforces the incompressibility constraint.

7.5.4. Ingredient 4: Magnetostrictive Deformation

We assume a multiplicative split of the total deformation gradient into *stress-free (magnetostrictive)* and *stress-producing* parts. The former, denoted by $\bar{\boldsymbol{\mathcal{E}}}$ is assumed to be a *volume-preserving spatial stretch tensor*, dependent on the current magnetization $\boldsymbol{\mu}$. A simple example construction is as follows. Consider the stretch tensor

$$\boldsymbol{\mathcal{E}}^{-1}(\boldsymbol{\mu}) := \boldsymbol{1} + c\boldsymbol{\mu} \otimes \boldsymbol{\mu} \ , \tag{7.42}$$

which is dependent on the magnetostrictive coefficient c and describes a magnetostrictive deformation aligned with the magnetization. The determinant of this tensor is $J_\mu := \det[\boldsymbol{\mathcal{E}}^{-1}] = 1 + c|\boldsymbol{\mu}|^2 > 0$. Note that the above deformation $\boldsymbol{\mathcal{E}}^{-1}$ does not preserve the volume of the polymer network. The desired *isochoric stretch mode* is obtained as

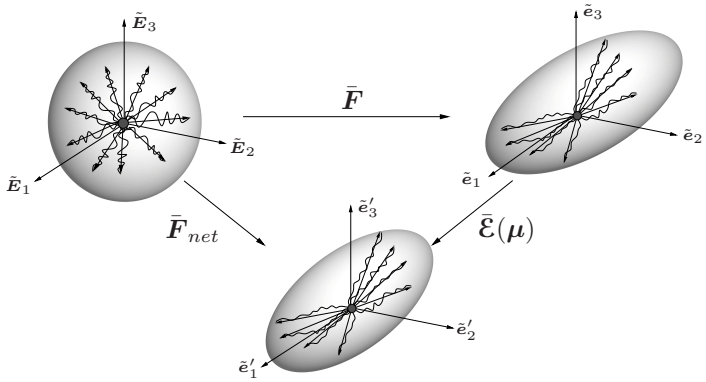

Figure 7.1: Multiplicative decomposition of isochoric part of deformation gradient into network contribution $\bar{\boldsymbol{F}}_{net}$ and local magnetically-induced deformation $\bar{\boldsymbol{\mathcal{E}}}$. We consider a *left multiplicative decomposition* $\bar{\boldsymbol{F}}_{net} = \bar{\boldsymbol{\mathcal{E}}}(\boldsymbol{\mu})\bar{\boldsymbol{F}}$.

the isochoric part of (7.42), governed by the multiplicative definition $\bar{\boldsymbol{\mathcal{E}}}^{-1} := J_\mu^{-1/3}\boldsymbol{\mathcal{E}}^{-1}$. Taking into account the inverse of the sum of two square matrices, see e.g. Miller [123], we obtain a closed-form kinematic assumption for the *inverse isochoric stretch* associated with the spatial magnetization

$$\bar{\boldsymbol{\mathcal{E}}}(\boldsymbol{\mu}) = J_\mu^{1/3}\left[\boldsymbol{1} - \frac{c}{J_\mu}\boldsymbol{\mu}\otimes\boldsymbol{\mu}\right] \ . \tag{7.43}$$

It is used in the subsequent treatment as a part of the constitutive structure. Thus we can define the *elastic network deformation* $\bar{\boldsymbol{F}}_{net}$

$$\bar{\boldsymbol{F}}_{net} := \bar{\boldsymbol{\mathcal{E}}}\bar{\boldsymbol{F}} \tag{7.44}$$

7.5.5. Ingredient 5: Local Isochoric Mechanical Network Kernel

Contribution to the Free-Energy: An important aspect of this work is the modular constitutive structure of magneto-elasticity, that allows to include micromechanically-based network models for polymers without any change. This *micromechanical kernel* is assumed to define the energy $\bar{\Psi}_{mec}$ in (7.41) by the constitutive assumption

$$\bar{\Psi}_{mec}(\bar{\boldsymbol{F}}, \boldsymbol{\mu}, \boldsymbol{\mathcal{I}}) = \bar{\Psi}^e_{net}(\bar{\boldsymbol{F}}_{net}) + \bar{\Psi}^v_{net}(\bar{\boldsymbol{F}}_{net}, \boldsymbol{\mathcal{I}}) \tag{7.45}$$

in terms of the *viscoelastic network storage function* $\bar{\Psi}_{net}$. This function is considered to be known from statistical approaches to finite elasticity of crosslinked polymer networks. We consider closed-form representations in that are described shortly.

The Dissipation Function: For the viscoelastic response, we require a dissipation functional $\Phi(\dot{\boldsymbol{\mathcal{I}}})$ that models the rate-dependent dissipation. Here one may use micromechanically motivated dissipation functionals that come from the underlying phenomena causing viscoelasticity. In the idealized case considered here, the dissipative response is primarily due to the viscosity of the matrix (until Mullins-type damage occurs as described in Bednarek [5]). In this scenario we also assume the magnetic response of the filler particles to be non-dissipative. Thus, in our current approach the dissipation functional $\Phi(\dot{\boldsymbol{\mathcal{I}}})$ is taken from one of those describing the viscoelasticity of polymer networks. Therefore

$$\Phi(\dot{\boldsymbol{\mathcal{I}}}) = \Phi_{net}(\dot{\boldsymbol{\mathcal{I}}}) \tag{7.46}$$

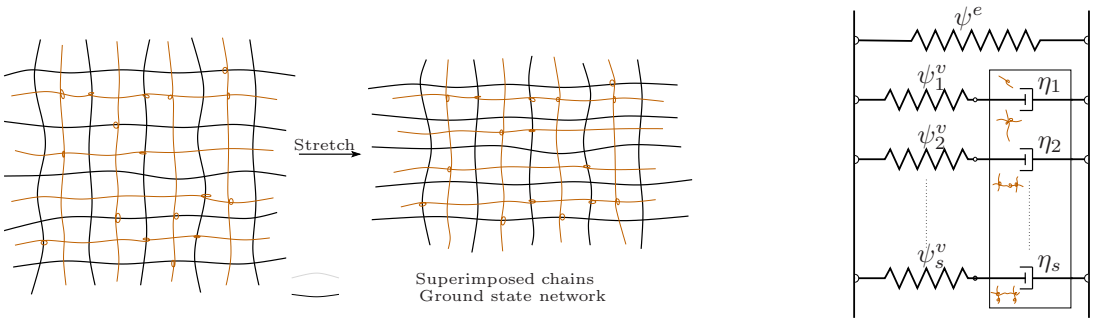

Figure 7.2: The micromechanical mechanism of viscoelasticity is shown on the left with a spectrum of superimposed non-equilibrium networks as indicated by the brown chains that retract by brownian motion yielding the relaxation of the non-equilibrium stresses. On the right is the equivalent Maxwellian type rheological model to capture this relaxation where each branch corresponds to a different subnetwork.

Now we only have to specify the functions $\tilde{\Psi}_{net}$ and Φ_{net}. As before, although we will use the micropshere model for this purpose, in principle, any other model may be used instead. A discussion on the elastic contribution $\tilde{\Psi}^e_{net}$, is not repeated here, and we refer the reader to the discussion in this term in the previous chapter.

The modeling of finite rubber viscoelasticity have been tackled by many researchers. As a result a variety of approaches have been developed by the engineering and chemistry communities. A complete review on viscoelasticity models of polymer networks is out of the scope of this work, however we may identify two broad categories, within the available phenomenological approaches, on the basis of internal variables used.

- Stress-like internal variables: The formulations of Simó [140], Govindjee & Simo [64], Holzapfel & Simó [69], Lion [105], Kaliske & Rothert [86] that employ convolution integrals, usually exploiting the structure of linear viscoelastic solids.
- Strain-like internal variables: The formulations of Sidoroff [139], Lubliner [107], Simo [140], Reese & Govindjee [131], Bergström & Boyce [7] use a *multiplicative split of the deformation gradient* into elastic and inelastic parts whereas Miehe & Keck [117] use the notion of evolving metric tensors.

We also mention several molecular theories have been developed in the past decade to describe the viscous behaviour of polymers. The main models of interest in this field are, *bead-spring type models* Zimm [169], the *reptation-type tube models* Doi & Edwards [40] and the *transient type tube models* by Green & Tobolsky [65]. Ideas of the reptation model has already been utilized in the macroscopic model in Bergström & Boyce [7].

Here, in the same vein as the elastic response, we use the viscoelastic contributions from the viscoelastic microsphere approach in Miehe & Göktepe [116] for our model. For brevity, we will outline only the chain contributions of that model. The viscoelastic part however makes an affine stretch assumption $\lambda = \bar{\lambda}$. The non-equilibrium part of the macroscopic energy is obtained by homogenizing the 1D response over the microsphere using the overstress contribution of a single chain ψ^v, the micro-dissipation function ϕ^v, and the internal variables $\epsilon^1....\epsilon^s$ for s Maxwell branches as

$$\psi^v = \frac{1}{2}\sum_{a=1}^{s} \mu^a (\ln \bar{\lambda} - \epsilon^a)^2 \quad \text{and} \quad \phi^v = \sum_{a=1}^{s} \frac{\delta^a}{\eta^a(1+\delta^a)} (\eta^a \, |\dot{\epsilon}^a|)^{(1+\delta^a)/\delta^a} \,, \tag{7.47}$$

in terms of the $3s$ material parameters $\{\mu^a, \eta^a, \delta^a\}^{a=1...s}$. Thus the macro-contributions are

$$\tilde{\Psi}^v(\boldsymbol{F}_{net}, \boldsymbol{\mathcal{I}}) = \langle \psi^v(\bar{\lambda}, \epsilon^1 .... \epsilon^s) \rangle \quad \text{and} \quad \Phi_{net}(\dot{\boldsymbol{\mathcal{I}}}) = \langle \phi^v(\dot{\epsilon}^1 ... \dot{\epsilon}^s) \rangle \tag{7.48}$$

For complete details regarding the viscoelastic microsphere, we refer the reader to Miehe & Göktepe [116]. For an alternative approach, the reader is referred to Ask, Menzel & Ristinmaa [3, 4] in which the second approach (multiplicative split of the deformation gradient) to model viscoelasticity of electroactive polymers is used.

7.6. The Stress and Magnetic Induction

With the structure of the energy-enthalpy function at hand, the material stresses take the form

$$\boxed{\boldsymbol{P} = U' J \boldsymbol{F}^{-T} + \bar{\boldsymbol{P}}_{net} : \mathbb{D} + \boldsymbol{P}_{Max}} \tag{7.49}$$

in terms of the penalty-type elastic pressure contribution, a deviatoric contribution due to the network deformation and a Maxwell-type magnetostatic contribution. The second term on the RHS of (7.49) includes the material deviatoric projection tensor defined as

$$\mathbb{D} := \partial_{\boldsymbol{F}} \bar{\boldsymbol{F}}_{net} = J^{-1/3} \bar{\boldsymbol{\mathcal{E}}} [\mathbb{I} - \tfrac{1}{3} \boldsymbol{F} \otimes \boldsymbol{F}^{-T}] \tag{7.50}$$

in terms of the fourth-order identity tensor $\mathbb{I}_{ijkl} = \delta_{ik}\delta_{jl}$.

The viscoelastic network stress kernel

$$\bar{\boldsymbol{P}}_{net} = \partial_{\bar{\boldsymbol{F}}_{net}} \bar{\Psi}_{net}(\bar{\boldsymbol{F}}_{net}, \boldsymbol{\mathcal{I}}) \ . \tag{7.51}$$

that takes into account the network structure of crosslinked polymer chains. One may use a variety of models for the mechanical kernels within this framework. Here, we use the microsphere model and specify the remaining expressions, namely the stress kernel, for completeness. Owing to the decomposition of the free energy into elastic an viscous parts, the stress kernel decomposes similarly as

$$\bar{\boldsymbol{P}}_{net} = \bar{\boldsymbol{P}}^e_{net} + \bar{\boldsymbol{P}}^v_{net} \ , \tag{7.52}$$

with $\bar{\boldsymbol{P}}^e_{net} = \partial_{\bar{\boldsymbol{F}}_{net}} \bar{\Psi}^e_{net}$ and $\bar{\boldsymbol{P}}^v_{net} = \partial_{\bar{\boldsymbol{F}}_{net}} \bar{\Psi}^v_{net}$. We may derive these elastic, and viscous overstress parts explicitly as

$$\bar{\boldsymbol{P}}^e_{net} = n\psi^{e\prime} \langle \bar{\lambda} \rangle_p^{1-p} \langle \bar{\lambda}^{p-2} \boldsymbol{t} \otimes \boldsymbol{r} \rangle \quad \text{and} \quad \bar{\boldsymbol{P}}^v_{net} = \langle \psi^{v\prime} \ \bar{\lambda}^{-1} \boldsymbol{t} \otimes \boldsymbol{r} \rangle \ , \tag{7.53}$$

with the Eulerian orientation vectors $\boldsymbol{t}$ related to their Lagrangian counterparts via $\boldsymbol{t} = \bar{\boldsymbol{F}}_{net} \boldsymbol{r}$. For brevity, we have not repeated the *tube* contributions of Miehe & Göktepe [116] but they have been implemented for the simulations

The Lagrangian magnetic induction $\widetilde{\boldsymbol{B}}$ was already obtained in $(6.26)_2$ and is repeated here for convenience

$$\boxed{\widetilde{\boldsymbol{B}} = \mu_0 (J \boldsymbol{C}^{-1} \widetilde{\boldsymbol{H}} + \rho_0 \boldsymbol{F}^{-1} \boldsymbol{\mu})} \tag{7.54}$$

In a similar fashion, to the stress variables above the total Maxwellian magnetic field $\boldsymbol{h}$ appears as a conjugate to the magnetization $\boldsymbol{\mu}$ and the local balance of magnetomechanical microtractions may be written as

$$\boxed{\mu_0 \boldsymbol{h} = \mu_0 \boldsymbol{h}_{mag} + \bar{\boldsymbol{P}}_{net} : \mathbb{G} \ .} \tag{7.55}$$

The first term comes from the contribution of the pure magnetic response and hence $\mu_0 \boldsymbol{h}_{mag} = \partial_{\boldsymbol{\mu}} \hat{\Psi}_{mag}$ depends on the model chosen for rigid magnetic response. The second term on the RHS of (7.55) arises due to the magnetostriction and includes the tensor

$$\mathbb{G}_{ijk} := \left[\partial_{\boldsymbol{\mu}} \bar{\boldsymbol{F}}_{net}\right]_{ijk} = cD^{-2/3} \left[\frac{2}{3}\mu_k \delta_{ia} - \mu_a \delta_{ik} - \mu_i \delta_{ak} + \frac{4c}{3}\frac{\mu_i \mu_a \mu_k}{D}\right] \bar{F}_{aj} \ . \tag{7.56}$$

Note that $\bar{\boldsymbol{P}}_{net}$ also includes a viscous contributions. In this manner, the model has a time dependent magnetic response arising due to the viscous contribution in the mechanics alone. The constitutive equations (7.49), (7.54) and (7.55) highlight the modularity of the presented approach since everything is explicitly specified except the *pure magnetic kernel* $\mu_0 \boldsymbol{h}_{mag}$ and the *stress kernel* $\bar{\boldsymbol{P}}_{net}$ *in the isochoric elastic deformation space*. This allows to include a variety of micromechanically based magnetic response functions and, more importantly, all viscoelastic network models for polymers.

7.7. Numerical Results

In the examples that follow, we demonstrate the capability of the complete finite deformation magneto-viscoelasticity modeling framework. As a micromechanical network kernel, we choose the microshere model of Miehe & Göktepe [116]. For the pure magnetic response we use the simple paramagnetic expression $\Psi_{mag} = \frac{C_m}{2}\boldsymbol{\mu} \cdot \boldsymbol{\mu}$. The structural model employs eight-node brick finite elements for the space discretization. The degrees of freedom at the nodes are the displacements $\boldsymbol{u} = \boldsymbol{\varphi} - \boldsymbol{X}$ and magnetic potential of the self-field $\widetilde{\phi}$. The material parameters used in for the simulations of the boundary value problems are given in Table 7.1.

7.7.1. Qualitative Demonstration of Magnetic Relaxation

In this problem we observe the response of the material on application of a rapidly increasing magnetic field $\overline{\boldsymbol{h}}$ on the body while constraining its free deformation. Due to

Table 7.1: Magneto-Elastic Material Parameters.

No.	Parameter	Name	Matrix	Inclusion	Unit
1.	κ	Bulk modulus	6.00×10^2	6.00×10^4	N/mm^2
2.	μ	Shear modulus	2.07×10^{-1}	2.07×10^1	N/mm^2
3.	N	Number of chain segments	4.31	4.31	–
4.	p	Non-affine averaging parameter	6.22	6.22	–
5.	U	Tube constant	5.00	5.00	–
6	q	Non affine tube parameter	2	–	
7.	c	Magnetostrictive coefficient	1.00×10^{-1}	0.00	–
8.	m_s	Saturation magnetization	1.00	0.00	–
9.	C_m	Paramagnetic coefficient	10.00	N/A^2	

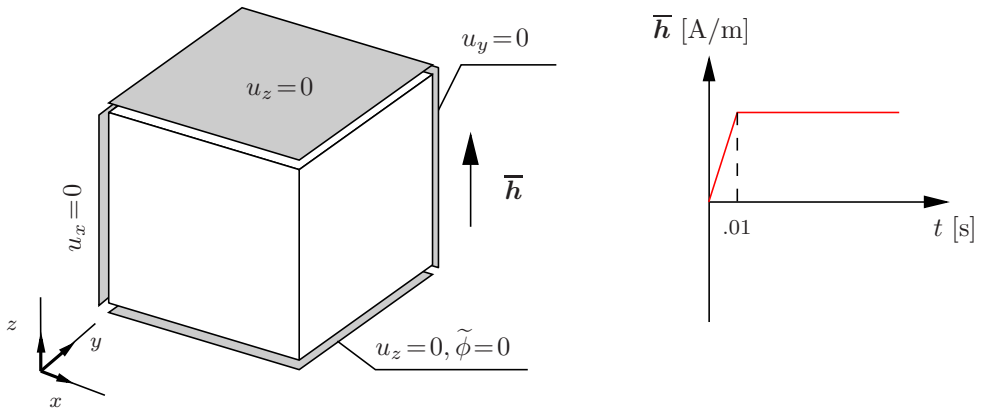

Figure 7.3: Boundary conditions for the magnetic relaxation simulation. The magnetic field $\overline{\boldsymbol{h}}$ is applied in the z-direction as shown in the figure.

magnetostriction, a mechanical stress in created in the body. It must be noted here that there will be no stress induced in the body if the deformation of the body is not constrained, this is due to the fact that according to the multiplicative split of the deformation gradient, the magnetostrictive part is stress-free. This particular problem is similar to a relaxation test conducted on standard viscoelastic models where a sudden strain is applied, and the consequent stress relaxation over a period of time is observed. The boundary conditions of this problem are shown in Figure 7.3. The magnetoelastic parameters are in Table 7.1 and the viscous parameters are $\mu_f = (0.6157, 0.1345, 0.1802)$ MPa, $\mu_c = (2.190, 0.951, 1.430)$ MPa, $\delta_f = (2.974, 2.465, 24.46)$, $\delta_c = 1.022, 2.048, 16.47$, $\tau_{f,c} = (0.1, 10, 1000)$ where f and c, just like in Miehe & Göktepe [116], denote the parameters for the free stretch and tube constraint respectively. As shown, a magnetic field is applied suddenly and then is held constant. This sudden application of the mag-

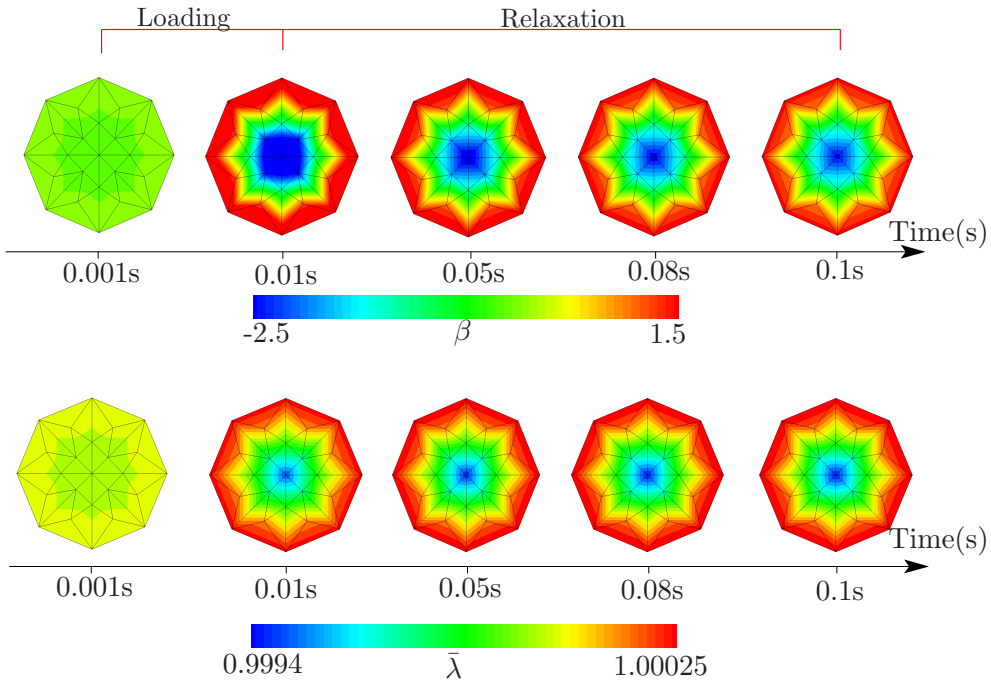

Figure 7.4: Pole-figures for the driving force β and the mechanical stretch $\bar{\lambda}$. The figures from a) to e) correspond to the different time steps a) 0.001s b) 0.01 c) 0.05s d) 0.08s e) 0.1s

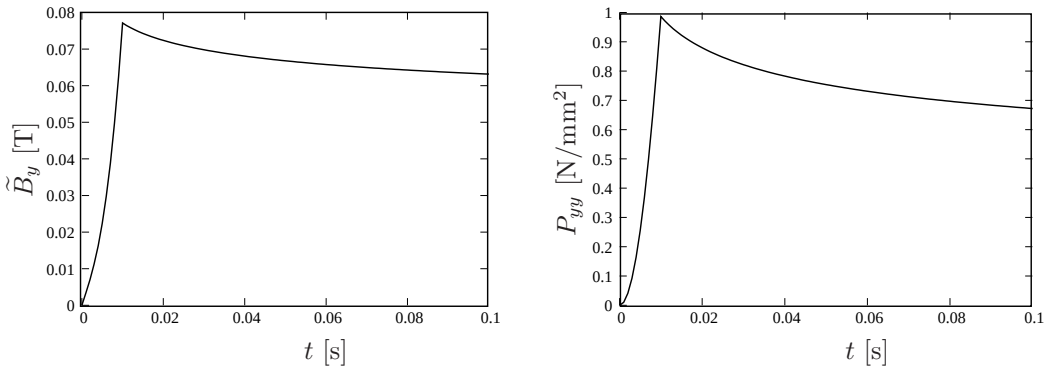

Figure 7.5: The plots for the induced magnetic induction $\widetilde{B}_2$ and the mechanical stress P_{22}, in the direction of the applied magnetic potential difference. The values are ploted at the same Gauss point as the pole-projection figures. Viscous effects in mechanical, as well as magnetic responses are observed.

netic field causes a mechanical stress in the body due to the chosen boundary conditions. Figure 7.4 shows the pole figure projection of the microsphere at a specific Gauss point for the internal variable β and the stretch $\bar{\lambda}$. The sudden change in the values of β and $\bar{\lambda}$ at time t=0.01s, is due to this applied magnetic field. This is denoted as loading in Figure 7.4 . After $t = 0.01$ s, the magnetic potential difference is held constant. The change in the pole projection from time $t = 0.01$ s to $t = 0.1$ s , is due to the relaxation of the viscoelastic model. This is denoted as the relaxation phase. This particular example shows the viscous coupling of the magnetic and the mechanical fields. The values of the magnetization $\boldsymbol{\mu}$ and the mechanical stresses P_{22} are plotted vs time in Figure 7.5, at the same Gauss point as the pole-projection figures. It can be clearly seen that the stress relaxation effect, generally observed in viscoelastic materials is observed in both the fields.

7.7.2. Dynamic Compression Test

One of the objectives of this thesis was to show the capability of the proposed model by fitting the parameters to get the experimental results. To show all the capabilities of our model, the dynamic compression test results are taken from Kallio [87]. Due to the lack

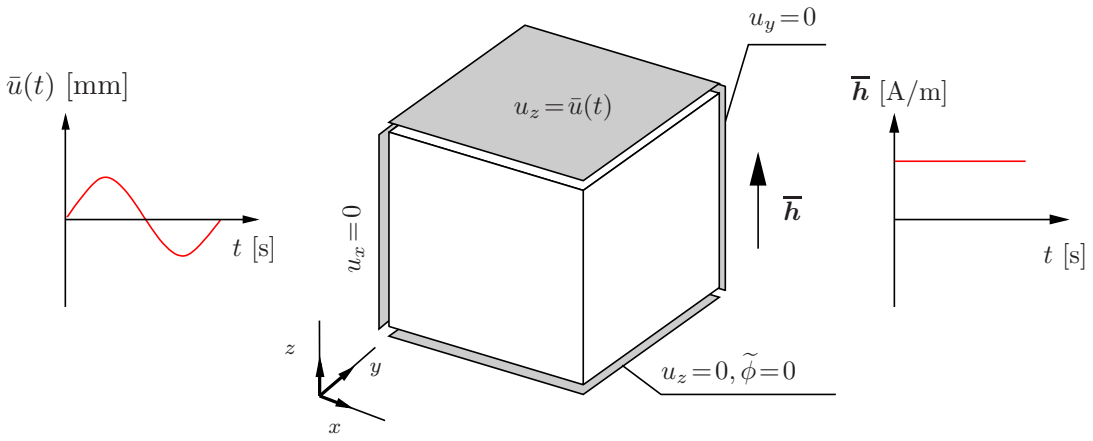

Figure 7.6: Boundary conditions for the magnetic relaxation simulation. The magnetic field $\overline{\boldsymbol{h}}$ is applied in the z-direction as shown in the figure.

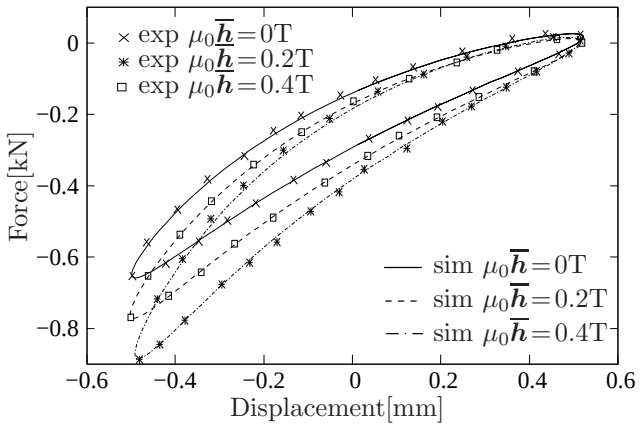

Figure 7.7: Comparison of experiment and simulation for the finite deformation magneto-viscoelastic models. Experimental data taken from KALLIO [87]. Viscous parameters identified for the fit are $\mu_f = (0.6157, 0.1345, 0.1802)$ MPa, $\mu_c = (2.190, 0.951, 1.430)$ MPa, $\delta_f = (2.974, 2.465, 24.46)$, $\delta_c = 1.022, 2.048, 16.47$, $\tau_{f,c} = (0.1, 10, 1000)$

of information available on viscoelasticity of isotropic MREs, the experimental results are of an anisotropic MRE under cyclic sinusoidal loading with and without the magnetic field are matched against the model. The magnetic field is applied in the direction of the deformation. Force vs displacement plots for the same are presented by KALLIO [87] which are used here for comparison. To simulate the results we use a single element and apply the boundary conditions as shown Figure 7.6. A sinusoidal displacement boundary condition is applied on the top surface while a constant magnetic field is applied in the z-direction. It should be noted here that the magnetic field is applied as a ramp load first so that the viscous effects due to the magnetic field are not induced in the deformation of the material (or kept to a minimum). The force and the displacement at the top surface are plotted. First, the simulation is run without any magnetic field so that the elastic and the viscoelastic parameters can be fitted. There are in all 28 parameters where we have 6 parameters for the elastic free and tube part, 1 parameter for the definition of the number of viscoelastic branches used (we use 3 branches here to get the viscoelastic behavior over a wide spectrum of loading conditions), 18 viscoelastic parameters 2 magnetic parameters and 1 magnetoelastic parameter. The mechanical parameters were first adjusted to get the proper viscoelastic behavior. It is seen from the first graph in Figure 7.7 that the

Table 7.2: Magnetoelastic Material Parameters for Calibration against Experiment.

No.	Parameter	Name	Matrix	Unit
1.	κ	Bulk modulus	6.00×10^2	N/mm^2
2.	μ	Shear modulus	8.00×10^{-4}	N/mm^2
3.	N	Number of chain segments	5.00	–
4.	p	Non-affine averaging parameter	1.16	–
5.	U	Tube constant	5.00	–
6	q	Non affine tube parameter	0.126	–
7.	c	Magnetostrictive coefficient	-12.00	–
8.	m_s	Saturation magnetization	1.00	0.00 –
9.	C_m	Paramagnetic coefficient	10.00	N/A^2

model shows a good fit to the experimental data The values used for the simulation are shown in Tab. 7.2. After fitting the material parameters for the elastic and viscoelastic parts, we fit the curve for applied magnetic field of $\mu_0\overline{h}_z = 0.2$ T. For this the magnetic constants c, κ_m and η were fitted to get the required stiffening in the material to get the curves. The final values for the same are given in Table 1. The same values have been used to generate the third plot for $\mu_0\overline{h}_z$=0.4 T. It is observed that the model is quite consistent with the experimental data. It should be noted here that this model is generally used for isotropic MR elastomer but taking the magnetostrictive coefficient as a negative value results in a behavior similar to an anisotropic MRE.

8. Conclusion

This work presented new variational principles for numerical simulations in magnetomechanics. In the stationary setting, these were based on three-field formulations. These ideas were then extended to time-dependent dissipative scenarios. The presented approaches allowed for mechanical and magnetic loadings and the construction of constitutive models was described in detail taking into account the micromechanics of the materials concerned. Finally, the implementation of these principles in finite element frameworks was outlined in detail and numerical simulations were presented for each case. We briefly summarize the salient features of the work, specific to the two general cases of materials considered in the following subsections.

8.1. Computational Micro-Magneto-Mechanics

We presented a *new geometrically exact, three-field rate-type variational principle for dynamic dissipative micro-magneto-mechanics.* This was done by first constructing functionals of micro-magneto-elasticity based on three fields which govern the coupled problem. Of utmost importance are the energy-enthalpy and dissipation functionals. They were formulated in terms of a general framework of an objective, first-order gradient-type material. Inside of the solid domain, the energy density splits up into a free space or vacuum contribution plus a term due to the solid matter. The latter contains the stored elastic energy, including the magnetostrictive coupling, the non-convex magnetic anisotropy density that determines the easy axes of magnetization (due to spin-orbit interactions) and the so-called exchange energy (due to spin-spin interactions) that contains the gradient of the magnetization director. We assumed a Rayleigh-type function for the dissipation. and introduce mechanical and magnetic loading functionals by focussing on magnetic-field-driven as well as stress-driven scenarios. The mechanical loading functional contains a *prescribed average macro-stress within the solid domain.* The magnetic loading functional is defined in terms of a *prescribed average macro-field within the full space*, including solid domain and free space. With these functionals at hand, we developed variational principles for the coupled evolution problem. We commenced by outlining the variational principle for stationary problems in a continuous setting in line with the classical work of Brown [21], formulated however, in terms of the loading quantities stated above.

A central and new aspect of the work was the formulation of an *incremental variational principle for dynamic (quasi-static) evolution problems.* This incremental principle, which governs the rates of the primary variables was based on a potential, that was formulated in terms the energy-enthalpy and the dissipation functionals. We showed that the Euler equations of this variational principle are the static stress equilibrium condition, the magnetostatic equilibrium condition, often denoted as the third Maxwell equation or the Gauss' law for magnetism, and the Landau-Lifshitz equation for the evolution of the magnetization director.

Based on this framework, we developed *a new geometrical consistent finite element model of micro-magneto-elasticity*, that accounts for the geometric structure of the magnetization director $\boldsymbol{m} \in \mathcal{S}^{d-1}$. Starting from the algorithmic version of the variational principle for dynamic evolution problems associated with finite time increments, we proposed a finite element method which preserved exactly this geometric property of the director field at the nodes of the mesh. This time-space-discrete formulation being variational in

nature, yielded a symmetric monolithic system of the coupled multifield problem. The key ingredient was the *exact rotational treatment of the magnetization director*, that resulted in nonlinear incremental updates of the nodal variables. The method preserved the geometric structure in each iteration step of a typical Newton-Raphson update. As a consequence of the nonlinear update of the magnetization director, the finite element tangent matrix split into characteristic material and geometric contributions. We outlined the formulation in the full three-dimensional context. Its reduction to two-dimensional problems yielded a substantial simplification due to the scalar nature of the incremental rotation. Numerical simulations to demonstrate the modeling capacity of the proposed formulation for domain wall motions in magnetic field- and stress-driven loading processes, including their coupling with the surrounding free space were presented.

We went further to develop a *projection method based on an operator split* as an alternative computational approach to the above monolithic solution strategy. This method was based on the same variational principles mentioned above, but avoided the nonlinear update and geometric matrices of the geometrically exact method thus leading to straightforward and efficient implementation. The unity constraint of the magnetization director was preserved by a post-processing projection step and a staggered solution scheme was employed for solving for the primary variables. Also, due to the successful implementation of both methods, *a comparison* of computational performance between the geometrically exact method and projection method has was possible for the first time.

8.2. Finite Strain Computational Modeling of MREs

A *new incremental variational principle for dissipative magneto-mechanics of MREs in the finite deformation regime* has was formulated in this dissertation. We first considered the non-dissipative elastic scenario. This was based on the classical work on elastic dielectrics by Toupin [156] and the work on MREs by Kankanala & Triantafyllidis [88, 89]. A *three-field formulation in terms of the deformation map, magnetization (per unit mass) and magnetic scalar potential of the self-field* was presented. In a similar manner to Miehe & Ethiraj [115], we began with constructing the required functionals. Of foremost importance was the energy enthalpy functional of finite deformation magnetoelasticity. The loading contributions were taken in terms of the applied magnetic field and mechanical body forces and tractions. With these functionals at hand, we constructed the variational principle for finite deformation magnetoelasticity. The Euler equations of the variational principle are the balance of linear momentum, the Gauss' law for magnetism, the (time-discrete) Biot equation for the evolution of the internal variables and a local equation relating the magnetic field with the magnetization.

From the material modeling perspective, we have presented *a modular framework for the construction of constitutive models for isotropic MREs that allow the incorporation of statistically based kernels*. The presented framework was shown to have two salient features that were highlighted. Firstly, we employed a *multiplicative split of the deformation gradient into stress-free (magnetostrictive) and stress-producing parts*. This gave rise to the second salient feature namely *the exploitation of micromechanically-motivated, statistically-based (network) kernels* in the model without any change. While we used an Ising model for the pure magnetic response, the elastic response was governed by the non-affine microsphere model of Miehe, Göktepe & Lulei [118].

We further extended the above methods to cover irreversible effects. Here, we focussed

on the viscoelastic response that arises due to the rubber matrix. With the functionals for the reversible (magnetoelastic) case defined, we presented a *new four-field incremental variational principle for magneto-viscoelasticity* with the fourth field representing viscous strain-like variables. This was based on the construction of a rate-type variational potential that yielded in addition to the balance equations of the elastic case, the Biot equation for the local evolution of the viscous strain-like variables as the Euler equations. The incremental variational potential followed by an algorithmic time integration. Following this, the modular framework for free-energy functions for magnetoelasticity of MREs was extended to cover magneto-viscoelasticity. This involved an addition to the energetic part of the model and a dissipation function as well. Once again the modular framework allowed the inclusion of the *statistically-based network kernels,* this time, *for viscoelasticity.* For our specific implementation, we use the viscoelastic model of Miehe & Göktepe [116].

We have implemented the frameworks for finite deformation magnetoelasticity and magneto-viscoelasticity within a finite element code and thus are able to perform fully-coupled magnetomechanical simulations for application-oriented problems.

References

[1] Arruda, E. M.; Boyce, M. C. [1993]: *A three–dimensional constitutive model for the large stretch behavior of rubber elastic materials.* Journal of the Mechanics and Physics of Solids, 41: 389–412.

[2] Arthur, J. W. [2008]: *The fundamentals of electromagnetic theory revisited.* IEEE Antennas and Propagation Magazine, 50: 19–65.

[3] Ask, A.; Menzel, A.; Ristinmaa, M. [2012]: *Phenomenological modeling of viscous electrostrictive polymers.* International Journal of Non-Linear Mechanics, 47(2): 156–165.

[4] Ask, A.; Menzel, A.; Ristinmaa, M. [2012]: *Electrostriction in electro-viscoelastic polymers.* Mechanics of Materials, 50: 9–21.

[5] Bednarek, S. [1999]: *The giant magnetostriction in ferromagnetic composites within an elastomer matrix.* Applied Physics A, 68(1): 63–67.

[6] Bellan, C.; Bossis, G. [2002]: *Field dependence of viscoelastic properties of MR elastomers.* International Journal of Modern Physics B, 16(17–18): 2447–2453.

[7] Bergström, J. S.; Boyce, M. C. [1998]: *Constitutive modeling of the large strain time–dependent behavior of elastomers.* Journal of the Mechanics and Physics of Solids, 46: 931–954.

[8] Bertram, H. N. [1994]: *Theory of Magnetic Recording.* Cambridge University Press, Cambridge, UK.

[9] Borcea, L.; Bruno, O. [2001]: *On the magneto-elastic properties of elastomer-ferromagnet composites.* Journal of the Mechanics and Physics of Solids, 49: 2877–2919.

[10] Borovik-Romanov, A. S. [1960]: *Piezomagnetism in the antiferromagnetic fluorides of cobalt and manganese.* Journal of Experimental and Theoretical Physics, 11: 786–793.

[11] Borovik-Romanov, A. S. [1994]: *Piezomagnetism, linear magnetostriction and magnetooptic effect.* Ferroelectrics, 162: 153–159.

[12] Böse, H.; Rabindranath, R.; Ehrlich, J. [2012]: *Soft magnetorheological elastomers as new actuators for valves.* Journal of Intellegent Material Systems and Structures, 14: 743–765.

[13] Boyce, M. C.; Arruda, E. M. [2000]: *Constitutive models of rubber elasticity: A review.* Rubber Chemistry and Technology, 73: 504–523.

[14] Bozorth, R. M. [1940]: *The physical basis of ferromagnetism.* Bell System Technical Journal, 19: 1–39.

[15] Bozorth, R. M. [1951]: *Ferromagnetism.* Wiley-IEEE Press, New York, reissue of 1951 Edition.

[16] Brigadnov, I. A.; Dorfmann, A. [2003]: *Mathematical modeling of magneto-sensitive elastomers.* International Journal of Solids and Structures, 40: 4659–4674.

[17] Brown Jr., W. F. [1951]: *Electric and magnetic forces: A direct calculation. i.* American Journal of Physics, 19: 290–304.

[18] Brown Jr., W. F. [1951]: *Electric and magnetic forces: A direct calculation. ii.* American Journal of Physics, 19: 333–350.

[19] Brown Jr., W. F. [1962]: *Magnetoelastic Principles in Ferromagnetism*, Vol. 1. North-Holland Publishing Company.

[20] Brown Jr., W. F. [1963]: *Micromagnetics.* Interscience Publishers.

[21] Brown Jr., W. F. [1966]: *Magnetoelastic Interactions*, Vol. 9 of *Tracts in Natural*

Philosophy. Springer-Verlag.

[22] Brown Jr., W. F. [1984]: *Tutorial paper on dimensions and units*. IEEE Transactions on Magnetics, 2: 112–117.

[23] Bustamante, R.; Dorfmann, A.; Ogden, R. W. [2006]: *Universal relations in isotropic nonlinear magnetoelasticity*. The Quaterly Journal of Mechanics and Applied Mathematics, 59(3): 435–450.

[24] Bustamante, R.; Dorfmann, A.; Ogden, R. W. [2007]: *On variational formulations in nonlinear magnetoelastostatics*. Mathematics and Mechanics of Solids, 13(8): 725–745. In Press.

[25] Bustamante, R.; Dorfmann, A.; Ogden, R, W. [2007]: *A nonlinear magnetoelastic tube under extension and inflation in an axial magnetic field: numerical solution*. Journal of Engineering Mathematics, 59: 139–153.

[26] Chattock, A. P. [1887]: *On a magnetic potentiometer*. The London, Edinburgh, and Dublin Philosophical Magazine and Journal of Science, 24 (146): 94–96.

[27] Chatzigeorgiou, G.; Javili, A.; Steinmann, P. [2014]: *Unified magnetomechanical homogenization framework with application to magnetorheological elastomers*. Mathematics and Mechanics of Solids, 19: 193–211.

[28] Cullity, B. D. [1972]: *Introduction to Magnetic Materials*. Addison-Wesley, Reading, MA.

[29] Danas, K.; Triantafyllidis, N. [2014]: *Instability of a magnetoelastic layer resting on a non-magnetic susbstrate*. Journal of the Mechanics and Physics of Solids, 69: 67–83.

[30] Danas, K.; Kankanala, S. V.; Triantafyllidis, N. [2012]: *Experiments and modeling of iron-particle-filled magnetorheological elastomers*. Journal of the Mechanics and Physics of Solids, 60: 120–138.

[31] Davis, L. C. [1999]: *Model of magnetorheological elastomers*. Journal of Applied Physics, 85(6): 3348–3351.

[32] DeSimone, A. [1993]: *Energy minimizers for large ferromagnetic bodies*. Archive for Rational Mechanics and Analysis, 125: 99–143.

[33] DeSimone, A.; James, R. [2002]: *A constrained theory of magnetoelasticity*. Journal of Mechanics and Physics of Solids, 50: 283–320.

[34] DeSimone, A.; Kohn, R. V.; Müller, S.; Otto, F. [2004]: *Recent analytical developments in micromagnetics*. Technical report, Max-Planck-Institut für Mathematik in den Naturwissenschaften, Leipzig.

[35] DeSimone, A.; Kohn, R. V.; Müller, S.and Otto, F. [2005]: *Recent analytical developments in micromagnetics*. In *The Science of Hysteresis*. Elsevier Academic Press.

[36] Diguet, G. [2010]: *Huge Magnetostriction of magneto-rheological composite*. Ph.D. Thesis, Université de Grenoble.

[37] Diguet, G.; Beaugnon, E.; Cavaillé, J. Y. [2009]: *From dipolar interactions of a random distribution of ferromagnetic particles to magnetostriction*. Journal of Magnetism and Magnetic Materials, 321: 396–401.

[38] Dixon, R. C.; Eringen, A. C. [1964]: *A dynamical theory of polar elastic dielectrics I*. International Journal of Engineering Science, 3: 359–377.

[39] Dixon, R. C.; Eringen, A. C. [1964]: *A dynamical theory of polar elastic dielectrics II*. International Journal of Engineering Science, 3: 379–398.

[40] Doi, M.; Edwards, S. F. [1986]: *The Theory of Polymer Dynamics*. Clarendon

Press, Oxford.

[41] Donahue, M. J.: *μmag – micromagnetic modeling activity group.*

[42] Dorfmann, A.; Ogden, R. W. [2003]: *Magnetoelastic modelling of elastomers.* European Journal of Mechanics A/Solids, 22: 497–507.

[43] Dorfmann, A.; Ogden, R. W. [2004]: *Nonlinear magnetoelastic deformations of elastomers.* Acta Mechanica, 167(1–2): 13–28.

[44] Dorfmann, A.; Ogden, R. W. [2004]: *Nonlinear magnetoelastic deformations.* The Quaterly Journal of Mechanics and Applied Mathematics, 57(4): 599–622.

[45] Dorfmann, A.; Ogden, R. W. [2005]: *Some problems in nonlinear magnetoelasticity.* Zeitschrift für Angewandte Mathematik und Physik ZAMP, 56: 718–745.

[46] Dorfmann, A.; Ogden, R. W.; Saccomandi, G. [2005]: *The effect of rotation on the nonlinear magnetoelastic response of a circular cylindrical tube.* International Journal of Solids and Structures, 42: 3700–3715.

[47] Dzialoshinskii, I. E. [1957]: *Thermodynamic theory of "weak" ferromagnetism of antiferromagnetics.* Soviet Journal of Experimental and Theoretical Physics, 5: 1259–1272.

[48] Dzialoshinskii, I. E. [1958]: *The problem of piezomagnetism.* Soviet Journal of Experimental and Theoretical Physics, 6: 621–622.

[49] Eerenstein, W.; Mathur, N.; Scott, J. [2006]: *Multiferroic and magnetoelectric materials.* Nature, 442: 759–765.

[50] Ericksen, J. L. [2006]: *A modified theory of magnetic effects in elastic materials.* Mathematics and Mechanics of Solids, 11: 23–47.

[51] Ericksen, J. [2002]: *Electromagnetic effects in thermoelastic materials.* Mathematics and Mechanics of Solids, 7(2): 165–189.

[52] Ericksen, J. [2007]: *Theory of elastic dielectrics revisited.* Archive for Rational Mechanics and Analysis, 183: 299–313.

[53] Eringen, A. C.; Maugin, G. A. [1990]: *Electrodynamics of Continua I — Foundations and Solid Media.* Springer-Verlag.

[54] Ethiraj, G. [2009]: *Theory and numerical aspects of constitutive modeling in finite deformation magnetomechanics.* Master's thesis, University of Stuttgart.

[55] Ethiraj, G.; Miehe, C. [2015]: *Multiplicative magneto-elasticity of magnetosensitive polymers incorporating micromechanically-based network kernels.* Proceedings of the Royal Society A, Submitted.

[56] Ethiraj, G.; Sridhar, A.; Miehe, C. [2015]: *Variational modeling and homogenization in dissipative magneto-mechanics.* GAMM Mitteilungen.

[57] Ethiraj, G.; Zäh, D.; Miehe, C. [2013]: *A finite deformation microsphere model for magneto-visco-elastic response in magnetorheological elastomers.* Proceedings in Applied Mathematics and Mechanics, 13: 197–198.

[58] Fiebig, M. [2005]: *Revival of the magnetoelectric effect.* Journal of Physics D: Applied Physics, 38: R123–R152.

[59] Flory, P. J. [1989]: *Statistical Mechanics of Chain Molecules.* Clarendon Press, Oxford.

[60] Galipeau, E.; Ponte Castañeda, P. [2012]: *The effect of particle shape and distribution on the macroscopic behavior of magnetoelastic composites.* International Journal of Solids and Structures, 49: 1–17.

[61] Galipeau, E.; Ponte Castañeda, P. [2013]: *Giant field-induced strains in magnetoactive elastomer composites.* Proceedings of the Royal Society of London

A, 469.

[62] Gilbert, T. L. [1956]: *Formulation, foundations, and applications of the phenomenological theory of ferromagnetism*. Ph.D. Thesis, Illinois Institute of Technology.

[63] Gilbert, T. L. [2004]: *A phenomenological theory of damping in ferromagnetic materials*. IEEE Transacctions on Magnetics, 40: 3443–3449.

[64] Govindjee, S.; Simó, J. C. [1992]: *Mullins' effect and the strain amplitude dependence of the storage modulus*. International Journal of Solids and Structures, 29: 1737–1751.

[65] Green, M. S.; Tobolsky, A. V. [1946]: *A new approach to the theory of relaxing polymeric media*. The Journal of Chemical Physics, 14: 80–92.

[66] Griffiths, R. B. [1964]: *A proof that the free energy of a spin system is extensive*. Journal of Mathematical Physics, 5: 1215–1222.

[67] Griffiths, R. B. [1968]: *Free energy of interacting magnetic dipoles*. Physical Review, 176: 655–659.

[68] Hirohata, A.; Takanashi, K. [2014]: *Future perspectives for spintronic devices*. Journal of Physics D: Applied Physics, 47: 193001:1–40.

[69] Holzapfel, G. A.; Simó, J. C. [1996]: *A new viscoelastic constitutive model for continuous media at finite thermomechanical changes*. International Journal of Solids and Structures, 33: 3019–3034.

[70] http://www.etrema.com/: *Etrema products, inc.*

[71] http://www.feonic.com/: *Feonic - developers of sound and ultrasonic transducer technology*.

[72] Hubert, A.; Schäfer, R. [2001]: *Magnetic Domains*. Springer-Verlag, New York.

[73] Hutter, K.; Ven, A. A. F. van de [1978]: *Field Matter Interactions in Thermoelastic Solids*, Vol. 88 of *Lecture Notes in Physics*. Springer-Verlag, New York.

[74] Ivaneyko, D.; Toshchevikov, V.; Saphiannikova, M.; Heinrich, G. [2011]: *Magneto-sensitive elastomers in a homogeneous magnetic field: A regular rectangular lattice model*. Macromolecular Theory and Simulations, 20(6): 411–424.

[75] Ivaneyko, D.; Toshchevikov, V.; Saphiannikova, M.; Heinrich, G. [2012]: *Effects of particle distribution on mechanical properties of magneto-sensitive elastomers in a homogeneous magnetic field*. Condensed Matter Physics, 15: 33601: 1–12.

[76] Ivaneyko, D.; Toshchevikov, V.; Saphiannikova, M.; Heinrich, G. [2014]: *Mechanical properties of magneto-sensitive elastomers: unification of the continuum-mechanics and microscopic theoretical approaches*. Soft Matter, 10: 2213–2225.

[77] Iwasaki, S.; Takemura, K. [1975]: *An analysis for the circular mode of magnetization in short wavelength recording*. IEEE Transacctions on Magnetics, 11: 1173–1175.

[78] Iwasaki, S.; Takemura, K. [1978]: *The magnetic field distribution of a perpendicular recording head*. IEEE Transactions on Magnetics, 14: 436–438.

[79] James, H. M.; Guth, E. [1943]: *Theory of elastic properties of rubber*. The Journal of Chemical Physics, 11: 455–481.

[80] James, R. D.; Kinderlehrer, D. [1990]: *Frustration in ferromagnetic materials*. Continuum Mechanics and Thermodynamics, 2: 215–239.

[81] James, R. D.; Kinderlehrer, D. [1993]: *Theory of magnetostriction with ap-*

plications to $Tb_xDy_{1-x}Fr_2$. Philosophical Magazine B, 68(2): 237–274.

[82] Javili, A.; Chatzigeorgiou, G.; Steinmann, P. [2013]: *Computational homogenization in magneto-mechanics*. International Journal of Solids and Structures, 50(25–26): 4197–4216.

[83] Jolly, M. R.; Carlson, D.; Muñoz, B. C.; Bullions, T. A. [1996]: *The magnetoviscoelastic response of elastomer composites consisting of ferrous particles embedded in a polymer matrix*. Journal of Intelligent Material Systems and Structures, 7: 613–612.

[84] Joule, J. P. [1842]: *On a new class of magnetic forces*. Annals of Electricity, Magnetism, and Chemistry, 8: 219–224.

[85] Joule, J. P. [1847]: *On the effects of magnetism upon the dimensions of iron and steel bars*. The London, Edinburgh and Dublin Philosophical Magazine and Journal of Science, 30: 76–87, 225–241.

[86] Kaliske, M.; Rothert, H. [1997]: *Formulation and implementation of three–dimensional viscoelasticity at small and finite strains*. Computational Mechanics, 19: 228–239.

[87] Kallio, M. [2005]: *The Elastic and Damping Properties of Magnetorheological Elastomers*. Ph.D. Thesis, Tampere University of Technology.

[88] Kankanala, S. V.; Triantafyllidis, N. [2004]: *On finitely strained magnetorheological elastomers*. Journal of Mechanics and Physics of Solids, 52: 2869–2908.

[89] Kankanala, S. V.; Triantafyllidis, N. [2008]: *Magnetoelastic buckling of a rectangular block in plane strain*. Journal of the Mechanics and Physics of Solids, 56: 1147–1169.

[90] Kittel, C. [1949]: *Physical theory of ferromagnetic domains*. Reviews of Modern Physics, 21(4): 541–583.

[91] Kittel, C. [1956]: *Introduction to Solid State Physics*. John Wiley & Sons, New York, 2nd Edition.

[92] Kittel, C. [1996]: *Introduction to Solid State Physics*. John Wiley & Sons, New York, 7th Edition.

[93] Kittel, C.; Galt, J. K. [1956]: *Ferromagnetic domain theory*. Solid State Physics, 3: 437–564.

[94] Kovetz, A. [2000]: *Electromagnetic Theory*. Oxford University Press, Oxford.

[95] Kružík, M.; Prohl, A. [2006]: *Recent developments in the modeling, analysis, and numerics of ferromagnetism*. SIAM Review, 48: 439–483.

[96] Kuepper, K.; Buess, M.; Raabe, J.; Quitmann, C.; Fassbender, J. [2007]: *Dynamic vortex-antivortex interaction in a single cross-tie wall*. Phys. Rev. Lett., 99: 167202.

[97] Kuhn, W. [1934]: *über die gestalt fadenförmiger moleküle in lösungen*. Kolloid-Zeitschrift, 68: 2–15.

[98] Kuhn, W. [1936]: *Beziehungen zwischen molekülgröße, statistischer molekülgestalt und elastischen eigenschaften hochpolymerer stoffe*. Kolloid-Zeitschrift, 76: 258–271.

[99] Kuhn, W.; Grün, F. [1942]: *Beziehungen zwischen elastischen Konstanten und Dehnungsdoppelbrechung hochelastischer Stoffe*. Kolloid Zeitschrift, 101: 248–271.

[100] Landau, L. D.; Lifshitz, E. M. [1935]: *On the theory of the dispersion of magnetic permeability in ferromagnetic bodies*. Physikalische Zeitschrift der Sowjetunion, 8: 153–169.

[101] Lee, E. W. [1955]: *Magnetostriction and magnetomechanical effects*. Reports on

Progress in Physics, 18: 184–230.

[102] Lewis, D.; Nigam, N. [2003]: *Geometric integration on spheres and some interesting applications.* Journal of Computational and Applied Mathematics, 151: 141–170.

[103] Li, L. J.; Yang, Y.; C., S. Y.; Y., L. J. [2010]: *Continuum theory and phase-field simulation of magnetoelectric effects in multiferroic bismuth ferrite.* Journal of the Mechanics and Physics of Solids, 58: 1613–1627.

[104] Linnemann, K.; Klinkel, S.; Wagner, W. [2009]: *A constitutive model for magnetostrictive and piezoelectric materials.* International Journal of Solids and Structures, 46: 1149–1166.

[105] Lion, A. [1996]: *A constitutive model for carbon black filled rubber. experimental investigations and mathematical representations.* Continuum Mechanics and Thermodynamics, 8: 153–169.

[106] Lorentz, H. A. [1900]: *Theory of Electrons.* Dover Publications, New York, reprint (1952) Edition.

[107] Lubliner, J. [1985]: *A model of rubber viscoelasticity.* Mechanics Research Communications, 12: 93–99.

[108] Martin, J. E. [2005]: *Using triaxial magnetic fields to create optimal particle composites.* Composites: Part A, 36: 545–548.

[109] Maugin, G. A. [1988]: *Continuum Mechanics of Electromagnetic Solids*, Vol. 33 of *North-Holland Series in Applied Mathematics and Mechanics.* Elsevier Science Publishers, Amsterdam.

[110] Maugin, G. A.; Eringen, A. C. [1977]: *On the equations of the electrodynamics of deformable bodies of finite extent.* Journal de Mécanique, 16: 101–147.

[111] Menzel, A.; Waffenschmidt, T. [2009]: *A microsphere-based remodelling formulation for anisotropic biological tissues.* Philosophical Transactions of the Royal Society A, 367: 3499–3523.

[112] Miehe, C. [1995]: *Entropic thermo–elasticity at finite strains: Aspects of the formulation and numerical implementation.* Computer Methods in Applied Mechanics and Engineering, 120: 243–269.

[113] Miehe, C. [1995]: *Discontinuous and continuous damage evolution in ogden–type large–strain elastic materials.* European Journal of Mechanics A / Solids, 14: 697–720.

[114] Miehe, C. [1996]: *Numerical computation of algorithmic (consistent) tangent moduli in large-strain computational inelasticity.* Computer Methods in Applied Mechanics and Engineering, 134: 223–240.

[115] Miehe, C.; Ethiraj, G. [2012]: *A geometrically consistent incremental variational formulation for phase field models in micromagnetics.* Computer Methods in Applied Mechanics and Engineering, 245: 331–347.

[116] Miehe, C.; Göktepe, S. [2005]: *A micro–macro approach to rubber–like materials. part ii: The micro–sphere model of finite rubber viscoelasticity.* Journal of the Mechanics and Physics of Solids, 53: 2231–2258.

[117] Miehe, C.; Keck, J. [2000]: *Superimposed finite elastic–viscoelastic–plastoelastic stress response with damage in filled rubbery polymers. experiments, modelling and algorithmic implementation.* Journal of the Mechanics and Physics of Solids, 48: 323–365.

[118] Miehe, C.; Göktepe, S.; Lulei, F. [2004]: *A micro–macro approach to rubber–*

like materials. part i: The non–affine micro–sphere model of rubber elasticity. Journal of the Mechanics and Physics of Solids, 52: 2617–2660.

[119] Miehe, C.; Kiefer, B.; Rosato, D. [2011]: *An incremental variational formulation of dissipative magnetostriction at the macroscopic continuum level.* International Journal of Solids and Structures, 48: 1846–1866.

[120] Miehe, C.; Rosato, D.; Kiefer, B. [2011]: *Variational principles in dissipative electro-magneto-mechanics: A framework for the macro-modeling of functional materials.* International Journal for Numerical Methods in Engineering, 86: 1225–1276.

[121] Miehe, C.; Zäh, D.; Rosato, D. [2012]: *Variational-based modeling of micro-electro-elasticity with electric field- and stress-driven domain evolution.* International Journal for Numerical Methods in Engineering, 91(2): 115–141.

[122] Miguel, J.; Sànchez-Barriga, J.; Bayer, D.; Kurde, J.; Heitkamp, B.; Piantek, M.; Kronast, F.; Aeschlimann, M.; Dürr, H. A.; Kuch, W. [2009]: *Time-resolved magnetization dynamics of cross-tie domain walls in permalloy microstructures.* Journal of Physics: Condensed Matter, 21: 496001–496007.

[123] Miller, K. S. [1981]: *On the inverse of the sum of matrices.* Mathematics Magazine, 54(2): 67–72.

[124] Nan, C.-W.; Bichurin, M.; Dong, S.; Viehland, D.; Srinivasan, G. [2008]: *Multiferroic magnetoelectric composites: Historical perspective, status, and future directions.* Journal of Applied Physics, 103: 031101.

[125] Pao, Y. H.; Hutter, K. [1975]: *Electrodynamics for moving elastic solids and viscous fluids.* Proceedings of the IEEE, 63(7): 1011–1021.

[126] Penfield Jr., P.; Haus, H. A. [1967]: *Electrodynamics of Moving Media*, Vol. 40 of *Research Monographs.* M. I. T. Press, Cambridge, MA.

[127] Piratla, S. [2009]: *Fully-coupled characterization of thermo-electro-magneto-mechanical materials.* Master's thesis, The Ohio State University.

[128] Ponte Castañeda, P.; Galipeau, E. [2011]: *Homogenization-based constitutive models for magnetorheological elastomers at finite strain.* Journal of the Mechanics and Physics of Solids, 59: 194–215.

[129] Prohl, A. [2001]: *Computational Micromagnetism.* Teubner.

[130] Rave, W.; Hubert, A. [2000]: *Magnetic ground state of a thin-film element.* IEEE Transactions on Magnetics, 36: 3886–3899.

[131] Reese, S.; Govindjee, S. [1998]: *A theory of finite viscoplasticity and numerical aspects.* International Journal of Solids and Structures, 35: 3455–3482.

[132] Rosato, D. [2010]: *On the Formulation and Numerical Implementation of Dissipative Electro-Mechanics at Large Strains.* Ph.D. Thesis, Institute of Applied Mechanics (CE), Chair I, University of Stuttgart.

[133] Salas, E.; Bustamante, R. [2014]: *Numerical solution of some boundary value problems in nonlinear magneto-elasticity.* Journal of Intelligent Material Systems and Structures.

[134] Sansour, C.; Skatulla, S.; Arunachalakasi, A. [2010]: *A generalized framework and a multiplicative formulation of electro-mechanical coupling.* In Maugin, G. A.; Metrikine, A. V. (Editors), *Mechanics of Generalized Continua*, Vol. 21 of *Advances in Mechanics and Mathematics*, pp. 287–294. Springer New York.

[135] Saxena, P.; Hossain, M.; Steinmann, P. [2013]: *A theory of finite deformation magneto-viscoelasticity.* International Journal of Solids and Structures, 50: 3886–3897.

[136] Saxena, P.; Hossain, M.; Steinmann, P. [2014]: *Nonlinear magneto-viscoelasticity of transversally isotropic magneto-active polymers.* Proceedings of the Royal Society A, 470: 1–23.

[137] Schabes, M. E.; Bertram, H. N. [1988]: *Magnetization processes in ferromagnetic cubes.* Journal of Applied Physics, 64: 1347–1357.

[138] Schrade, D.; Müller, R.; Xu, B. X.; Gross, D. [2007]: *Domain evolution in ferroelectric materials: A continuum phase field model and finite element implementation,.* Computer Methods in Applied Mechanics and Engineering, 196: 4365–4374.

[139] Sidoroff, F. [1974]: *Un modèle viscoélastique non linéaire avec configuration intermédiaire.* Journal de Mécanique, 13: 679–713.

[140] Simó, J. C. [1987]: *On a fully three–dimensional finite–strain viscoelastic damage model: Formulation and computational aspects.* Computer Methods in Applied Mechanics and Engineering, 60: 153–173.

[141] Simo, J. C.; Fox, D. D. [1989]: *On stress resultant geometrically exact shell model. part i: formulation and optimal parametrization.* Computer Methods in Applied Mechanics and Engineering, 72: 267–304.

[142] Simo, J. C.; Fox, D. D.; Rifai, M. S. [1990]: *On a stress resultant geometrically exact shell model. part iii: computational aspects of the nonlinear theory.* Computer Methods in Applied Mechanics and Engineering, 79: 21–70.

[143] Simo, J.; Miehe, C. [1992]: *Associative coupled thermoplasticity at finite strains: Formulation, numerical analysis and implementation.* Computer Methods in Applied Mechanics and Engineering, 98: 41–104.

[144] Smith, R. C. [2005]: *Smart Material Systems: Model Development.* Society for Industrial and Applied Mathematics, Philadelphia, PA.

[145] Smith, R. C.; Dapino, M. J.; Seelecke, S. [2003]: *Free energy model for hysteresis in magnetostrictive transducers.* Journal of Applied Physics, 93(1): 458–466.

[146] Smith, R. C.; Dapino, M. J.; Braun, T. R.; Mortensen, A. P. [2006]: *A homogenized energy framework for ferromagnetic hysteresis.* IEEE Transactions on Magnetics, 42: 1747–1769.

[147] Spaldin, N. A. [2003]: *Magnetic Materials: Fundamentals and Device Applications.* Cambridge University Press, Cambridge.

[148] Steigmann, D. J. [2004]: *Equilibrium theory for magnetic elastomers and magnetoelastic membranes.* International Journal of Non-Linear Mechanics, 39: 1193–1216.

[149] Stratton, J. A. [2007]: *Electromagnetic Theory.* John Wiley & Sons.

[150] Tavger, B. A.; Zaitsev, V. M. [1956]: *Magnetic symmetry of crystals.* Soviet Journal of Experimental and Theoretical Physics, 3: 430–436.

[151] Thylander, S.; Menzel, A.; Ristinmaa, M. [2012]: *An electromechanically coupled micro-sphere framework—Application to the finite element analysis of electrostrictive polymers.* Smart Materials and Structures, 21: 094008.

[152] Tiersten, H. F. [1964]: *Coupled magnetomechanical equations for magnetically saturated insulators.* Journal of Mathematical Physics, 5(9): 1298–1318.

[153] Tiersten, H. F. [1965]: *Variational principle for saturated magnetoelastic insulators.* Journal of Mathematical Physics, 6 (5): 779–787.

[154] Tiersten, H. F. [1987]: *On the interaction of the electromagnetic field with de-*

formable solid continua. In *Proceedings of the IUTAM Symposium: Electromagnetomechanical Interactions in Deformable Solids and Structures, Tokyo, Japan, 12–17 October, 1986*, pp. 277–284.

[155] Tiersten, H. F. [1990]: *A Development of the Equations of Electromagnetism in Material Continua*, Vol. 36 of *Tracts in Natural Philosophy.* Springer-Verlag, New York.

[156] Toupin, R. A. [1956]: *The elastic dielectric.* Archive for Rational Mechanics and Analysis, 5: 849–915.

[157] Treloar, L. R. G. [1944]: *Stress–strain data for vulcanised rubber under various types of deformation.* Transactions of the Faraday Society, 40: 59–70.

[158] Treloar, L. R. G. [1975]: *The Physics of Rubber Elasticity.* Clarendon Press, Oxford, 3rd Edition.

[159] Truesdell, C.; Toupin, R. [1960]: *The classical field theories.* In Flügge, S. (Editor), *Principles of Classical Mechanics and Field Theory*, Vol. III/1 of *Encyclopedia of Physics*, pp. 226–795. Springer-Verlag, Berlin.

[160] Varga, Z.; Filipcsei, G.; Zrínyi [2005]: *Smart composites with controlled anisotropy.* Polymer, 46: 7779–7787.

[161] Varga, Z.; Filipcsei, G.; Zrínyi [2006]: *Magnetic field sensitive functional elastomers with tunable elastic modulus.* Polymer, 47: 227–233.

[162] Venkataraman, V. [2012]: *A projection method in incremental variational formulation for phase field models in micromagnetics.* Master's thesis, University of Stuttgart.

[163] Weinan, E.; Wang, X.-P. [2000]: *Numerical methods for the landau-lifshitz equation.* SIAM Journal on Numerical Analysis, 38: 1647–1665.

[164] Williams, H. J.; Bozorth, R. M.; Shockley, W. [1949]: *Magnetic domain patterns on single crystals of silicon iron.* Physical Review, 75: 155–178.

[165] Yung, K. W.; Landecker, P. B.; Villani, D. V. [1998]: *An analytic solution for the force between two magnetic dipoles.* Magnetic and Electrical Separation, 9: 39–52.

[166] Zhang, J. X.; Chen, L. Q. [2005]: *Phase-field microelasticity theory and micromagnetic simulations of domain structures in giant magnetostrictive materials.* Acta Materialia, 53: 2845–2855.

[167] Zhang, J. X.; Chen, L. Q. [2005]: *Phase-field model for ferromagnetic shape-memory alloys.* Philosophical Magazine Letters, 85: 533–541.

[168] Zhang, W.; Bhattacharya, K. [2005]: *A computational model of ferroelectric domains. Part I: Model formulation and domain switching.* Acta Materialia, 53: 185–198.

[169] Zimm, B. H. [1956]: *Dynamics of polymer molecules in dilute solution: Viscoelasticity, flow birefringence and dielectric loss.* The Journal of Chemical Physics, 24: 269–278.

Curriculum Vitae

Personal Data

Name	Gautam Ethiraj
Date of Birth	March 22, 1985
Place of Birth	Chennai, India
Parents	Geeta Ethiraj Dwarak Ethiraj
Marital Status	Unmarried

School Education

1990-1993	Bishop's School Pune, India
1993-2000	St. Mary's School Pune, India
2000-2002	Fergusson College Pune, India

University Education

2003-2007	B.Tech in Mechanical Engineering, IIT Madras
2007-2008	M.Sc. in Computational Mechanics, Swansea University
2008-2009	M.Sc. in Computational Mechanics, University of Stuttgart

Professional Occupation

2009-2014	Research Associate and COMMAS Course Director Institute of Applied Mechanics, Civil Engineering, University of Stuttgart

In dieser Schriftenreihe bisher erschienene Berichte:

I-1(1996) *Theoretische und algorithmische Konzepte zur phänomenologischen Beschreibung anisotropen Materialverhaltens*, J. Schröder, Dissertation, 1996.

I-2(1996) *Zur Theorie und Numerik finiter elastoplastischer Deformationen von Schalentragwerken*, B. Seifert, Dissertation, 1996.

I-3(1996) *Zur Modellierung des künstlichen Infrarot-Dichroismus in Poymerfolien bei großen Verformungen*, J. Buhler, Dissertation, 1996.

I-4(1998) *Verfahren zur Ermittlung der Erdbebenlasten mit Berücksichtigung des stochastischen Charakters des Bebens*, S. Zhang, Dissertation, 1998.

I-5(1998) *Zur Beschreibung finiter Deformationen von Polymeren: Experimente, Modellbildung, Parameteridentikation und Finite-Elemente- Formulierung*, J. Keck, Dissertation, 1998.

I-6(1999) *Berechnungsverfahren instationär erregter Systeme im Frequenzbereich*, A. Jaworek, Dissertation, 1999.

I-7(2000) *Homogenisierungsmethoden der nichtlinearen Kontinuumsmechanik unter Beachtung von Stabilitätsproblemen*, J. Schröder, Habilitation, 2000.

I-8(2002) *Theorie und Numerik von Materialinstäbilitaten elastoplastischer Festkörper auf der Grundlage inkrementeller Variationsformulierungen*, M. Lambrecht, Dissertation, 2002.

I-9(2002) *Mikromechanisch motivierte Modelle zur Beschreibung finiter Deformationen gummiartiger Polymere: physikalische Modellbildung und numerische Simulation*, F. Lulei, Dissertation, 2002.

I-10(2003) *Adaptive Finite-Elemente-Berechnungen der nichtlinearen Festkörpermechanik bei kleinen und großen Verzerrungen*, A. Koch, Dissertation, 2003.

I-11(2003) *Theorie und Numerik der Parameteridentikation von Materialmodellen der finiten Elastizität und Inelastizität auf der Grundlage optischer Feldmeßmethoden*, G. Scheday, Dissertation, 2003.

I-12(2004) *Approaches to the Description of Anisotropic Material Behaviour at Finite Elastic and Plastic Deformations, Theory and Numerics*, N. Apel, Dissertation, 2004.

I-13(2004) *Temperaturabhängige Beschreibung visko-elasto-plastischer Deformationen kurzglasfaserverstärkter Thermoplaste: Modellbildung, Numerik und Experimente*, S. Rieger, Dissertation, 2004.

I-14(2005) *Zur Parameteridentikation komplexer Materialmodelle auf der Basis realer und virtueller Testdaten*, A. Rieger, Dissertation, 2005.

I-15(2005) *Viskoelastisches Verhalten von Elastomeren bei finiten Verzerrungen: Experimente, Modellierung und Simulationen*, H. Zecha, Dissertation, 2005.

I-16(2005) *Mehrskalenmodelle in der Festkörpermechanik und Kopplung von Mehrgittermethoden mit Homogenisierungsverfahren*, C.G. Bayreuther, Dissertation, 2005.

I-17(2005) *Static and Dynamic Homogenization Analyses of Discrete Granular and Atomistic Structures on Different Time and Length Scales*, J. Dettmar, Dissertation, 2005.

I-18(2006) *Incompatibility and Instability Based Size Effects in Crystals and Composites at Finite Elastoplastic Strains*, M. Becker, Dissertation, 2006.

I-19(2007) *Aspects of Energy Minimization in Solid Mechanics: Evolution of Inelastic Microstructures and Crack Propagation*, E. Gürses, Dissertation, 2007.

I-20(2007) *Micro-Macro Approaches to Rubbery and Glassy Polymers: Predictive Micromechanically-Based Models and Simulations*, S. Göktepe, Dissertation, 2007.

I-21(2008) *Material Forces in Finite Inelasticity and Structural Dynamics: Topology Optimization, Mesh Refinement and Fracture*, D. Zimmermann, Dissertation, 2008.

I-22(2010) *Thermoviscoplasticity of Glassy Polymers: Experimental Characterization, Parameter Identification and Model Validation*, J. Méndez Diez, Dissertation, 2010.

I-23(2010) *On the Formulation and Numerical Implementation of Dissipative Electro–Mechanics at Large Strains*, D. Rosato, Dissertation, 2010.

I-24(2011) *A Variational Framework for Gradient-Extended Dissipative Continua. Application to Damage Mechanics, Fracture, and Plasticity*, F. Welschinger, Dissertation, 2011.

I-25(2013) *Variational Multifield Modeling of the Formation and Evolution of Laminate Microstructure*, F. Hildebrand, Dissertation, 2013.

I-26(2013) *On the Computational Modeling of Micromechanical Phenomena in Solid Materials*, C.Linder,Habilitation, 2013.

I-27(2013) *Hybrid Micro-Macro Modeling of Texture Evolution in Polycrystal Plasticity Based on Microstructural Reorienation Continua*, I. Zimmermann, Dissertation, 2013.

I-28(2014) *Finite Element based Electronic Structure Calculations*, V. Schauer, Dissertation, 2014.

I-29(2014) *A Thermodynamically Phase Field Approach to Fracture* , M. Hofacker, Dissertation, 2014.

I-30(2014) *Multi-level Description of Failure Phenomena with Strong Discontinuity Approach*, A. Raina, Dissertation, 2014.

I-31(2014) *Phase Field Modelin of Fracture in Ruberry and Glassy Polymers at Finite Thermo-Viscoelastic Deformations*, L. Schänzel, Dissertation, 2014.

I-32(2014) *Variational Homogenization in Electro-Mechanics: From Micro-Electro-Elasticity to Electroactive Polymers*, D. Zäh, Dissertation, 2014.

I-33(2014) *Computational Modeling of Ferromagnetics and Magnetorheological Elastomers*, G. Ethiraj, Dissertation, 2014.